

This item was submitted to [Loughborough's Research Repository](#) by the author.  
Items in Figshare are protected by copyright, with all rights reserved, unless otherwise indicated.

## **Knock modelling in spark-ignition engines and a study of the effect of combustion instability on knock**

PLEASE CITE THE PUBLISHED VERSION

PUBLISHER

© Gopal Ganti

PUBLISHER STATEMENT

This work is made available according to the conditions of the Creative Commons Attribution-NonCommercial-NoDerivatives 4.0 International (CC BY-NC-ND 4.0) licence. Full details of this licence are available at: <https://creativecommons.org/licenses/by-nc-nd/4.0/>

LICENCE

CC BY-NC-ND 4.0

REPOSITORY RECORD

Ganti, Gopal. 2019. "Knock Modelling in Spark-ignition Engines and a Study of the Effect of Combustion Instability on Knock". figshare. <https://hdl.handle.net/2134/16606>.

BLDSC No. - D 80418

LOUGHBOROUGH  
UNIVERSITY OF TECHNOLOGY  
LIBRARY

AUTHOR/FILING TITLE

GANTI, G

ACCESSION/COPY NO.

014743/02

VOL. NO.

CLASS MARK

LOAN COPY

- 6 JUL 1990

date due:-

13 DEC 1983

LOAN 3 WKS. + 3

UNLESS RECALLED

CHESTER

CHESTER

date due:- 21 NOV 1994

- 9 DEC 1994

- 4 DEC 1996

26 JUN 1991

29 JUN 1988

14 APR 89

LOAN 3 WKS. + 3

UNLESS RECALLED

CHESTER

date due:-

- 5 JUL 1989

LOAN 3 WKS. + 3

UNLESS RECALLED

CHESTER

date due:-

17 JAN 1989

LOAN 3 WKS. + 3

UNLESS RECALLED

1/2/89

25 JUN 1999

001 4743 02





KNOCK MODELLING IN SPARK-IGNITION ENGINES

AND

A STUDY OF THE EFFECT OF COMBUSTION INSTABILITY ON KNOCK

by

GOPAL GANTI B.Tech, M.S.

A Doctoral Thesis

Submitted in partial fulfilment of the  
requirements for the award of

Doctor of Philosophy  
of Loughborough University of Technology

October 1987

Supervisor: Professor J C Dent, PhD, CEng  
Department of Mechanical Engineering

© by Gopal Ganti

Loughborough University	
of Technology Library	
Date	Dec 87
Class	
Acc. No.	014743/02

## Abstract

One of the limiting factors for improved performance of the spark ignited internal combustion engine is the phenomenon of knock.

The present investigation makes a survey of the available models for auto-ignition for introduction into an existing phenomenological combustion model. A mathematical model of knock, based on a degenerate branched chain mechanism for the prediction of autoignition delay time, was considered and introduced into the combustion model. Experiments were carried out on a single cylinder variable compression ratio engine to validate the model.

The interaction of acoustic waves with unsteady combustion leading to unstable combustion and thus triggering knock is considered. This work examines the relationship between the variation in the power of the frequency component corresponding to the natural frequency of the combustion chamber, and the occurrence of knock.

A model based on the relaxation oscillation phenomenon is developed to calculate the oscillating frequency of the flame front. This model was developed on the basis that the gas contents of the combustion chamber in an internal combustion engine can be considered as a 'lumped parameter' spring mass damper system.

Analysis of the frequency spectrum of flame ionization data show a favourable comparison with the predictions from the model, thus, opening the possibility of future work on correlating the acoustic instability in the combustion chamber to knock in spark ignition engines.

## ACKNOWLEDGEMENTS

The Author wishes to express his grateful appreciation to the following:

Professor J C Dent for his guidance and supervision throughout the work.

Dr G M Chapman for his help with the Fast Fourier Analyser.

Messrs. G Manship, S Taylor, S Line and all the members of the technical staff.

Geoff Harris and members of the Computer Centre.

Mrs Janet Redman for the drawings and Mrs Janet Smith for typing the difficult parts and giving the manuscript the professional touch.

All friends who have helped in different ways throughout the project and last but in no way least Miss Sue Taylor for her encouragement and support throughout the project.

## NOTATIONS

A	Pre-experiment factor in Rate Equation
E	ACTIVATION ENERGY
Gr	Grashof Number
Nu	Nusselt Number
P	Pressure
Re	Reynolds Number
T	Temperature
t	Time
$\rho$	Density
$\tau$	Ignition delay
$\tau_1$	Delay time for first stage ignition
$\tau_2$	Delay time for second stage ignition

## ABBREVIATIONS

ATDC	After Top Dead Centre
A/F	Air Fuel Ratio
BTDC	Before Top Dead Centre
°C	Degrees Centigrade
F	Fuel Air Equivalence Ratio
FFT	Fast Fourier Transformation
KLCR	Knock Limited Compression Ratio
KLIMEP	Knock Limited Indicated Mean Effective Pressure
KLIP	Knock Limited Inlet Pressure
PRF	Primary Reference Fuel
TDC	Top Dead Centre
TEL	Tetra Ethyl Lead

## CONTENTS

	<u>Page No</u>
Abstract . . . . .	i
Acknowledgements . . . . .	ii
Notations . . . . .	iii
Abbreviations . . . . .	iv
CHAPTER I: REVIEW OF LITERATURE ON KNOCK	
1.1 Introduction . . . . .	1
1.2 Hydrocarbon Combustion and Two-Stage Ignition . . . . .	7
1.3 Experiments with Closed Vessels . . . . .	9
1.4 Experiments with Rapid Compression Machines . . . . .	12
1.5 Flame Vibrations . . . . .	18
1.6 Flame Propagation in Closed Vessels . . . . .	19
1.7 Types of Vibratory Flames . . . . .	20
1.8 Interaction of Compression Waves with Flame Front . . . . .	21
1.9 Overview of the Literature Survey . . . . .	22
CHAPTER II: REVIEW OF KNOCK MODELS	
2.1 Introduction . . . . .	24
2.2 Requirements of a Knock Model . . . . .	27
2.3 Selection of Kinetic Model . . . . .	28
2.4 The Model Due to Halstead et al (Shell Model) . . . . .	29
2.5 The Mathematical Scheme of the Kinetic Model . . . . .	31
2.6 Preliminary Model of Schapertons et al . . . . .	33
2.7 Model due to Cox and Cole . . . . .	35
2.8 Selection of Model for Incorporation in Combustion Model . . . . .	37
2.9 Solution Technique . . . . .	37
2.10 Validation of Shell Model . . . . .	41

CHAPTER III:	THE COMBUSTION MODEL	
3.1	Introduction . . . . .	44
3.1.1	Phenomenological Models . . . . .	44
3.1.2	Multi-Dimensional Models . . . . .	44
3.2	Thermodynamic Models . . . . .	45
3.3	Sub-Models for Burn Rate . . . . .	46
3.4	Burning Law . . . . .	50
3.5	Basis of the Combustion Model . . . . .	54
3.6	Governing Equations and Solution Technique	55
3.7	Validation of Combustion Model . . . . .	58
3.8	Incorporation of Knock Model . . . . .	60
3.9	Comparison of Results from Models of Halstead et al and Douaud and Eyzat . . .	62
CHAPTER IV:	DATA ACQUISITION AND ANALYSIS	
4.1	Introduction . . . . .	64
4.2	Pressure Data Measurement and Analysis . .	64
4.3	Dynamic Pressure Measurement in Engine . .	65
4.4	Application of Flame Ionization Probe to Engine Studies . . . . .	67
4.5	Flame Ionization Probe: Principle of Operation . . . . .	71
4.6	Ionization Probe Construction and Manu- facture . . . . .	71
4.7	Probe Calibration . . . . .	72
4.8	Data Acquisition and Preparation . . . . .	72
4.9	Data Analysis . . . . .	76
CHAPTER V:	APPLICATION OF RELAXATION OSCILLATION MODEL TO ENGINE COMBUSTION . . . . .	78
5.1	Introduction . . . . .	78
5.2	Preknock Vibrations . . . . .	78
5.3	Application of Relaxation Oscillation to Engine Geometry . . . . .	83

	<u>Page No</u>
5.4    Compression Waves in Bombs and Engines . .	84
5.5    Application of Equation of Relaxation Oscillation . . . . .	85
5.6    Solution of Equation for Relaxation Oscillation . . . . .	86
5.7    Modelling Data from Lancaster's Thesis . .	88
5.8    Effect of Fluctuating Flame Front on the Unburned Gas . . . . .	89
CHAPTER VI:    RESULTS AND DISCUSSION	
6.1    Introduction . . . . .	91
6.2    Comment on the Experimental Procedures . .	92
6.3    Experimental Results from Tests with Propane	94
6.4    Results with Premium Grade Gasoline . . .	96
6.5    Results with 70 Octane PRF . . . . .	98
6.6    Discussion of Results . . . . .	100
CHAPTER VII:    SUMMARY, CONCLUSIONS AND RECOMMENDATIONS FOR FUTURE WORK	
7.1    Introduction . . . . .	104
7.2    Summary . . . . .	104
7.3    Conclusions . . . . .	108
7.4    Recommendations for Future Work . . . . .	109
REFERENCES . . . . .	110
APPENDIX A:    Calculation of Mass Fraction Burned from Experimental Data . . . . .	
	120
APPENDIX B:    Parameters to Control Subroutine DO2QBF . .	123
APPENDIX C:    The Idea of Relaxation Oscillation . . . . .	140
APPENDIX D:    ACS1 Program to Solve the Equation of Relaxation Oscillation . . . . .	142

## CHAPTER I

### REVIEW OF LITERATURE ON KNOCK

#### 1.1 INTRODUCTION

The Four-stroke Spark-Ignited Internal Combustion engine follows the otto cycle, which, as an ideal process can be represented by Fig.1.1. The first stroke draws in the mixture of fuel and air. During the second stroke, this is compressed, ignited near the end of compression, by an electric discharge and, ideally, instantaneously burned. In the third stroke, the burned gases expand and perform work. During the fourth stroke, the burned gases are exhausted to the atmosphere.

In actual practice the engine cycle follows Fig.1.2. The first stroke, also referred to as the induction stroke draws in a mixture of air and fuel which mixes with some residual exhaust gases. The temperature and pressure of this mixture, usually referred to as the charge, increases as the second or compression stroke starts, just before the end of the compression stroke the charge is ignited by the aid of a spark. After an initial period of delay a flame front develops which progresses the unburned gases increasing the pressure and temperature within the cylinder. As the flame front progresses the unburned gases are subjected to very high temperatures due to compression from piston motion, compression by the flame front and heat transfer from the burned zone. Due to these high temperatures most fuels are subjected to rapid oxidation. Depending on whether the flame progresses through the entire chamber before this rapid oxidation turns into an explosion or not, smooth or knocking combustion is said to occur.

The third stroke is the expansion stroke also referred to as the power stroke, as, it is this stroke that produces all the power developed by the engine. The fourth is the exhaust stroke when the products of combustion are expelled from the engine.

Complete and instantaneous combustion at the top dead centre (TDC) would be the ideal form of combustion to obtain maximum power and efficiency from a Spark ignition engine, since this is not feasible in practice, to obtain maximum efficiency it is necessary to get as close as possible to the ideal otto cycle. Increasing the power output and efficiency by increasing the compression ratio of an engine has been restricted by the onset of knock. The cause, effect and possible cure of knock has been the subject of research since it was first noticed by Nernst, Clerk and their contemporaries in the early 20th Century {Refer review by Oppenheim [1]}.

Over the years the terms "pinking" and "detonation" have been used synonymously with knocking. Knocking in spark ignition engines is defined as the autoignition of the unburned charge ahead of the flame front.

The early theories as to the cause of knock were :

- a. The Autoignition Theory of knock.
- b. The Detonation Theory.
- c. The "Flame Vibration Theory".

- a. "The Auto-ignition Theory":

The Autoignition theory was first proposed by Ricardo [2]. According to Ricardo knock is caused by the sudden inflammation of residual unburned charge owing to its compression by the expanding burned and burning portion. The heat due to compression is augmented by radiant and conducted heat. The complete unburned gas is considered to explode causing a rapid rise in pressure and generating vibrations in the cylinder wall as if struck by a hammer.

b. "The Detonation Theory":

The Detonation Theory proposed by Maxwell and Wheeler [3] suggests that a knocking explosion in an internal combustion engine is due to the initiation of a stationary pressure wave in the burned and burning gases, followed by a maintained shock wave when the accelerated, vibrating flame impinges on the wall of the combustion chamber. The nature of the fuel and its concentration determining the amount of residual energy available to maintain a shock wave when the recoil takes place.

c. "The Flame Vibration Theory":

Studying the rate of flame propagation and nature of vibrations in mixtures with air of methane and Birmingham coal gas in closed tubes of 12 inches (30 cm) and 24 inches (60 cm) long, Morgan [4] found, that in the longer tube, flame vibrations developed that led to a high pitched note resembling knock in an internal combustion engine. Based on this similarity Morgan [4] suggested that the two phenomena were closely connected, and suggested that knock depended on (a): the rate of heat generation, and, its association with, (b): an appropriate frequency in the gas along the direction of motion of the flame. The frequency of the vibrations is a function of the length of the gas column, therefore maintaining a fixed point of ignition, only factor (a) would operate, thus, implying that the vibrations are most likely to occur when the most inflammable mixture is used.

Maxwell [5] in his study of the various theories as to the cause of knock rejects the theory of Morgan on the grounds that it does not provide a cause for knock.

The most widely accepted theory has been the autoignition theory first proposed by Ricardo [2] and later substantiated with photographic evidence by Boyd and Withrow [6].

The operating variables that effect knock either individually or in combination are:

- a. Spark Timing
- b. Engine Speed
- c. Inlet Pressure and Compression Ratio
- d. Inlet Temperature
- e. Cylinder Coolant Temperature
- f. Air-Fuel Ratio
- g. Fuel Quality

Knocking and the limitations thereby imposed on the range of practical operations are so important in practice that the evaluation and division of fuels for spark ignition engines is based upon the knock properties. The knock rating of a fuel (given as Octane Number) is found by comparing the knock characteristics (i.e. tendency to knock) of a given fuel to that of a blend of Primary Reference Fuels (PRF). The Primary Reference Fuels being n-heptane with an octane number of 0, as it has a very high tendency to knock and Iso-octane (2,2,4- Trimethyl Pentane) with an octane number of 100. An Octane number of, say, 75 for any fuel would mean that the said fuel would have the same knock characteristics as that of a blend of iso-octane and n-heptane in a volumetric ratio of 75 and 25 respectively.

Fuels that have anti knock characteristics better than that of Iso-octane, are defined as 100 plus the number of milliliters of tetra-ethyl-lead added to a litre of petrol.

Octane number requirement increases as the spark is advanced or the engine speed is reduced as has been shown in Fig.1.3 by Taylor and Taylor [7]. Increasing the inlet pressure (Fig.1.4) or Compression ratio (Fig.1.5) causes the engine to knock. The inlet pressure and compression ratio when incipient knocking is observed are the Knock Limited Inlet Pressure (KLIP) and Knock Limited Compression Ratio (KLCR) respectively. The Indicated mean effective pressure when

knocking starts to occur is known as the Knock Limited Indicated Mean Effective Pressure (KLIMEP). To extend the range of defining the performance of a fuel over 100 Octane the term Performance Number was introduced, which is defined as the ratio of the Knock Limited Indicated Mean Effective Pressure of a fuel to the Knock Limited Indicated Mean Effective Pressure using iso-octane. The tendency of an engine to knock increases with increase in the inlet temperature (Fig.1.6) or increasing the cylinder coolant temperature (Fig.1.7). The overall effect of increasing any one or a combination of the above variables is, the reduction in the reaction time of the end gases. Depending on this reaction time Hydrocarbon combustion has been categorised into three types :

1. Catalytic Oxidation - taking place at relatively low temperatures sometimes noticeable below 100 C.
2. Slow Oxidation - taking place in the gas phase in a range from 200-300 C to about 500-600 C.
3. Explosive Combustion - fast spontaneous oxidation

It is the slow oxidation that is of interest in the study of knocking combustion. Slow oxidation of Hydrocarbons are known to follow a typical course of an auto-catalytic reaction[8], i.e. a reaction that has one of its products act as a catalyst to enhance the rate of the reaction. As the oxidation of Hydrocarbons takes place the reaction rate rises and falls. The slow rise and fall of this reaction rate depicts an auto-catalytic reaction (Fig.1.8. Curve 1), Curve 2 shows a case when the thermal equilibrium is disturbed and the auto-catalytic reaction ends in an explosion. Curve 3 depicts a normal explosion where the thermal equilibrium is disturbed from the start of the reaction.

In the study of knock three different approaches have been used over the years to reduce or eliminate the tendency to knock in an engine. The physical aspects of flame propagation on the occurrence of knock was studied by Ricardo [2] by developing various geometries for the combustion chamber, so that the propagating flame reaches completion before the end-gas could autoignite. This involved changing the shape of the cylinder head and the piston top. Some of the different designs tested by Ricardo are shown in Fig. (1.19).

It can be seen that with central ignition the engine did not knock where as the maximum tendency to knock was with the spark plug at a corner [Fig. 1.19 (g)(i)(k)], thus providing further evidence that the longer the flame travel, the higher the tendency to knock as the residence time for the end gases to autoignite is greater.

Kettering, Boyd and co-workers developed chemical means 'doping' the fuel with anti-knock agents, like tetra-ethyl-lead, and using fuels of high octane number like triptane. Gussak et. al [9] developed chemical-kinetic means for direct control of the combustion process like the LAG (Lavinnia Aktivatsia Gorennia or Avalanche Activated Combustion Process). Essentially, this principle is such, that the ignition initiation and propagation of combustion, of the working mixture in a prechamber of a spark ignition engine, is obtained by a low temperature torch of the chemically active products of combustion of a rich mixture in the auxiliary chamber.

Combustion of fuels with additives such as tetra-ethyl-lead lead to exhaust products like lead oxide that are poisonous and have a detrimental effect on life (animal and vegetation).

Environmental restrictions have forced the need to restrict or completely eliminate the use of anti-knock agents such as tetra-ethyl-lead. Manufacturing constraints would restrict the use of complicated geometries to eliminate knock. Thereby, forcing the need to find a solution to the problem of knock by chemical-kinetic means or a combination of chemical-kinetic and physical means.

## 1.2 Hydrocarbon Combustion and Two-Stage Ignition

As the end gases in the engine undergo autoignition, it would be appropriate to study the oxidation and autoignition characteristics of hydrocarbons. The Hydrocarbons above Butane have a form of oxidation that follows what is usually referred to as a two stage ignition. In this form of ignition the hydrocarbon slowly oxidizes increasing the temperature and pressure of the system, after it reaches a temperature of about 250 C the temperature gradient is very low and bluish flames are noticed which have a very low emissivity and low heat release as compared to a hot (normal) flame. These flames are called "cool flames". Table(1.2) shows the pressure data during a reaction of pentane and oxygen in a constant volume combustion bomb from data presented by Lewis and Von-Elbe [10]. The data typifies the phenomenon of two stage ignition with its two separate induction periods, which are usually denoted as  $t_1$  and  $t_2$ . The induction period  $t_1$  is considered to be the time from the beginning of the reaction to the appearance of the cool flames, and the second induction period ( $t_2$ ) is the time from the appearance of cool flames to the onset of violent explosion. Extension of constant volume studies to rapid compression machines also show the two stage ignition (Fig. 1.9). Ball [11] confirmed the presence of cool flames in an operating engine, and showed the possibility of a relatively high rate of propagation for the cool flames, and the occurrence of autoignition subsequent to the appearance of cool flames.

Sturgis [12] conducted experiments in motored engines in which the temperatures and pressures of the entire fuel-air mixtures were varied to simulate the conditions present in the end gas of a fired engine. The elimination of combustion pressure in a motored engine resulted in longer reaction times for the cool flames thus making the process easier to study.

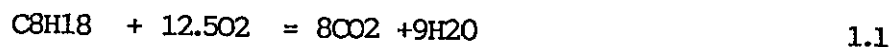
As a result of cool flames, Sturgis [12] found the presence of radiation which was measured with a sensitive radiation detector placed in the head of the motored engine. Increasing the compression

ratio increased the radiation levels till autoignition occurred. On the basis of these end gas analysis and radiation level measurement Sturgis [12] suggests a four stage scheme for hydrocarbon oxidation.

Pre-Cool flame region  
Cool flame region  
Blue flame region  
and Hot flame region

The initial period of oxidation in which the intermediates necessary for the cool-flame formation are produced in the pre-cool flame region, this is usually about 25-40 C below the temperature required for cool-flame formation. Fig. 1.14 shows three of the four stages of hydrocarbon oxidation namely, pre-cool flames, cool-flames and hot flames. Though most hydrocarbons give rise to blue flames just prior to autoignition it is seen more often in lean mixtures.

The complete combustion of a hydrocarbon such as Iso-octane would follow the (equation 1.1) :



This does not occur in one stage but in a series of intermediate reactions over a number of stages. A generalised scheme would follow Fig 1.13, where the reactions could be defined as formation of peroxides, decomposition of which leads to the formation of Aldehydes, ketones, acids and carbon oxides.

The decomposition of peroxides takes place in two ways (Fig.1.15), the first which is the fission of the peroxide molecule to yield two radicals each of which can help initiate further oxidation of the hydrocarbon and comprises the pre-cool flame stage, while the thermal decomposition to aldehydes, ketones, acids and/or olefins makes up the cool flame stage.

The formation of formaldehyde and hydrogen peroxide (lowest aldehyde and peroxide respectively) are considered to be the blue flame stage while the reactions forming carbon oxides and water are the final stage.

Mathematical modelling of knock in engines requires knowledge of the chemical reactions occurring during the autoignition of hydrocarbons. The experiments conducted in constant volume combustion bombs, rapid compression machines, motored engines and fired engines have resulted in the development of empirical models for the simulation of autoignition delay times based on single global reaction rates and on more complicated kinetic models.

### 1.3 Experiments with Closed Vessels

Due to the absence of compression in constant volume bombs the temperatures and pressures are much lower than those in engines. This results in longer reaction times for the oxidation or autoignition of any fuel. The reproduction of knocking combustion in such bombs gives an idea, as to the variables effecting the induction periods for hydrocarbon combustion. Fig.1.10 shows the variation of the two induction periods and the complex nature of the variation of  $t$  ( $= t_1 + t_2$ ) with temperature and pressure. Rogener defined the induction times for n-heptane, n-pentane and n-butane (Table 1.11). Though the numerical values hold no great significance it is seen that  $t_1$  always decreases with temperature while  $t_2$  increases with temperature, and both  $t_1$  and  $t_2$  decrease with pressure. Attempts to define a single scheme to calculate the total induction period required the need to understand the chemistry of hydrocarbon oxidation. Investigations into the behaviour of various hydrocarbons during combustion have been made by observing:

- a. Slow oxidation rates by flow methods or statically in bulbs.
- b. Absorption and emission spectra of burning hydrocarbons.
- c. Self-Ignition temperatures under various conditions.
- d. Knock in Engines

Egerton [13] noticed that, the kinetics of Hydrogen-Oxygen reactions and Hydrocarbon-Oxygen reactions shared a common feature in the chain branching phenomenon, though, the Hydrocarbon-Oxygen system was more complex in nature. Chain branching is a phenomenon whereby a reaction leads to self multiplication of free radicals. Lewis and Von Elbe [10] show that the first stage of hydrocarbon oxidation is governed by chain branching reactions. The chain branching phenomenon is one of the important features taken into account while modelling any kinetic scheme to simulate two-stage ignition.

Spectroscopic studies by Rasswieler and Withrow [14] of the combustion in engines showed the presence of formaldehyde during the occurrence of knock. The formation of peroxides and their depletion to aldehydes occurs in the first stage of hydrocarbon oxidation. The aldehydes decompose to form acids and end products like CO<sub>2</sub> and H<sub>2</sub>O.

The amount of aldehyde present has an influence on the induction time and this is clearly shown by Lewis and Von-Elbe [10]. Fig.1.11 shows the results of bomb experiments with the addition of acetaldehyde to a mixture of pentane-oxygen. The reduction in induction time is nearly exponential. The decomposition of aldehydes is dependent on the square of its concentration as shown by Schapertons et. al.[15]. Reducing the formation of aldehydes would increase the delay time. Addition of aniline was found to have this effect.

Though Tetra-ethyl-lead (TEL) increased the delay time it did not have any effect on the formation of aldehydes as was found by Rasswieler and Withrow [14]. Sturgis [12] suggests that TEL has a negligible effect on the formation and decomposition of Peroxides and higher Aldehydes, Ketones or Olefins during the oxidation of n-heptane, though it was found to deactivate radicals formed by organic peroxide decomposition which carried out further stages in the reaction leading to hydrogen peroxide formation and to knock.

The displacement of the autoignition limits to regions of higher temperatures and pressures due to addition of TEL are shown in Fig 1.18. The effect of TEL on the concentration of various intermediates analysed from the exhaust while running on n-heptane are shown in Figs 1.15 and 1.16. The reduction of the rate of decomposition of aldehydes and ketones with the addition of TEL is quite clear, thus comparing favourably with Lewis and Von-Elbe's results showing the variation of induction time with the addition of acetaldehyde (Fig.1.11).

Increasing the delay time for the second stage ignition as was found by Rogener, increases the time available for the end gases to autoignite, but it would also allow the flame to propagate through to completion, thus pre-empting knock.

Sturgis [12] points out the fact that the flame travel time has a strong influence on the characteristics of combustion, the larger the distance travelled by the flame travel the greater the chances of knocking in the combustion chamber. This concurs with the finding of Maxwell and Wheeler [3] that mixtures of pentane and oxygen that did not knock in short tubes would knock if the length of the tube was increased. The appearance of vibratory flames and the increase in their amplitude in conditions where knock occurred suggest the possibility that these vibrations could contribute to the cause of knock.

#### 1.4 Experiments with Rapid Compression Machines

As has been seen in the previous section the autoignition of fuel and air requires a finite time interval, which is, in general, a complex function of the physical state, (as defined by the temperature, pressure) and chemical constitution of the mixture. For the special case when the physical state of the fuel-air mixture can be regarded as constant, this time interval has been called ignition delay.

To simulate the above mentioned special case so as to be able to measure the delay period rapid compression machines (RCM) have been used. This device rapidly increases the temperature and pressure of the mixture of air and fuel, and allows it to remain at this elevated state for the duration of the delay period. Development of mathematical models for the combustion in spark ignition engines required the availability of pressure and temperature histories of the end gas. Based on experiments with rapid compression machines Livengood and Wu [16] proposed an expression correlating the fuel-air ratio, absolute temperature, absolute pressure and time, to the concentration of pertinent reaction products such as chain carriers.

This took the form:

$$d(x)/dt = \phi_1(P, T, t), \phi_2(F, \text{chemical composition}) \quad 1.2$$

where (x) = concentration of pertinent reaction products  
(i.e. chain carriers).

t = time

P = absolute pressure

T = absolute temperature

$\phi_1, \phi_2$  = empirical functions or constants

F = Fuel-air ratio

This equation implies that, for a given fuel-air mixture there exists a fixed functional relationship between the rate of the

global reaction, the instantaneous physical state, and time. The assumption that the ultimate consequence of the global reaction of equation (1.2) was a sudden transition to a process which then proceeds to complete the combustion reaction within a time interval which is smaller by orders of magnitude than the preceding delay period led to the concept of critical concentration  $(x)_c$ .

The concept of a critical concentration provides a limit for an integration process during which the concentration of chain carriers builds up. Hence, once the relationship between physical state and the low speed reaction rate is known, and the critical limit is determined, it should be possible to predict the time of occurrence of the high speed autoignition during any state-time process for the fuel-air mixture in question. This relationship has been expressed as ignition delay data. The general form of the empirical expression defining the delay time is given as

$$\tau = c \cdot \exp(-b/T) p^n \quad 1.3$$

where  $\tau$  = ignition delay

$T$  = mixture temperature

$p$  = mixture pressure

$c, b, n$  = empirical constants

The critical concentration being constant for a given fuel air composition a functional relationship between the concentration ratio  $(x)/(x_c)$  and the relative time  $(t/\tau)$  could be assumed. Thus giving

$$d/dt[x/x_c] = \phi(t/\tau) \quad 1.4$$

integrating equation 1.4 over the limits  $t(0)$  to  $t(k)$ ; where  $t(0)$  is the start of combustion and  $t(k)$  is the time knock occurs we get:

$$[x]/[x_c] = \int_{t_0}^{t_k} (1/\tau) dt = 1 \quad 1.5$$

The function  $\phi$  cannot be obtained from ignition delay data, however if it is assumed that the reaction rate does not change with time during a fixed state process then:

$$\phi(t/\tau) = 1/t \quad 1.6$$

and

$$[x/x_c] = \int_{t(0)}^{t(k)} \phi(t/\tau) dt = 1 \quad 1.7$$

Some of the expressions proposed for the delay time are given below.

Rifkin and Walcutt [17] obtained a expression based on rapid compression machine tests, this expression was derived for tests where compression pressures ranged from 7 to 34 Bars. with the corresponding temperature range of 640 to 830 K, and is given as:

$$t = 0.017095 P^{-1.49} \exp(7457/T) \quad 1.6$$

$t$  = induction time in milliseconds

$P$  = Compression pressure in Bars.

$T$  = Compression temperature in K.

Using a continuous flow reactor Burwell and Olson [18] obtained an induction time relation for isooctane-air mixtures. Compression pressures and temperatures were varied over a narrow range, the pressure range being 1.25 to 2.0 Bars, and temperature between 850 and 900 K. The equivalence ratio was varied between 0.5 and 2.2. The induction time was given as:

$$t = 0.916 \cdot 10^{-12} \phi^{-1.04} P^{-2.57} \exp(32400) \quad 1.7$$

where  $\phi$  = equivalence ratio

Though the expression has validity over a range of fuel air mixtures, the pressure and temperature range would limit its application in terms of knock in an engine.

Based on data obtained from experiments conducted in shock tubes and a study of hydrocarbon ignition behind reflected shock waves, Vermeer, et. al [19]. used the pressure rise to define the induction time for iso-octane mixed in stoichiometric proportions with oxygen and argon.

$$t = 10^{-3}(P/(R*T))^{-0.72}\exp(-9.387 + 16319/T) \quad 1.8$$

where R = Universal gas constant

The compression temperatures ranged from 1200 K to 1700 K while compression pressures were varied from 1 to 4 Bars. The high range of temperatures being selected because of a problem of ignition occurring behind the reflected shock waves rather than at the reflecting wall at the lower end of the temperature range used for these experiments.

Douaud and Eyzat [20] used firing engine experiments along with the method proposed by Livengood and Wu [16] to derive an induction time relation for Primary Reference Fuel (PRF) blends based on experimentally determined pressure and calculated temperature histories in a CFR test engine.

Coefficients and exponents for the resulting induction time relation were determined by least squares minimisation of the difference between the Livengood and Wu integrand and unity using knocking engine cycle histories. The relation includes a pre-exponential term that is a power function of the PRF octane number, and is given as:

$$t = 0.01869 (ON/100)^{3.4107} P^{-1.7} \exp (3800/T) \quad 1.9$$

ON = Octane Number

The constants in the above expression were obtained for a constant fuel air equivalence ratio of F=1.1. The equivalence ratio in the present investigation is defined as the ratio of Stoichiometric Air-

Fuel ratio to the Actual Air-Fuel ratio.

$$\text{i.e.} \quad \phi = \frac{(A/F)_{st}}{(A/F)_{actual}} \quad 1.10$$

$$\text{therefore we obtain } \phi = 1/F \quad 1.11$$

The expression given by Douaud and Eyzat[20] for the delay time is for  $\phi = 0.9$ . To overcome the shortcomings of the equation (i.e. no effect of changing air-fuel ratio), Douaud [35] proposed an expression to modify the pre-exponential factor in equation 1.9.

The modified pre-exponential factor  $A_f$  was related to the pre-exponential factor in the original expression (eqn.1.9) as follows:

$$\frac{A_F}{A_{1.1}} - 1 = 0.9625 \left( \frac{F}{1.1} - 1 \right) + 5.445 \left( \frac{F}{1.1} - 1 \right)^2 + 8.32 \left( \frac{F}{1.1} - 1 \right)^3 \quad 1.12$$

$$A_{1.1} = 0.01869$$

The Data of Rifkin and Walcutt [17] were obtained from rapid compression machine tests. Though the pressures considered are closer to those obtained in motored engines they would be much less than those in fired engines, also the temperatures under consideration are much lower. The relation being for stoichiometric air-fuel mixtures, it would be inapplicable where the mixtures used were other than stoichiometric.

The expressions formulated by Burwell and Olson [18] and by Vermeer et. al. [19] have been obtained under specific conditions and therefore limiting their application to specific ranges of temperature, pressure or fuel quality (or type). Of the above expressions the only expression formulated on the basis of data obtained from a fired engine is that of Douaud and Eyzat [20], and considers pressure temperature and Octane number and the modified version [35] also takes into account the air-fuel ratio.

Though the above expressions are valid in a limited way, predicting the ignition delay and thus the occurrence of knock in a spark

ignition engine is a more complex undertaking. Which would require a detailed study of the chemical kinetics and their use in calculating the delay time, thus providing a more realistic reproduction of the autoignition characteristics of hydrocarbons over a complete range of engine conditions as well as fuel types. Halstead et. al. [21] proposed a chemical kinetic model based on the degenerate branched chain mechanism for the simulation of the two stage autoignition characteristics of hydrocarbons. The knock point as predicted by Douaud's model for ignition delay and the Shell model have been compared in chapter III.

Schapertons et. al. [15] proposed a model that was based on data obtained from Sokolik's experiments on bombs. Warnatz [22] proposed a model using elementary reactions occurring in the oxidation of hydrocarbons to describe the mechanism of Propane and Butane oxidation. The data was obtained based on experiments conducted with premixed laminar flames at lean and moderately rich conditions, this mechanism was later extended to the higher alkanes such as iso-octane [23]. Pitz, et. al. [36], considered experimental data from shock tubes, premixed laminar flames and turbulent flow reactors to extend a mechanism proposed by Westbrook and Pitz [37] for the oxidation and pyrolysis of Propane and Propene to describe the oxidation of n-Butane. Cox and Cole [24] proposed a model based on empirical data, and similar to that of Halstead et. al., but taking into consideration individual species rather than three parameters representing groups of species of a kind. Some of the models relevant to oxidation and autoignition of commercial petrol and iso-octane are discussed in the next chapter.

There is evidence in the literature to suggest that apart from the strong chemical kinetic process that contribute to knock, there appears to be a coupling between the pressure fluctuations in the propagating flame front and the onset of knock. It is therefore of interest to review the early research in this area in an attempt to better understand the mechanism of the process involved.

## 1.5. Flame Vibrations

Flame propagation studies in closed and open tubes by Egerton [13] have shown the interaction between combustion waves and flame vibrations. Though the flame propagation in closed vessels and open tubes are quite different due to the level of freedom available to the propagating flame, it is still possible to draw on the results from literature dealing with flame propagation in open vessels.

The presence of shock waves, intense pressure fluctuations and flame and gas vibrations have been noticed at the time and after knock [3,25,26]. Maxwell and Wheeler [3] noticed in explosions with rich mixtures the presence of vibrating flames prior to the occurrence of knock. They also noticed that the pressure fluctuations were synchronous with the flame vibrations and were of the same frequency. Increasing the initial pressure in the combustion bomb increased the amplitude of these vibrations. Using the variations in the pressure to density ratios as a basis for their argument Maxwell and Wheeler suggest that the striations formed in the photographic records of the flames are due to the establishment of stationary longitudinal waves in the gas columns.

In an investigation to study the effect of artificially induced waves on knock, Rothrock and Spencer [25] carried out experiments where they artificially induced shock waves by exploding a copper wire stretched inside an engine. A 2 microfarad condenser charged to 30,000 volts was discharged through a 0.004 inch diameter copper wire to cause an explosion. Knock was found to occur intermittently and the authors did not think that knock was influenced by the shock waves from the exploding wire, though it was found that exploding the wire in the early stages of combustion resulted in the charge knocking while exploding the wire at a later stage of the combustion did not result in knock.

Though shock waves caused by exploding a copper wire may not set up knock Rothrock and Spencer mention a case where every time the wire was exploded behind the flame front knocking combustion was obtained. Thus introducing the possibility that though the vibrations may not actually cause knock, they could possibly trigger a highly volatile and unstable mixture into knock. This could be evidence to collaborate Paymans [26] view that shock waves originating at or behind the flame front may traverse the charge at a velocity greatly in excess of the flame velocity and gain such intensity as to cause autoignition.

Miller and Logan [27] observed vibration prior to knock and studied the effect of TEL on these vibrations. The single cylinder engine used to take the photographs was motored and then a single cycle fired. Careful observation of Fig 1.12 shows the delay in occurrence of knock with increasing amounts of TEL. The flame front vibrations corresponding to the different conditions show an increase in the frequency of the vibrations with increase in the amount of TEL (Fig.1.20). One way of interpreting this data is that the resistance of the end gases to autoignition is increased due to the addition of TEL therefore giving a longer time to observe the preknock burst of vibrations.

## 1.6 Flame Propagation in Closed Vessels

The presence of pre-knock vibrations have been referred to in the previous section. The behaviour of flame travel in open and closed tubes ( i.e. tubes open at one end and closed at the other) and closed vessels is quite relevant to the study of flame instability in spark ignition engines and its effect on the occurrence of knock.

Flame propagation varies according to the freedom offered to the burned products. A mixture which is ignited at the open end of a tube so that the products from the flame can expand without rise of pressure will usually propagate the flame at uniform speed for some distance along the tube towards the closed end; Whereas, in a

mixture which is ignited at a closed end so that the products cannot escape, the pressure rises and the flame accelerates. Flame propagation in constant volume bombs would be entirely different to that under constant pressure conditions.

Flame propagation at top dead centre in a reciprocating engine can be likened to a constant volume combustion case as, the change in volume over a span of 10 to 15 degrees crank angle can be considered negligible over the total volume of the combustion chamber volume.

### 1.7 Types of Vibratory Flames

The development of vibratory flames can be considered to be due to any of the following three factors:

- a. those caused due to the acoustical properties of the vessel.
- b. those caused by regions of pressure difference and,
- c. those resulting from the presence of compression waves.

Each of these types of disturbance may cause the average rate of burning to increase [28]. The formation of these disturbances can be explained as follows:

When an explosive mixture contained in a vessel, open at one end, is ignited at the open end the flame propagating towards the closed end reaches a point where the pressure rise cannot dissipate towards the atmosphere. At this point the flame may either a) If it were a fast burning medium accelerate continuously, or, vibrate and surge backwards and forwards with variable but generally increasing amplitude, or b) in the case of a slow burning mixture those variations may not occur, but, the flame envelope itself may vibrate by continual alteration of form like a flexible diaphragm. These movements have been shown to be influenced by the acoustical properties of the tube. Frazer [28] quotes the work of Mason and Wheeler, where they found these movements to be caused as a direct result of the resonance of the column of gas lying between the flame

front and the close end of the tube. The frequency of the vibrations were found to agree closely with the frequency calculated for organ pipes of the same dimensions as the portion of the tube remaining ahead of the flame front.

Working on the proposals of Khitrin, that, the development of the oscillations in closed vessels may be compared to those observed in open-closed tubes, Leyer and Mason [29] showed that the vibratory phenomenon of flame propagation in open-closed tubes are similar to those in closed vessels.

An interesting feature of the pressure records and flame motion pictures of Leyer and Mason [29] was the closeness of the frequency of pressure oscillations following the first contact between the flame and the wall and the fundamental frequency of the longitudinal acoustic mode of the vessel. The fundamental frequency being calculated with different mean sound velocities for the burned and the unburned gases.

### 1.8 Interaction of Compression Waves with Flame Front

Egerton [13] has shown in experiments with open-closed tubes that flame instability could set up compression waves. Based on the work of Bone et. al. [30] it was suggested that compression waves set up by the flame itself brings about conditions in which detonation may occur.

Kogarko and Ryzhkov [31] show that the compression waves passing through the flame front amplify and consider this to be due to an increase in the speed of energy emission in the chemical reaction zone of the flames during the time that the flame is located within the wave. Though not all conditions were conducive to the amplification of the compression waves, it was in rich mixtures and at initial pressures greater than 2 Bars that the compression waves showed marked amplification.

## 1.9 Overview of the Literature Survey

From the results of Rothrock and Spencer [25] and Miller and Logan [27] it is seen that vibrations set up in the combustion chamber tend to trigger knock. Kogarko and Ryzhkov's [31] work opens further avenues with respect to the interaction of compression waves with the flame front and its reaction on the unburned gases. Increasing the temperature and density of the combustion zone during the relaxation period (i.e. the period when the combustion wave retracts and the combustion zone expands) of a combustion wave would effect the unburned zone by heat transfer and molecular diffusion.

The Mathematical analysis [15 to 24] of autoignition takes into account only the chemistry or the physics of the situation. The possibility of an interaction between the acoustic properties of the combustion chamber and the chemical kinetics of the autoignition phenomenon have been totally ignored.

Of the available kinetic models for the simulation of autoignition of the end gases, the model proposed by Halstead et. al. [21] has been well proven by various authors [24,32,33]. The aim of this investigation is to incorporate this model into an existing combustion model and test its application with experimental data, also the global scheme proposed by Livengood and Wu [16] to obtain the knock point by integrating the reciprocal of the ignition delay time is incorporated into the combustion model with Douaud's [35] expression for the delay time. The results from both models are compared with each other and with experimental data in chapter III.

A model for relaxation oscillation of the gas column in a ramjet combustor is considered for application to the engine combustion chamber. The system of burned gases, flame front and unburned gases is considered as lumped system rather than as individual zones.

Development of a model demands the further objective of validating the results. Spectral Analysis is used for studying the flame vibrations in the signal obtained by the use of flame ionisation probes.

Table 1.1

EMPIRICAL EQUATIONS FOR  $\tau_1$  AND  $\tau_2$  (RÜGENER)<sup>a</sup>

$n$ -heptane	$\left\{ \begin{array}{l} \tau_1 = 8.1 \times 10^{-12} \times p^{-0.66} \times e^{15,100/T} \\ \tau_2 = 0.5 \times p^{-1.82} \times e^{-1,400/T} \end{array} \right.$
$n$ -pentane	$\left\{ \begin{array}{l} \tau_1 = 2.7 \times 10^{-9} \times p^{-0.69} \times e^{11,600/T} \\ \tau_2 = 4.5 \times p^{-1.54} \times e^{-3,030/T} \end{array} \right.$
$n$ -butane	$\left\{ \begin{array}{l} \tau_1 = 5.8 \times 10^{-6} \times p^{-1.35} \times e^{8,330/T} \\ \tau_2 = 2.35 \times 10^4 \times p^{-2.96} \times e^{-5,220/T} \end{array} \right.$

Stoichiometric mixtures of Fuel in air  
 $\tau$  is in seconds;  $p$  and  $T$  are pressure in atms.,  
 and temperature in  $^{\circ}$  K at the end of compression  
 and before occurrence of appreciable chemical reaction

Table 1.2

## INCREASE OF PRESSURE DURING REACTION OF PENTANE AND OXYGEN

Seconds	0	8	8.2	8.4	8.6	8.8	9.0	9.2	9.21
$\Delta p$ , mm. Hg	0	0	2	35	48	52	54	57	explosion

( Ref. 10 )

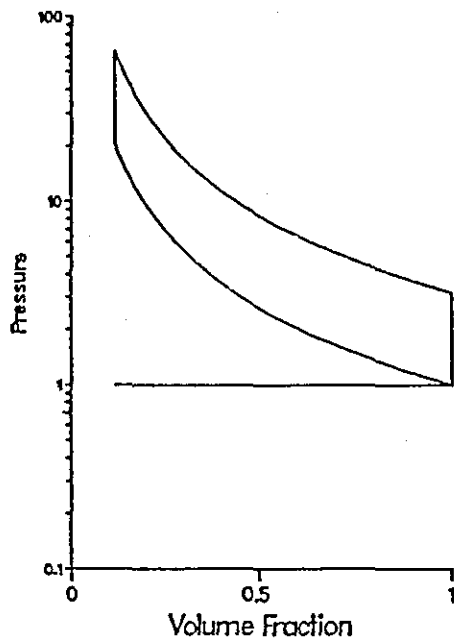


Fig. 1.1 Ideal Otto Cycle

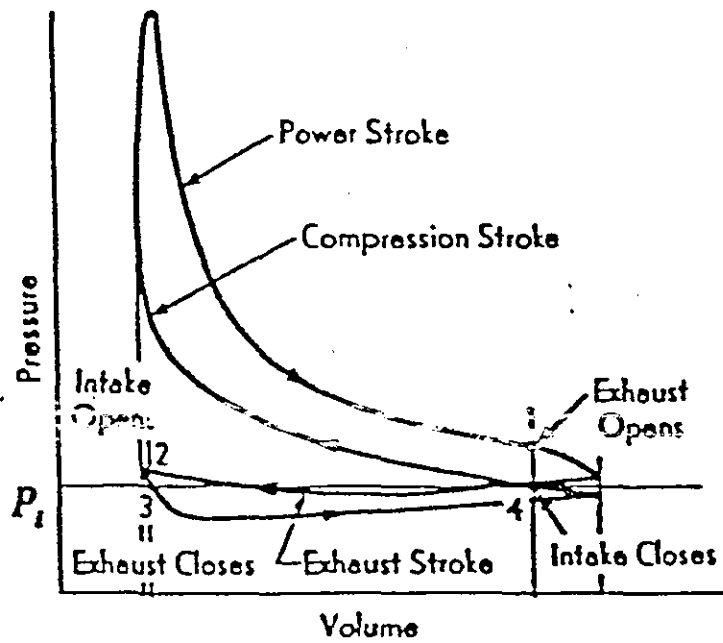


Fig 1.2 Experimental Otto Cycle

( Ref. 81)

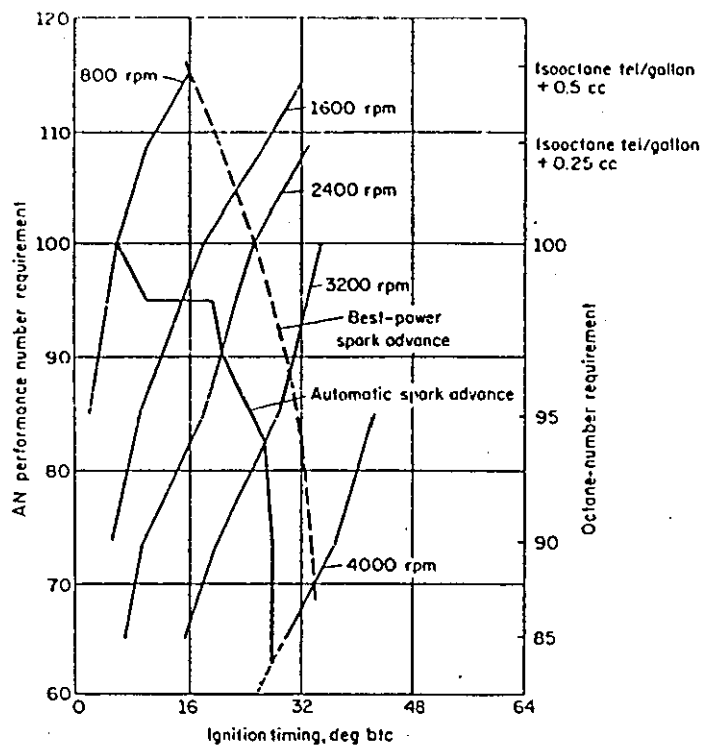


Fig.1.3 Variation of Performance Number Requirement with Spark Timing and Engine Speed (ref 7)

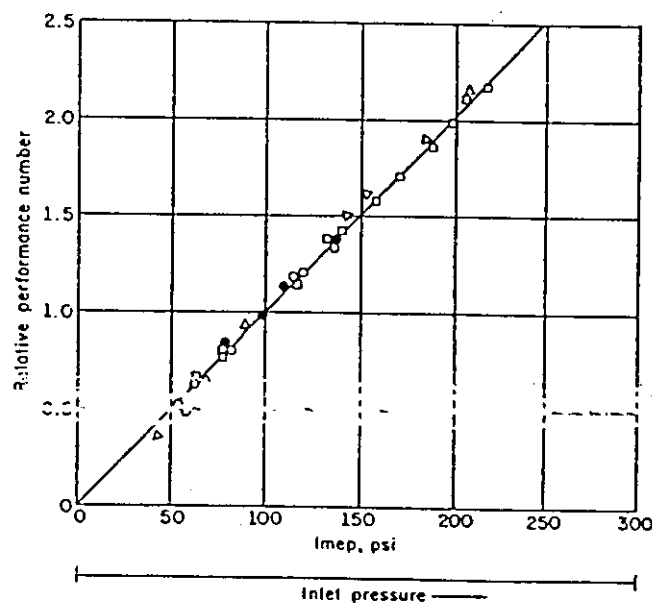


Fig.1.4 Variation of Relative Performance Number with Inlet Pressure (ref 7)

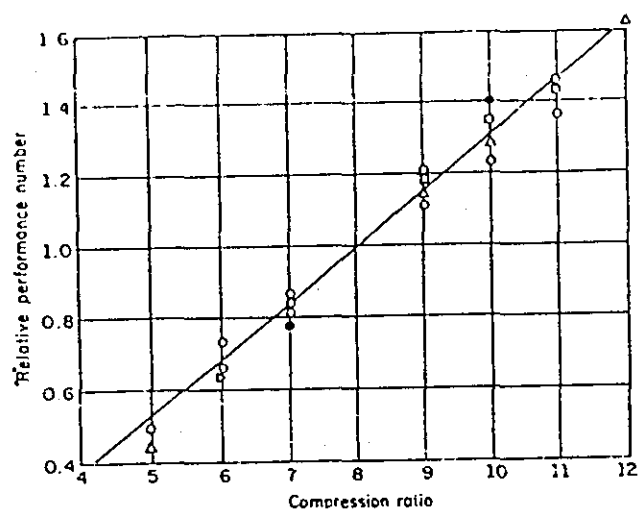


Fig.1.5 Variation of Relative Performance Number with Compression Ratio (ref 7)

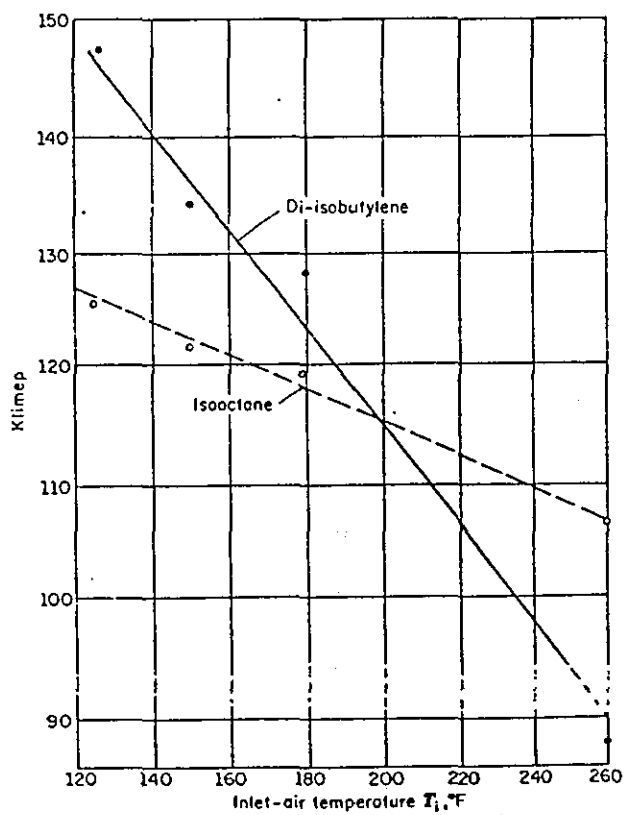


Fig.1.6 Variation of KLIMEP with Inlet Air Temperature (ref 7)

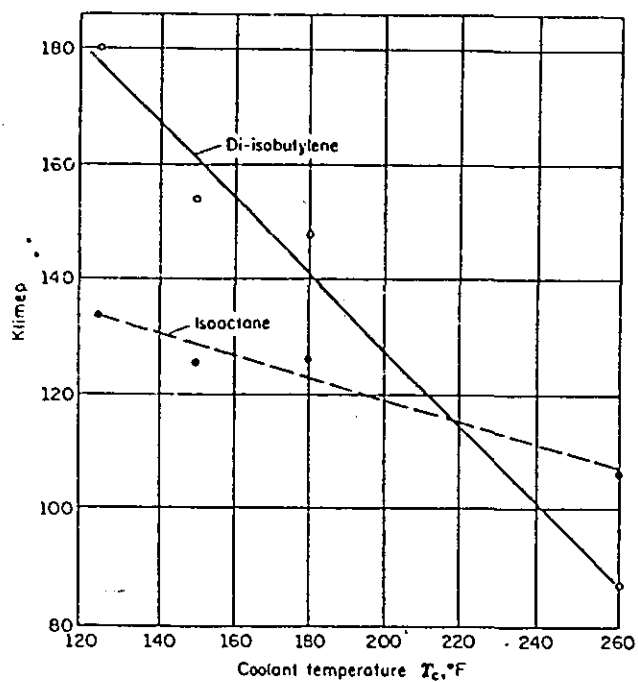


Fig.1.7 Variation KLIMEP with Coolant Temperature (ref 7)

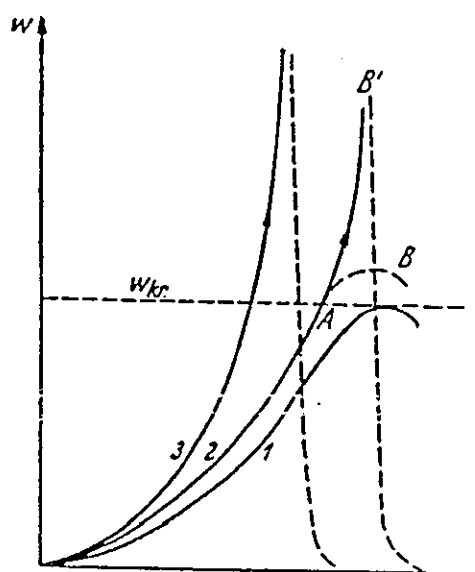


Fig.1.8 Time Variation of Reaction Velocities (ref 8)

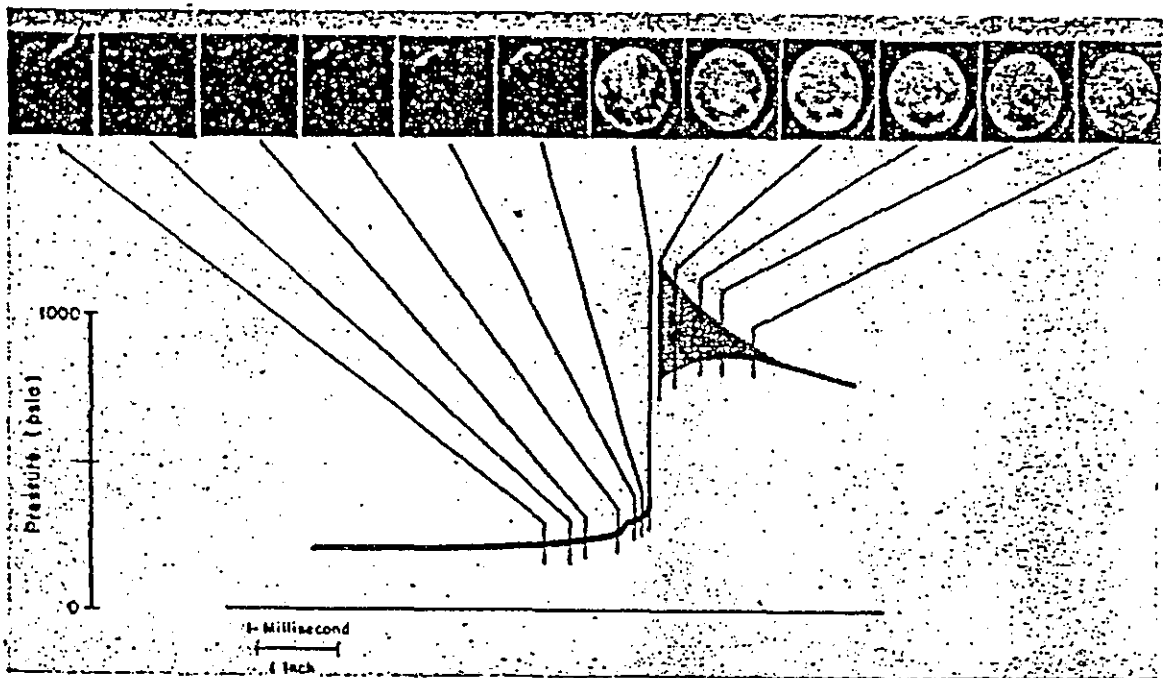


Fig.1.9 Photographs of luminosity within the combustion chamber corresponding to indicated points on the pressure-time record  
 Fuel — n-heptane, Fuel-Air Ratio = 0.066, Compression Ratio = 8.3  
 atmospheric pressure and 150F. before compression  
 Start of pressure record corresponds to instant of completion of compression stroke

( Ref. 10 )

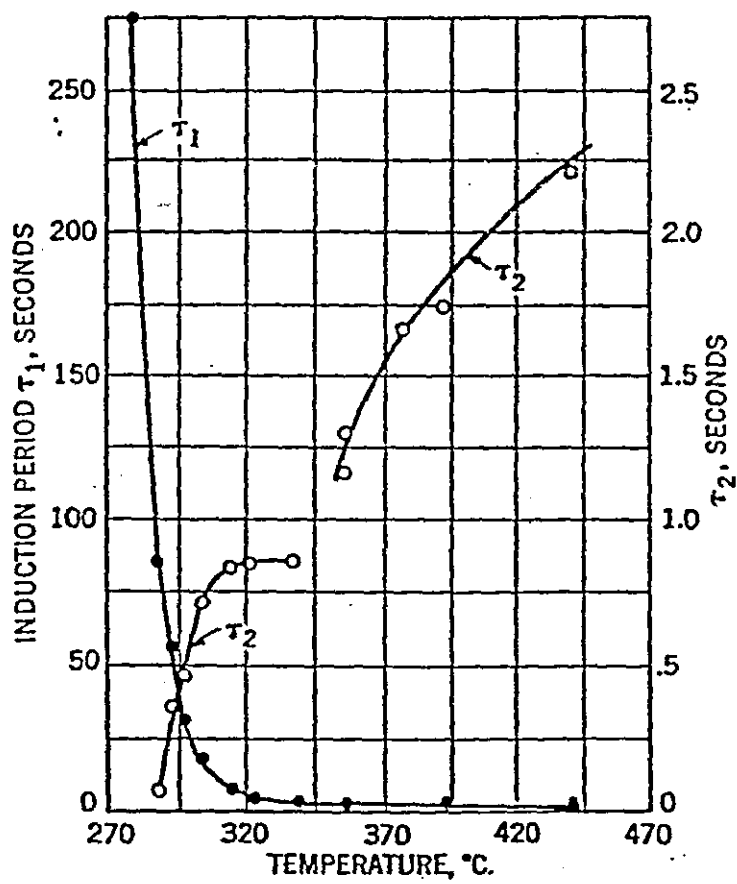


Fig.110 Induction periods  $\tau_1$  and  $\tau_2$   
 For  $C_4H_{10} + O_2$  at 380 mm Hg.  
 ( Ref. 10 )

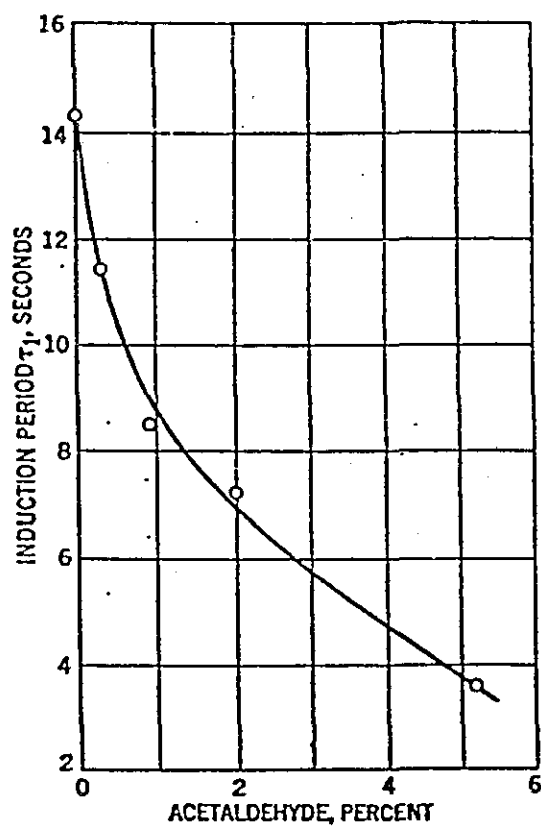


Fig.1-11 Effect of addition of acetaldehyde on induction period  $\tau_1$  of  $C_5H_{12} + 2O_2$  at 200 mm.Hg and  $329^\circ C$   
( Ref. 10 )

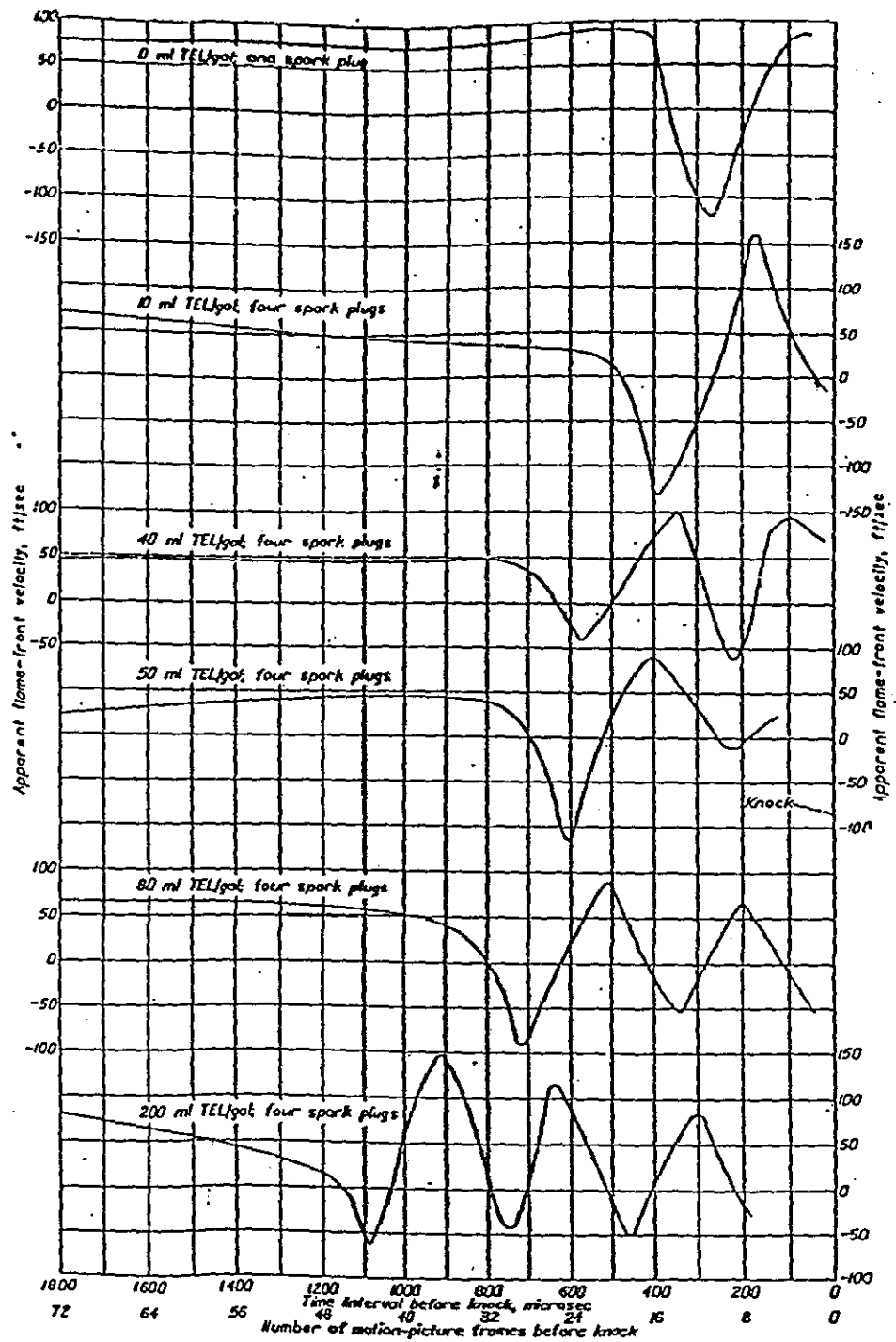


Fig. 1.12 Apparent upper flame front velocities in an engine cylinder as affected by preknock explosive  
( Ref. 27 )

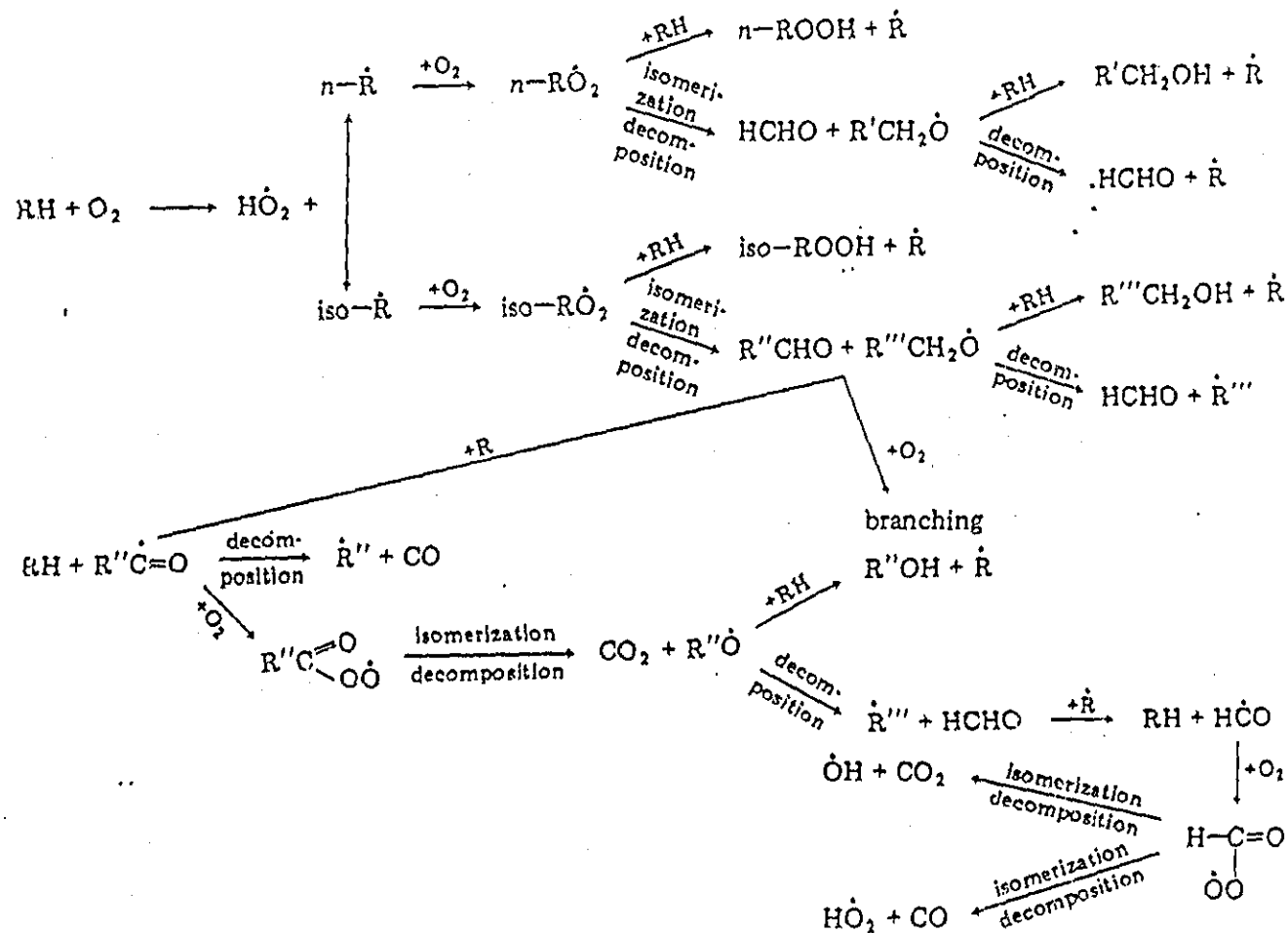


Fig. 1.13 Scheme for Autoignition of Hydrocarbons

( Ref. 34 )



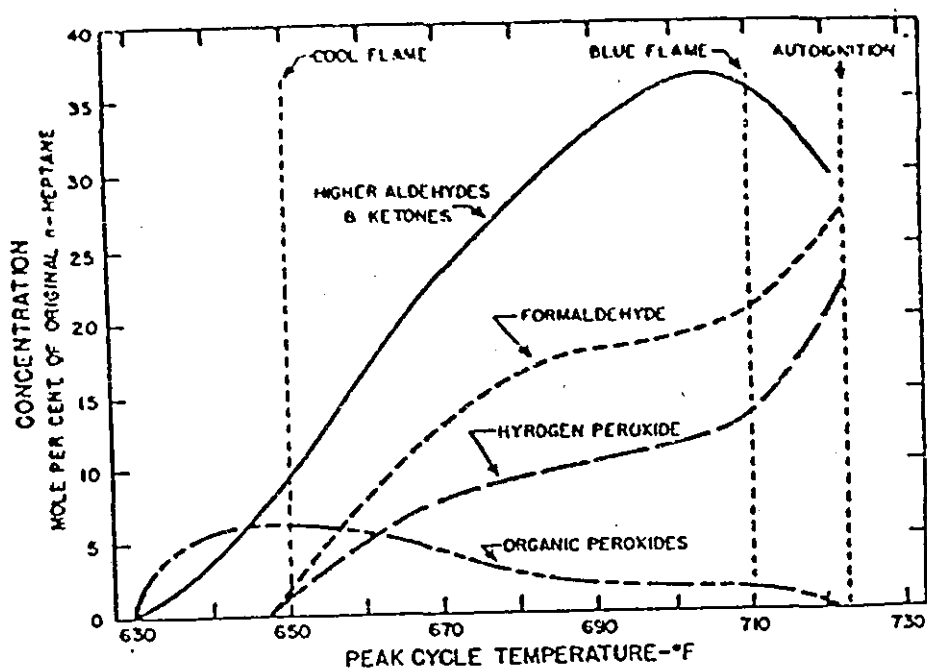


Fig.1.16 Effect of Blue Flame on Exhaust-Gas Composition, n-heptane( Ref. 12 )

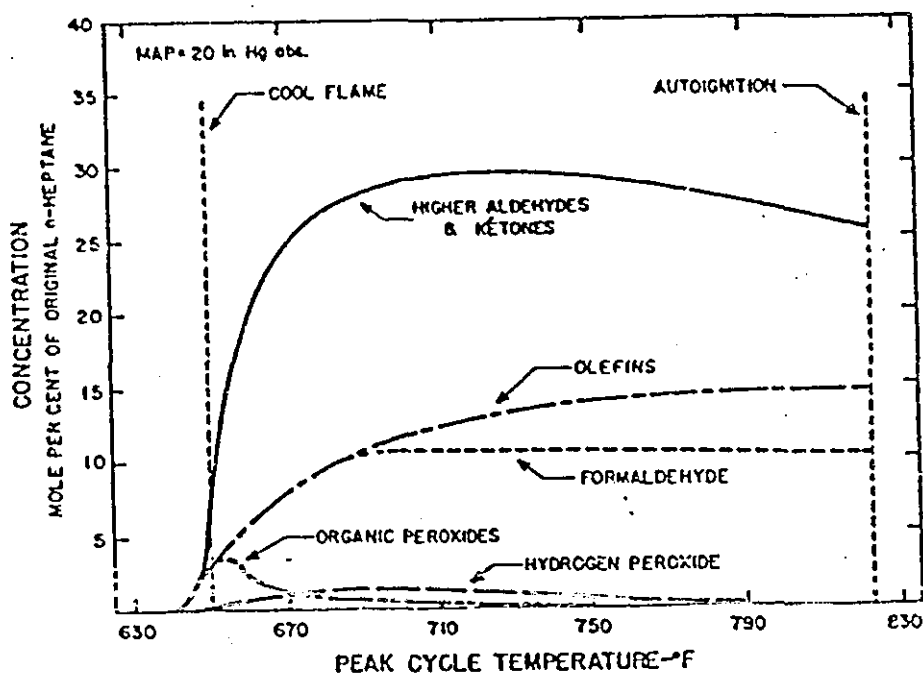


Fig. 1.17 Exhaust GAs Composition, n-heptane + 3 ml TEL per Gallon (Ref. 12)

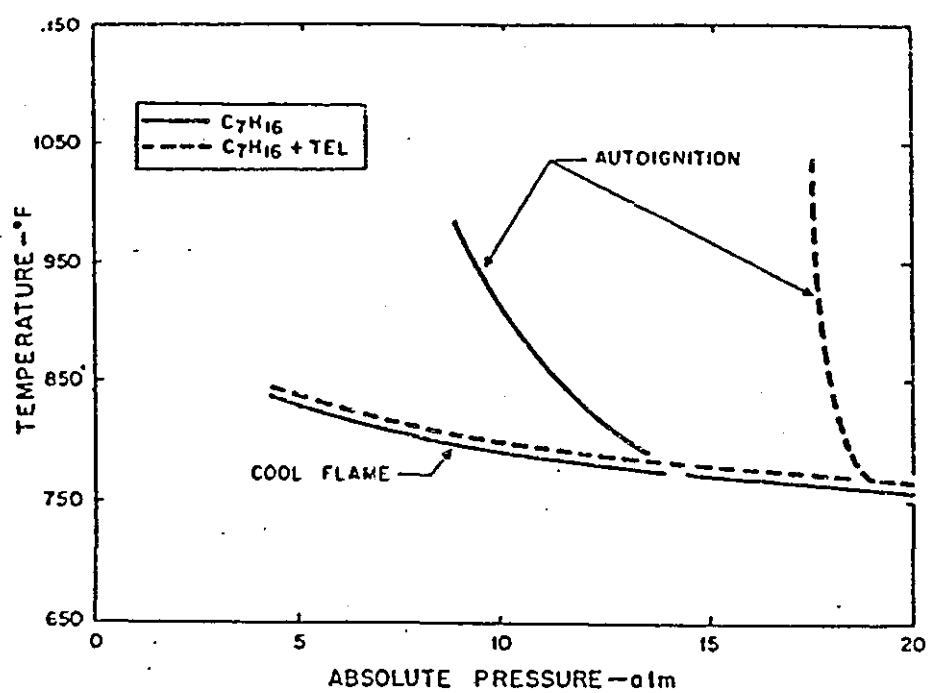


Fig. 1.18 Effect of TEL on ignition limits of n-heptane  
( Ref. 12 )

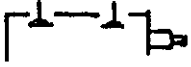
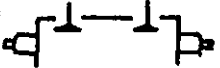





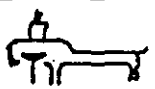



	Type of Combustion Chamber	Remarks
(a)		Slight tendency to Detonate
(b)		Slight tendency to Detonate
(c)		No Detonation under any circumstances
(d)		Slight tendency to Detonate
(e)		Slight tendency to Detonate
(f)		Excessive Detonation only with Benzol
(g)		Severe Detonation
(h)		Very little Detonation
(i)		Severe Detonation
(j)		No Detonation
(k)		Severe Detonation

Fig. 1.19 Combustion Chamber Shapes Tested by Ricardo  
( Ref. 2 )

Note: The term detonate is used by Ricardo to imply Knock

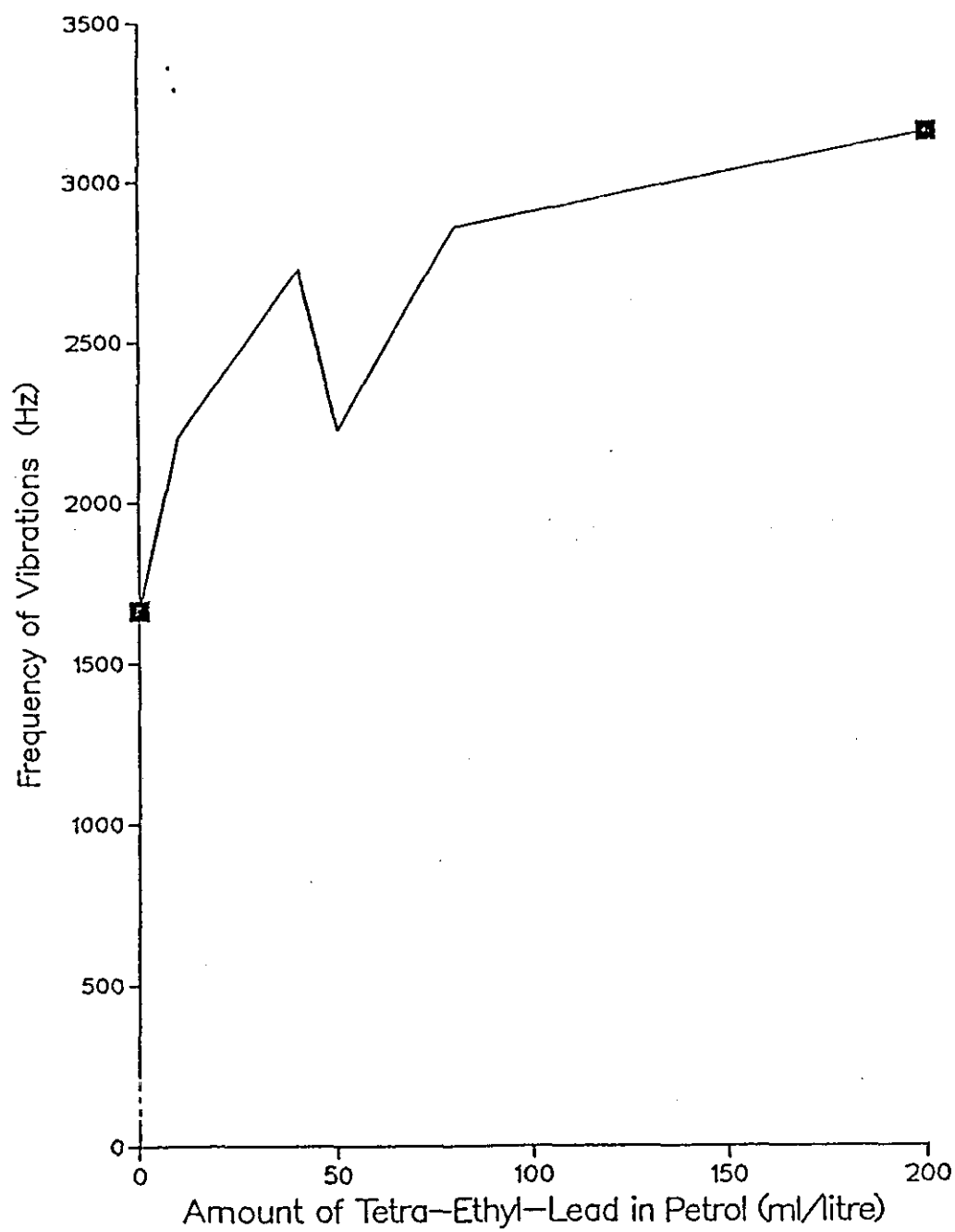


Fig. 1.20 Variation of Frequency of Gas Vibrations with amount of TEL, Frequency Calculated from Fig. 1.12

## CHAPTER II

### REVIEW OF KNOCK MODELS

#### 2.1 Introduction

Phenomenological knock modelling mainly consists of predicting the auto-ignition delay time of the end gases in the combustion chamber. Simple models based on empirical relationships for the ignition delay with respect to pressure, temperature, equivalence ratio and fuel octane number have been proposed assuming a global kinetic reaction to describe the auto-ignition mechanism [17 to 20]. These models treat knock more as an explosion rather than a two-stage ignition.

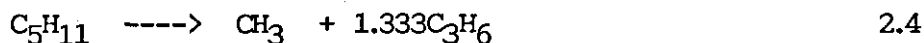
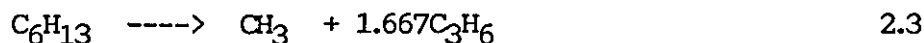
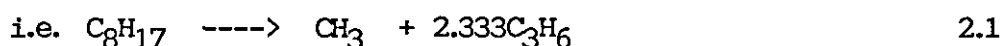
Empirical formulae for induction periods or reaction rates are incompatible with the essential nature of the autoignition of more complex hydrocarbons. Hydrocarbon autoignition is a degenerating branched chain reaction, whose rate depends on the accumulation of branching agents and therefore on the history of the reaction as well as the instantaneous state of the system. Also the development of the reaction is critically dependent on the coupling between the chemical-kinetics of the reaction and the physical state (i.e. temperature and pressure) of the system as, the reaction rate is dependent on the temperature of the system and also, the concentration of different species produced during the reaction, while the heat released by the preflame reactions effects the temperature and therefore the pressure and density of the end gas during the induction period.

As the number of carbon atoms in a hydrocarbon increases so does the complexity of its combustion reactions. During the oxidation of any hydrocarbon it is known that hydrocarbons with large number of carbon atoms decompose to form radicals with lesser number of carbon atoms and these inturn would either react or further decompose to finally form carbon dioxide and water.

Scarcity of reaction rates for the oxidation of higher hydrocarbons such as isooctane has curtailed the development of kinetic models based on first principles of the chemical reactions.

Starting from first principles Warnatz [22] has shown the complexity of hydrocarbon oxidation. Just considering Propane and Butane the number of reactions involved in the formation and consumption of various intermediates add up to One Hundred and twentythree. From this work on high temperature combustion of Propane and Butane, Warnatz has also shown that the alkyl radical formed in the initial reaction is decomposed to smaller alkyl radicals by elimination of alkenes.

Since the detailed mechanisms for the reactions of saturated hydrocarbons (alkanes), its radicals (alkyl) or unsaturated compounds (alkenes) is very scarce and highly unreliable, Warnatz [23] considered the attack on the higher alkanes by H, O and OH radicals forming alkyl radicals. As the alkyl radical decomposition by alkene elimination and subsequent alkene oxidation are not a rate-limiting processes, the complex alkyl radical decomposition reactions are replaced by a simple reaction path leading to only one small alkyl radical and only one small alkene. The simple decomposition reactions used by Warnatz are given below.



For Hydrocarbons above butane Warnatz considers a representative mechanism which includes the simple decomposition to alkyl radicals and alkenes with 3 or less carbon atoms and detailed reactions for the C1/C2/C3-hydrocarbon oxidation mechanism.

Esser et. al. [38] used the model developed by Warnatz [22] and simulated knock in an engine run on n-Butane. This model was extended to simulate knock with iso-octane using the simple mechanism for the decomposition of the higher radicals to hydrocarbons with 3 or less carbon atoms. The delay time for end gases in an engine were calculated with the temperature and pressure being obtained from experiments. Though the results obtained for n-Butane were found comparable with experimental data for 81 RON PRF the predicted knock point was 10 degrees after the experimental value (Fig. 2.8).

Westbrook and Pitz [37] developed a scheme based on the elementary reactions occurring in hydrocarbon combustion. This scheme is similar to that proposed by Warnatz [22,23] but considers experimental data from premixed laminar flames, shock tubes and turbulent flow reactors as against data from laminar flames of Warnatz. The mechanism proposed by Westbrook and Pitz was for Propane and Propene but was later extended by Pitz et. al. [36] to consider n-Butane. This mechanism consisted of 248 elementary reactions taking into account 47 different species. The models proposed by Warnatz [22,23] and Pitz, et. al. [37] only consider oxidation of hydrocarbons up to n-Butane, extending it further even to iso-Butane is complicated.

The global schemes for defining the ignition delay are expressed as a single differential equation while the kinetic model of Shell [41] describes the autoignition phenomenon by 5 differential equations, the model of Cox and Cole [24] requires the description of 15 equations. The models proposed by Warnatz et. al. [22] and Pitz et. al. [36] require the description of 123 and 248 reactions respectively.

Introduction of any knock model into a phenomenological requires the solution of the differential equations assuming the unburned gas as a single unit. Introducing the ignition delay model of Douaud's into the combustion model called "copred.fortran" does not effect the computation time appreciably but introducing the Shell model

increases the computation time from 64 seconds to 147 seconds on the Honeywell Multics computer. The computing time required for integrating a set of differential equations increases with the number of equations. Introduction of either of the models based on the first principles of hydrocarbon oxidation would increase the computation time phenomenally.

In multi-dimensional models the kinetic scheme would have to be solved at every node, and depending on the complexity of the mesh chosen the number of nodes increases and so will the computational time. The accuracy of the results obtained by Warnatz (Fig. 2.8) does not warrant the use of complex and time consuming knock models in phenomenological models.

The computing time being a major constraint, kinetic models with smaller number of equations, though developed on empirical basis, were considered suitable for testing and inclusion into an existing combustion model.

## 2.2 Requirements of a Knock Model.

Any model describing the autoignition of a hydrocarbon whose oxidation occurs in two stages with the cool flames occurring in the intermediate stage (Fig. 2.4) should be capable of simulating the following features [21]:

- a. Sharp, well defined two stage ignition on a millisecond time scale, with first and second stage induction periods in the range 0 - 30 ms {Fig. 2.4 (a)};
- b.  $\Delta T$ , the temperature rise during the cool flame ranging up to 200K; during the pulse the rate of temperature rise being typically  $10^5$  K/s.
- c. rapid and, under many conditions, complete quenching of the cool

flame yielding close to zero temperature rise during an extended period prior to the onset of ignition;

- d. rapid acceleration of the reaction rate after the onset of ignition;
- e. a transition from two stage to single stage ignition with increasing temperature { Fig. 2.4(b)};
- f. a region of 'negative temperature coefficient' to the overall induction period. ( a region of negative temperature coefficient for a reaction being that region where the reaction rate decreases with increase in temperature rather than increase as is usually the case ).

In addition, the model must ultimately be capable of reproducing the variation with concentration and composition of the lengths of the induction periods  $\tau_1$  and  $\tau_2$ .

### 2.3 Selection of Kinetic Models

The kinetics of chemical reactions leading to auto-ignition, even in simple pure hydrocarbons is complex [39]. Based on empirical considerations Halstead et. al. [21] of Shell Research Centre (for convenience this model will be referred to as the "Shell Model") first proposed a model that grouped the different species formed during the oxidation of hydrocarbons into three groups depending on their nature, namely Radicals, Branching agents and Quenching agents. In this mechanism it is assumed that the reaction chain may be propagated by any number of radical reactions, but that each propagation step shows a first order dependence on the radical involved. The model is further simplified by assuming that the radical concentrations are in a steady-state relation to each other, that is , in any one cycle the rate of the individual propagation steps are equal.

Schapertons et. al. [15] assumed a simple scheme which consists of 5 consecutive reactions to describe the autoignition process. This model assumed the formation of Radicals, Peroxides and aldehydes in series as the first stage of ignition. The conversion of Aldehydes to the final products was assumed to be through intermediate products which are usually acids and ketones [40].

The third model considered is one proposed by Cox and Cole [24] of Harwell Research Centre (this model will be referred to as the "Harwell Model"), which is based in principle on the degenerating branched chain mechanism of the model proposed by Halstead et. al. [21] but takes into account the isomerisation of  $RO_2$  (i.e alkylperoxy radical) and the formation and decomposition of Hydrogen peroxide. Individual species have been defined rather than the use of global parameters.

#### 2.4 The Model due to Halstead et. al.

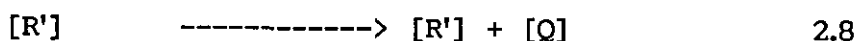
In the model proposed by Halstead et. al. [21] autoignition of hydrocarbons is described by a thermokinetic free radical chain mechanism in which the time evolution of the radical concentration and hence the rate of oxidation of the fuel is controlled by a degenerate branching agent. In this model, fuel molecules  $[RH]$  are oxidised in a chain process, propagated by radical  $[R]$ , with accompanying heat release. The chain is initiated by a slow reaction between fuel and oxygen, and the reaction rate accelerates due to formation of a degenerate branching agent,  $[B]$ , in a small fraction of the propagation steps. Both linear and quadratic termination reactions involving  $[R]$  are required to describe the first stage (cool flame) ignition. The second stage "hot" ignition is caused by the formation of an intermediate,  $[Q]$ , which provides a secondary source of branching agents at the higher temperature following the cool flame. Chemical heat release is based on an assumed overall reaction stoichiometry, and heat loss from the gas is treated in a simple convective model.

The key reactions used by the Shell model and which are considered to be the minimum required for a chain branching mechanism are as follows:

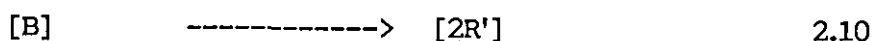
#### Initiation



#### Propagation



#### Branching



#### Linear Termination



#### Quadratic Termination



This scheme is based upon the "steady state approximation" which assumes that all propagation -chain radicals always exist in the same relative concentrations. They are not, therefore, treated individually, but as their cumulative concentration  $[R']$ . In addition to the radicals the scheme involves the fuel  $[RH]$ , oxidant  $[O_2]$ , products  $P$ , Branching agents  $[B]$  and the intermediate product  $[Q]$ .  $[Q]$  was introduced to assure a rapid chain acceleration at the second stage of ignition.

The rate coefficients and the factor for the propagation reactions are expressed in the Arrhenius form.

$$k = Ae^{(-\frac{E}{RT})}$$

## 2.5 The Mathematical Scheme of the Knock Model

The mathematical equations defining the generalised auto-ignition mechanism due to Halstead et. al. [41] are as follows :

$$1/V^* \{dnR/dt\} = 2\{Kq[RH][O_2] + Kb[B] - Kt[R][R] - f3Kp[R] \} \quad \text{--} \quad 2.13$$

$$1/V^* \{dnB/dt\} = f1*Kp[R] + f2*Kp[Q][R] - Kb[B] \quad \text{--} \quad 2.14$$

$$1/V^* \{dnQ/dt\} = f4*Kp[R] - f2*Kp[Q][R] \quad \text{--} \quad 2.15$$

$$1/V^* \{dnO_2/dt\} = -pKp[R] \quad \text{--} \quad 2.16$$

$$dT/dt = 1/cv/ntot * Qk - Ql - ntot/V^* R^* T^* dV/dt \quad \text{--} \quad 2.17$$

$$nRH = (nO_2 - nO_2(t=0))/(p^*m) + nRH(t=0) \quad \text{--} \quad 2.18$$

Where V = Instantaneous Volume

nR = number of moles of Radicals

nB = number of moles of Branching Agents

nQ = number of moles of Quenching Agents

nO<sub>2</sub> = number of moles of Oxygen

nRH = number of moles of Fuel

[RH] = Concentration of Fuel (moles/cc)

[O<sub>2</sub>] = Concentration of Oxygen (moles/cc)

[R] = Concentration of Radicals (moles/cc)

[B] = Concentration of Branching Agents (moles/cc)

[Q] = Concentration of Quenching Agents (moles/cc)

T = Temperature (K)

t = Time (Seconds)

K<sub>p</sub> defines the chain propagation rate as a function of the total Radical concentration.

K<sub>q</sub> is the quenching rate coefficient

K<sub>b</sub> is the branching rate coefficient

K<sub>t</sub> is the termination rate coefficient

The terms f<sub>1</sub>, f<sub>3</sub>, f<sub>4</sub> are defined as the ratio of the rate of formation of Branching Agents, rate of Linear termination, and the rate of formation of Q with respect to the linear main propagation rate respectively. m is the number of carbon atoms plus 1.

$$p = [n(2-z)+m]/2m$$

C<sub>v</sub> is the specific heat of the unburned gas at constant volume.

n<sub>tot</sub> is the total number of moles in the charge.

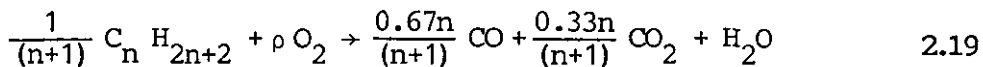
$$Q_k = K_p \cdot q \cdot V[R]$$

q is the exothermicity of the fuel molecule

Q<sub>l</sub> - Heat loss

Equations (2.13) to (2.16) give the molar concentrations of the Radicals, Branching Agents, Quenching Agents and Oxygen. Equation (2.17) is the energy balance equation giving the rate of temperature rise. Equation (2.18) balances the Oxygen and fuel concentrations after each step.

Fuel consumption is assumed to occur at a rate of a single (-CH<sub>2</sub>-) entity for each propagation cycle. Thus on each occurrence of the reaction OH + RH ( C<sub>n</sub>H<sub>2n+2</sub>) only a fraction 1/(n+1) of the RH molecule is removed. The number of moles of oxygen consumed per propagation cycle is defined from the assumed overall reaction stoichiometry



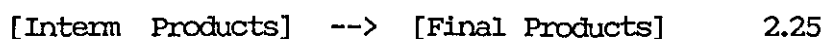
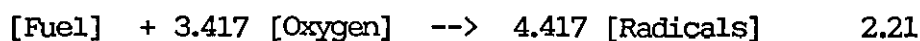
The heat release rate is calculated from the reaction rate, the stoichiometry and the exothermicity of the propagation cycle. The rate of temperature rise in the system is given by the energy balance equation (2.17) with terms for the chemical heat release,  $Q_k$ , and the rate of heat loss,  $Q_l$ , expressed in Seminov form.

$$\text{i.e. } Q_l = a (T - T_w) \quad 2.20$$

where 'a' is the heat transfer coefficient and  $(T - T_w)$  the temperature difference between the gas and the surrounding walls.

## 2.6 Preliminary Model of Schapertons et. al.

Based on the the measured autoignition data in a constant volume cylinder of Sokoliks , Shapertons et. al. [15] proposed a model for the autoignition of iso-octane. This model comprised of five chemical reactions. The reactions being expressed as follows:



The authors [15] assume that most of the chemical energy is released in the last reaction.

The authors assume that only formaldehyde is formed by the oxidation of alcohol. Benson [40] has shown that the production of Aldehydes is through an intermediate stage of producing alcohols and ketones. In this cycle the peroxides decompose to form alcohols and

aldehydes. The alcohols further oxidise to give formaldehyde and a lower alcohol till finally water is obtained. The formation as well as the oxidation of aldehyde is a very rapid process. Though Schapertons et. al. [15] have not defined the intermediate products Benson [40] has shown that the final stages of formation of carbon dioxide and water from aldehydes is through the production of acids.

Following [15] the kinetic Scheme for the auto-ignition of Iso-octane can be written as follows :

$$\begin{aligned}
 d[R]/dt &= 8.0e05*[F] \exp(-8000/T) & 2.26 \\
 d[Per]/dt &= 1.0e09*[R]*[R]*(1+500[Per]/[R])\exp(-8000/T) & 2.27 \\
 d[Ald]/dt &= 6.0e11*[Per]*[Per]\exp(-8000/T) & 2.28 \\
 d[P1]/dt &= 3.0e06*[Ald]*[Ald] & 2.29 \\
 d[PF]/dt &= 3.0e12*[P1]\exp(15100/T) & 2.30
 \end{aligned}$$

where [F] = Fuel Concentration

[R] = Radical Concentration.

[Ald] = Aldehyde (mainly formaldehyde) Concentration

[P1] = Intermediate Product Concentration.

[PF] = Final Product Concentration.

The above kinetic scheme would be termed a series reaction as the concentration of any product is dependent only on the concentration of the product of the earlier stage or its own concentration. The intermediate products being acids [40]. As this mechanism does not take into account degenerate branching the autoignition simulation is more like an explosion rather than like a Branching process and two stage ignition.

## 2.7 Model due to Cox and Cole

The model proposed by Cox and Cole [24] embodies the essential features proposed by Halstead et. al. [21] to simulate two stage ignition but also expands the chemical scheme to take into account the available information from the kinetic and mechanistic data base relating to hydrocarbon oxidation at intermediate temperatures.

The Chemical scheme followed takes into account 15 reactions to define the oxidation process instead of 8 as in the Shell Model and has 10 species as compared to 3 generalised parameters in the Shell model.

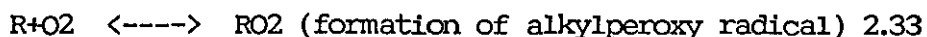
The chemical scheme considered is as follows :

Initiation :

The initiation of the chain reaction, which is in effect the same as that in the Shell model, is assumed to occur homogeneously by reaction of a fuel molecule with O<sub>2</sub> and expressed as follows:



The propagation sequence involves the reaction of an OH radical with a fuel molecule or one of the intermediate products ( all designated as RH) to give an alkyl radical, which adds O<sub>2</sub> to form an alkylperoxide radical, RO<sub>2</sub>: and are represented as



This scheme takes into account the isomerisation of the alkylperoxy radical by internal H - abstraction and is shown as



## The Formation and Decomposition of Branching Agent.

The formation of the Branching Agent is by Cleavage and internal rearrangement of a hydroperoxyalkylperoxy radical formed by reversible addition of O<sub>2</sub> to ROOH radical and is expressed as



Benson [40] considers this internal isomerisation-branching mechanism of long chain hydrocarbons to be the cause of their high susceptibility to knock.

## Formation and Reaction of Intermediate, Q

As in the Shell model, the description of the sharp second stage ignition is by the participation of a secondary source of branching agent via an intermediate product Q. (referred to as a Quenching agent). Aldehydes which are formed as products of the cool flame chemistry contain H atoms which are more readily abstractable than in the fuel molecule thus inducing the reaction to reach a level whereby it would cause an explosion.

## The Termination Reactions :

Adequate description of the cool flame characteristics is obtained by introducing both linear and quadratic chain termination just as in the Shell model.

## Formation and removal of Hydrogen Peroxide

The formation and removal of hydrogen peroxide is considered to play a major role in promoting hot (second stage) ignition, this is in contradiction to Halstead et. al. [41] finding that a mechanism involving branching due to hydrogen peroxide was incompatible with their diagnosis of two stage ignition at high pressure. The complete set of reactions and the rate constants used in this model are given

in table (2.1).

Though the model gave more information as to the influence of fuel structure, comparison with experimental data did not improve.

## 2.8 Selection of Model for Incorporation in Combustion Model

From previous sections it is seen that the Shell model and Harwell model are capable of simulating the two stage ignition. The Shell model has been analysed and tested by various researchers [24,32,33] including the authors of the Harwell model [24] and it has been recommended as a model that fulfills the requirement of having a few but essential steps to simulate the auto-ignition of hydrocarbons. Cox and Cole [24] found that their model gave most satisfactory results when using the same parameters as used by Halstead et. al. [41]. In a review of different knock models By et. al. [39] have also recommended the Shell model where a kinetic model is preferred but have also suggested further development and testing of the model proposed by Douaud and Eyzat [20] which is considered to be very promising.

## 2.9 Solution Technique

Equations (2.13) to (2.17) in section 2.5 are differential equations which have large differences in their time constants. The time constant being the term that defines the rate of decay. Considering for example, the equation  $y' = \lambda y$  has the solution  $Ce^{\lambda t}$ . If  $\lambda$  is negative, then  $y$  decays by a factor of  $e^{-1}$  in time  $-1/\lambda$ . This is the time constant. The more negative  $\lambda$ , the shorter the time constant. When the time constants for a set of equations have a very large difference then the equations are considered to be stiff. The fast reactions in any set of reactions control the stability of the method used. To solve a set of stiff equations it is necessary to use an integrating technique that incorporates variable time steps and variable orders.

To integrate the set of equations (2.13) to (2.17) a package available on the main frame computer was used. This routine uses Gear's method to integrate a set of ordinary first order differential equations over a step of length H, where H is specified by the user, but is controlled by the subroutine to control the estimated error within a specified tolerance. Gear's method of integration has an inbuilt automatic control of step size and order. The routine uses a multi-step predictor corrector method (Adams Moulton) whose order is automatically chosen by the subroutine as the integration proceeds. This starting procedure is automatic and the information retained by the program about previous steps is stored in such a way as to make the interpolation to a non-mesh point straight forward.

The Nag library subroutine for integrating a set of equations using Gear's method of integration is called `d02qbf.fortran`.

The subroutine `d02qbf` permits a number of options defined by the user including :

- a. Specifying the type of error bound to be used,
- b. Specifying minimum and maximum permitted stepsizes,
- c. Specifying an initial stepsize,
- d. Varying constants used in the choice of stepsize,
- e. Specifying an interrupt to the calculation to check the progress of the integration

The subroutine offers 5 types of error tests.

- a. mixed error test

$$\frac{1}{N} \sum_{I=1}^N E(I)^2 \leq \text{TOL} \times \max \{1.0, \frac{1}{N} \sum_{I=1}^N Y(I)^2\}$$

- b. absolute error test

$$\frac{1}{N} \sum_{I=1}^N E(I)^2 \leq \text{TOL}$$

c. relative error test

$$\frac{1}{N} \sum_{I=1}^N E(I)^2 \leq \text{TOL} \times \max \left\{ \frac{1}{N} \sum_{I=1}^N Y(I)^2, \text{dwarf/macheps} \right\}$$

d. mixed error test applied componentwise

$$\frac{1}{N} \sum_{I=1}^N \left( \frac{E(I)}{W(I,19) \times \max(W(I,20), |Y(I)|)} \right)^2 \leq \text{TOL}$$

e. absolute error test applied componentwise

$$\frac{1}{N} \sum_{I=1}^N \{E(I)/W(I,19)\}^2 \leq \text{TOL}$$

N is the number of equations, E(I) is the error at the current time step for equation I, TOL the tolerance set by the user, Y(I) the values of the dependent variables calculated by the routine, W(I,19) and W(I,20) values specified by the user and are dependent on the range of the values of the dependent variables.

The initial values for Y(1) to Y(3) were 0.0, the value of Y(4) was around 3.5e-4 (could be varied depending on the oxygen concentration chosen but was always in the same range), the value of Y(5) which the temperature the value was 373.0 (this value was changed depending on the initial conditions chosen, but was always in terms of hundreds). As the integration progresses the values of Y(1) to Y(3) increase at varying rates coming up to around 1.0e-8 or 1.0e-10 for Y(1) and Y(2) but around 0.5 to 25.0 for Y(3). The large variations in the variables would mean that the error in each case would be in a different range, thus requiring the need for the error to be checked individually, therefore the fifth type of error test (i.e. Absolute error test applied componentwise ) was chosen.

On the Honeywell multics mainframe computer the usage is:

```
call d02qbf (x,xend,n,y,cin,tol,fcn,comm,const,cout,nped,
            pederv,pw,w,iw,iwl,ifail)
```

where :

x = initial value of the independent variable T  
xend = end point of the range of integration

n = number of differential equations  
y = before calling the subroutine y contains the initial values of the dependent variables, and on exit contains the computed values of the dependent variables

cin = an array of real values to indicate that the user intends to set the control parameters.

In the present case the following values were set :

cin(1) = 1.0 Indicating that the user intends to set all parameters

cin(2) = 4.0 indicating that the user wishes to apply the absolute error test componentwise

cin(3) = 0.0 this is the minimum step size permitted

cin(4) = 0.0 This value indicates to the routine that the maximum step size to be used is the communication step. If the communication step is greater than  $1.0e-4$  it is recommended that a smaller value be given for cin(4).

cin(5) = This value is used in the calculation of the initial stepsize. If cin(5) = 0.0 then the initial stepsize is calculated internally by d02qbf.

tol = this value specifies a positive tolerance for bounding the local error.

w(i,19) = is the reduction factor for checking the error against the tolerance for convergence.

All other variables used in the calling statement are defined in

## Appendix (B)

### 2.10 Validation of Shell model

Before incorporating the Shell model into the phenomenological combustion model the consistency of its use was tested. Fig(2.1) shows the flow chart for the program simulating the combustion in a rapid compression machine based on the data published by Halstead et. al. [41]. The present program simulates the rapid compression machine from start of compression. Till time equals 12ms the effect of compression, due to the moving piston, on the autoignition reactions are considered, after which, as the piston comes to a halt, the reactions occurring are solely due to autoignition of the hydrocarbon air mixture.

The change in volume due to piston motion is given by the following expressions:

Time	Decrease in Volume with Time
0 - 2.58 ms	$v = 429.9 - 28.71t$
2.58 - 10.02 ms	$v = 461.8 - 41.11t$
10.02 - 12.00 ms	$v = 76.01 - 2.605t$

where  $v$  is the instantaneous gas volume in cc and  $t$  is the time in milliseconds.

The heat transfer is given by the expression :

$$Q_1 = \Phi * V(T - T_w)$$

where  $\Phi$  is the heat product of the heat transfer coefficient  $a$  and the surface to volume ratio.

and where  $\Phi = \Phi(1)$  up to the end of compression

## Appendix (B)

### 2.10 Validation of Shell model

Before incorporating the Shell model into the phenomenological combustion model the consistency of its use was tested. Fig(2.1) shows the flow chart for the program simulating the combustion in a rapid compression machine based on the data published by Halstead et. al. [41]. The present program simulates the rapid compression machine from start of compression. Till time equals 12ms the effect of compression, due to the moving piston, on the autoignition reactions are considered, after which, as the piston comes to a halt, the reactions occurring are solely due to autoignition of the hydrocarbon air mixture.

The change in volume due to piston motion is given by the following expressions:

Time	Decrease in Volume with Time
0 - 2.58 ms	$v = 429.9 - 28.71t$
2.58 - 10.02 ms	$v = 461.8 - 41.11t$
10.02 - 12.00 ms	$v = 76.01 - 2.605t$

where  $v$  is the instantaneous gas volume in cc and  $t$  is the time in milliseconds.

The heat transfer is given by the expression :

$$Q_1 = \Phi * V(T - T_w)$$

where  $\Phi$  is the heat product of the heat transfer coefficient  $a$  and the surface to volume ratio.

and where  $\Phi = \Phi(1)$  up to the end of compression

$\Phi = \Phi(2) \cdot \exp[-(t-12.0)/t_0] + \Phi(3)$  after compression.

$\Phi(1)$ ,  $\Phi(2)$  and  $\Phi(3)$  are related to the Nusselt number  $\{Nu(i)\}$  by the expression

$$Nu(i) = \Phi(i)(v/s)(d/k)$$

where  $v/s$  is the volume to surface ratio,  $d$  the characteristic length (in this case the diameter of the combustion chamber), the Nusselt number itself is related to the Reynolds number ( $Re$ ) and Grashoff number ( $Gr$ ) by the following expressions.

$$Nu(1) \sim 0.017 Re^{0.87}$$

$$Nu(2) \sim 0.073 Re^{0.76}$$

$$Nu(3) \sim 0.23 Gr^{0.39}$$

$$t_0 \sim (88\text{ms}) Re^{-0.40}$$

Fig. 2.2 is the output from the above program for the initial conditions of 373K, initial charge density  $3.3 \times 10^{-5}$  mole/cc (i.e. 1.0 Bar or 100 kPa), 0.9 equivalence ratio and 90 RON fuel-Air mixture, which correspond to the conditions from [41] of end of compression temperature of 690K and charge density of  $3.2 \times 10^{-4}$  moles/cc. The variation of species concentration and temperature is seen to be in comparison with that published (Fig. 2.3).

Further validation of the application of the model was done by plotting the induction time (calculated from the time of deceleration of the piston, i.e. 10ms from start of compression) against, temperature at end of compression (Fig. 2.5), charge density (Fig. 2.6) and against equivalence ratio (Fig. 2.7), along with data published by Halstead et. al. [41].

The values predicted by the model are very close to those published by Halstead et. al. [41] as can be seen from the figures. The slight discrepancies in the results could be attributed to a) the value of specific heat of the gas at constant volume which was taken as a constant through out this exercise and b) the calculation of Reynolds number and Grashof number to obtain the Nusselt number in the heat transfer calculations where in approximate relations were used in the calculation of viscosity and bulk modulus for calculating the Reynolds Number and Grashof number.

Since the heat transfer and heat release calculations were already developed in the main combustion model (these are dealt with in the next chapter) it was considered necessary to obtain the results from the rapid compression machine calculations close to those published within the limits of error imposed by the assumptions made in the heat transfer and heat release calculations.

Incorporation of the Shell model into the phenomenological model and its validation are dealt with in the next chapter.

TABLE 2.1  
Rate Coefficients for Reactions Incorporated in Chemical Mechanism for Autoignition of C<sub>8</sub> Hydrocarbon/Air Mixtures

Reaction Number	Reaction <sup>a</sup>	Arrhenius Parameters <sup>b</sup>	
		A	E/R
(1)	$RH + O_2 \rightleftharpoons R + HO_2$	9.0(-11)	20,000
(2)	$R + O_2 \rightleftharpoons RO_2$	1.67(-12)	0 <sup>c</sup>
(3)	$RO_2 \rightleftharpoons ROOH$	forward	9680
		reverse	5900
(4)	$ROOH = \text{epoxide} + OH$	1.1(11)	7942
(5)	$ROOH = \text{olefin} + RCHO + OH$	2.5(14)	15,500
(6)	$ROOH + O_2 \rightleftharpoons OOROOH$	0.66(-14)	0 <sup>c</sup>
(7)	$OOROOH = RO_2H + OH$	6.5(10)	10,830
(8)	$RO_2H = R + OH$	1.0(17)	20,110
(9)	$OH + RH = H_2O + R$	1.67(-10)	1000
(10)	$R + O_2 = \text{olefin} + HO_2$	2.5(-12)	5050
(11)	$R + R = RH_2$	3.3(-9)	0
(12)	$RO_2 + RCHO = RO_2H + R$	5.25(-13)	4350
(13)	$HO_2 + HO_2 = H_2O_2 + O_2$	2.5(-12)	0
(14)	$HO_2 + RCHO = H_2O_2 + R$	8.3(-13)	4350
(15)	$H_2O_2 + M = OH + OH + M$	2.0(-7)	22,900

<sup>a</sup> Since reactions (1)-(15) are generalized reactions and not balanced chemical equations, R does not represent a unique chemical entity but a general carbon skeleton of undefined length and functional group content.

<sup>b</sup> Units are A, cm<sup>3</sup> molecule<sup>-1</sup> s<sup>-1</sup> for bimolecular reactions and s<sup>-1</sup> for unimolecular reactions; E/R, °K.

<sup>c</sup> Reverse reaction calculated from  $Nk_f/K_{eq}$ , where  $K_{eq}$  is the equilibrium constant given by

$$K_{eq} = RT \exp((15,520/T) - 17.33 - 1.961 (\ln 298/T + (T-298)/T))$$

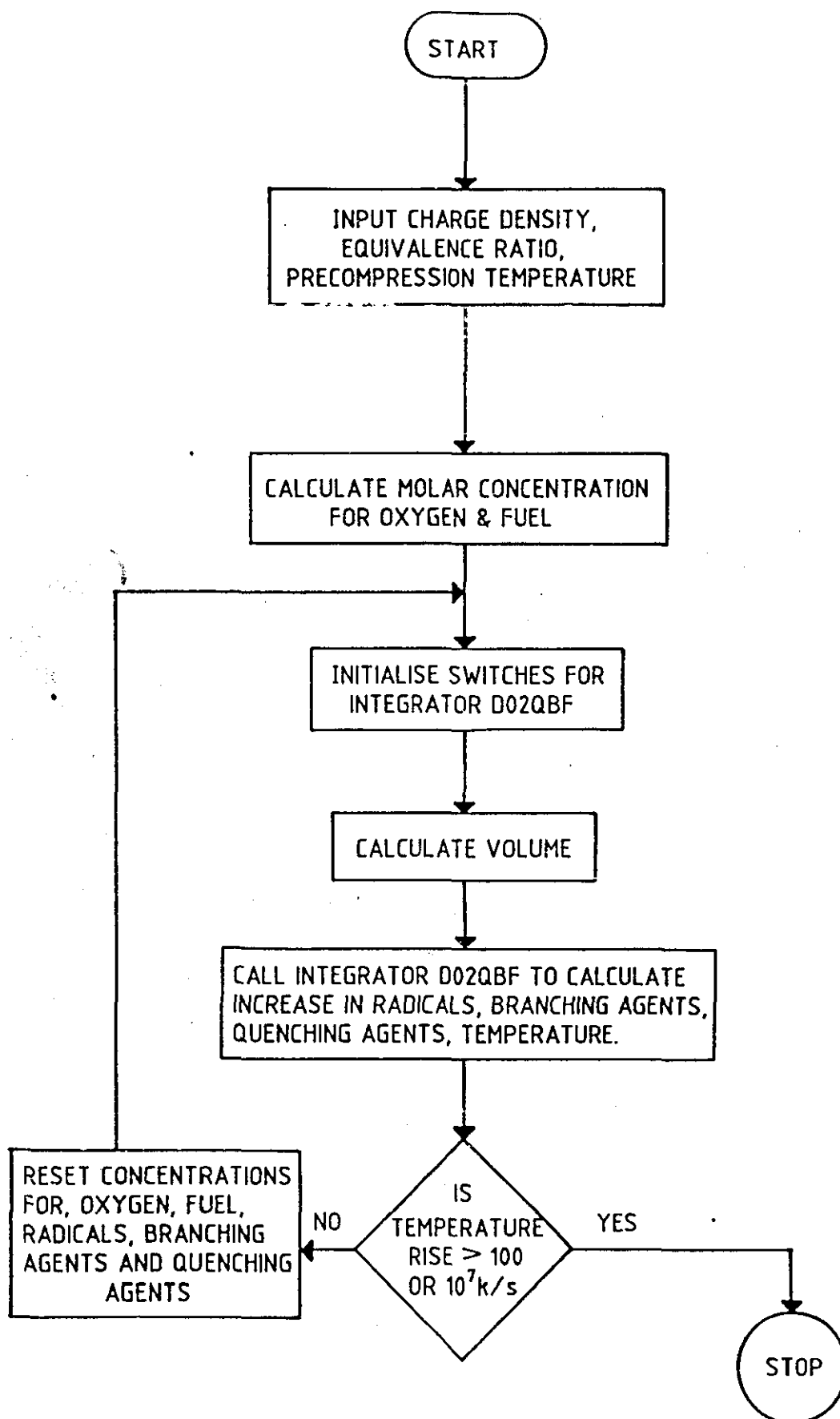


FIG. 2.1 FLOWCHART TO SIMULATE TWO-STAGE IGNITION IN A RAPID COMPRESSION MACHINE.

# Simulation of Two Stage Ignition in a Rapid Compression Machine

Conducted by the Author

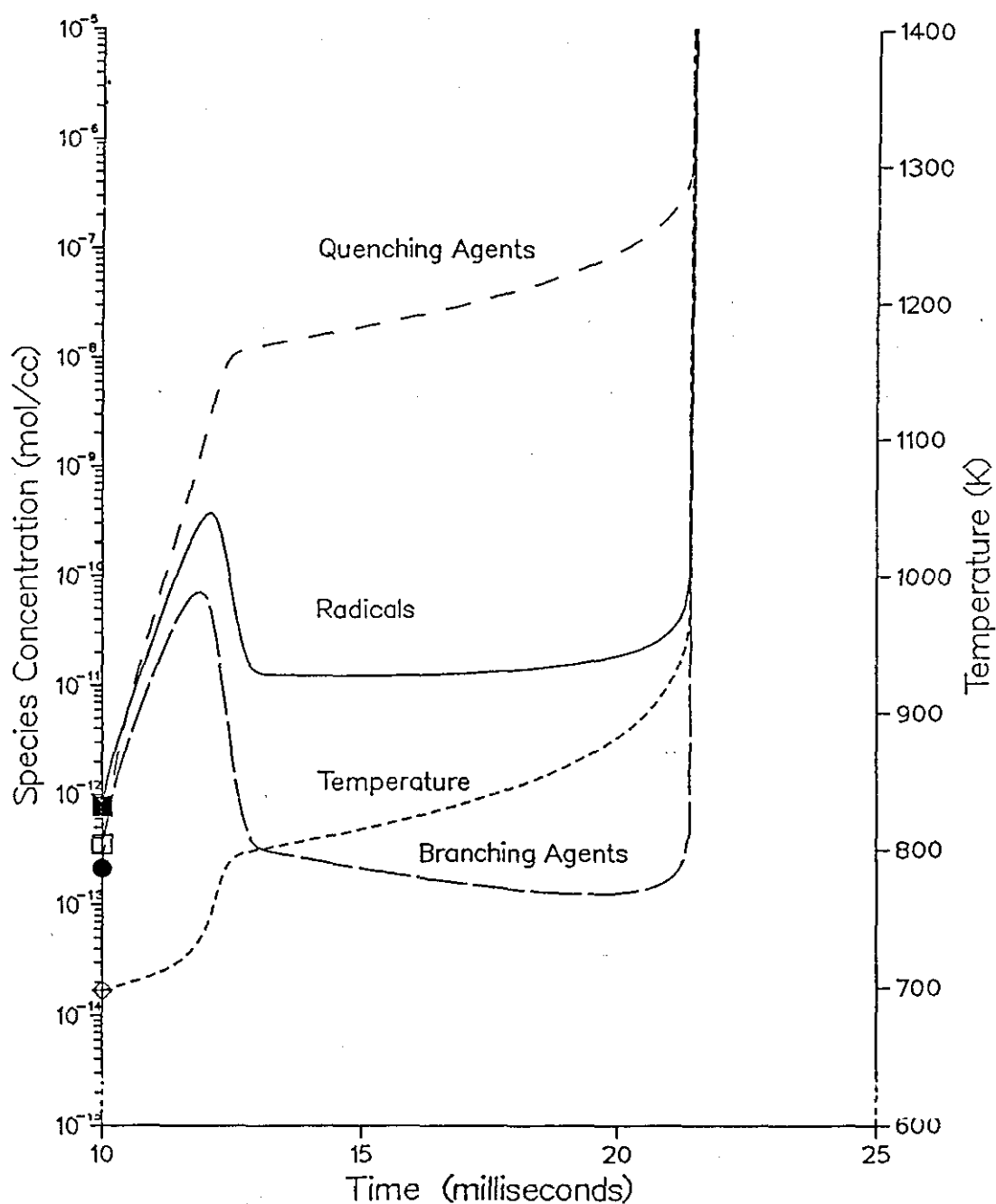


Fig. 2.2 Variation of Temperature and Species Concentration with Time  
 Equivalence Ratio = 0.9 Precompression Temperature 373°K  
 Precompression Charge Density  $3.33 \times 10^{-5}$  mol/cc

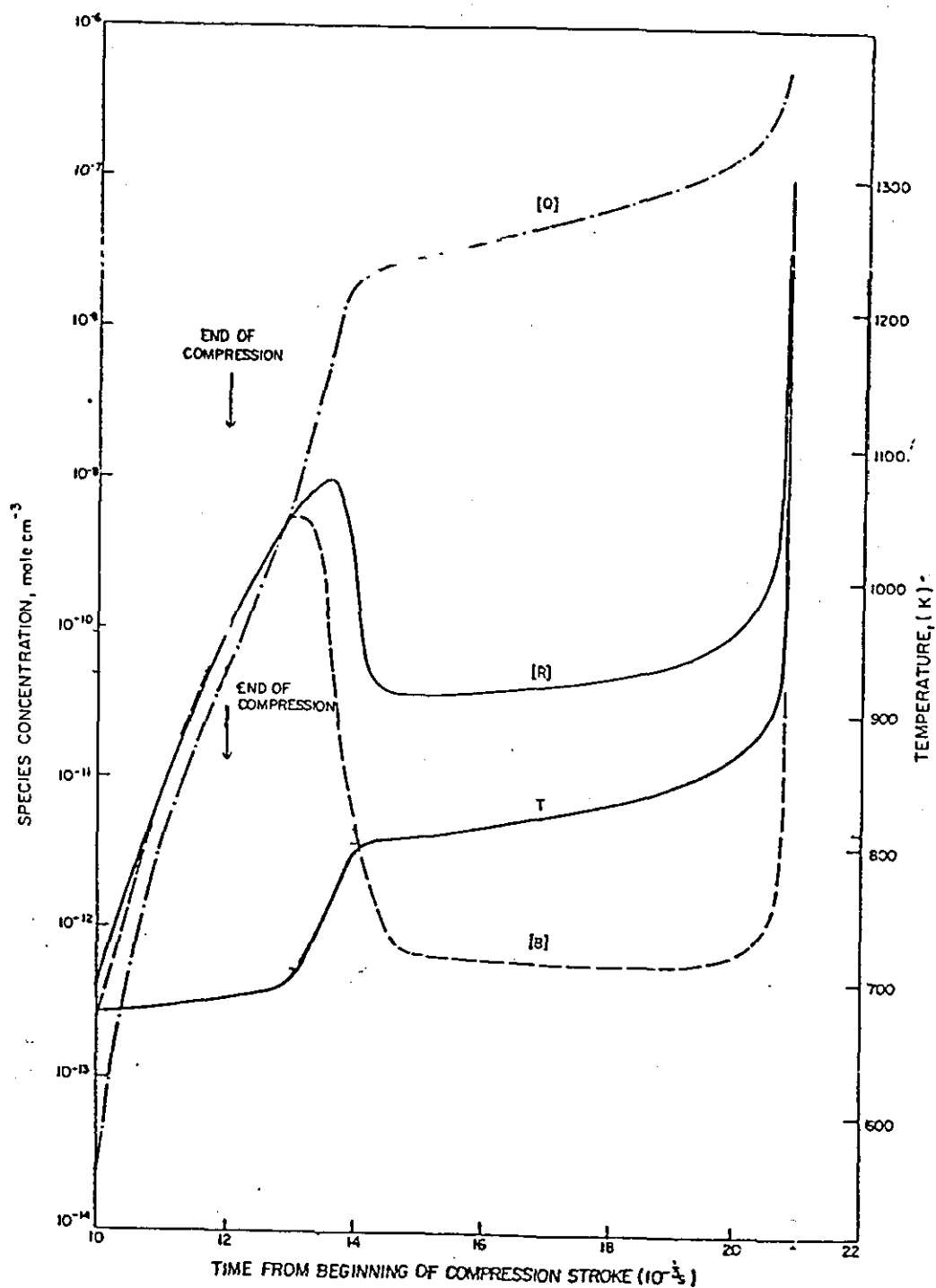
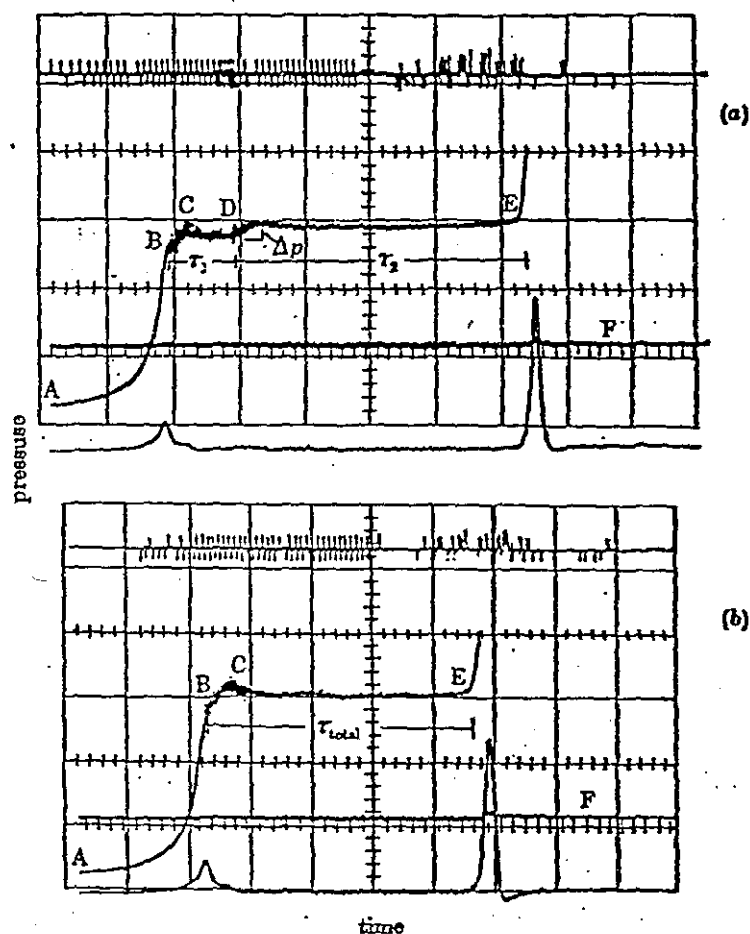


Fig. 2.3 Typical Simulation of Two-Stage Ignition  
in a Rapid Compression Machine

Results from Reference 41



**Fig 2.4.** Typical oscilloscope records of the autoignition of a 0.9 stoichiometric mixture of iso-octane with air in a rapid-compression machine. (a) Two-stage ignition at a pressure and temperature of 1.86 MPa and 686 K; (b) single-stage ignition at a pressure and temperature of 2.12 MPa and 787 K. Trace ABCDE is the pressure record; the vertical scale corresponds to 690 kPa per large division. Trace F is the timing trace with markers at millisecond intervals. The total gas concentration at the end of compression is in both cases  $3.3 \times 10^{-4} \text{ mol cm}^{-3}$ .

(Ref. 21)

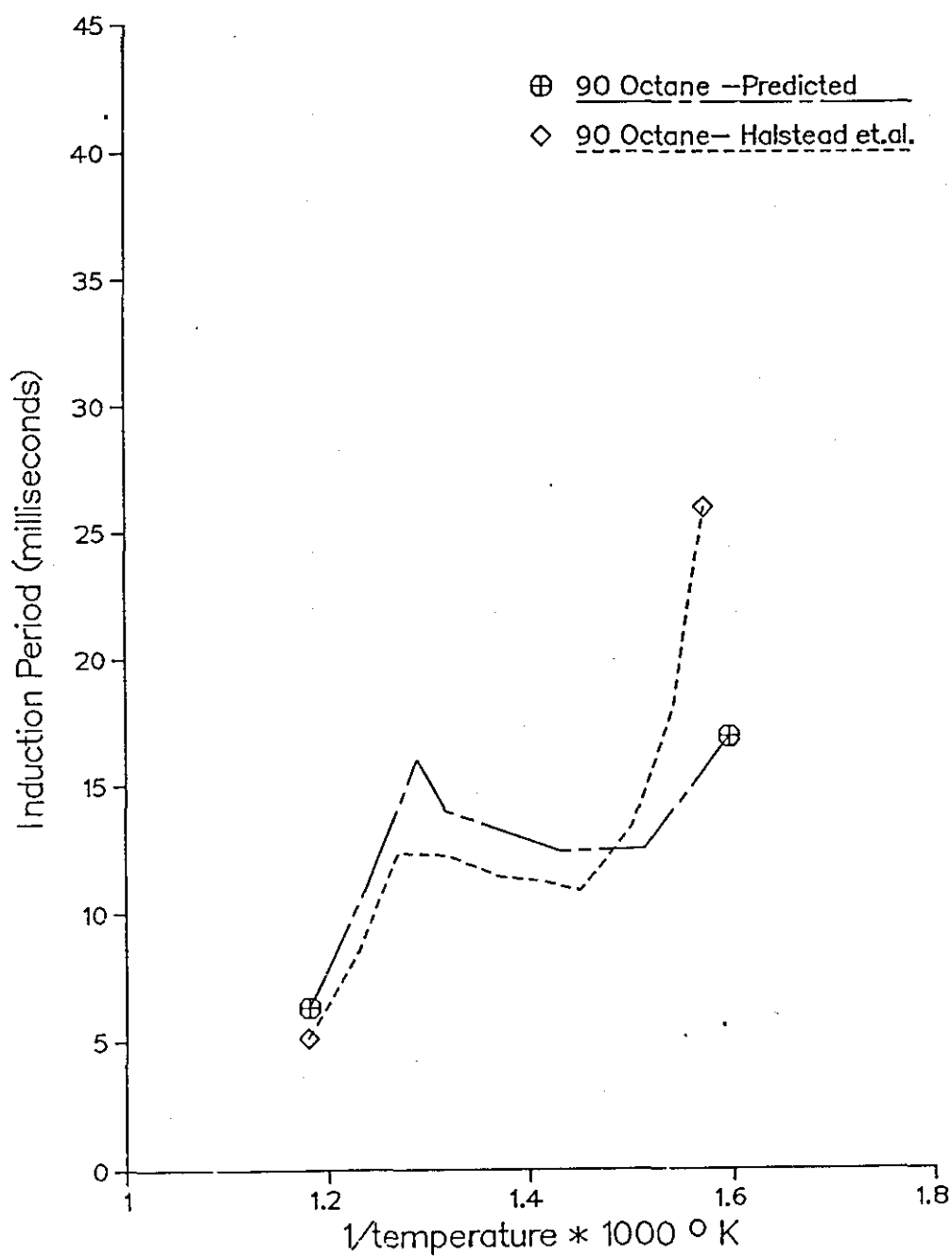


Fig. 2.5 Induction Period v/s Temperature (EOC)  
 Equivalence Ratio = 0.9  
 Precompression charge density  $3.33 \times 10^{-5} \text{ mol/cc}$   
 EOC = End of Compression

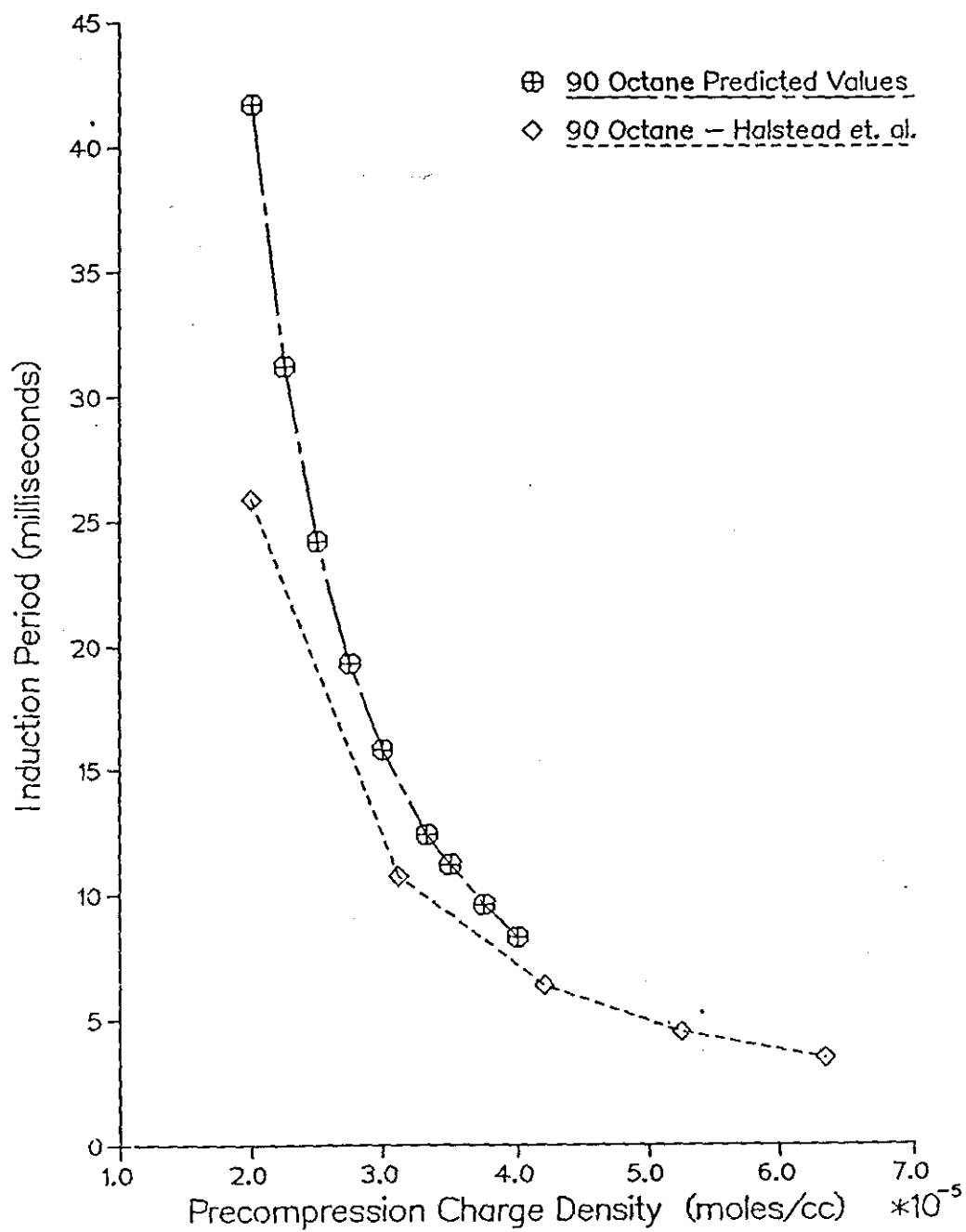


Fig. 2.6 Induction Time v/s Charge Density  
Equivalence Ratio = 0.9  
Precompression Temperature  $^{\circ}$  K

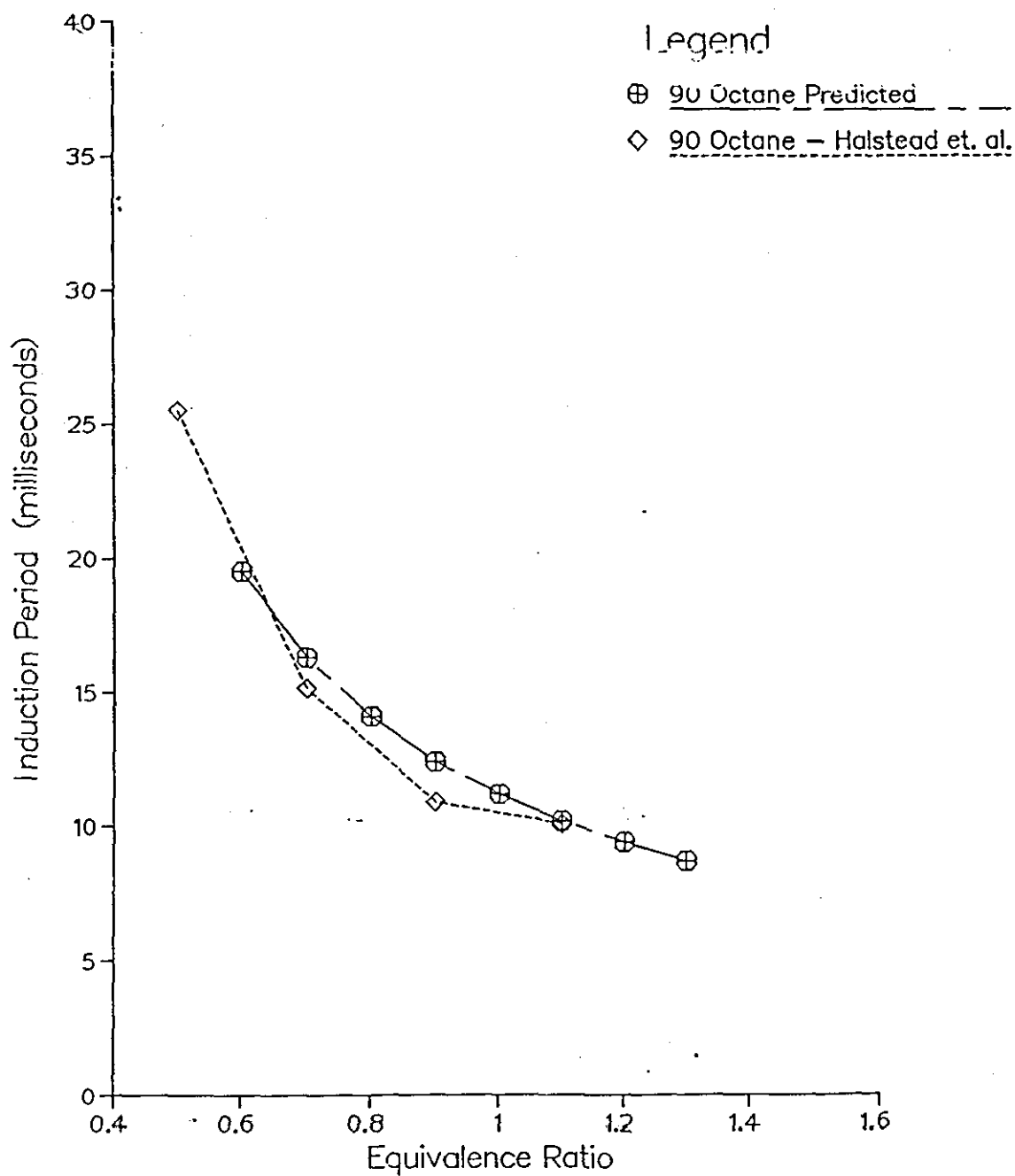


Fig. 2.7 Induction Period v/s Equivalence Ratio  
Precompression Temperature  $373^{\circ}\text{K}$   
Precompression charge density  $3.33\text{e}-05\text{ mol/cc}$

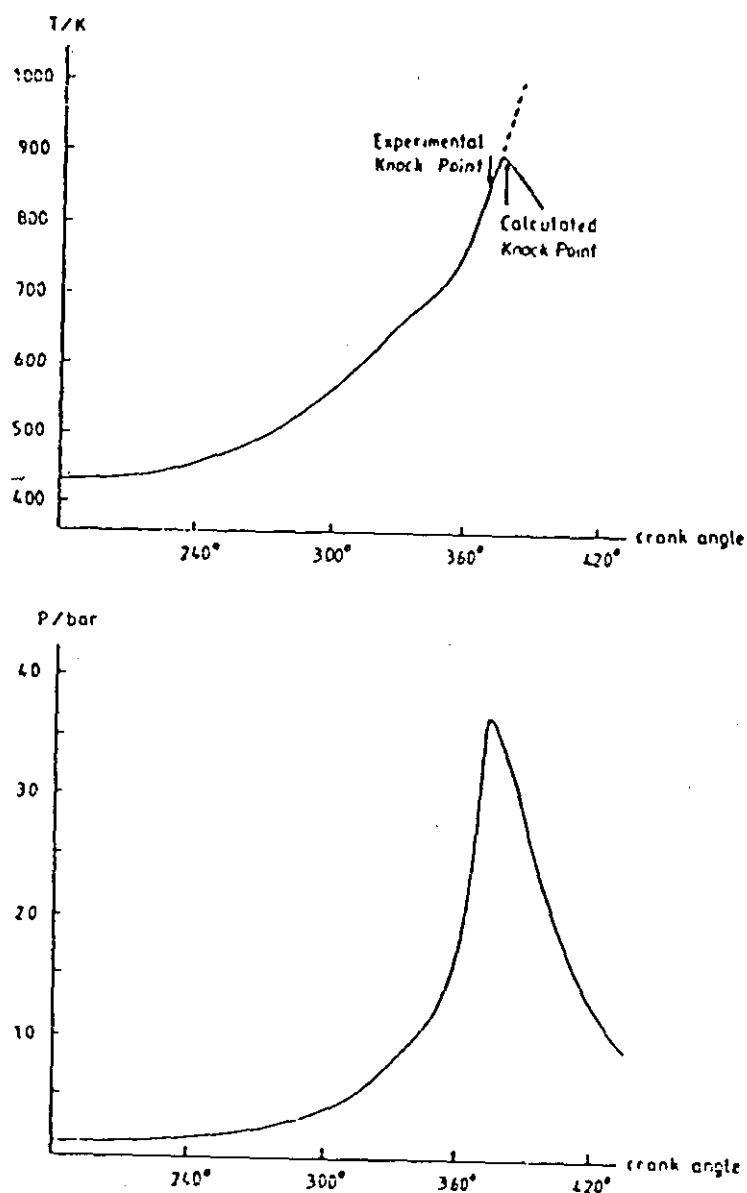


Fig. 2.8 Measured and Calculated Knocking behaviour  
in an engine fueled with 81 RON PRF  
(Ref. 38)

## CHAPTER III

### THE COMBUSTION MODEL

#### 3.1 INTRODUCTION

Combustion in spark ignition engines as in any internal combustion engine is a complex problem. Mathematical modelling of the engine cycle helps to understand the effects of various operating variables on the running of the engine. To compute the autoignition delay time of the endgases with any of the models described in chapter II, it would be necessary to predict the temperature and pressure histories of the unburned gas at any given time in the cycle. The mathematical models available can be broadly classified into two groups. Multi-dimensional models and Thermodynamic or Phenomenological models.

##### 3.1.1. Phenomenological Models.

These models are also referred to as thermodynamic models as they are based on the thermodynamic analysis of engine cylinder contents and empirical or semi-empirical process descriptions. Depending on the process description they are classified as zero-dimensional or quasi-dimensional models. In the zero-dimensional models the details of the combustion process are fixed as an input to the calculation in the form of a burning law whereas in a quasi-dimensional model an attempt is made to couple the combustion process to the thermodynamic state inside the engine cylinder.

##### 3.1.2 Multi-Dimensional Models.

Multi-dimensional models are models that have, in principle, the capability of predicting details of fluid flow within the engine cylinder and the propagation rate and geometrical shape of the flame. The governing equations are conservation equations that are

solved numerically, along with appropriate sub models which describe the turbulence processes, chemical processes, boundary layer processes, subject to the appropriate boundary conditions. Multi-dimensional models have an advantage over thermodynamic models where engine geometry and flow are most important. For parametric studies of the effects of changes in design and operating variables on engine performance, efficiency and emissions the thermodynamic models are better suited due to their simplicity and comparatively smaller computational time and costs.

### 3.2. Thermodynamic Models.

Thermodynamic models consider the cylinder charge prior to ignition to be a homogeneous mixture of air, fuel and residual gas. The flame is assumed to propagate spherically from the point of ignition. Mass and energy conservation laws are applied to the burned and unburned gases (this includes heat transfer). The complete cycle analysis including exhaust emissions can be represented as in Fig. 3.1.

The flow into the engine cylinder during the induction process is handled using quasi-steady one dimensional flow equations. Mass flows past valves and other restrictions are modelled by the equations for isentropic adiabatic flow through an orifice. A discharge coefficient is used to relate the effective area for the particular constriction (an intake valve, high-aspect-ratio connecting passage, sharp-edge orifice, etc.) to the ideal area for the isentropic flow. System pressures upstream and downstream of the restriction are used for the pressure ratio in these calculations. Unless pipe dynamics are of interest, plenum assumptions are commonly used for intake and exhaust manifolds.

Where pipe dynamics are important, these are calculated using one-dimensional unsteady gas flow equations, which are solved using the method of characteristics. These calculations generally include friction, heat transfer, and area change in the pipes. Empirical constants are used to determine boundary conditions at pipe

junctions, valves and open ends.

The unburned charge is assumed to be a mixture of air, fuel vapour, and residual gas of frozen composition appropriate to the particular engine type and operating conditions being modelled. The specific heat of each component gas in the gas mixture is modelled using polynomial functions of temperature. For most engine geometries under throttled-engine operation, burned gases flow into the intake during the gas exchange process. When this occurs, it is assumed that the burned gases that leave the cylinder do not mix with the fresh intake charge and are the first gases to be pulled into the cylinder during the intake process. This assumption has proved useful for calculating the residual gas fraction in the chamber.

For both zero-dimensional and quasi-dimensional modelling the analysis of the induction, compression, expansion and exhaust are the same. In the zero-dimensional models the combustion rate (or burn rate) is defined by an empirical expression which is obtained by matching with experimental data. In a quasi-dimensional model an attempt is made to predict the rate of burning from more fundamental physical quantities such as, turbulent flame velocity, eddy size and laminar flame speed.

### 3.3 Sub-models for Burn Rate

Distinction between zero-dimensional and quasi-dimensional models is made on the basis of the definition of the burn rate. In the zero-dimensional class of models the burn rate is defined by a functional relationship obtained by matching with previous experimental data. Typical functional forms used for specifying the combustion rate are the cosine function:

$$X(I) = (1/2)\{1. - \text{Cos}(\pi)[(I-I_S)/(I_e - I_S)]\} \quad 3.1$$

or a Wiebe function:

$$X(I) = 1 - \exp\{-a[(I-I_s)/(I_e-I_s)]^{m+1}\} \quad 3.2$$

where  $X(I)$  is the mass fraction burned at  $I$ ,  $I_s$  is the crank angle at the start of combustion,  $I_e$  is the crank angle at the end of combustion, ' $a$ ' is the duration parameter and ' $m$ ' is the shape parameter. The heat release rate is calculated from the analysis of the first law of thermodynamics as shown in appendix 'A', the best fit curve through a set of burn rates obtained from experimental pressure data would give the burn rate from which the parameters ' $a$ ' and ' $m$ ' can be obtained for a particular engine. One of the major drawbacks of zero-dimensional models is the need to specify the burn rate in advance. This has led to the development of quasi-dimensional models.

Quasi-dimensional models attempt to predict the rate of burning from more fundamental physical quantities such as, turbulent intensity ( $u'$ ), the turbulent integral length scale ( $L$ ), the turbulent micro-scale ( $\lambda$ ) and the kinetics of the fuel-oxidation process. Thus, defining the ignition delay and combustion rate as a function of engine design and operating conditions.

One approach has been to model the burning process as a flame front of area  $A_f$  propagating through the unburned mixture at the turbulent flame speed  $S_t$ . Thus the mass burning rate is given as

$$dm_b/dt = \rho_u * A_f * S_t \quad 3.3$$

where  $S_t$  can be related to the laminar flame speed. One such relation as shown by Mattavi et. al. [42] is given by eqn. 3.4

$$S_t = S_l + 4.01 * u'/S_l \quad 3.4$$

Blizard and Keck [43] suggest an alternate approach for modelling turbulent flame propagation. These authors developed a laminar

combustion scheme by considering turbulence to be the movement of discrete turbulent eddies. Each eddy in the fragmented turbulent combustion zone is assumed to burn inward from its outer surface at a constant laminar burning velocity. The eddies are entrained into the flame front at a turbulent burning velocity  $U_e$  taken to be equal to the turbulence intensity  $U'$ .

Here the propagating flame front is considered to be of finite thickness, the entrainment front defines the boundary at which turbulent eddies enter the burning zone and begin to burn up. The model considers the eddy structure to be represented by three length scales, the integral or macro scale  $L$  which specifies the overall characteristic dimension of the eddies, the Taylor micro-scale  $\lambda$ , which determines the internal structure of the eddy, and represents the scale at which laminar burning is dominant, and the Kolmogorov scale  $\eta$  which is the characteristic dimension of the vortex tubes that subdivide the eddy into numerous laminar burning zones.

The mass entrained into the front is given by  $m_e$

$$\text{where} \quad \frac{dm_e}{dt} = \rho_u A_f U_e \quad 3.5$$

$A_f$  = Area of the flame front

$\rho_u$  = density of Unburned gas

where  $U_e$  is the entrainment velocity assumed proportional to the turbulent intensity and the rate of mass burned is given by

$$\frac{dm_b}{dt} = (m_e - m_b)/t \quad 3.6$$

where  $t$  is the characteristic reaction time to burn the mass of an eddy of size  $L$ .

Blizard and Keck [43] assumed that the characteristic reaction time  $t$  and the entrainment velocity were constant rather than time-varying in value thereby not reflecting the change in geometry or

thermodynamic conditions during the turbulent combustion process. In an attempt to rectify these drawbacks Tabaczynski et. al.[44] assumed that:

- a) The turbulent integral scale at the initiation of spark is proportional to the instantaneous chamber height.
- b) The turbulent intensity at the time of spark is proportional to engine speed and does not vary with spark advance.
- c) The turbulent entrainment speed is proportional to the turbulent intensity.
- d) After the beginning of measurable heat release, taken as 1% mass fraction burned, the turbulent intensity and integral scale of the unburned gas are governed by the conservation of angular momentum of the individual eddies. This assumption of conservation of angular momentum for rapidly compressed gases is known catagorically as a rapid distortion theory. The effect of this assumption is that leaner mixtures or dilute mixtures will burn slower than near stoichiometric mixtures since there is less compression of the turbulence in the unburned gases.

Though the above assumptions were made by Tabaczynski et. al. [44] based on indirect evidence, physical intiution and to a certain extent mathematical convenience, their results do show trends that would be expected in an engine with change in engine design and operating parameters.

Hires et. al. [49] extended the model of Tabaczynski et. al. [44] to predict the ignition delay and combustion duration. The expressions for ignition delay and combustion duration in terms of crank angle as follows :

$$\Delta\theta_{ig} = C_{ig}(S_p^\eta)^{1/3}(h/S_1)^{2/3} \quad 3.7$$

$$\Delta\theta_c = \int_{x=0}^{x=1} [C_c(A_b/A_f)(p_i/p_u)^{10/9}(S_p\eta)^{1/3}(h_i/S_1)^{2/3}]dx \quad 3.8$$

where  $\Delta\theta_{ig}$  = Ignition delay in terms of crank angle duration

$\Delta\theta_c$  = Combustion duration in terms of crank angle

$S_p$  = Average piston speed

$\eta$  = Kinematic viscosity

$h$  = instantaneous chamber height

$S_1$  = Laminar flame speed

$A_f$  = effective flame surface area

$A_b$  = cross-sectional area of the cylinder bore

$p_i$  = density of the unburned gas at the end of the  
ignition delay

$p_u$  = density of the unburned gas

$C_{ig}$  and  $C_c$  are constants unique to the engine geometry  
but independent of operating conditions.

The values of both these constants  $C_{ig}$  and  $C_c$  are determined by an iterative comparison of model prediction with the corresponding experimental value of the ignition delay and combustion intervals.

Lakshminarayanan and Dent (45) found that though comparison of predicted and experimental pressures and flame areas were good under stoichiometric and rich conditions, under lean mixture conditions and part throttle conditions further refinement in the evaluation of the constant  $C_c$  was considered necessary.

### 3.4 Burning Law

As mentioned in section 3.3 the burn rate can be defined either by a Cosine function or a Wiebe function, from equations 3.1 and 3.2 it can be seen that both these functions require that the Start and end of combustion be defined. Application of the cosine burn law to the combustion model resulted in very low pressures as compared to experimental values, these were found to be due to the fact that the end of combustion was defined very late in the cycle, especially in cases where the last phase of burning was very slow compared to the

early stages of combustion. Lavoie and Blumberg [46] proposed the use of 5% and 95% burn points instead of the start and end of combustion as the 0% and 100% burned points are difficult to determine accurately from an experimental trace thus rewriting equation 3.1 as:

$$X = 0.5 \{1 - \cos[180/1.16((I - I_{0.05})/(I_{0.95} - I_{0.05}))]\} \quad 3.9$$

where  $I_{0.05}$  and  $I_{0.95}$  are the crank angles at 5% burn and 95 % burn points respectively.

Determining the 95% burn point or 100% burn point for a knocking case would be meaningless as the angles defined would predetermine the occurrence of knock. On the contrary a point along the mass fraction burned curve that would not change drastically due to knock (provided it occurred late in the burn cycle) would be the 50% burn point. Lancaster [56] and Mattavi et. al. [42] have also preferred the 50% mass burn point as:

a) It occurs in region where geometry calculations are less sensitive to model uncertainties,

b) with MBT spark timing it was found to occur consistently at about 7 degrees after top dead centre for the wedge and open chamber and 12 degrees after top dead centre for the disc chamber,

also Mattavi et. al. found that the flame speed ratio in the vicinity of the 50% mass burn point was relatively closer to its peak value.

Another Mathematical function that is capable of depicting trends similar to the different burn rates is the chi-square distribution.

The chi-square distribution is expressed as :

$$F(x_n^2) = [2^{n/2} \Gamma(\frac{n}{2})]^{-1} [x]^{n/2-1} \exp[-\frac{x^2}{2}] d(x^2)$$

n is the number of degrees of freedom.

Varying n (the number of degrees of freedom), changes the distribution curves and the chi-square distribution with varying degrees of freedom are shown in Fig. 3.41. The rate of burning to a large extent is dependent on the engine type for a given fuel therefore, for a given engine and a given fuel the chi-square distribution can be defined by a given number of degrees of freedom for the chi-square distribution.

The end of delay period and start of combustion is taken as 1% burn point, as this is approximately the region where the mass fraction burn curve shows a deviation from the horizontal (showing the effect of heat release). The burn duration is defined as the difference in crank angle at any given point and the crank angle at 1% burn, similarly the 50% burn duration is the duration from 1% burn point to the 50% burn point in crank angle degrees. The mass fraction burned is plotted against the burn duration normalized to the 50% burn duration.

The Ricardo E6 engine was run using 4 star petrol ( 98 Octane) at conditions that took into account a variation in spark timing , compression ratio, air-fuel ratio and speed from a base condition of 1500 rpm, 8.7 CR, stoichiometric air-fuel ratio and MBT spark timing as shown in Table 3.1. The mass fraction burned points are plotted against the burn duration normalized to the 50% burn duration. The chi-square distribution that best fits this data is selected to represent the burn rate for this engine.

Table 3.1

Variable	Values		
	High	Base	Low
Speed	2000	1500	1000
Compression Ratio	9.7	8.7	7.7
Air-Fuel Ratio	18.1	15.6	12.7
Spark Timing	MBT+6	MBT	MBT-6

To obtain the expression for the rate of burning the fraction of mass burned  $dmb$  could be then equated to  $F(x^2)$  thus obtaining

$$\frac{dm_b}{m_b} = F(x_n^2) \quad 3.11$$

$$\frac{dm_b}{m_b} = \frac{[x^2]^{n/2-1} \exp[-x^2/2] d(x^2)}{[2^{n/2}] [\Gamma(n/2)]} \quad 3.12$$

$$\frac{dm_b}{m_b} = \frac{[x^2/2]^{n/2-1} \exp[-x^2/2] d(x^2/2)}{\Gamma(n/2)}$$

Normalising  $x^2$  with the 50% point we can write

$$\frac{x^2}{x_m^2} = \frac{x}{x_m} \quad 3.14$$

$$\frac{dm_b}{m_b} = \frac{(x_m^2/2)^{n/2-1} (\frac{x}{x_m})^{n/2-1} \exp[-x_m^2/2 (\frac{x}{x_m})] d(x_m^2/2) d(\frac{x}{x_m})}{\Gamma(n/2)} \quad 3.15$$

where  $x_m^2$  and  $x_m$  are values at the 50% point .

Pressure data obtained from the engine were used to find the mass fraction burned according to the method described in appendix A.

To extend the generality of the Chi-Square distribution as a burn rate law, pressure data obtained by previous investigators [53] using the Ford 4 cylinder engine with the Standard and the May

'fireball' heads were used to obtain the mass fraction burned curves and the chi-square distribution functions for the different engine geometries. Varying the number of degrees of freedom in the expression for chi-square distribution a smooth fit is obtained through the experimental data. Figs. 3.3 and 3.4 show the mass fraction burned curves for the Ford engine with the Standard head and the May 'fireball' heads respectively.

### 3.5. Basis of the Combustion Model.

The Thermodynamic model is that proposed by Lavoie et. al. [52] and coded and reported by Ferguson et. al. [47]. The model simulates the combustion from spark to exhaust valve opening. Compression till spark is assumed to be polytropic with an index of 1.3.

The development of the model was based on the following assumptions:

1. The flame surface separating the burned from unburned gas regions has negligible volume.
2. The gas within the cylinder consists of a burned fraction at thermodynamic equilibrium plus an unburned fraction frozen at its original composition
3. Gas temperatures in the burned and unburned gas regions are uniform. The model of Martin and Heywood [48] is used to calculate thermodynamic properties in the burned gas region, while the property calculations for the unburned region including the residuals is computed as per Hires et. al [49].
4. The cylinder pressure is uniform throughout the cylinder.
5. Heat transfer to the cylinder surface is according to Woschni [50] and is averaged over the whole combustion volume.

6. The flame front is assumed to be spherical, The flame areas and maximum flame radius are calculated as per the technique developed by P A Lakshminarayanan and J C Dent [51].

### 3.6 Governing Equations and Solution Technique

The thermodynamic model employed is that of Lavoie et. al. [52] modified to incorporate time dependent specific heats.

The system consists of burned and unburned gases seperated by a burning zone, assuming that the mass of burning gas is small compared to the mass in the cylinder it follows that :

$$V/m = X_b * v_b + (1-X_b) * v_u \quad 3.16$$

$$E/m = X_b * e_b + (1-X_b) * e_u \quad 3.17$$

where  $V$  = Cylinder volume  
 $E$  = Energy of the gases in the cylinder  
 $e$  = spatial average internal energy  
 $v$  = spatial average specific volume

The average internal energy or specific volume of the unburned or burned gases is computed using the average unburned or burned gas temperature and pressure.

The thermodynamic state functions for the burned gas are computed using the model of Martin and Heywood [48]

$$\text{i.e.} \quad e_b = e_b(T_b, p) \quad 3.18$$

$$v_b = v_b(T_b, p) \quad 3.19$$

For the unburned gases the state equations are from [47]

$$\text{i.e.} \quad e_u = e_u(T_u, p) \quad 3.20$$

$$v_u = v_u(T_u, p) \quad 3.21$$

The unburned gas is assumed to compress isentropically, thus making it a function of the pressure alone. giving equation 3.202

$$T_u = T_u(p) \quad 3.22$$

at any instant after ignition the first law of thermodynamics for the combustion volume can be expressed as

$$e_b + e_u = e_o - \int Q dt - \int dW dt \quad 3.23$$

where  $e_b$  = internal energy of the burned gases

$e_u$  = internal energy of the unburned gases

$e_o$  = Total internal energy of the system

$Q$  = heat lost form the system

$W$  = Expansion work by the system

The heat loss is computed using the heat transfer co-efficients from Woschnis [50] correlation. The heat transfer coefficients being given by 3.24 and 3.25 for the burned and unburned gases respectively.

$$H_b = 100d^{-0.2}p^{0.8}T_b^{-0.53}[C_1C_m + C_2 \frac{V_s T_1 (P-P_o)}{P_1 V_1}] \quad 3.24$$

$$H_u = 100d^{-0.2}p^{0.8}T_u^{-0.53}[C_1C_m + C_2 \frac{V_s T_1 (P-P_o)}{P_1 V_1}] \quad 3.25$$

where  $C_m$  = mean piston speed

$V_s$  = swept volume

$P_0$  = Instantaneous motoring Pressure

$C_1$  = 2.28

$C_2 = 3.24 \times 10^{-3}$  m/sec deg C

The constant  $C_1$  and  $C_2$  have been obtained by Woschni [50] from experimental heat transfer values.  $C_1$  is a constant relating the piston speed to the gas velocity and  $C_2$  is a constant relating the state of the working gas at a reference level (i.e. Spark) to an additional gas velocity introduced to account for the turbulence in the system due to combustion.

The datum pressure, temperature and volume are  $P_1$ ,  $T_1$ ,  $V_1$  respectively and are evaluated at the time of spark.

The heat loss from the burned and unburned sides being given as :

$$Q_b = H_b \cdot A_b \cdot (T_b - T_w)$$

$$Q_u = H_u \cdot A_u \cdot (T_u - T_w)$$

$$Q_t = Q_b + Q_u$$

where  $Q_b$  = heat loss from the burned gases

$Q_u$  = heat loss from the unburned gases

$Q_t$  = Total heat loss from the system

$T_b$  = temperature of the burned gases

$T_u$  = temperature of the unburned gases

$T_w$  = Wall temperature ( assumed 460 K)

The flow chart for the computer program is given in Fig. 3.5. The computer program simulating the combustion is called "copred.fortran" and the main subroutine is called BLZKCK, where, all switches initialising different events such as spark, end of delay (start of combustion), end of combustion and exhaust valve opening are set, also the control parameters for the integrator are initialised. The pressure and temperature at spark are calculated.

The pressure from the expression  $PV^n = \text{Constant}$  and the temperature from the universal gas law , i.e.  $T = P \cdot V / m / R$

The rate of burning defined by an empirical relation such as equation 3.13 coupled to the thermodynamic relations defined above together with initial conditions constitutes an initial value problem. Integration of the differential equations defining the rate of burning, the rate of heat lost and the rate of change of internal energy to obtain the total mass burned, the total heat lost to the surroundings and the total internal energy in the system at any given instant is performed using a subroutine employing a variable step, variable order method of integration using Adams-Falkner predictor and Adams-Moulton corrector co-efficients as proposed by Krogh [55] and coded and reported by Ferguson et. al. in reference [47]

### 3.7. Validation of Combustion Model.

To check the implimentation of the model and the working of the computer code, the pressure crank angle output from the program was plotted against those obtained from the engine. The experiments were carried out on a Ricardo E6 engine with variable compression ratio. The conditions at which the engine tests were carried out are given in Table 3.1. The heat release rate was calculated using the pressure data obtained from these experiments according to the method explained in Appendix A.

The test conditions at which the cylinder pressure data were measured were selected to include variation in speed, compression ratio, Air-fuel ratio and spark timing about a base set. Maintaining three variables in the base condition constant the fourth variable was varied thus obtaining 9 test points. This was done for four fuels, i.e 100 RON, 4 Star petrol (98 Octane), 95 RON and 90 RON fuels. With 70 RON the compression ratio at base condition had to be reduced due to heavy knock at 8.7 compression ratio and near

stoichiometric mixtures (on the lean side).

The computed cylinder pressure histories and the mass fraction burned for engine conditions representing variation of speed, air-fuel ratio and compression ratio are plotted against their respective experimental traces (Figs. 3.6 to 3.13). The pressure trace for retarded spark timing is also shown to represent variation in spark timing. The maximum deviation in the predicted peak pressure value is 5.79%, the predicted peak pressure occurring in most cases at the same crank angle as that found experimentally or 1 degree off the experimental value. The highest deviation in the peak pressure value occurs at 1000 rpm, stoichiometric air-fuel ratio and MBT spark timing. The mass fraction burned curves overplot in all the cases from around 15% burned to 85% burned. Though the rate of burning is slightly slower in the initial stages it does not have a large impact on the pressure calculation. The difference in the theoretical and experimental mass fraction burned curves during the last stages of combustion could be attributed to the assumptions made in the calculation of the mass fraction burned from the pressure data, such as:

- a) a constant ratio of specific heats
- b) that the chemical reaction reaches completion during the combustion duration.
- c) neglecting flame quenching, which could be significant towards the latter part of combustion.

Comparison of the pressure plots and mass fraction burned plots for the May engine show up favourably (Fig. 3.14 to Fig. 3.17). In the case of the standard engine (Fig. 3.18 to Fig. 3.21) there is a high degree of deviation in the predicted pressure data as compared to the experimental data. The standard engine is a slow burn engine as compared to the May engine and the scatter in the data being higher the chi-square distribution chosen did not represent the true nature

of the burning rate. A close match of the burn rate especially at the beginning and middle of the combustion tends to give a better comparison of the predicted and experimental pressure curves as shown for the Ricardo and May engine data.

### 3.8 Incorporation of Knock Model

The Shell model [41] originally developed from rapid compression machine experiments was modified to suit the combustion program. The flow chart of the subroutine to calculate the temperature rise and mass burned due to autoignition is shown in Fig. 3.22. The equations comprising the model are given below:

$$1/V \{dnR/dt\} = 2\{Kq[RH][O_2] + Kb[B] - Kt[R][R] - f3Kp[R] \} \quad -- \quad 2.13$$

$$1/V \{dnB/dt\} = f1*Kp[R] + f2*Kp[Q][R] - Kb[B] \quad -- \quad 2.14$$

$$1/V \{dnQ/dt\} = f4*Kp[R] - f2*Kp[Q][R] \quad -- \quad 2.15$$

$$1/V \{dnO_2/dt\} = -pKp[R] \quad -- \quad 2.16$$

$$dT/dt = 1/cv/ntot * Qk - Ql - ntot/V * R * T * dV/dt \quad -- \quad 2.17$$

$$nRH = (nO_2 - nO_2(t=0)) / (p * m) + nRH(t=0) \quad -- \quad 2.18$$

The solution of the set of equations 2.13 to 2.17 gives the rise in temperature due to autoignition in the given time step. Equation 2.18 gives the fuel consumed in the same time step based on the consumption of oxygen. Knowing the number of moles of fuel and oxygen consumed in a cycle the mass of fuel and air consumed in the given time step are calculated from the following expressions.

$$F_m = Y_f * 144$$

and

$$F_{air} = Y_{O_2} * 32 * 4.76$$

where  $Y_f$  and  $Y_{O_2}$  are the number of moles of fuel and oxygen consumed in the time step under consideration.

The mass burned due to autoignition  $F_{air}$  is added to the total mass burned on return to the main program thus adding the masses of gas burned due to normal combustion and autoignition for the next step. The occurrence of knock is defined as the time step in which the temperature rise is greater than  $100K$  in a one degree time step or  $10^7 K/s$ . It is assumed that all the remaining mass is burned at this stage.

The Ricardo E6 engine was run with commercial four star petrol having an Octane number of 98 and with a 90 RON fuel prepared from a mixture of Iso-octane and n-heptane. The pressure signal under knocking conditions was recorded on a 4 channel tape recorder, relevant details of which are given in Table 4.1. Details about the acquisition of pressure signals as well as the ionisation probe signals is dealt with in the next chapter.

The incorporation of the knock model into the combustion program was validated by simulating the different test runs with the two fuels. Fig. 3.23 through 3.27 show a mixed response. In three of the five cases the comparison is very good while in the two cases where the mixture ratio is on the lean side the pressure traces do not compare favourably. This could be attributed to the fact that with lean mixtures the cyclic variations at knock is much higher than with stoichiometric or rich mixtures, thus increasing the possibility of obtaining a cycle that is not a true representative of the general or average cycle under those conditions.

The charge mass, fed as an input for the program are calculated from the measured air-flow rates.

### 3.9 Comparison of Results from models of Halstead et. al. and Douaud and Eyzat

The model proposed by Halstead et. al. [41] takes into account a complex kinetic scheme to predict the ignition delay time for the end gases, though at the same time it gives a description of the chemistry during the process of knock. The model of Douaud and Eyzat [20] which was later extended by Douaud [35] considers a simple expression for the ignition delay which when incorporated into the integrand proposed by Livengood et. al. [eqn.1.5] gives the knock point.

Fig. 3.28 to Fig. 3.35 show the pressure traces for four air-fuel ratios at 1500 rpm and four speeds at stoichiometric air-fuel ratio under knocking conditions ( see Table 3.2 for conditions). The time knock occurs is calculated both by the model of Halstead et. al. (Shell Model) and that of Douaud [35]. It is shown that the time knock occurs as predicted by Douaud's model is always earlier with respect to the time predicted by the Shell model.

At 1500 rpm (Fig.3.28-Fig.3.31) both models predict knock ahead of the experimental value. One of the reasons being that the predicted pressures are higher than the experimental pressures. The Shell model predicts the time of knock closer to the experimental value as compared to that predicted by Douaud's model at higher speeds.

The knock timing as predicted by the Shell model and the model of Douaud's is plotted against the experimental value (Fig. 3.40) and it is seen that the predictions by the Shell model are closer to the line of equality (i.e. the line on which the points would fall if the predicted and experimental values were equal) as compared to that by Douaud's model.

To study the effect of mixture strength in terms of residuals a parametric study was performed, Figs 3.36 to 3.39 show the pressure plots predicted for fixed conditions of 1500 rpm, equivalence ratio

0.994, compression ratio 8.7 and exhaust gas residuals varying from 5% to 15 % in steps of 5%.

The effect of exhaust residuals is simulated by reducing the charge mass proportionately and making the mixture leaner, thereby assuming that an equivalent amount of Nitrogen has been added to the charge. The oxygen concentration calculation in the Shell model is calculated using the original air-fuel ratio to effect the reduction in oxygen concentration due to the exhaust residuals.

The change in spark timing and ignition delay from the measured values for increase in exhaust gas residuals (EGR) is obtained from the data presented by Young [54].

Hires et. al. [49] have shown that increasing the amount of EGR increases the combustion duration as also the ignition delay time. Morgan and Hetrich [84] have presented results which show the effect of EGR on the RON requirement for an engine run at three different air-fuel ratios at constant speed and full load. The slightly richer mixture (Air-fuel ratio 14.5) required higher octane number fuels with increasing EGR while with air-fuel ratios of 16:1 the octane requirement showed a decreasing trend and with 18:1 air-fuel ratios no effect of EGR was noticed on the octane requirement.

The results of the computer simulation of knock with the two models under consideration with increasing amounts of EGR are presented in Figs 3.36 to 3.39. Douaud's model predicts knock earlier than the Shell model though with 15% EGR no knock is predicted by either of the models. This compares favourably with the results presented by Morgan and Hetrich [84] for a case with 16:1 air-fuel ratio.

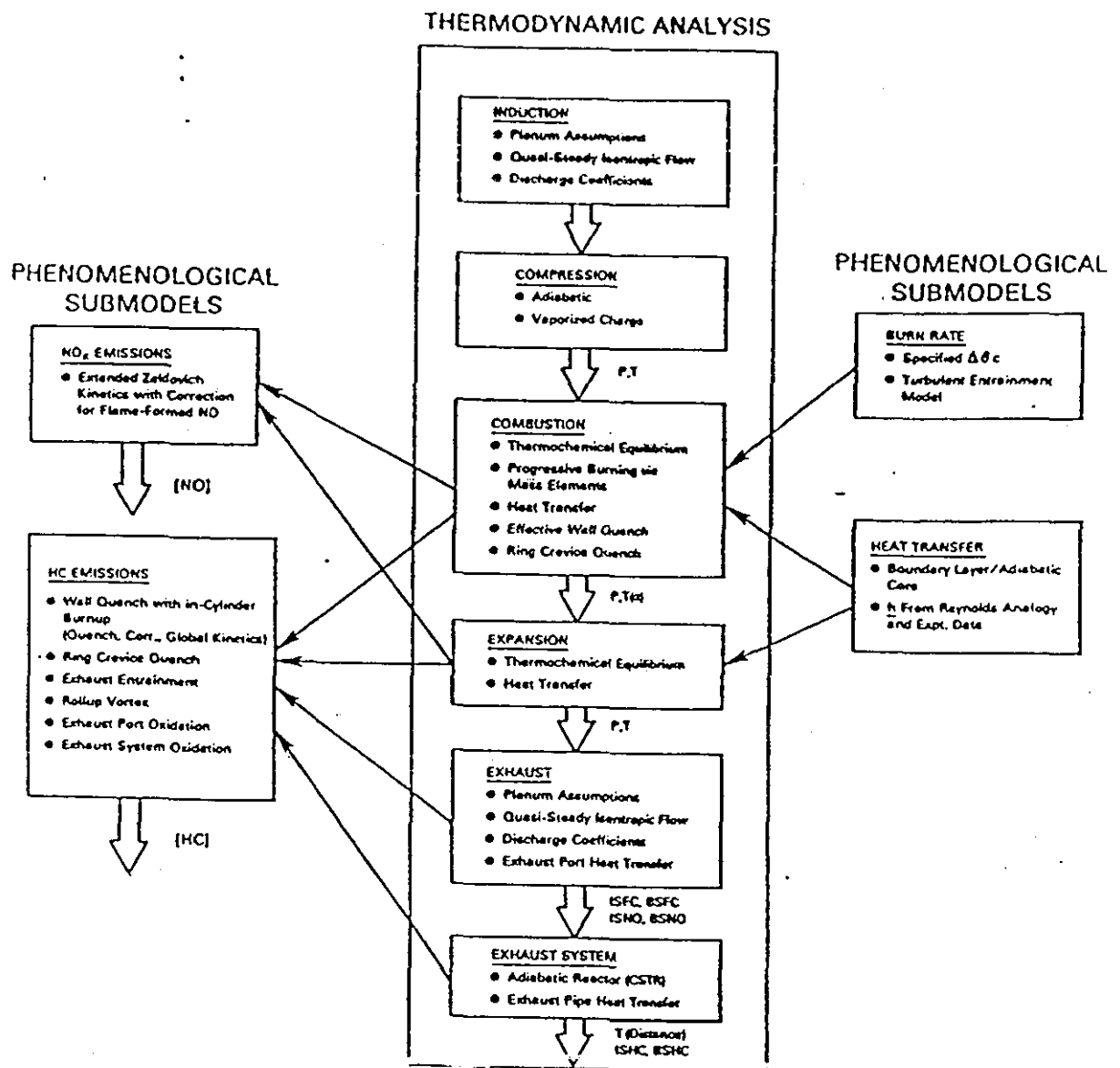


Fig. 3.1 Block Diagram Showing the Structure of Zero and Quasi-Dimensional Models

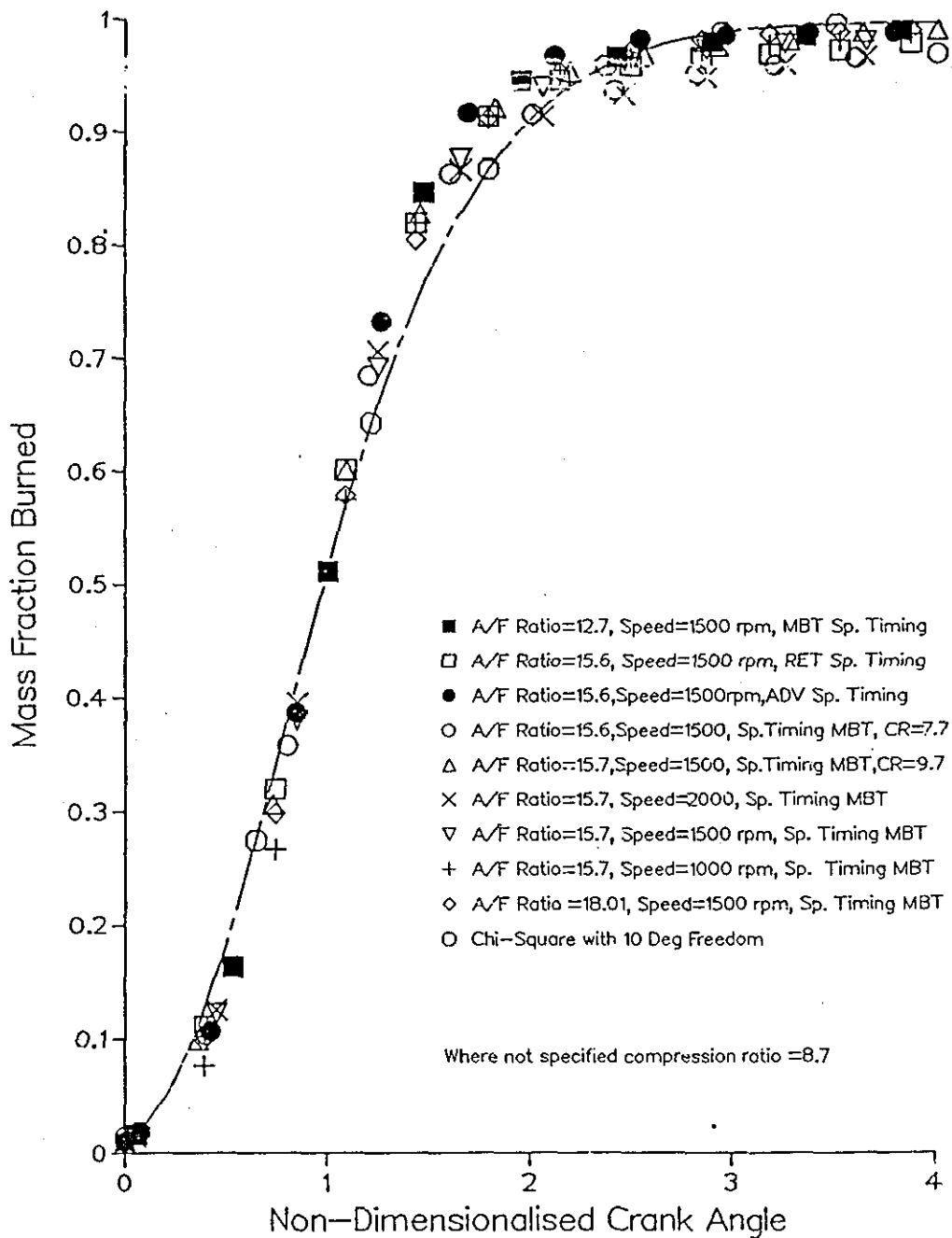


Fig. 3.2 Mass Fraction Burned v/s Non-Dimensionalised Crank Angle  
Data for Ricardo E6 Engine with 4 Star Petrol  
Chi-Square Distribution with 10 Degrees of Freedom

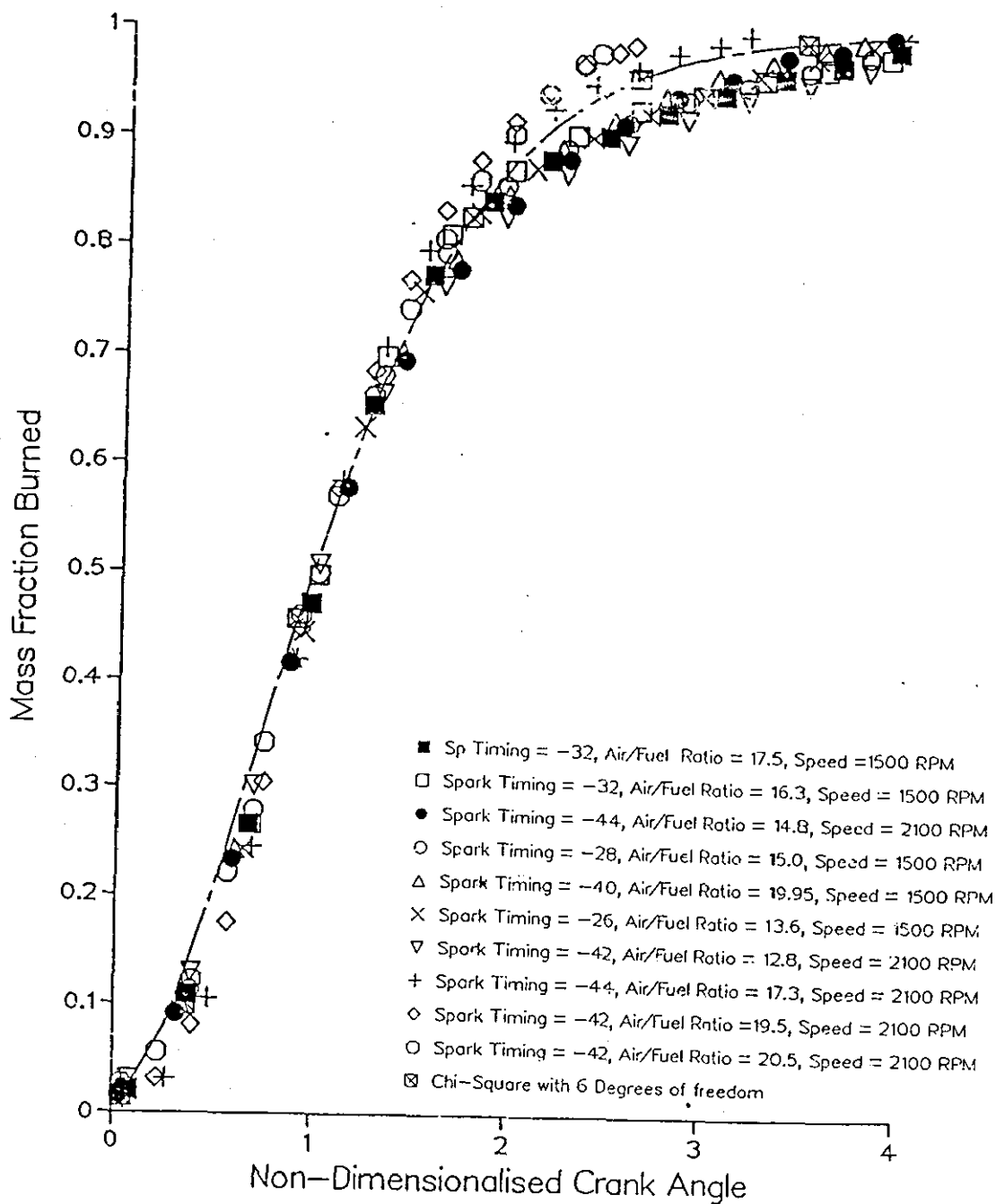


Fig.3.3 Mass Fraction Burned v/s Non-Dimensionalised Crank Angle  
Data For Ford Engine with Standard Head  
Chi-square Distribution with 6 Degrees of Freedom

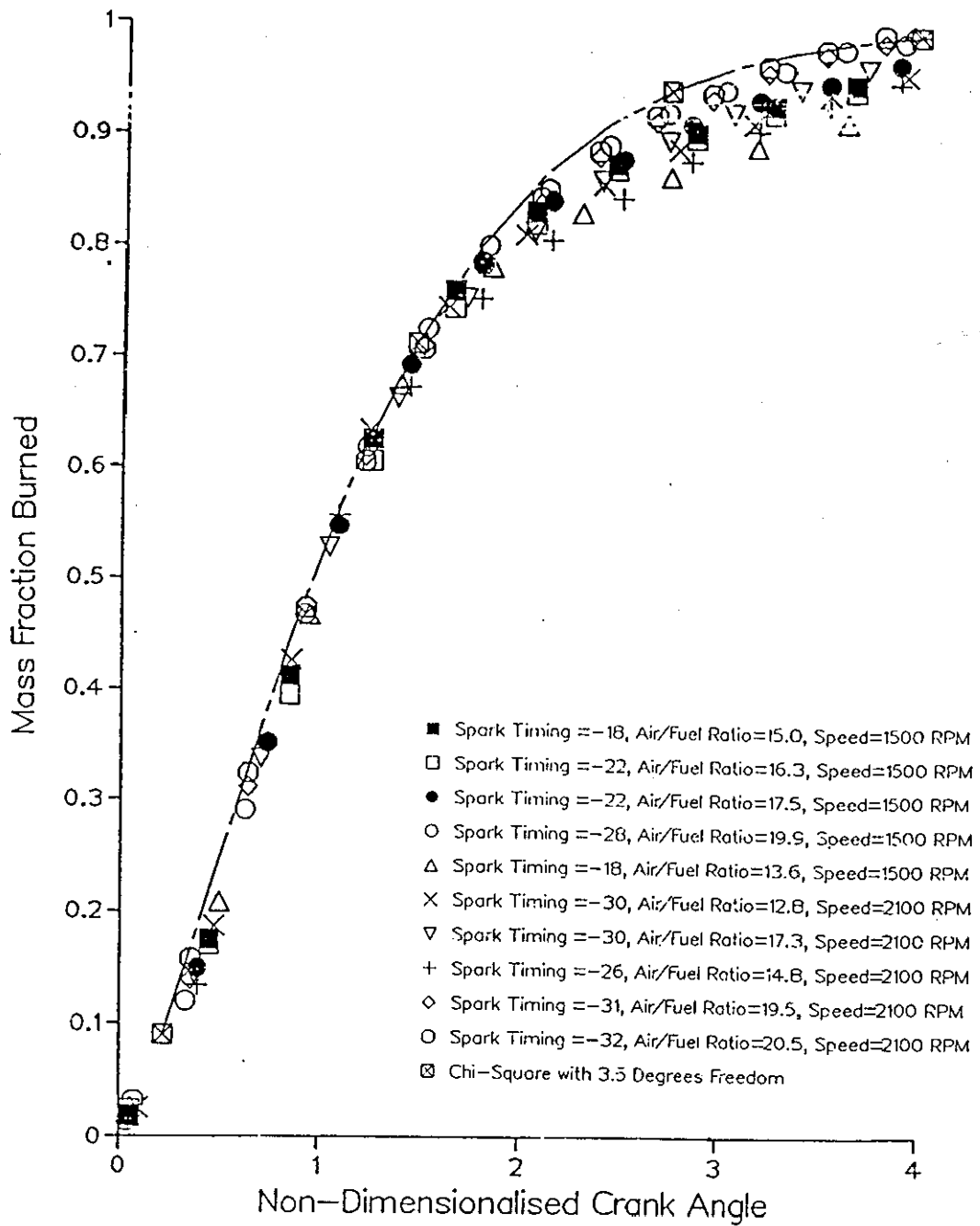


Fig.34 Mass Fraction Burned v/s Non-Dimensionalised Crank Angle  
Data For Ford Engine with May Head  
Chi-square Distribution with 3.5 Degrees of Freedom

# SUBROUTINE BLZKCK

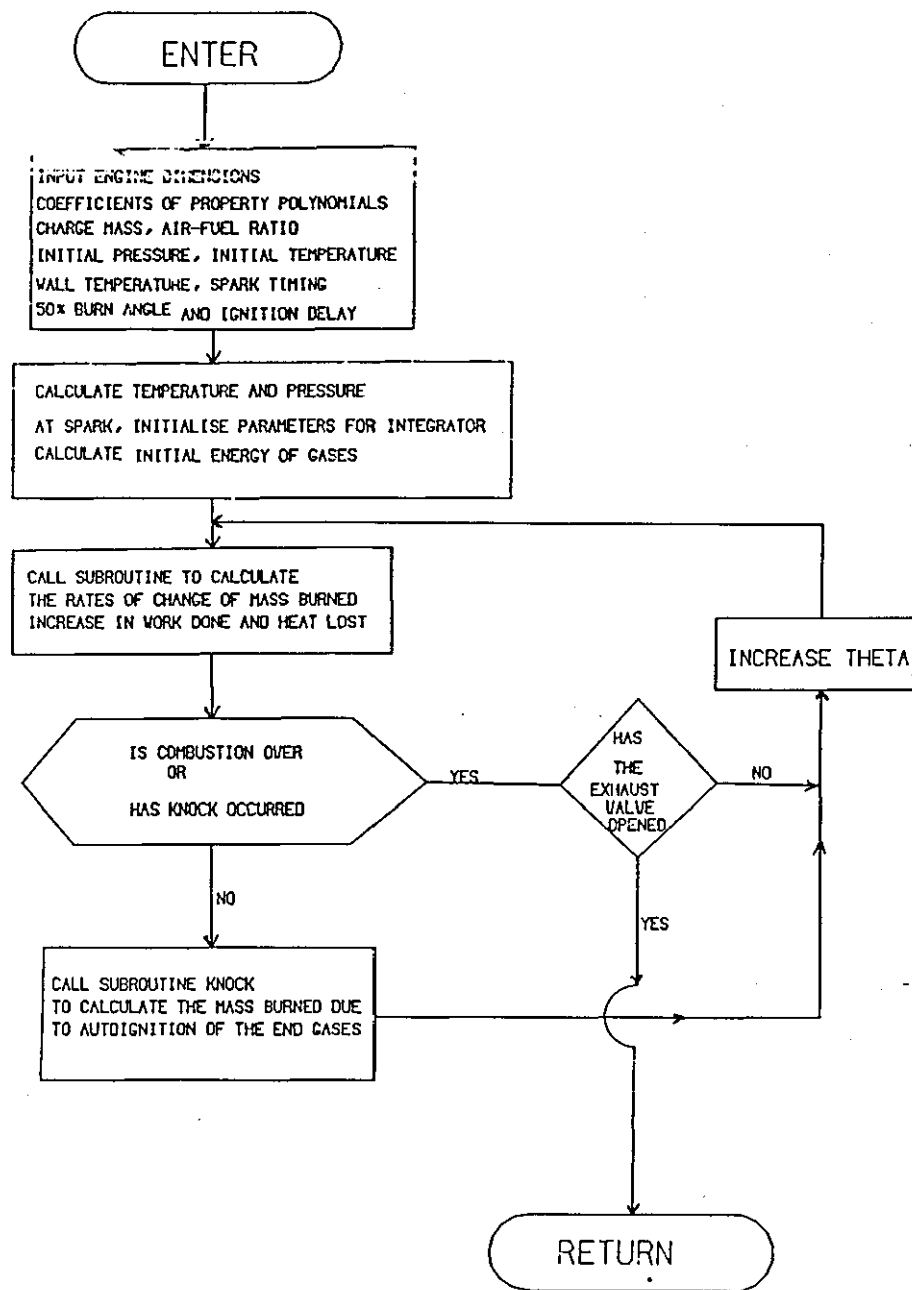


Fig. 3.5 Flow Chart of Main Subroutine

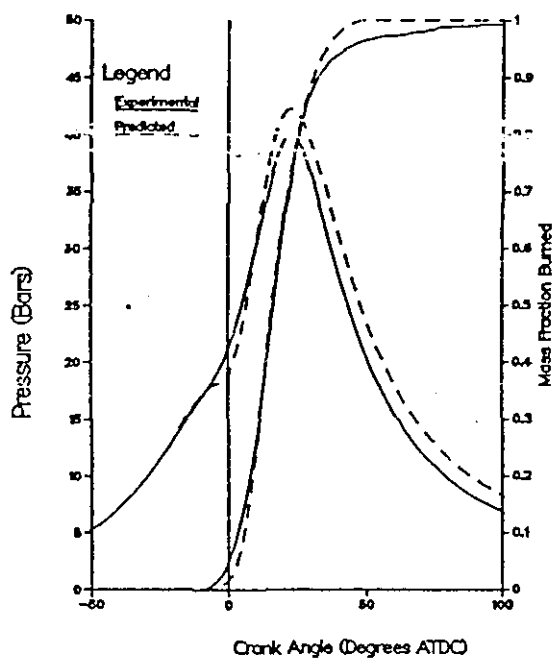


Fig. 3.6 Speed = 1000 rpm, Spark Timing =  $19^{\circ}$  BTDC (MBT)  
Air-Fuel Ratio = 15.69 Compression Ratio = 8.7

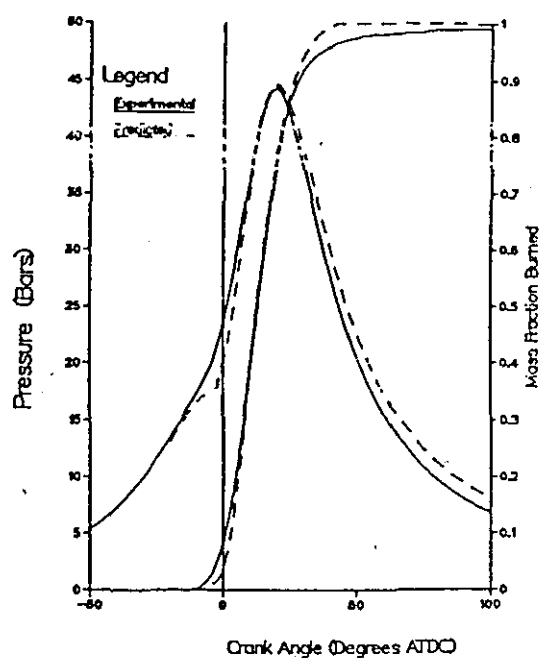


Fig. 3.7 Speed = 1500 rpm, Spark Timing =  $20^{\circ}$  BTDC (MBT)  
Air-Fuel Ratio = 15.58 Compression Ratio = 8.7

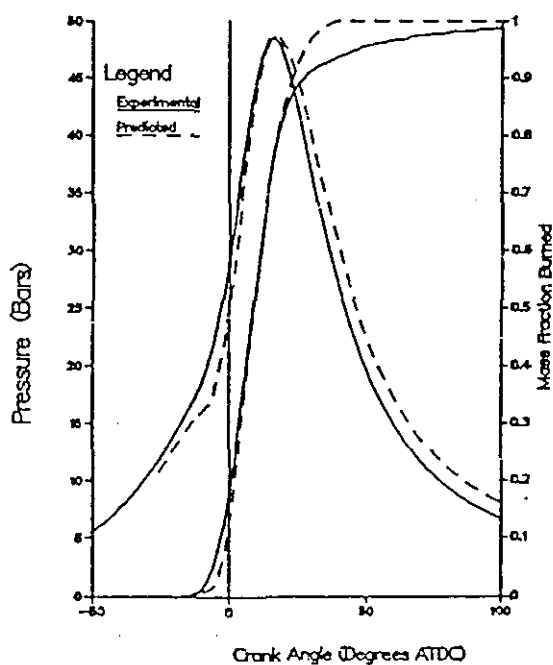


Fig. 3.8 Speed = 2000 rpm, Spark Timing =  $26^{\circ}$  BTDC (MBT)  
Air-Fuel Ratio = 15.69 Compression Ratio = 8.7

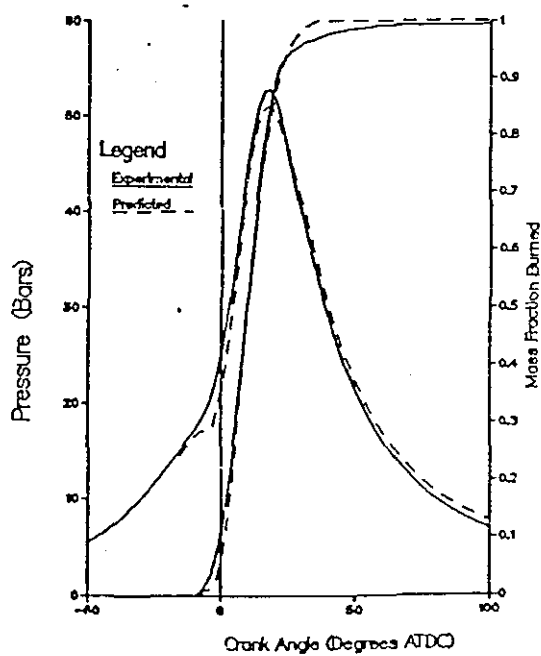


Fig. 3.9 Speed = 1500 rpm, Spark Timing =  $16^{\circ}$  BTDC (MBT)  
Air-Fuel Ratio = 12.72 Compression Ratio = 8.7

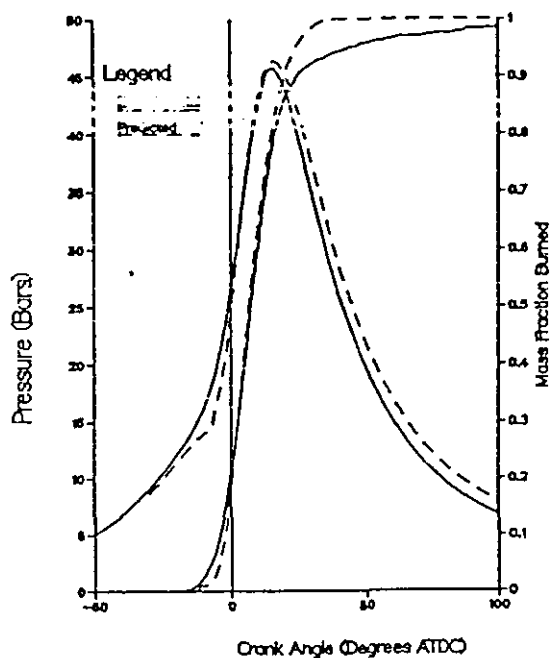


Fig. 3.10 Speed = 1500 rpm, Spark Timing = 30° BTDC (MBT)  
Air-Fuel Ratio = 15.69 Compression Ratio = 7.7

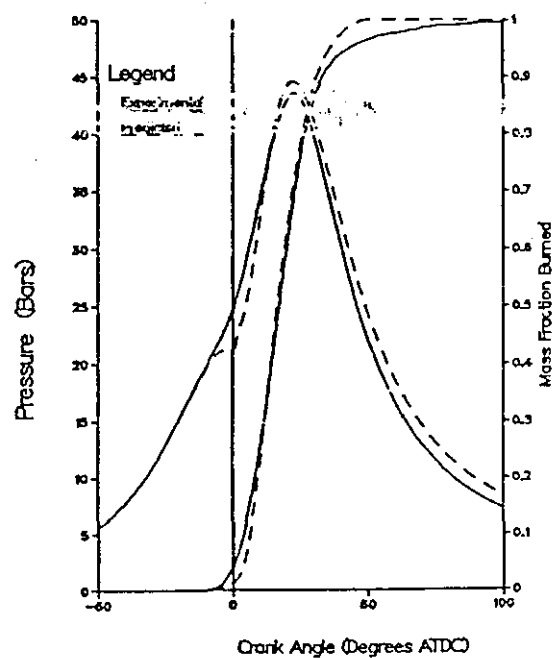


Fig. 3.11 Speed = 1500 rpm, Spark Timing = 16° BTDC (MBT)  
Air-Fuel Ratio = 15.69 Compression Ratio = 9.7

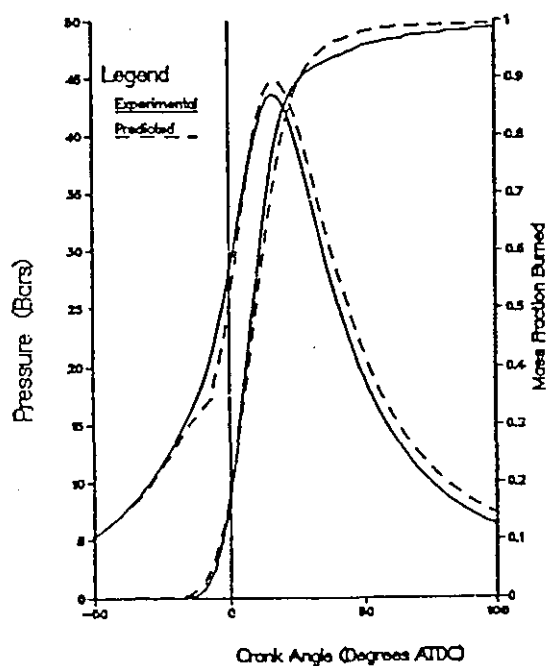


Fig. 3.12 Speed = 1500 rpm, Spark Timing = 36° BTDC (MBT)  
Air-Fuel Ratio = 13.10 Compression Ratio = 8.7

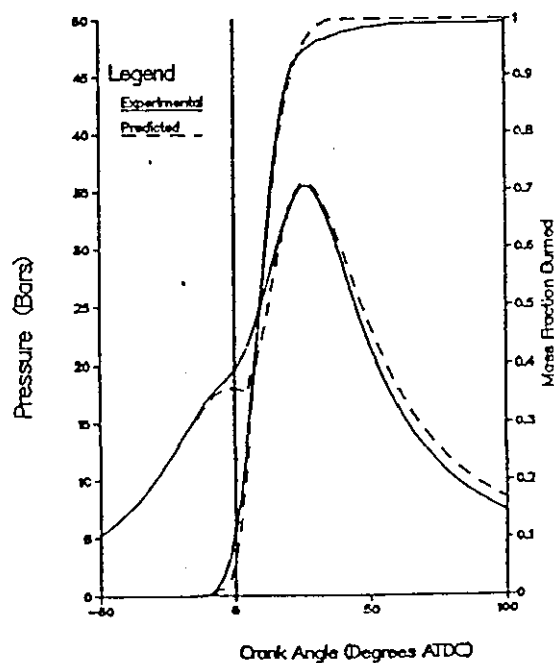


Fig. 3.13 Speed = 1500 rpm, Spark Timing = 14° BTDC (RET)  
Air-Fuel Ratio = 15.58 Compression Ratio = 8.7

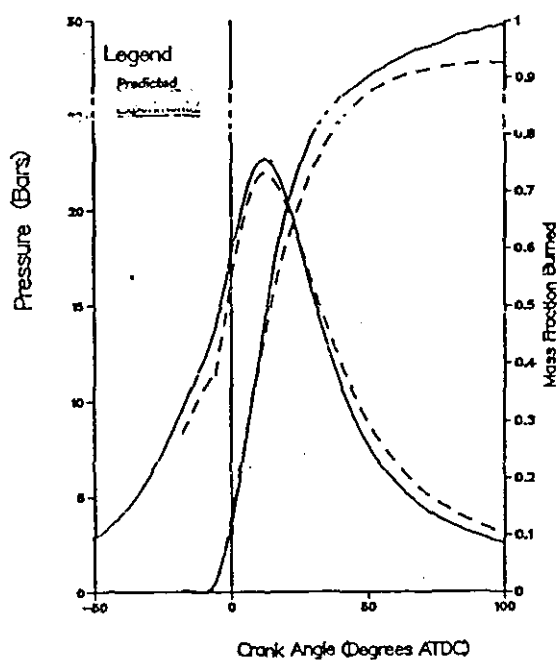


Fig. 3.14 Speed = 1500 rpm, Spark Timing =  $18^{\circ}$  BTDC (MBT)  
Air-Fuel Ratio = 15.0 Compression Ratio = 12.5

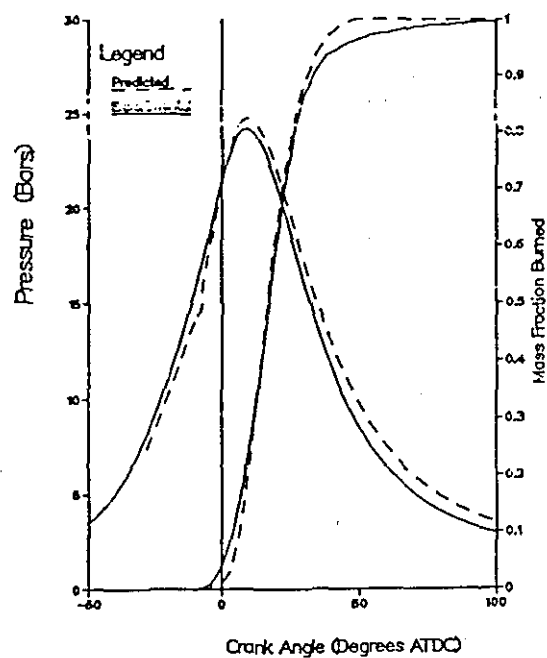


Fig. 3.15 Speed = 1500 rpm, Spark Timing =  $28^{\circ}$  BTDC (MBT)  
Air-Fuel Ratio = 19.95 Compression Ratio = 12.5

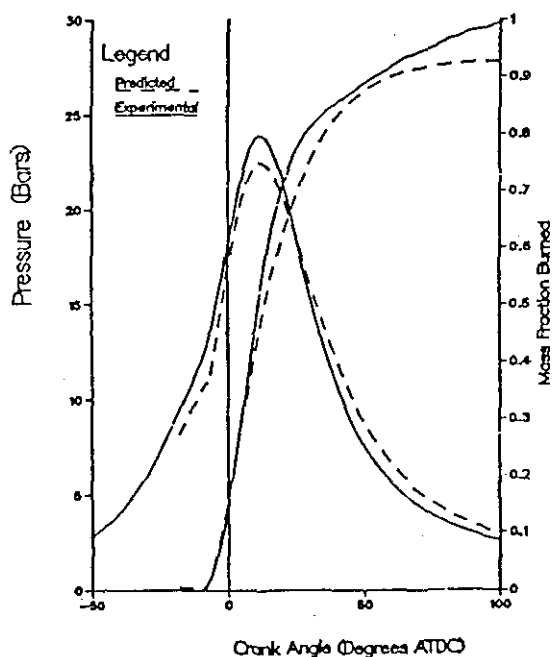


Fig. 3.16 Speed = 1500 rpm, Spark Timing =  $19^{\circ}$  BTDC (MBT)  
Air-Fuel Ratio = 13.6 Compression Ratio = 12.5

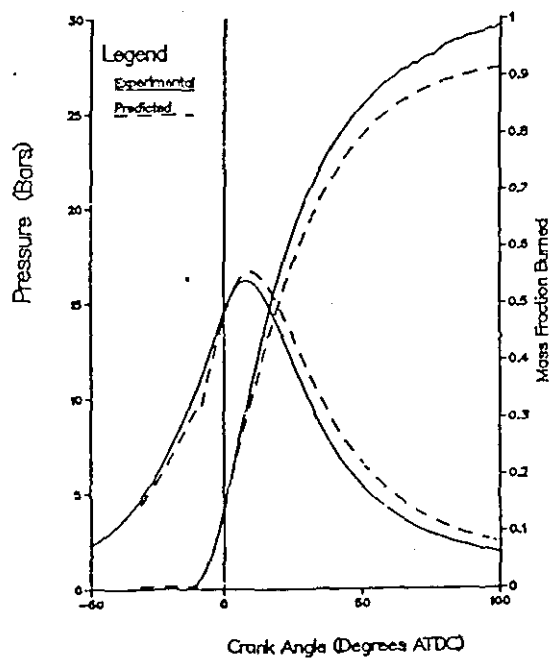


Fig. 3.17 Speed = 2100 rpm, Spark Timing =  $31^{\circ}$  BTDC (MBT)  
Air-Fuel Ratio = 19.5 Compression Ratio = 12.5

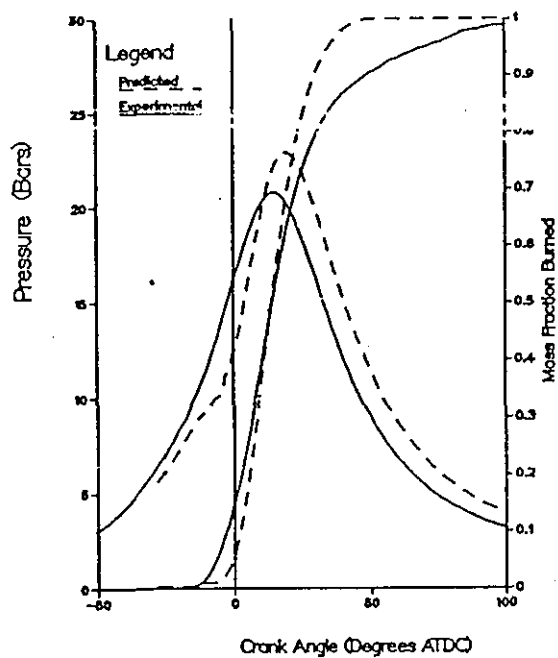


Fig. 3.18 Speed = 1500 rpm, Spark Timing =  $28^{\circ}$  BTDC (MBT)  
Air-Fuel Ratio = 15.0 Compression Ratio = 9.8

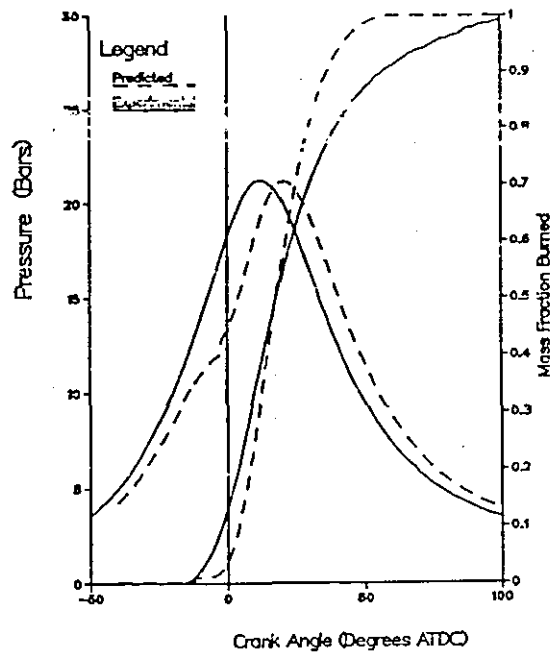


Fig. 3.19 Speed = 1500 rpm, Spark Timing =  $40^{\circ}$  BTDC (MBT)  
Air-Fuel Ratio = 19.95 Compression Ratio = 9.8

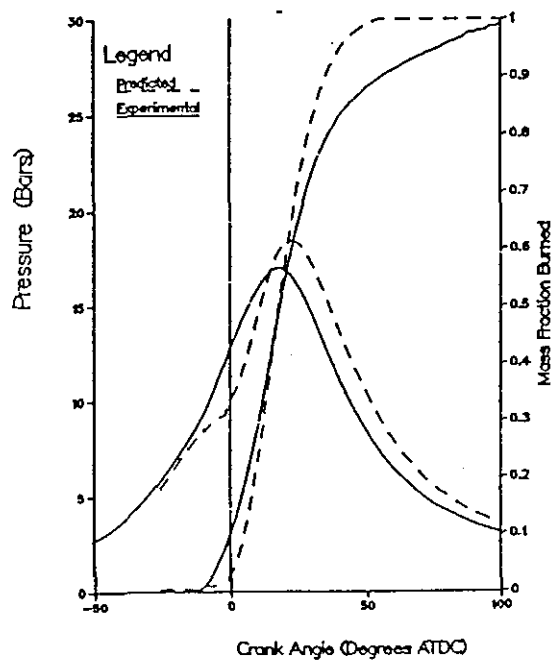


Fig. 3.20 Speed = 1500 rpm, Spark Timing =  $26^{\circ}$  BTDC (MBT)  
Air-Fuel Ratio = 13.6 Compression Ratio = 9.8

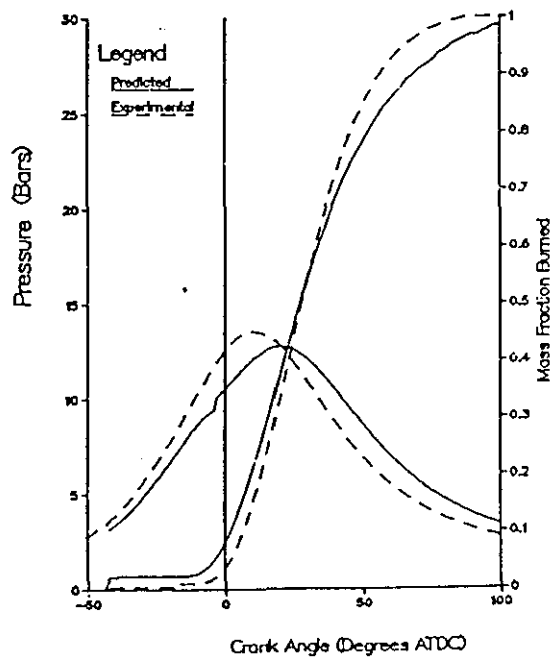


Fig. 3.21 Speed = 2100 rpm, Spark Timing =  $42^{\circ}$  BTDC (MBT)  
Air-Fuel Ratio = 19.5 Compression Ratio = 9.8

Subroutine Knock

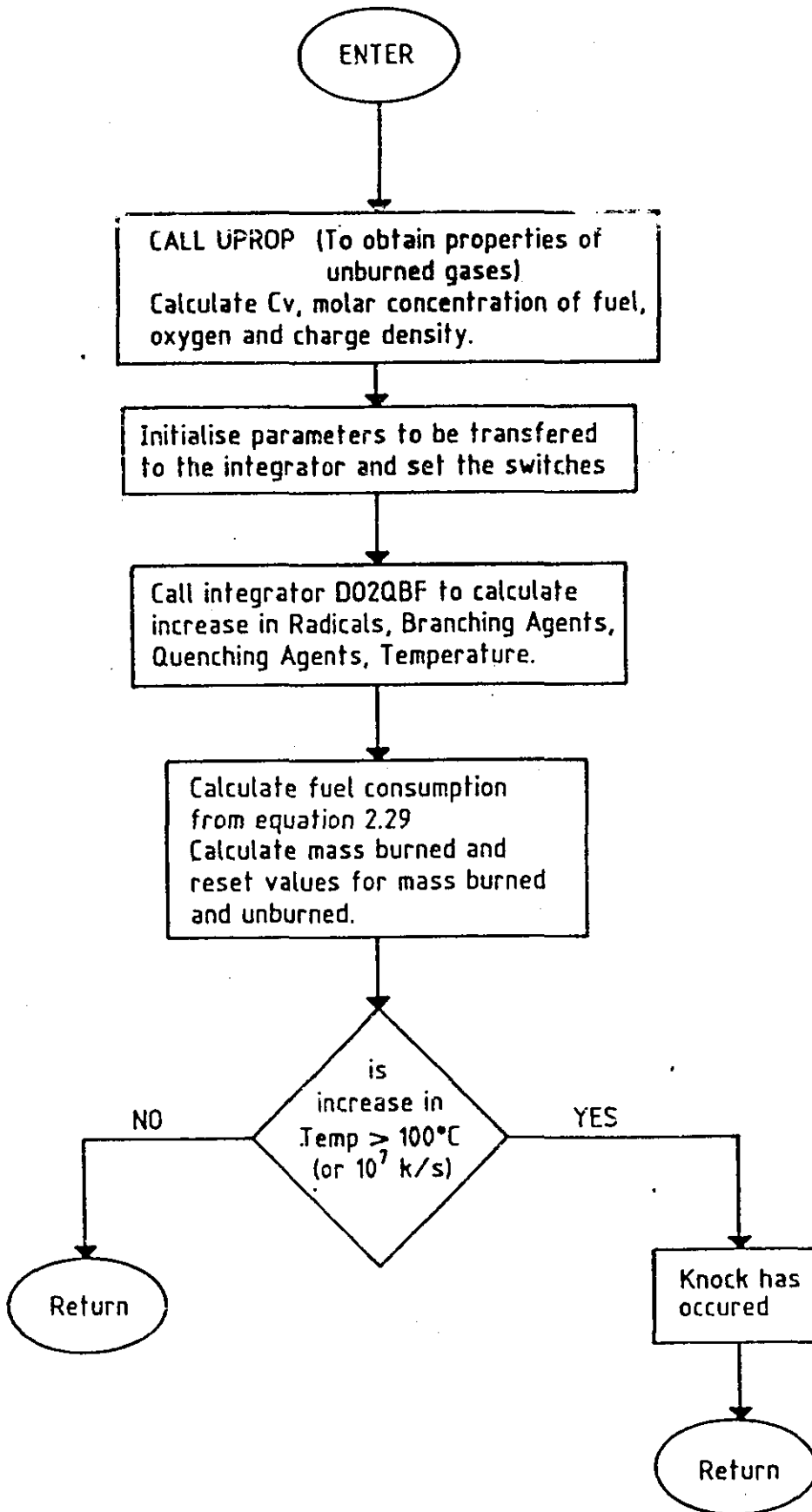
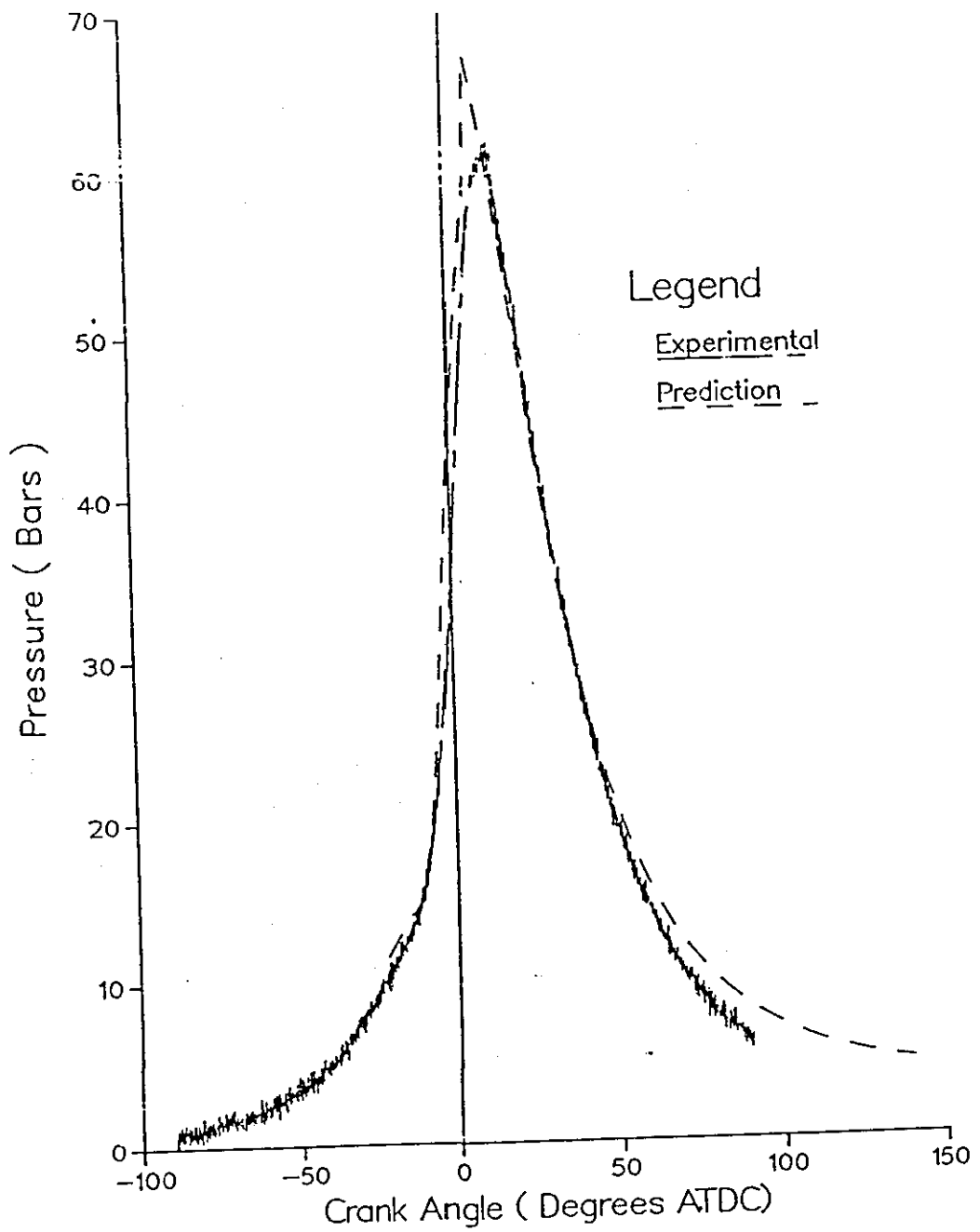
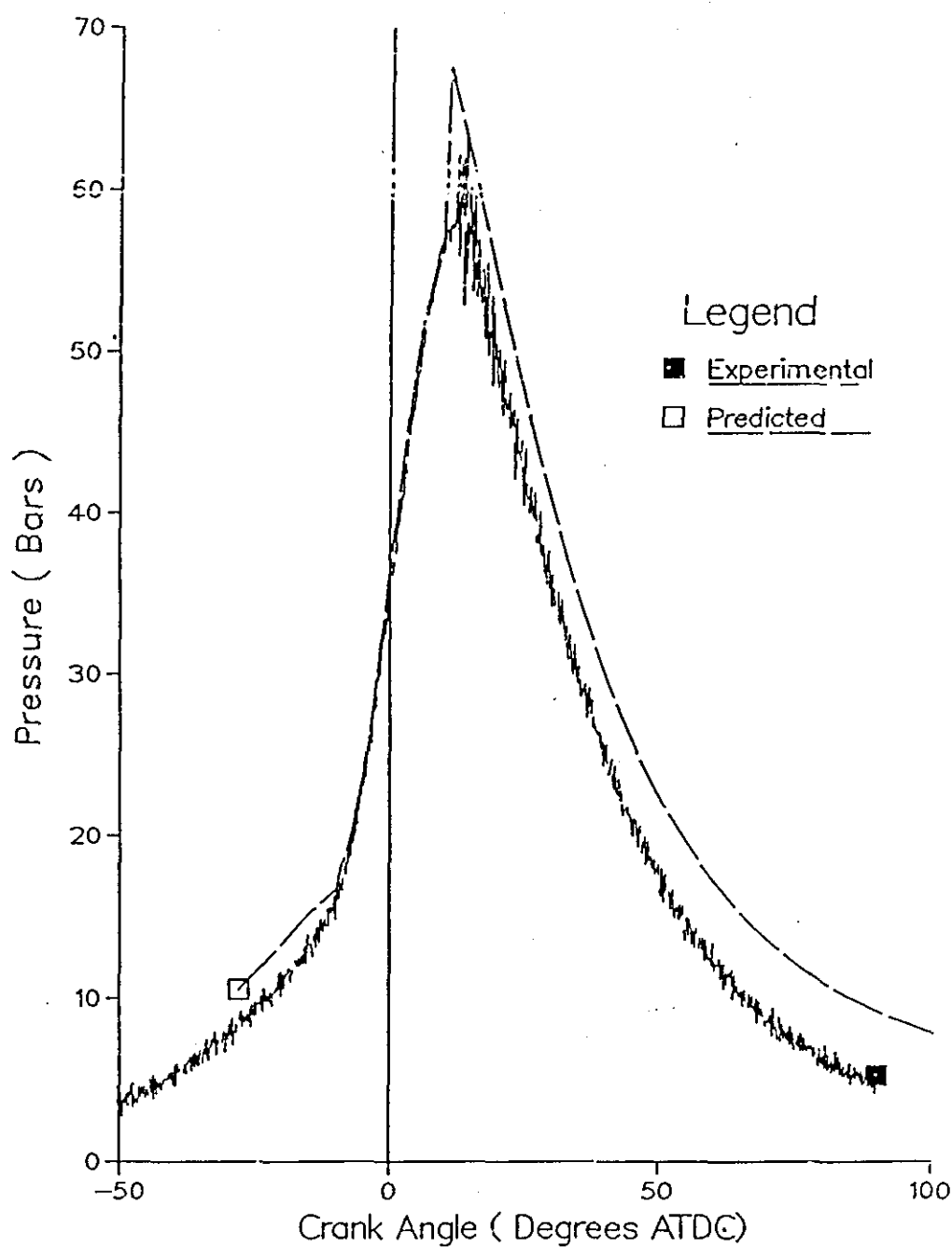


Fig. 3.22 FLOWCHART OF SUBROUTINE TO CALCULATE RISE IN TEMPERATURE AND MASS BURNED DUE TO AUTOIGNITION



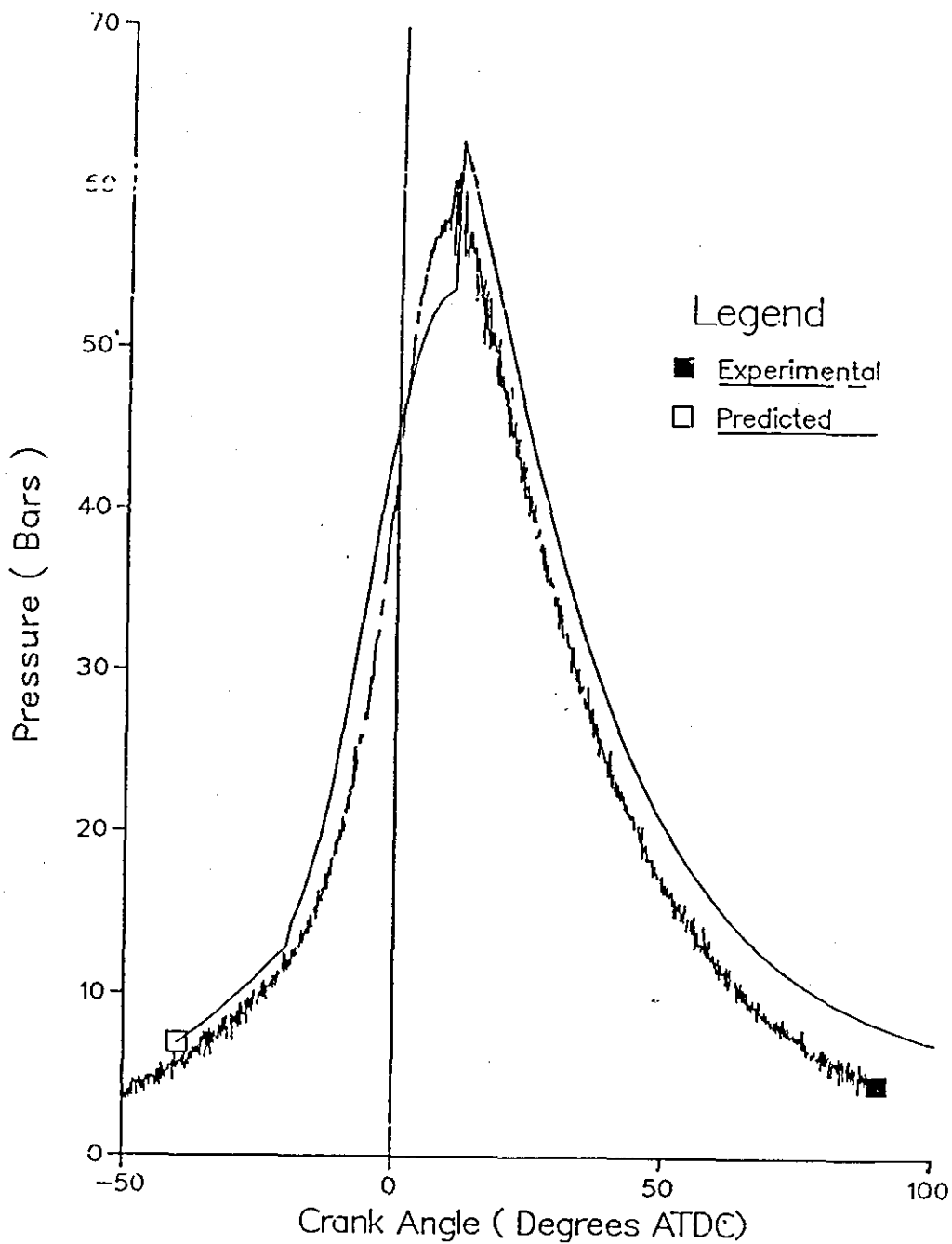
Spark Timing  $22^\circ$  BTDC ( $6^\circ$  Advanced)  
 Air-Fuel Ratio=13.0 Speed = 1500 RPM  
 Fuel Type --- Commercial 4\* Petrol  
 Ricardo E6 Engine ; Compression Ratio = 8.7

Fig. 3.23 Cylinder Pressure with Knock



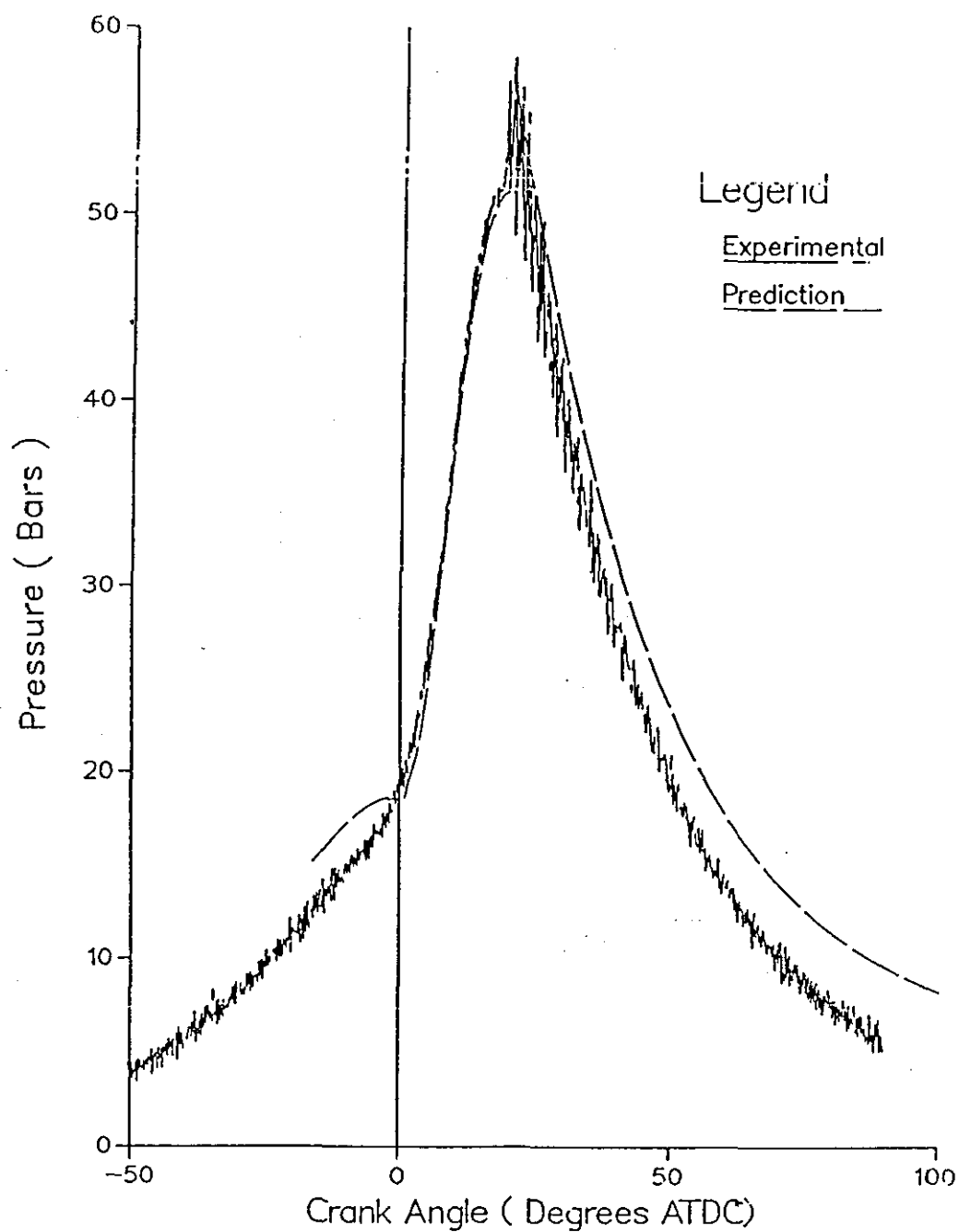
Spark Timing  $28^{\circ}$  BTDC ( $6^{\circ}$  Advanced)  
 Air-Fuel Ratio=15.5 Speed = 1500 RPM  
 Fuel Type — Commercial 4\* petrol  
 Ricardo E6 Engine ; Compression Ratio = 8.7

Fig. 3.24 Cylinder Pressure with Knock



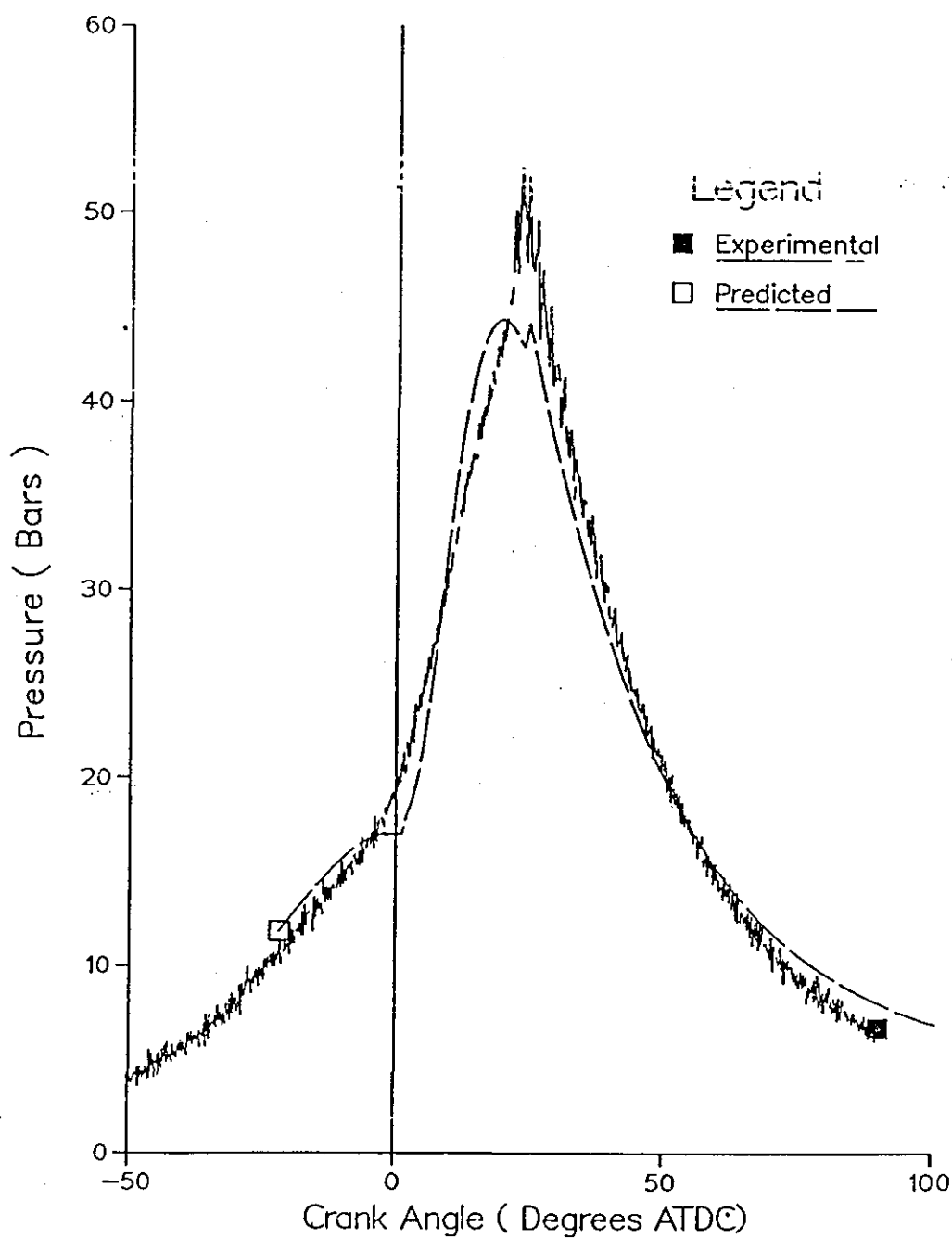
Spark Timing  $40^{\circ}$  BTDC ( $6^{\circ}$  Advanced)  
 Air-Fuel Ratio=17.6 Speed = 1500 RPM  
 Fuel Type --- Commercial 4\* petrol  
 Ricardo E6 Engine ; Compression Ratio = 8.7

Fig. 3.25 Cylinder Pressure with Knock



- Spark Timing  $16^\circ$  BTDC ( $6^\circ$  Advanced)
- Air-Fuel Ratio=15.0 Speed = 1500 RPM
- Fuel Type --- 90% iso-octane + 10% n-heptane
- Ricardo E6 Engine ; Compression Ratio = 8.7

Fig. 3.26 Cylinder Pressure with Knock



Spark Timing  $22^{\circ}$  BTDC ( $6^{\circ}$  Advanced )  
 Air-Fuel Ratio=17.6 Speed = 1500 RPM  
 Fuel Type --- 90% ISO-OCTANE + 10% n-Heptane  
 Ricardo E6 Engine ; Compression ratio = 8.7

Fig. 3.27 Cylinder Pressure with Knock

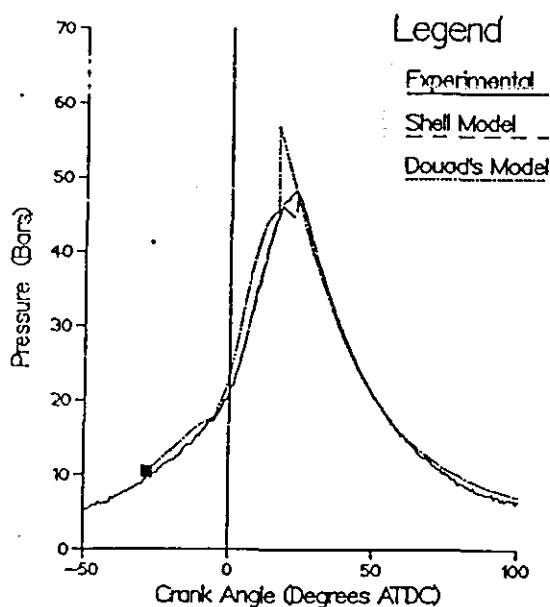


Fig. 3.28 Spark Timing  $28^\circ$  BTDC  
Air-Fuel Ratio = 18.4

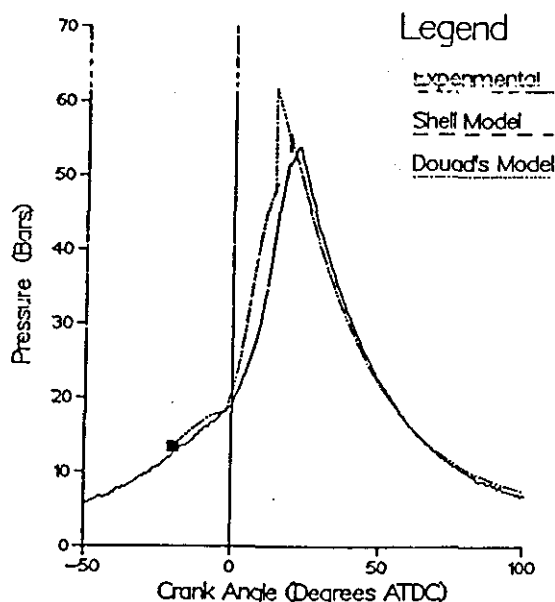


Fig. 3.29 Spark Timing  $20^\circ$  BTDC  
Air-Fuel Ratio = 16.9

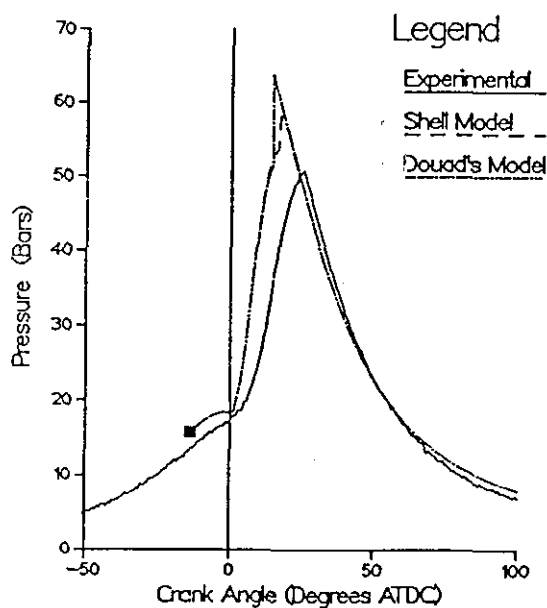


Fig. 3.30 Spark Timing  $14^\circ$  BTDC  
Air-Fuel Ratio = 15.42

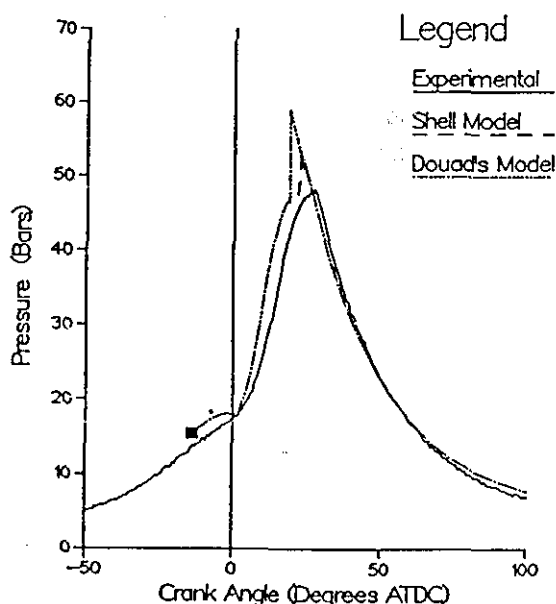


Fig. 3.31 Spark Timing  $14^\circ$  BTDC  
Air-Fuel Ratio = 11.96

Ricardo E6 Engine, Fuel — 90 RON PRF  
Compression Ratio = 8.7, Speed = 1500 RPM

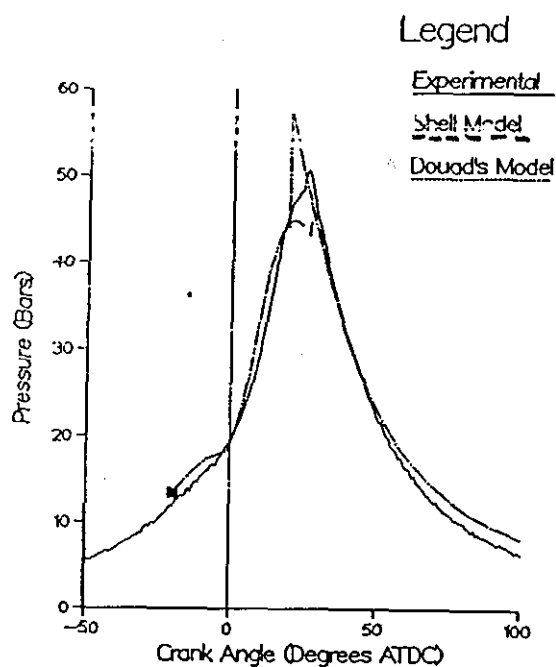


Fig. 3.32 Spark Timing  $20^{\circ}$  BTDC  
Air-Fuel Ratio = 15.11 Speed = 1750 RPM

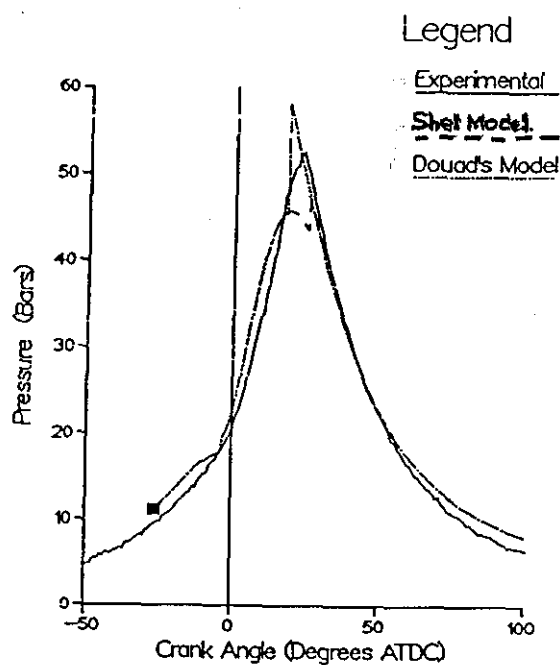


Fig. 3.33 Spark Timing  $26^{\circ}$  BTDC  
Air-Fuel Ratio = 15.67 Speed = 2000 RPM

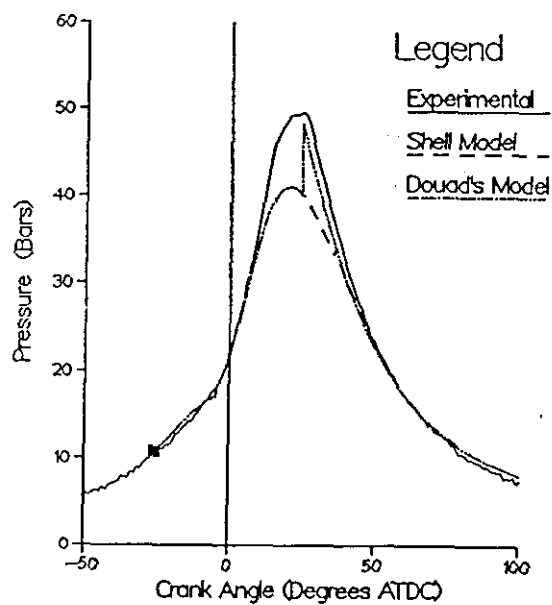


Fig. 3.34 Spark Timing  $26^{\circ}$  BTDC  
Air-Fuel Ratio = 15.31 Speed = 2250 RPM

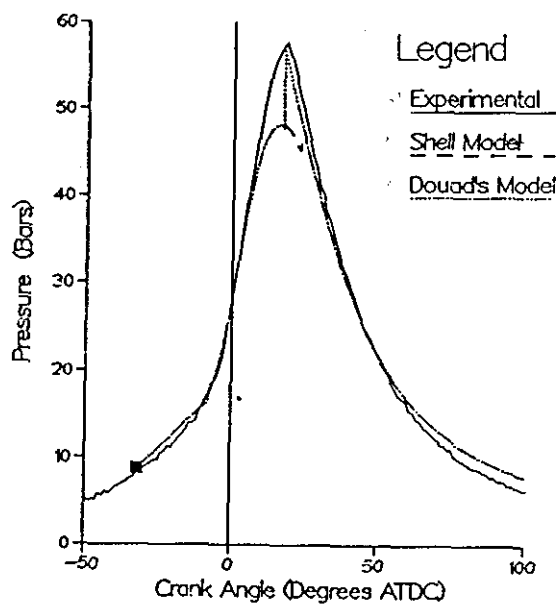


Fig. 3.35 Spark Timing  $32^{\circ}$  BTDC  
Air-Fuel Ratio = 15.44 Speed = 2500 RPM

Ricardo E6 Engine, Fuel — 90 RON PRF  
Compression Ratio = 8.7

## Simulated Knock Response with Increasing EGR

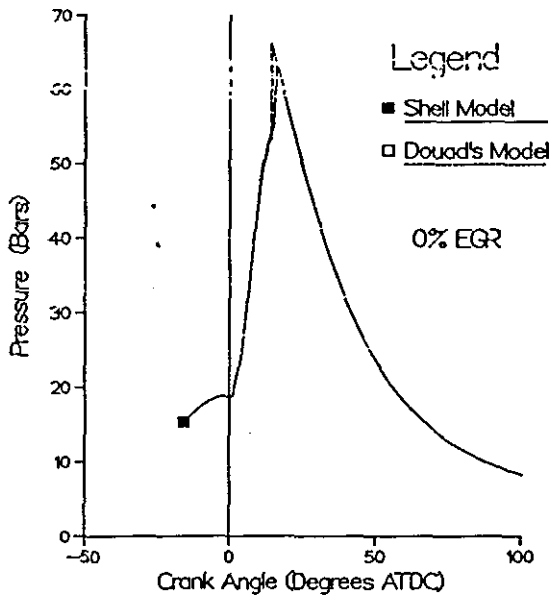


Fig. 3.36 Spark Timing  $16^\circ$  BTDC  
 Air-Fuel Ratio = 15.2

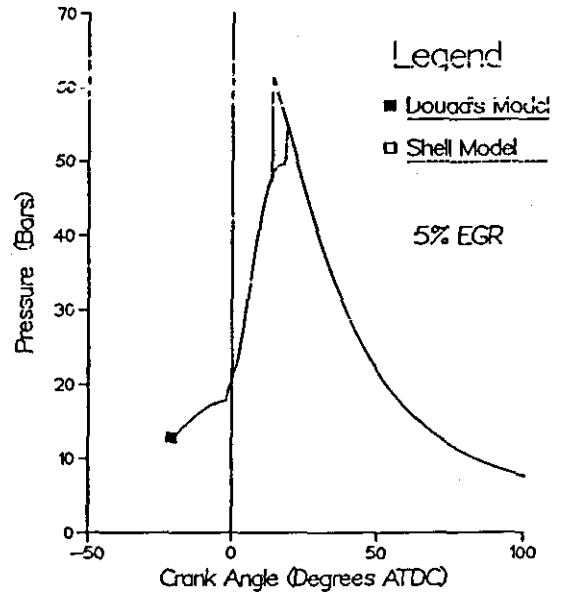


Fig. 3.37 Spark Timing  $21^\circ$  BTDC  
 Air-Fuel Ratio = 15.2

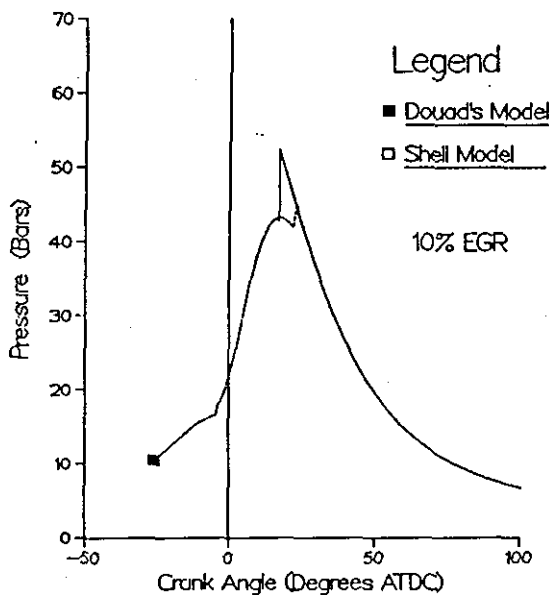


Fig. 3.38 Spark Timing  $26^\circ$  BTDC  
 Air-Fuel Ratio = 15.2

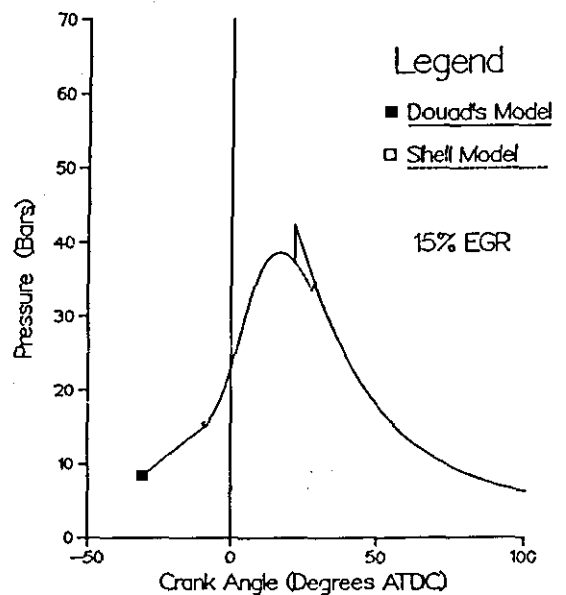


Fig. 3.39 Spark Timing  $31^\circ$  BTDC  
 Air-Fuel Ratio = 15.2

Ricardo E6 Engine, Fuel — 90 RON PRF  
 Compression Ratio = 8.7  
 Speed = 1500 RPM

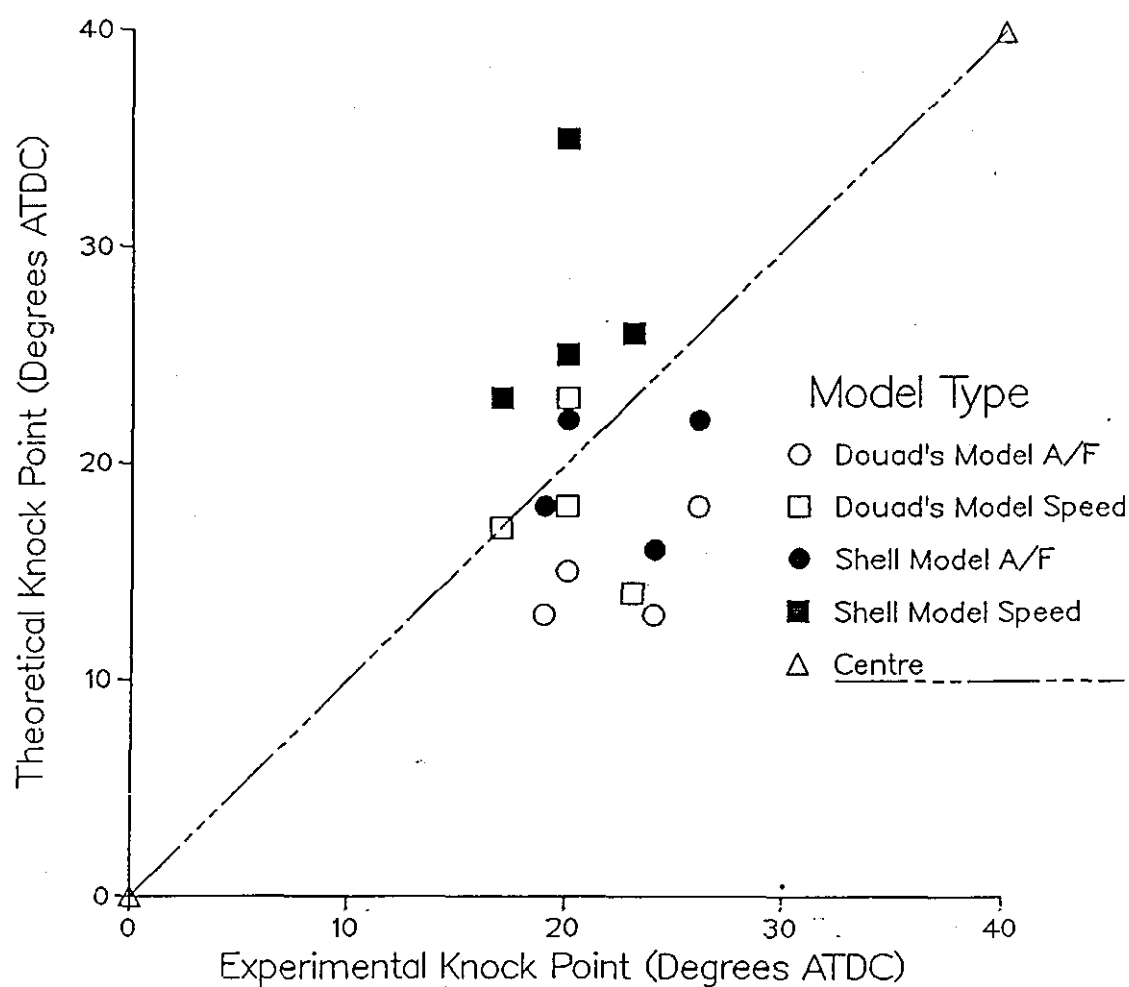


Fig. 3.40 Plot of Predicted Knock Point  
v/s  
Measured Knock Point  
Fuel Type --- 90 RON PRF

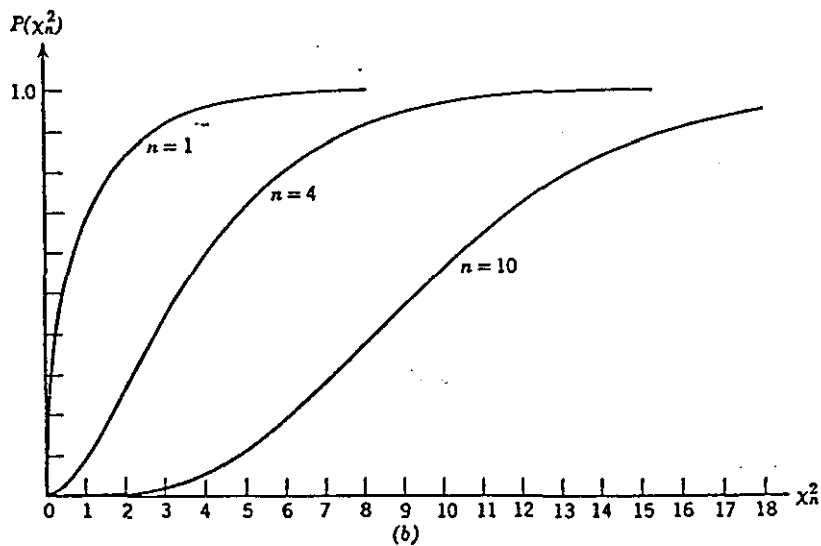
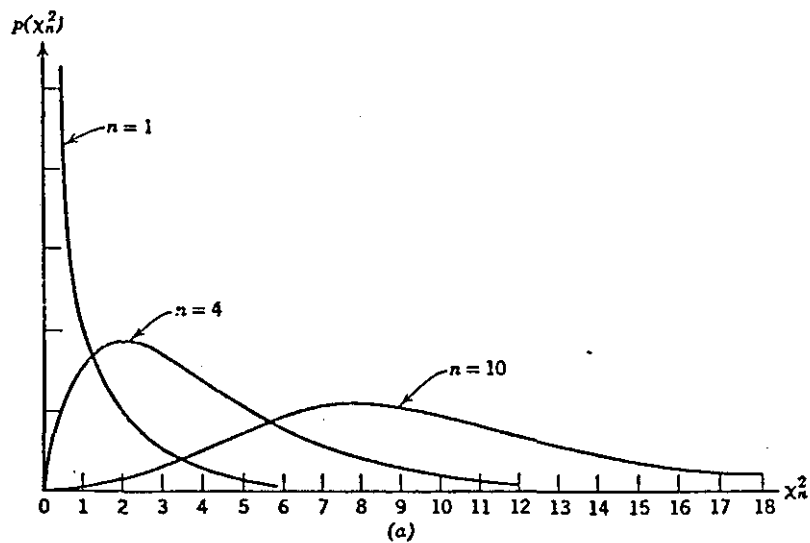


Fig 3.41 Chi-square probability density and distribution functions. (a) Probability density function. (b) Probability distribution function.

## Chapter IV

### DATA ACQUISITION AND ANALYSIS

#### 4.1. Introduction

This chapter deals with the measurement and analysis of pressure and ionization probe data. The first section deals with the measurement and analysis of the pressure data while the second section deals with the measurement and analysis of the flame ionization probe data.

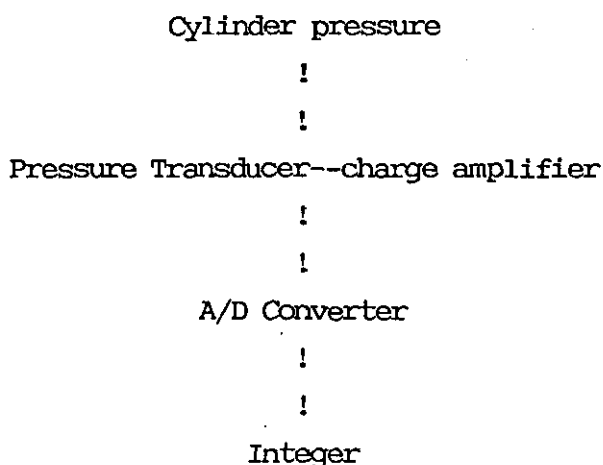
The computer used for the on line real time acquisition of pressure data was a Minc-23 micro-computer. The ionization probe data was recorded on a 4 channel FM tape recorder (relevant data given in Table 4.1) and digitized using a Nicolet 660 A Dual-Channel Fast Fourier Transform (FFT) analyser.

#### 4.2. Pressure Data Measurement and Analysis

The cylinder pressure was measured using a Kistler Type 601A piezo-electric pressure transducer and amplified using a Kistler Type 5001 charge amplifier. Calibration of the transducer and charge amplifier was done with reference pressures supplied with a dead weight tester, and the charge amplifier output monitored with a digital voltmeter. The pressure transducer was calibrated from 1 bar to 10 bars in steps of 1 bar and from 10 bar to 50 bar in steps of 10 bar. The correlation between the applied pressure and the output voltage was found to be linear within the range under consideration. A long time constant was used on the charge amplifier during the calibration but was switched on a short time constant during operation with engine pressure data.

#### 4.3. Dynamic Pressure Measurement in Engine

The pressure signal was digitized in synchronization with engine crank angle at every 2 degree interval. The conversion for the pressure signal took the following steps:



Where the integer is a value between 2048 and -2047 corresponding to an input voltage to the analog/digital converter of 5 or -5 volts.

The piezo-electric transducer measures relative rather than absolute pressures. The absolute values of each integer obtained in the data acquisition process was directly related to the absolute cylinder pressure. The integer obtained from the A/D converter was multiplied by a calibration factor (obtained from the dead weight tests) to obtain the relative pressure in bars. The absolute pressure at each crank angle was then obtained by adding a constant amount to the relative cylinder pressure at each crank angle. The amount to be added was determined by assuming that the cylinder pressure at bottom dead centre (BDC) of intake was equal to the mean intake manifold absolute pressure. This technique is similar to that adopted by Lancaster [56]. The difference between the mean intake manifold pressure and the relative pressure at BDC of intake was then added to each of the 360 points making up the complete cycle.

The computer was capable of digitizing 16 consecutive cycles at a

time before it was necessary to transfer the data from memory to disks for storage. Fig 4.1 is a sample plot of sixteen consecutive cycles plotted in a 3-Dimensional form showing cyclic variation. Fig. 4.2 is a plot of the minimum, average and maximum cycles of a total of 4 sets of 16 cycles each.

The synchronization of the pressure acquisition with the engine crank angle made it possible to associate an instantaneous cylinder volume with each pressure measurement. Thus enabling the calculation of mass fraction burned according to Appendix "A".

The pressure fluctuations during trace knock and light knock being higher than the acquisition rate of the computer, it was necessary to record the pressure signal on a tape recorder and then digitize it using the Nicolet Fast Fourier transform analyser. The highest rate at which a signal can be digitized using the Fast acquire program on the Minc-23 computer is 16.129 KHz , which would correspond to 1.79 points per degree crank angle if the engine were running at 1500 rpm. This rate is too low for a good resolution of the knocking period in a cycle. The highest rate at which an analog signal can be digitized on the Nicolet FFT analyser is 256 KHz. The Nicolet FFT analyser acquires 1024 points at any selected frequency thus limiting the window width for any given frequency. The time window to acquire 1024 points at 256 KHz is 0.004 seconds which would correspond to 36 degrees crank angle at 1500 rpm. To obtain a cycle from spark to exhaust valve opening so as to be able to compare with the output from the computer program, a data acquisition rate of 51.2 KHz was selected, which corresponds to a window of 0.02 seconds or 180 degrees crank angle at 1500 rpm. The Nicolet FFT analyser was triggered at 90 degrees before top dead centre of compression thus obtaining data till 90 degrees after top dead centre hence including the period where knock would generally occur.

#### 4.4. Application of Flame Ionization Probe to Engine studies

Flame ionization probes have been used to detect flame proximity with great success [57-60], Blizzard and Keck [43] used them to measure the position of the flame front as a function of crank angle. The existence of ions in hydrocarbon flames has been recognised since Calcote [61] showed that the increase in the orders of magnitude of carbon ions during combustion of hydrocarbon fuels gives rise to a similar increase in the conductivity of the reacting gases. This mechanism thus makes it possible to measure both the arrival and the degree of relaxation (i.e. reverse motion of the flame front due to oscillations) at a given point as a function of time, using the gas as a variable resistance in a detector circuit.

Flame ionization probes have been used by Denniston et. al. [62] to measure the most probable position of a combustion wave within the flame brush of a flame from a Bunsen burner. The probe used was a single electrode probe biased negatively by approximately 90 volts, therefore collecting only positive ions. Fig 4.3 shows the ionization density associated with a laminar combustion wave. It is seen that the highest level of ion concentration is just behind the flame front (i.e. the most luminous zone) and that it falls off sharply. This property of a sharp demarkation of the ion concentration about the flame front has been used by Denniston et. al. [62] to measure the most probable position of a combustion wave thus being able to determine a reference surface to calculate burning velocities, also they were able to determine the rms displacement of the wave from its most probable position. Instantaneous discontinuities in the ionization sheath could be seen from the fluctuations in the response of the probe thus giving a measure of flame stability.

The capability of the ionization probe to respond to the variation in the ionization levels led Denniston et. al. [62] to attempt measuring the combustion wave frequency with the aid of an ionization probe. To study the response of the probe to a

fluctuating combustion wave, a level of turbulence was created in the flame by setting the laminar flame into simple harmonic horizontal motion by means of a loud speaker driven by a sine wave oscillator. Fig. 4.4 shows the probe response before and after being passed through a pulse discriminator. The response before the discriminator shows peaks and valleys of varying heights. The variations of the signal is considered to be due to variable length of wire exposed to the low ion concentrations of the burned gas. The probability that the wire could be exposed to more than one surface of the flame at one time is envisaged.

Winch and Mayes [70] used a spark plug to act as an ionization probe (they called it an ionization gap) and studied the response of engine combustion with and without a voltage level applied across the gap. The use of the ionization gap was essentially to identify the occurrence of preignition.

Iinuma [71] made a detailed study of the response of an ionization gap to different types of combustion. Here too as in the case of Winch and Mayes [70], a spark plug was used to act as the ionization gap, thus implying that the gap was located close to the cylinder wall. The power supply to the probe was connected in series with a resistor as shown in Fig.(4.27). The voltage produced across the resistor by an ionization current was applied to an oscilloscope, the voltage gave the momentary variations in current flow across the gap.

The ionization current was found to be proportional to the source voltage in the range 1.5 V to 100 V only, though no mention is made of the highest voltage tested. The resistance in the circuit was found to effect the time over which the current trace could be observed on the oscilloscope.

An interesting feature noticed by Iinuma was that the peak values as well as the pattern of the current did not change significantly with change in the gap distance over a range 0.5mm to 2.0mm. A lack off

effect of a change in the polarity on the probe response is also reported.

The fact that the combustion waves effect the ionization level has been shown by Denniston et. al. [62], therefore the ionization current, which is dependent not only on the formation of ions and their lives but also on the structure and propagating characteristics of the combustion wave, would vary with engine conditions through these phenomenon. Iinuma found the peak current showed a maximum value at slightly rich mixtures and not at chemically correct mixtures. The slower burning rate for rich and lean mixtures were inferred from an increase in the duration of the current level.

Iinuma found the compression ratio to have no effect on the ionization current except when the engine set into knock. In an early paper Charch et. al. [69] found that the electrical conductivity of the combustion gases increased with the occurrence of knock, while Iinuma [71] found that the ionization current tended to increase abnormally just before audible knock was recorded. Kumagai and Kudo [58] also reported the occurrence of fluctuating current levels at the time of knock.

Using a two electrode probe in a closed vessel Ohigashi et.al[63]. obtained single peak response in laminar flames , and multiple peak responses with turbulent flames (Fig.4.5). Assuming that the laminar flame comprises of a single elementary zone of combustion, the turbulent flames are considered to be made up of several such reaction zones. The ion current in turbulence flames which has several peaks may thus be obtained by random superimposition of the individual currents of multiple "elementary zones of combustion"( Fig. 4.6).

The presence of multiple peaks in probe responses when applied to engine combustion studies has been reported by Harrow [64], Arrigoni et. al.[60] and Warren and Hinkemp [59]. The first peak in a

multiple peak response is considered to be due to the passage of the flame front thus being related to the chemi-ionization whereas the second peak is believed to be due to the reionization of the burnt gases at peak pressures and higher temperatures. In cases of knocking combustion pressure fluctuations start much before the actual occurrence of knock [64], Kumagai and Kudo [58] found that these pressure fluctuations that occur in the combustion chamber usually create changes in the ionization current at the probe electrodes, they therefore used this feature as a very convenient means of knock detection. In the present investigation it is this feature of flame ionization in combination with the fact that the ionization level varies with the frequency [62] that is used to obtain information regarding the flame front instability.

Any given random signal is considered to comprise of a set of pure signals at specific frequencies, the method of obtaining these frequencies is known as spectral analysis. One of the most common ways of obtaining the spectral content of any given signal is by performing the Fourier Transformation.

Following Ohigashi et. al.'s [63] argument that the signal contains a set of individual signals that are superimposed one on the other, spectral analysis of the signal would give the various frequencies present in the signal with their corresponding energy content. The approach is similar to that proposed by Dryden [65] for studying the energy distribution in hot wire anemometer signals to obtain a detailed picture of the spectral description of turbulence in a fluid flow. Though the ionization probe has the capability of recording very high frequencies Haghgoole et. al. [84] show the use of the ionization probe to record signals with a high frequency cut-off at 25KHz.

#### 4.5. Flame Ionization Probe : Principle of Operation.

The general principle of operation of a two-electrode flame ionization probe can be explained by reference to the circuit diagram in Fig. 4.7. The two electrodes A and B are maintained at a potential difference of 240 volts. The resistance R is fixed after varying the voltage V so as to be able to obtain the highest response for a particular condition. The voltage across the resistance R gives the variation of ion density across the electrodes A and B. The voltage and resistance found to give the best response were 240 Volts and 60 KOhms. The passing of a flame front or reaction zone which has a higher conductivity as compared to the normal charge due to the high ionization level would reduce the resistance between the two electrodes thus completing the circuit and displaying a voltage drop across the resistance R which would be stored on an oscilloscope and later photographed (in the case of Bomb Studies) or recorded on the Tape recorder for later digitization and analysis

#### 4.6. Ionization Probe Construction and Manufacture

The salient design details of the probes used in this investigation are shown in Fig. 4.8. The electrodes used were made of Tungsten. The Tungsten wires were passed through a ceramic tube with two holes spaced 2mm apart. This ceramic tube was then passed through a steel tube for restraint. The leads were connected to a co-axial lead with jack connections on the flying leads of a BNC type. The probes were checked for insulation between the two electrodes a resistance of X megaohms was considered a suitable insulation , a simple resistance box and a 240 Volt DC source were used.

#### 4.7. Probe Calibration

To check for confirmity of the working of the probe, a bomb was constructed with quartz windows on two sides. Fig 4.9 shows a sketch of the circular bomb used with the positions of the probe in relation to the spark plug. The quartz windows were covered with black paper with a pin hole pierced to allign with the tip of the probe. A photomultiplier tube (PMT) was aligned to record the flash of light emitted from the pin hole. The output signal from the PMT was displayed along with the ionization probe response on a Nicolet Storage oscilloscope and photographed. Fig. 4.10(a) shows the ionization probe response and the PMT signal for combustion in a quiescent chamber. The ionization probe signal shows a single peak while the PMT signal shows a peak and then a depression and a rise in voltage.

To generate turbulence during combustion a grid was placed in the combustion chamber perpendicular to the line of the spark plug and the ionization probe. Fig. 4.10 (b) shows the response of the ionization probe and the PMT signal. The ionization probe shows the double peak reported by Ohigashi et. al.[63] confirming the presence of multiple waves of ionized gases.

#### 4.8. Data Acquisition and Preparation

Fig. 4.26 shows a schematic diagram depicting the flame front at 4 positions as it progresses through the combustion chamber. To measure the ionization level due to the flame front at the different locations it would be necessary to locate the probes so that the electrode tip correspond to the position of interest. To measure the ionization signal when the flame arrives at four points in the same plane in a single line would require a probe with eight electrodes and four parallel circuits, also a device capable of recording more than four signals at the same time ( as the crank angle and TDC signals would also need to be recorded). A probe with eight

electrodes would be very bulky and would require the use of a very thick plate in between the cylinder head and engine block to locate the probe. Such a plate would reduce the compression ratio to levels where it would be very difficult to obtain knock with high octane rated fuels such as Propane, Iso-octane and 4 star commercial petrol.

The Flame ionization level at different points was measured by the use of probes and probe holders of varying lengths. The combination of probe and probe holders resulted in four different probe positions, one 4mm, one 14mm, one 18mm and the fourth 21mm from the cylinder wall.

A disc of 12 mm thickness was made to fit between the cylinder head and the engine block, to be able to locate the ionization probes. The engine was warmed up without the probe till the coolant water temperature reached around 80 C. The probe were then inserted and the engine now fired once in every three cycles, this was to prevent damage to the probes due to overheating. The output signal from the probe was recorded on a 4 channel tape recorder alongwith the TDC and crank angle signals on the other channels. Table 4.1 gives an abstract of some relevant specifications for the Racal Store 4 tape recorder. The data taken on tape was converted to digital form using the Nicolet Fast Fourier Analyser as a fast Analog to Digital converter. This data was then transferred to a floppy disc using a micro computer and then transferred to the main frame computer for processing.

From sampling theory [66] it is known that at least two samples per cycle are required to define a frequency component in the original data. The highest frequency that can be defined by sampling any set of data at time interval  $Dt$  is  $1/(2Dt)$  cycles per second which is called the cut off frequency or the Nyquist frequency or the folding frequency.

$$n_{\max} = 1/(2 Dt)$$

Frequencies in the original data over  $n_{\max}$  Hz will be folded back into the frequency range from 0 to  $n_{\max}$  and be confused with data in the lower range and cause what is known as "aliasing", an inherent problem with digital processing that is preceded by an analog to digital conversion. The phenomenon of aliasing can be explained with the help of Fig.4.11. Considering low frequency signal and a high frequency signal if the sampling rate is too low then the high frequency will appear as a low frequency or rather be indistinguishable from genuine low frequency components. In Fig. 4.11 it can be seen that digitizing a 'Low' frequency signal (Fig.4.11a) produces exactly the same set of discrete values as a result from the same process applied to a high frequency signal (Fig.4.11b). In the present investigation to overcome the problem two methods were applied, a.) The signal from the tape recorder was passed through a low pass filter with a cut off at 43 KHz and b.) the sampling rate was maintained at 128 KHz, which was well above 2.5 times the highest frequency of interest (i.e. 15KHz).

The number of sample points acquired by the Nicolet is 1024. The Nicolet plots only 400 of the 1024 points. Fig 4.12 shows the raw signal as obtained from the Nicolet FFT analyser and transferred to the main frame computer. The most efficient fast fourier transformation is performed with  $2^n$  points, where  $n$  is an integer. the number of points in a probe signal that contain the required information about the frequency fluctuations vary between 150 and 256 therefore any signal with less than 256 points was padded up with zeros to make up the required sample length. Newland [67] points out that the addition of zeros to increase the record length does not effect the power spectrum as the power spectrum is extrapolated to give frequencies over a smaller frequency step.

As a direct consequence of the need to take only a finite length of time history coupled with the assumption of periodicity (i.e. the signal under consideration occurs periodically), the problem of leakage is encountered. Leakage of a spectrum can be best illustrated by the two examples shown in Fig.4.13 in which two

sinusoidal signals of slightly different frequencies are subjected to the same analysis process. In the first case (Fig. 4.13a), the signal is perfectly periodic in the time window,  $T$ , and the resulting spectrum is a single line at the frequency of the sine wave. In the second case Fig.4.13b the periodicity assumption is not strictly valid and there is a discontinuity implied at each end of the sample. As a result, the spectrum produced for this case does not indicate the single frequency which the original time signal possessed but shows a set of frequencies close to the original one, where the energy from the original frequency component has leaked into.

One practical solution to the problem of leakage is the use of windowing. Windowing involves the imposition of a prescribed profile on the time signal prior to performing the fourier transform and the profiles or 'windows' are generally depicted as a time function.  $W(t)$ , as shown in Fig. 4.14 . The analysed signal is

$$x'(t) = x(t).W(t).$$

The first case shown is known as a rectangular window where the complete signal is considered with a sharp cutoff. The Hanning window is shown second and the cosine taper window the third. The Hanning and cosine taper window are typically used for continuous signals. The Exponential window (Fig. 4.14 d) is used for transient vibration applications where much of the important information is concentrated in the initial part of the time record and would be suppressed by any of the taper windows. The result of using a Hanning or cosine taper window on the signal in Fig 4.13 shows an improved spectrum (Fig.4.15). In the present investigation the cosine taper window has been used as it would retain the major portion of the information in the middle of the time record without change.

#### 4.9. Data Analysis

The flame ionization signal obtained from the probe circuit was recorded on the Racal store 4 FM tape recorder. The tape was then played back at the same speed as when recording the signal (60 in/sec). The probe signal from the tape recorder was passed through a signal conditioner with cutoff frequencies of 2Khz and 43 KHz. The signal in its unfiltered form is presented in Fig. 4.16 while the same signal when passed through the signal conditioner is shown in Fig 4.17. The part of signal of interest in both cases is shown in Figs 4.18 and 4.19. The need to filter the signal is seen in Fig. 4.22 where it can be seen that the d.c. component has overshadowed the rest of the frequency spectrum, thus making it impossible to obtain any relevant information from the power spectrum. A raised cosine window is applied to the signal of Fig. 4.19 to obtain a signal with its ends smoothed out (Fig. 4.20). The effect of adding zeros to increase the sample length is shown in Figs 4.21 and 4.23. The power in the signal has been distributed over the signal thus reducing the power content in individual signals but spreading a proportional amount into the neighbouring signals by extrapolation.

As the signal variation is quite large it is usually plotted in log form or in decibels where the reference voltage in the present study has been taken as 20 micro-volts so as to compare with the datum used in the calculation of sound pressure levels (i.e.  $20 \times 10^{-5}$  dynes/cm<sup>2</sup>). Fig. 4.24 shows Fig. 4.21 plotted with the y axis on log scales. To obtain a more representative frequency spectrum an ensemble average of 10 cycles was taken a sample plot is shown in Fig.4.25.

Table 4.1

Abstract of Some Relevant Specification of  
The Racal (Store 4) Tape Recorder (120)

Tape Speeds	60, 30, 15, 7.5 and 11/16 in/sec
Input Sensitivity	Selected by Input Attenuators in the following Range (peak for full Deviation) (+ 20 volts, + 10 volts, + 5 volts, + 2 Volts, + 1 volt, + 0.5 volt, + 0.2 volt, + 0.1 volt)
Output Level	Continuously Variable for 0 to + 2.5 for full deviation
Bandwidth	D C to 20 KHz at 60 in/sec.
Signal/Noise Ratio	48 dB at 60 in/sec.
Harmonic Distribution	< 1% at maximum modulation level

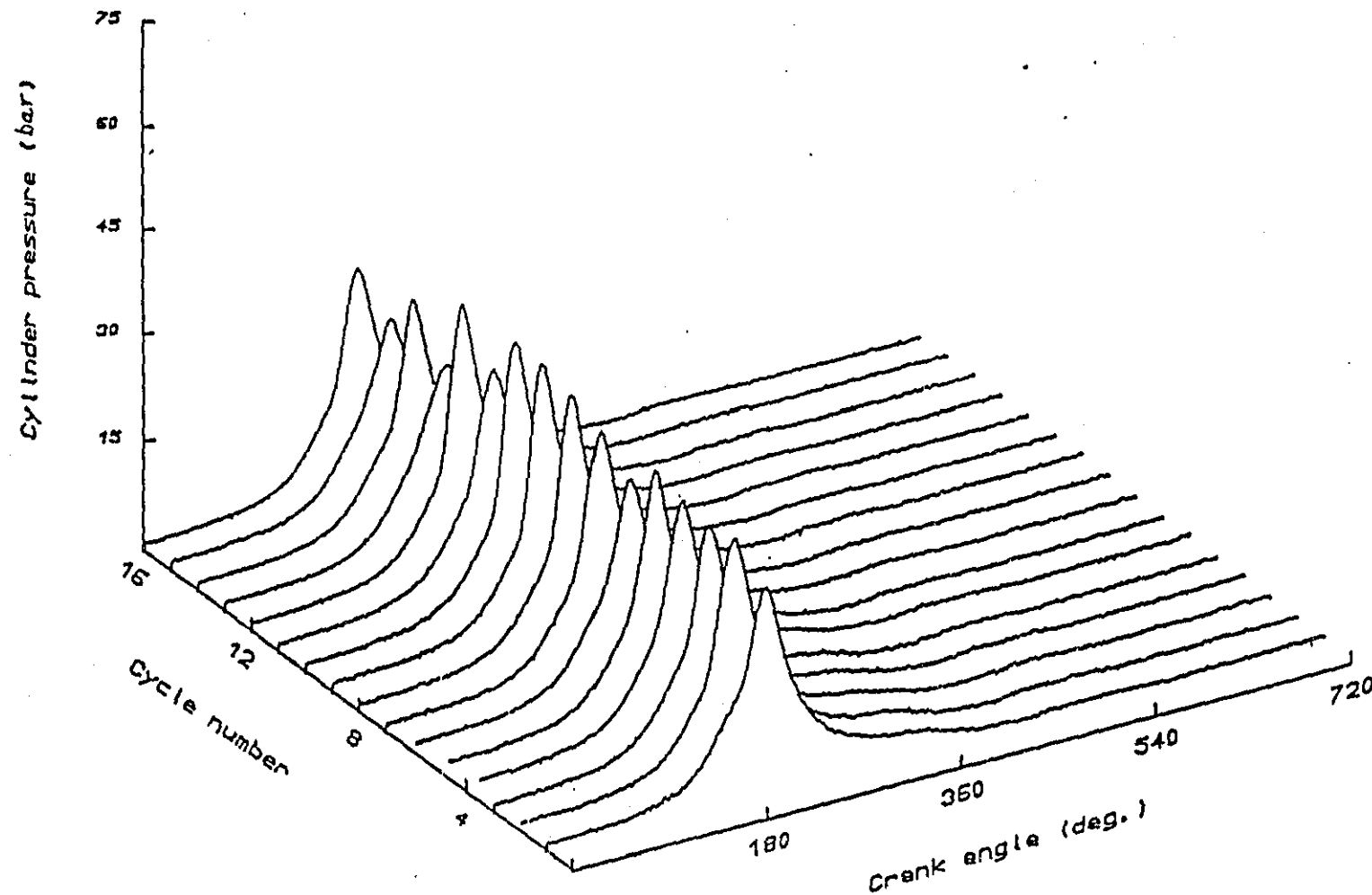


Fig.4.1.Cylinder pressure for 16 consecutive cycles

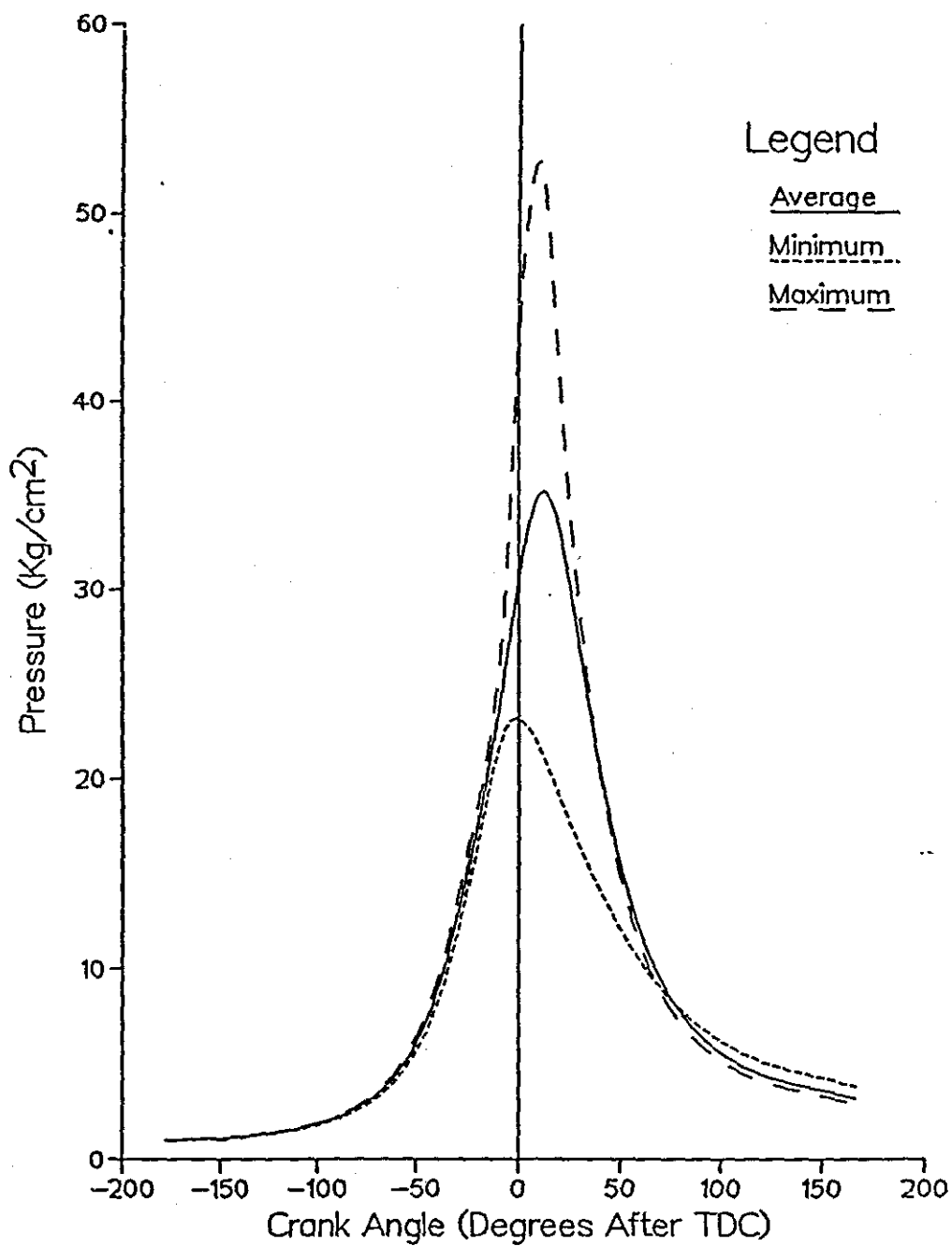
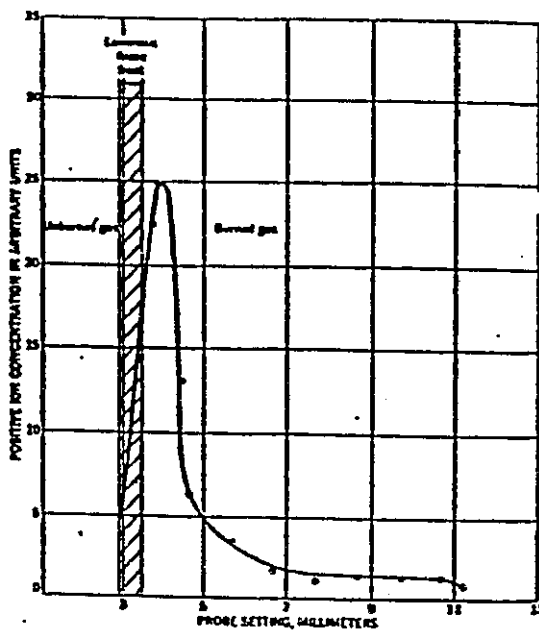
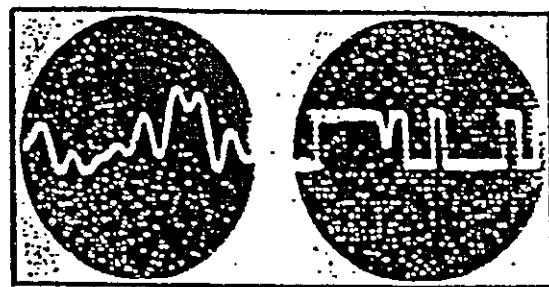


Fig. 4.2 Minimum Maximum and Average of 64 Cycles



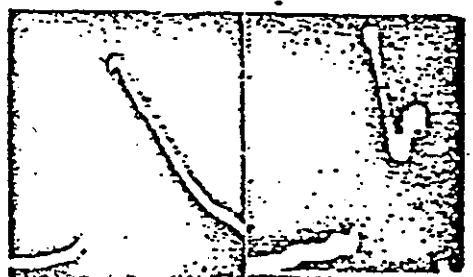
Distribution of positive ion concentration in the vicinity of a laminar flame front.

Fig. 4.3 (REF. 62)

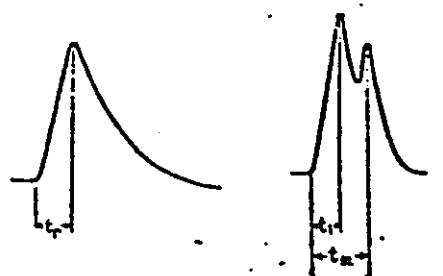


Simultaneous oscillograms of probe circuit response to turbulent flame, before (left) and after signal has passed the pulse-height discriminator.

Fig. 4.4 (REF. 62)

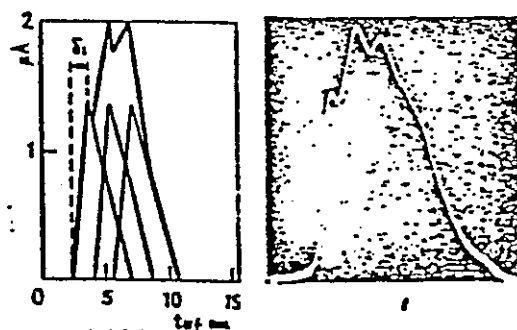
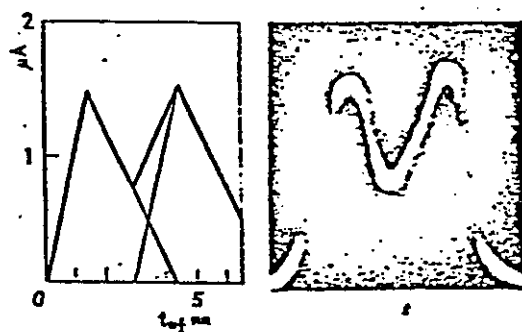


(a)  $\Delta U = 0 \text{ m/sec}$  (b)  $\Delta U = 1.37 \text{ m/sec}$   $\phi = 1.0$   
Examples of records of ion-currents



(a) Laminar flame (b) Turbulent flame  
Schematic diagrams of ion-currents

Fig. 4.5 (REF. 63)



Examples of composing the wave forms of turbulent ion-currents by superimposing fundamental ion-currents

Fig. 4.6 (REF. 63)

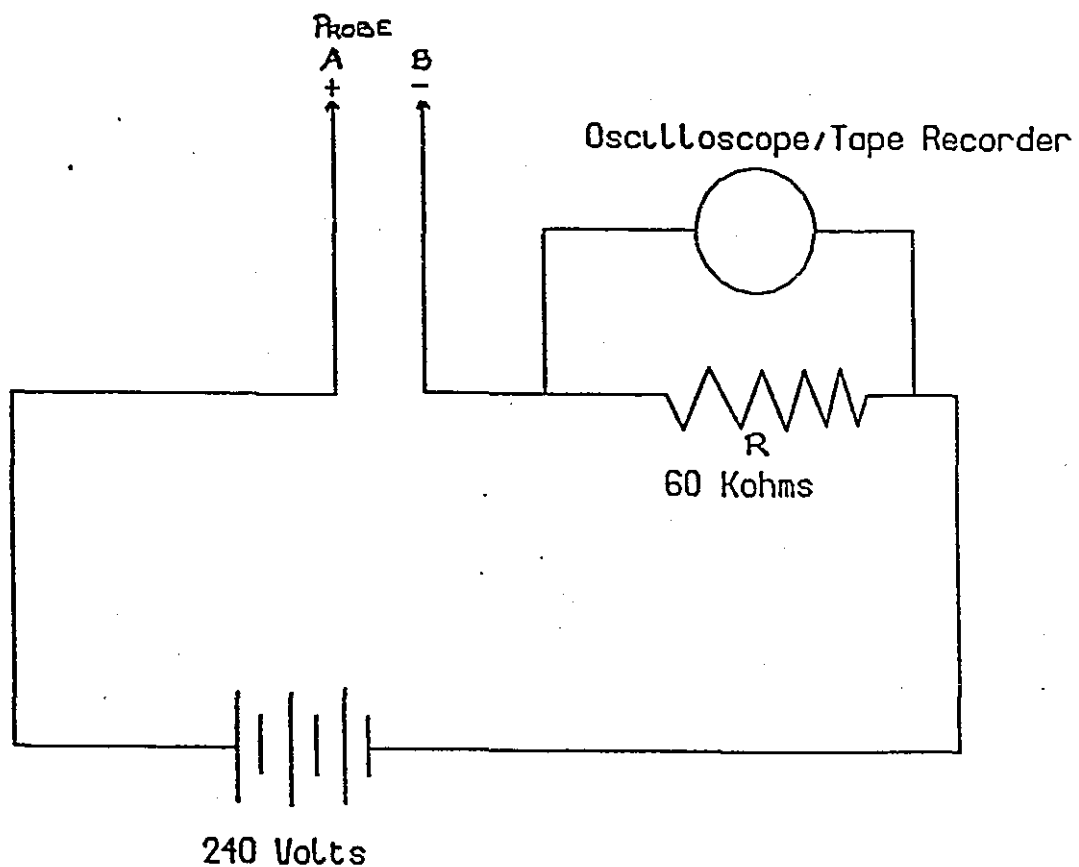


Fig. 4.7 Schematic Circuit of an Ionisation Probe

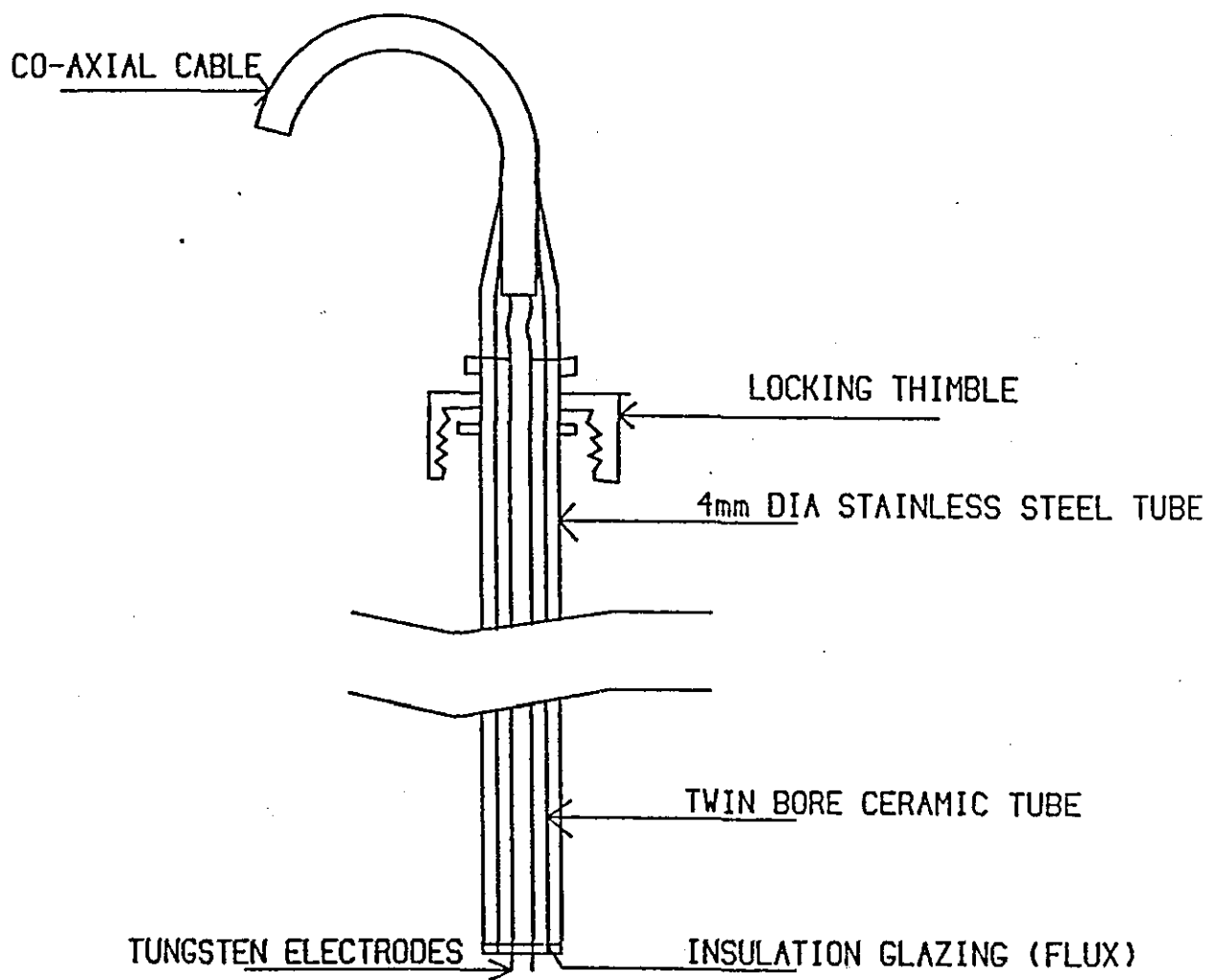


Fig. 4.8 Schematic Diagram of Ionisation Probe

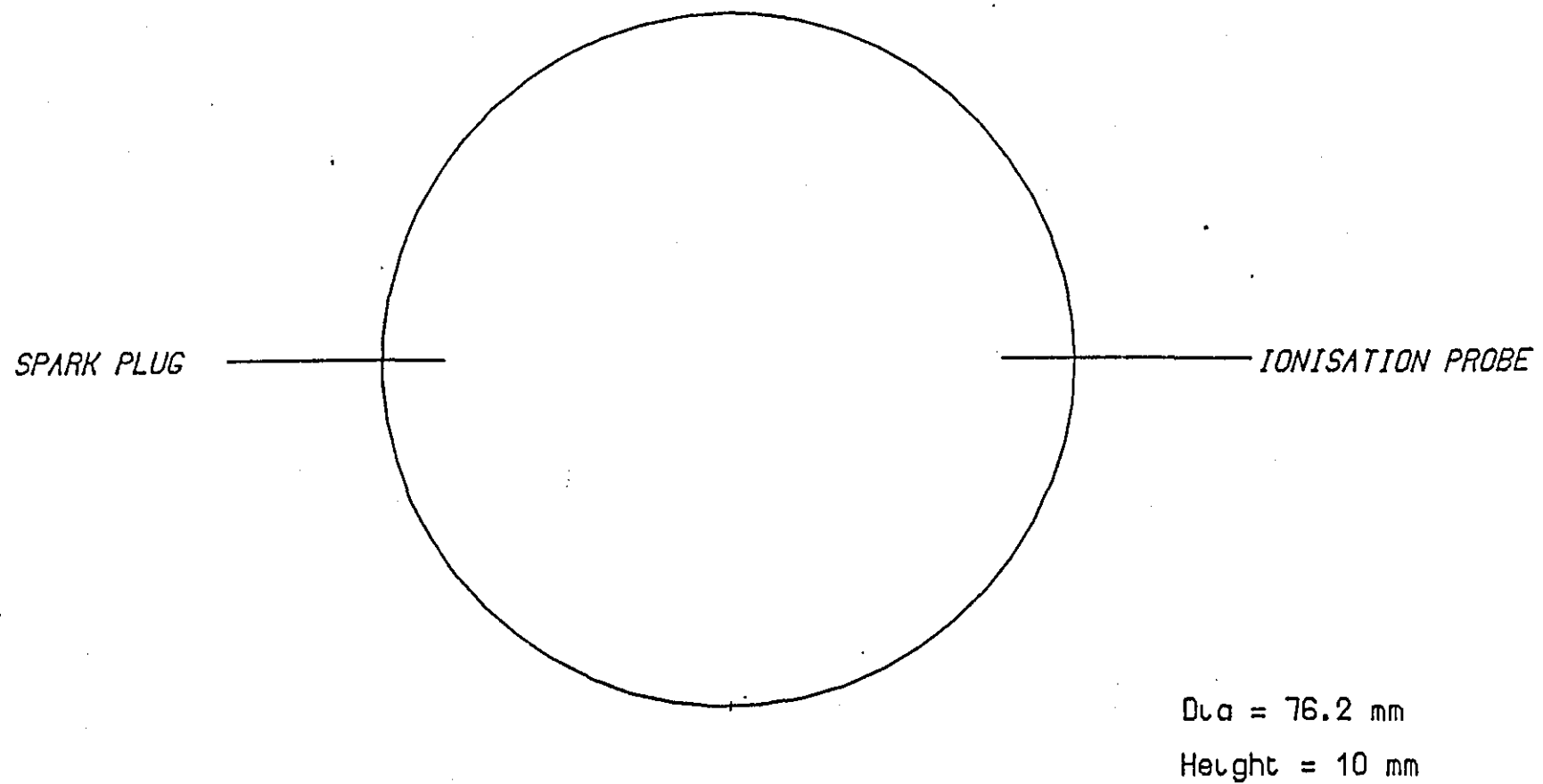
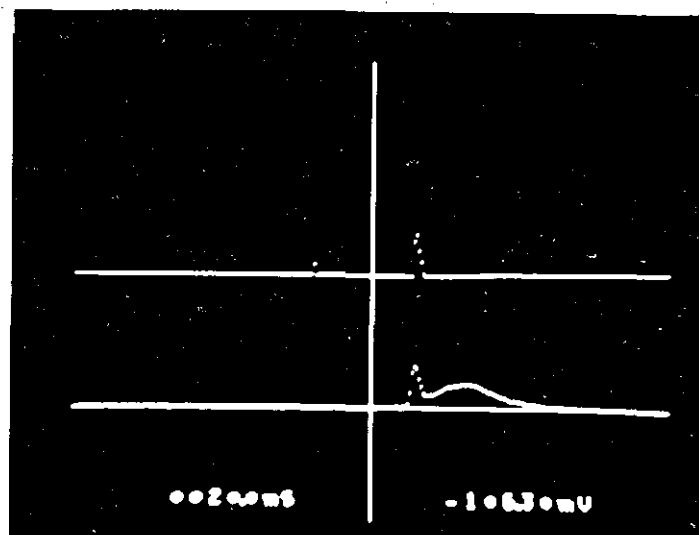


Fig. 4.9 Schematic Diagram of Bomb with Ionisation Probe Position relative to Spark Plug.

PROBE →

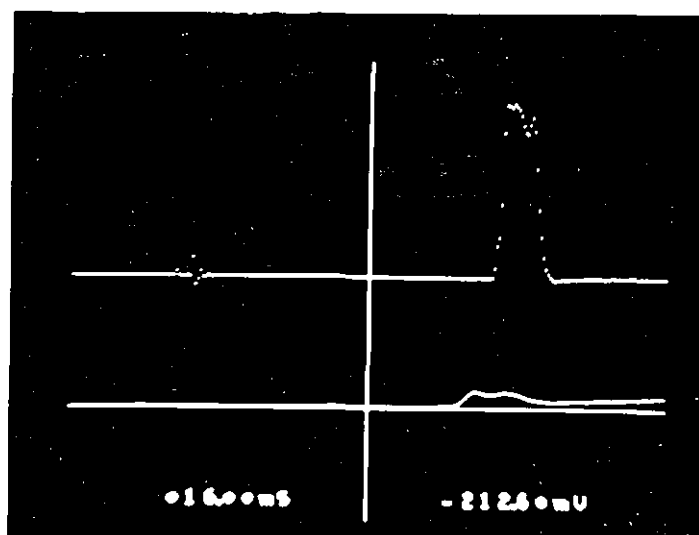
P M T →



(a) Quiescent Chamber

PROBE →

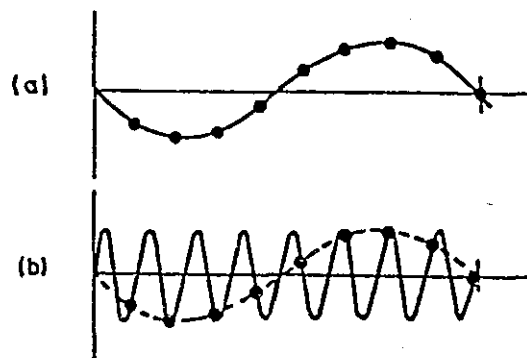
P M T →



(b) Turbulent Combustion

Fig. 4.10

IONIZATION PROBE AND  
PHOTOMULTIPLIER TUBE RESPONSE  
(Probe 15 mm from Periphery)



*Fig. 4.11. The Phenomenon of Aliasing* (REF. 68)  
(Ref. 14)

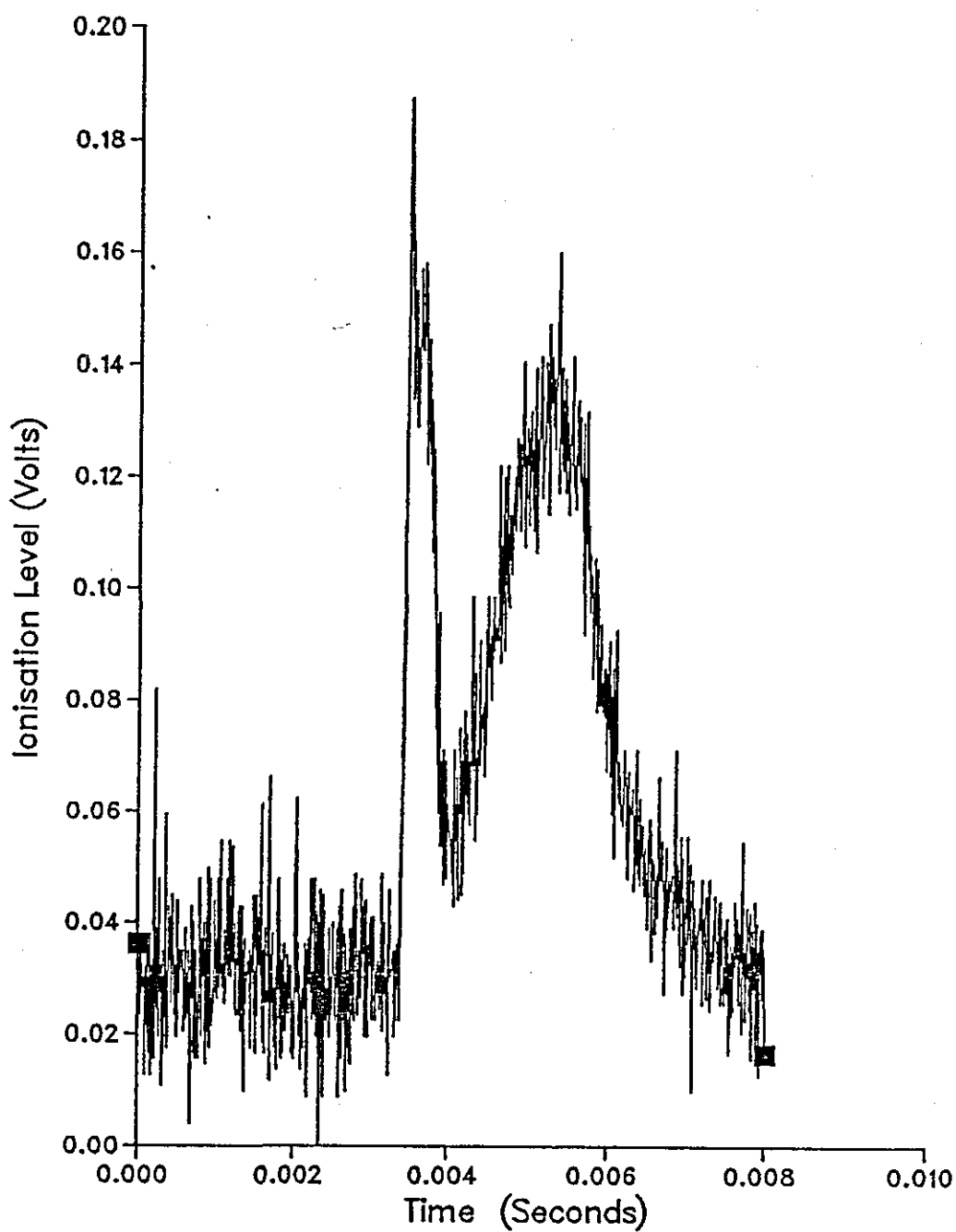


Fig 4.12 Unfiltered Ionisation Probe Signal

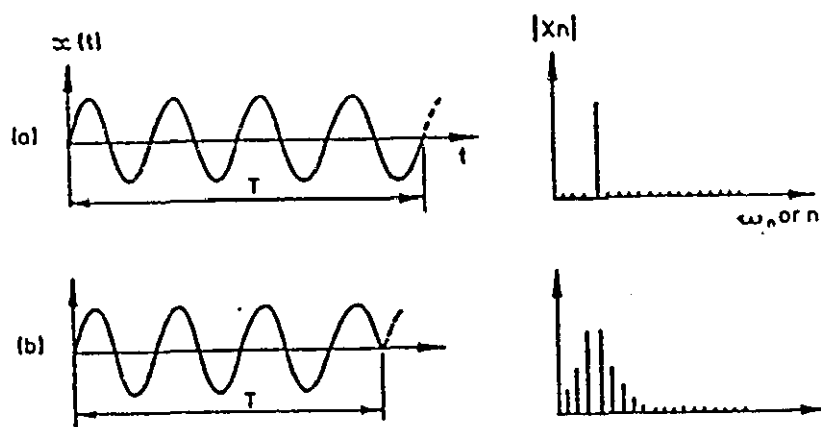


Fig. 4.13 Sample Length and Leakage of Spectrum (Ref. 68)

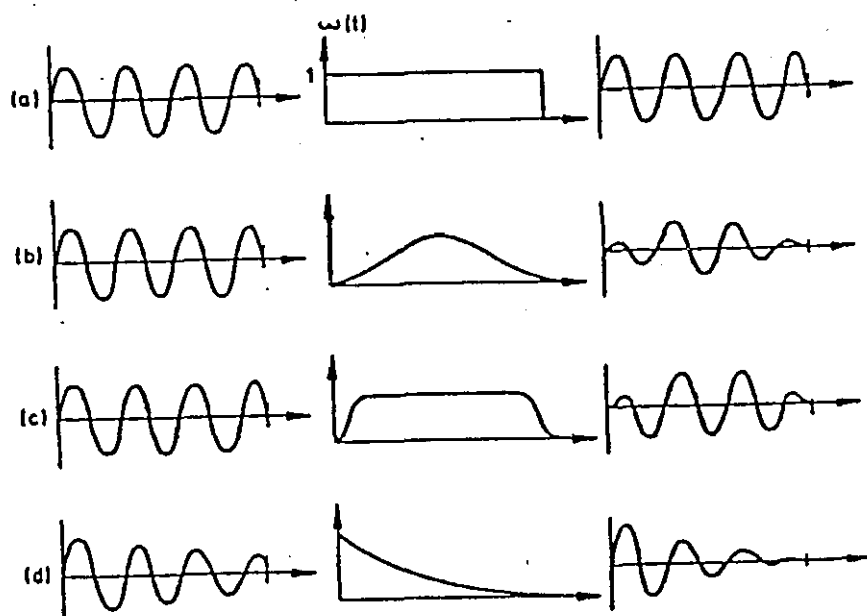


Fig. 4.14 Different Types of Window (Ref. 68)

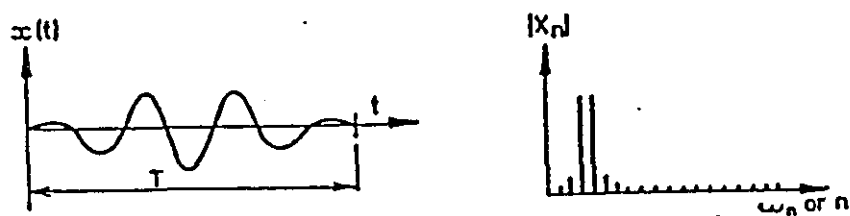


Fig. 4.15. Effect of Hanning Window on Finite Fourier Transform (Ref. 68)

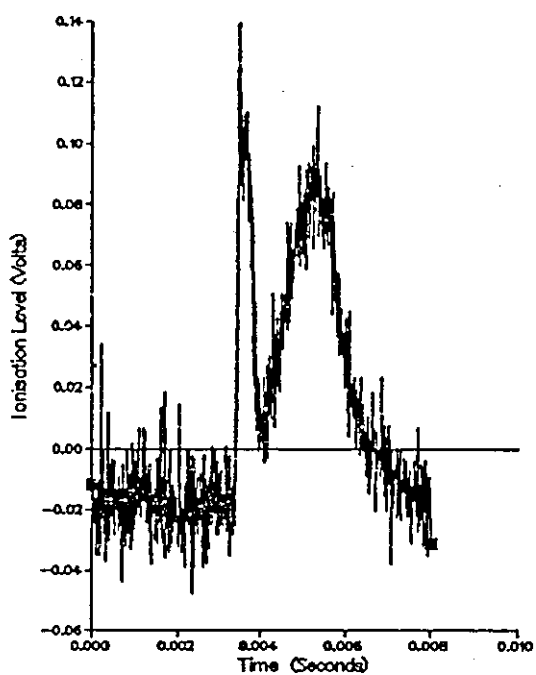


Fig 4.16 Unfiltered Ionisation Probe Signal

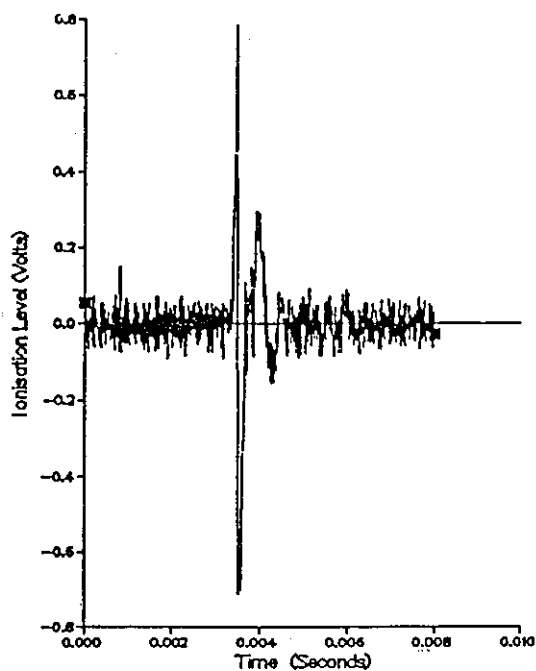


Fig 4.17 Filtered Ionisation Probe Signal  
Corresponding to Signal in Fig 4.16

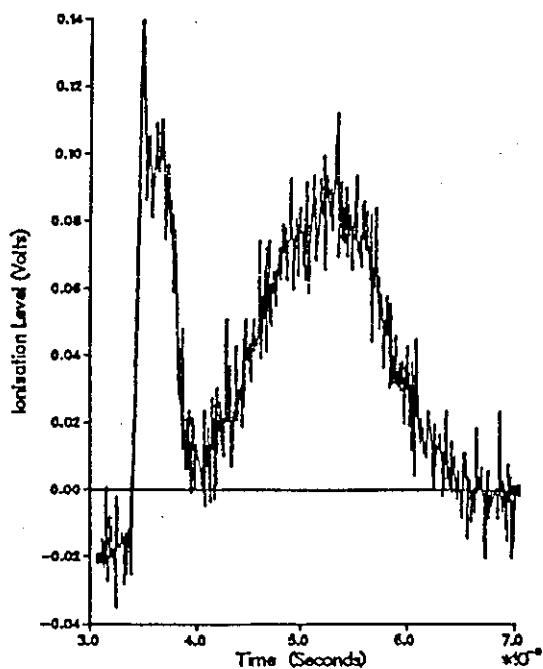


Fig 4.18 Unfiltered Ionisation Probe Signal  
Windowed over Pulse

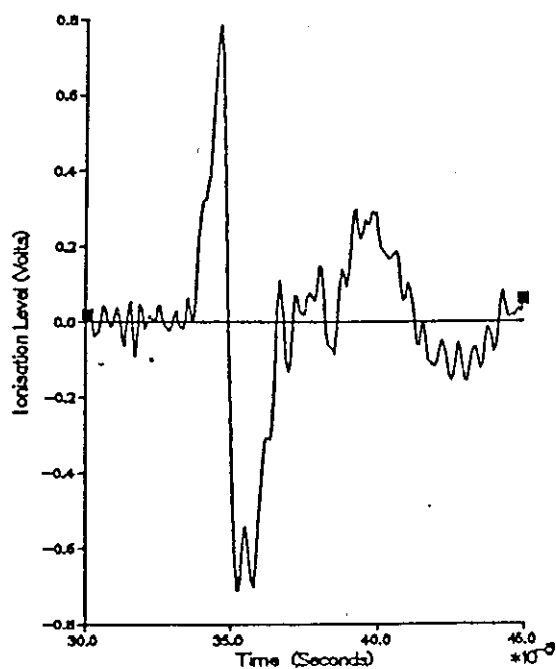


Fig 4.19 Filtered Ionisation Probe Signal  
Windowed over the Pulse

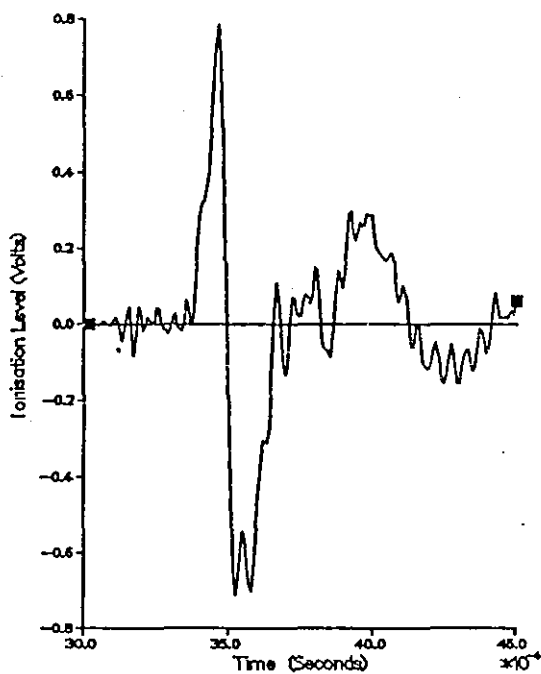


Fig. 4.20 Signal of Fig. 4.19 with raised Cosine Window

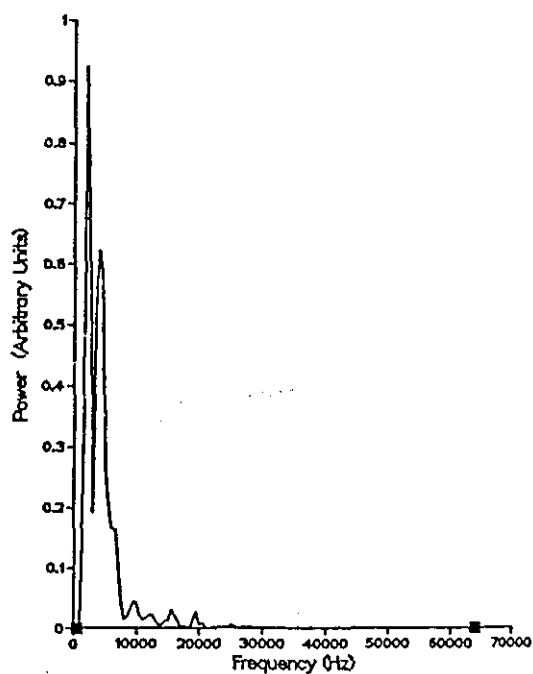


Fig. 4.21 Power Spectrum of Probe Signal Corresponding to Signal in Fig 4.14

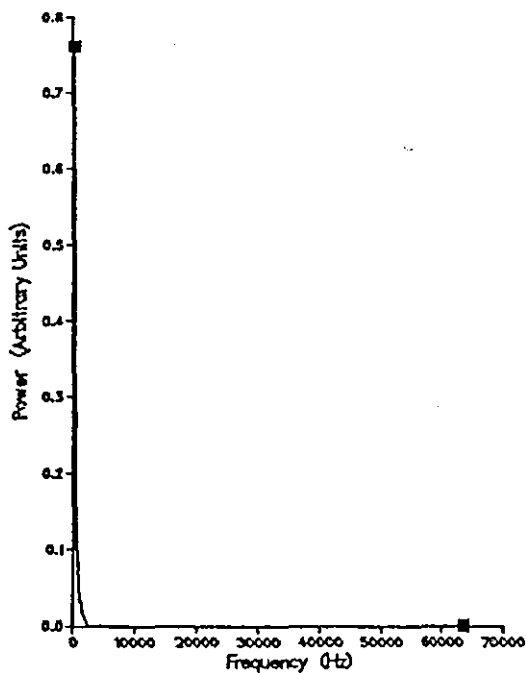


Fig. 4.22 Power Spectrum of Unfiltered Signal

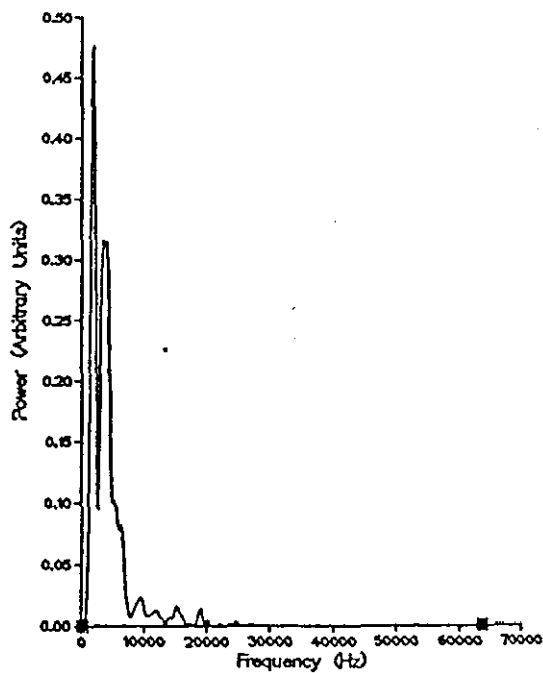


Fig. 4.23 Power Spectrum of Filtered Signal Record Length increased to 512 with zeros

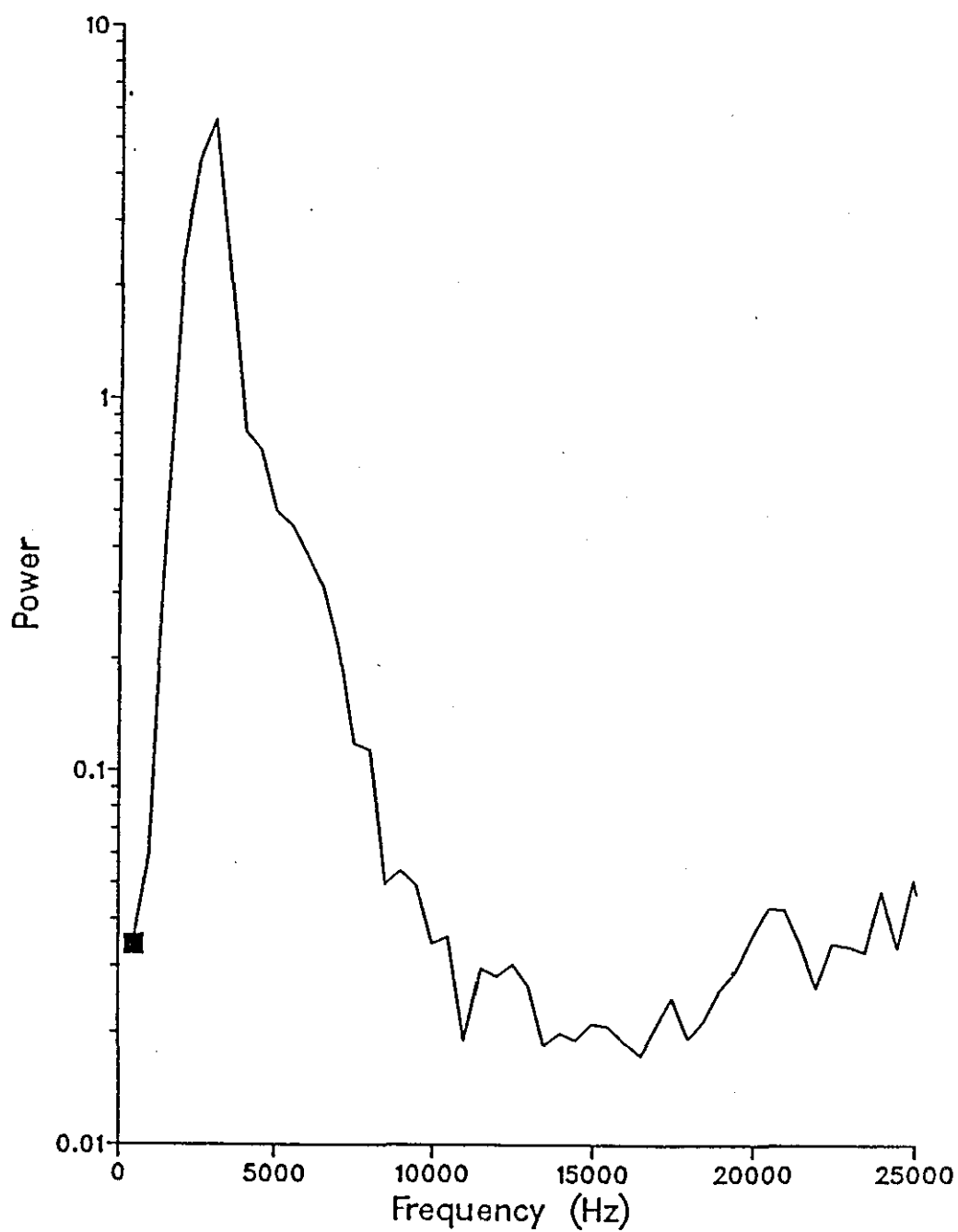


Fig 4.24 FREQUENCY SPECTRUM CORRESPONDING TO FIG 4.23

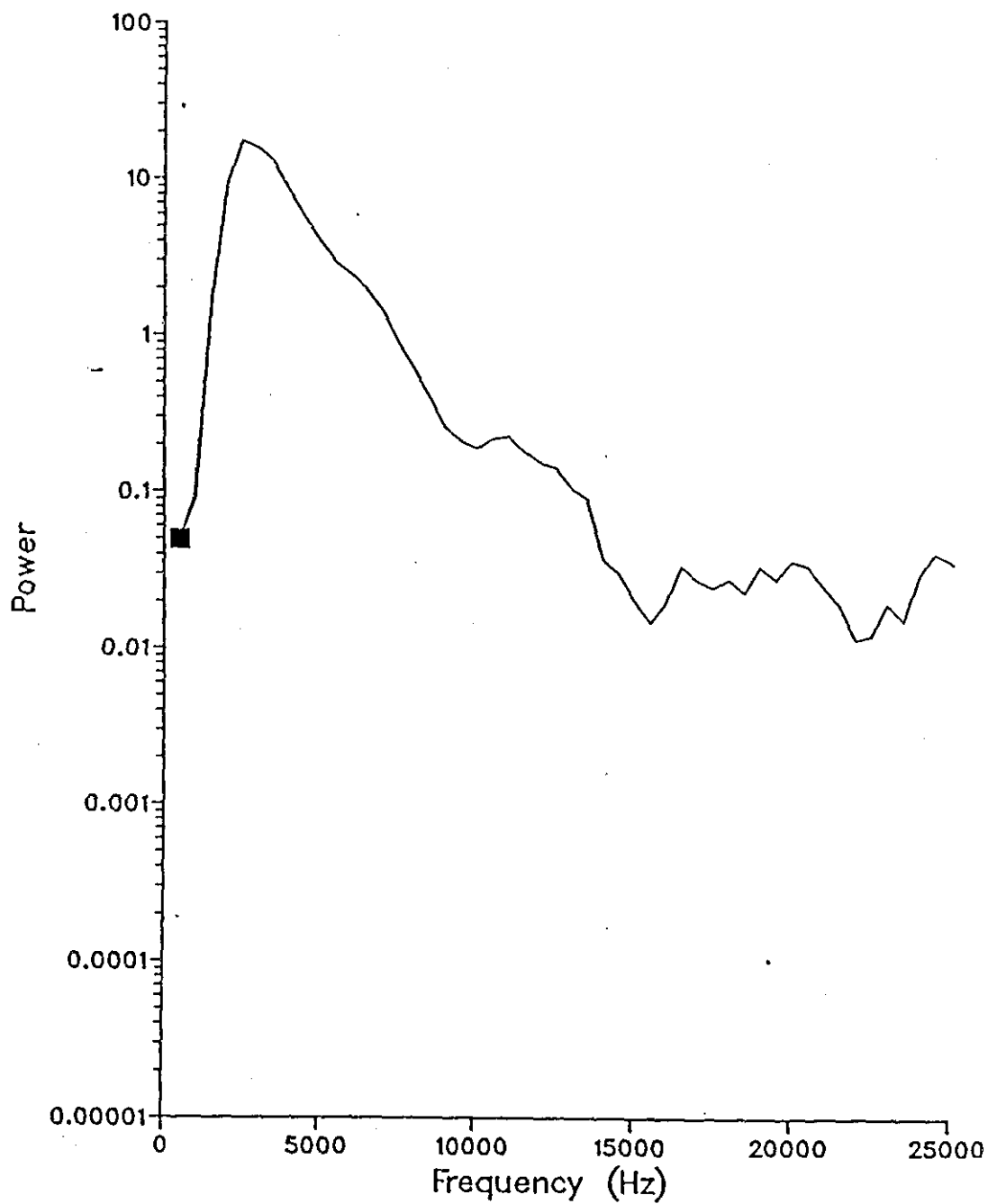


Fig. 4.25. ENSEMBLE AVERAGE OF 10 POWER SPECTRA

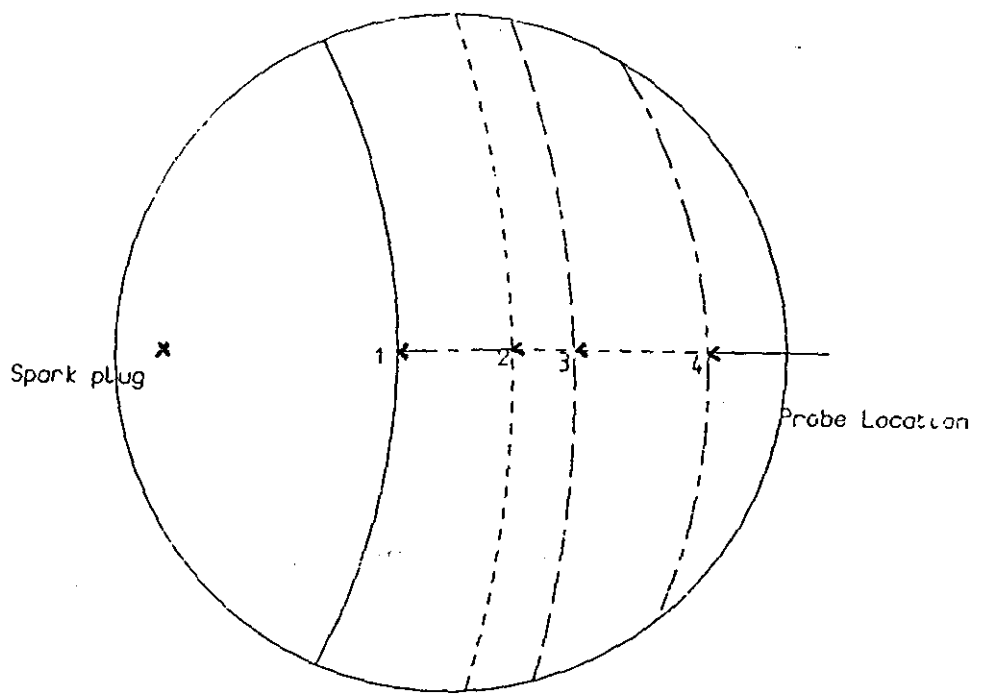


Fig. 4.26 Schematic of Probe Locations

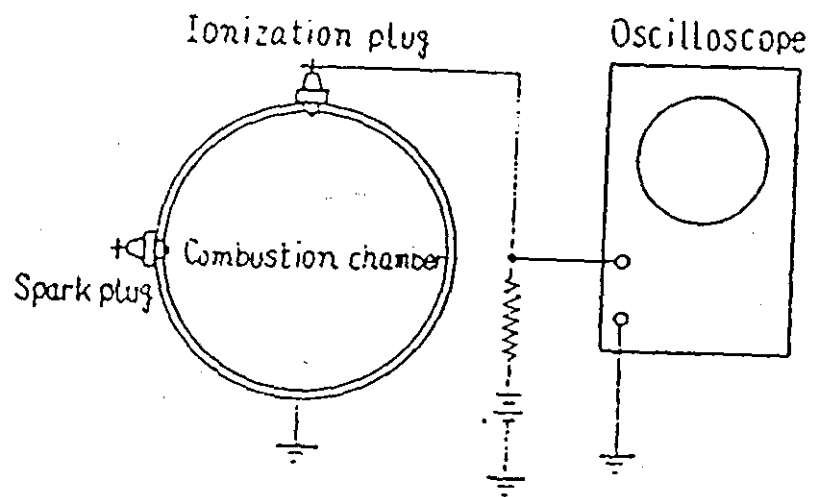


Fig 4.27

Schematic diagram of circuit for measuring ionization current

(Ref. 71)

## Chapter V

### APPLICATION OF RELAXATION OSCILLATION MODEL TO ENGINE COMBUSTION

#### 5.1 INTRODUCTION

Reference to preknock vibrations was made in section 1.5, and the possibility of these vibrations interacting with the end gas zone and enhancing the possibility of knock was considered.

This chapter attempts to correlate the preknock vibrations to the frequency of the flame front and the acoustic resonant frequency of the combustion chamber. The system of burned gas, flame front and unburned gas is considered as a lumped parameter system (Fig.5.1). An analogy is drawn with equivalent electrical systems and to oscillatory combustion in an equivalent duct.

#### 5.2 Preknock Vibrations

Based on high speed photographs taken of combustion in a spark ignition engine Miller and Logan [27] found presence of gas vibrations in the combustion chamber prior to the occurrence of knock, which they referred to as preknock vibrations. Fig. 1.12 shows the fluctuation of the flame velocity against time. To obtain these plots Miller and Logan [27] measured the displacement of the flame front over consecutive frames of the high speed photographs. The camera speed was maintained constant thus enabling an easy calculation of the flame velocity. Positive velocity is considered when the flame front displacement is into the unburned charge ahead and negative when the flame front displacement is in the opposite direction..

An interesting feature drawn from these plots is that the frequency of the vibrations increase with increase in the amount of tetra-ethyl-lead in the fuel, also it is seen that the duration of the

vibrations increase with increasing amounts of tetra-ethyl-lead. Fig. 1.20 is a plot of the frequencies calculated from Fig.1.12 and plotted against the amount of TEL in the fuel. The natural frequency of the combustion chamber with the complete charge burned and at a temperature of 2000K is 3430 Hz. The frequency calculated is the average over a period of crank movement and it would be of interest to find the variation of the frequency at different points as the flame front progresses along the combustion chamber.

Gas vibrations in bombs and engines can be of two types, one where the amplitude of the vibrations decay with time and the second where the amplitude increases, thus implying that amplification of the waves is occurring as the combustion progresses. The later type of vibratory combustion would require that the waves are gradually fed with energy over a period of many cycles. This gradual feeding in, of the energy could occur only if the vibrations themselves effected the local rate of combustion or energy release in such a manner as to speed up the combustion in the high pressure regions, thus, increasing the difference in pressures. This driving of these oscillations is similar to the Rayleigh criterion.

The Rayleigh criterion is a hypothesis proposed by Rayleigh [72] regarding the driving of oscillations by periodic release of heat in a gaseous medium, which states that, if heat is periodically added to a mass of oscillating gas, at the moment of highest pressure, or taken away from it at the moment of lowest pressure, the oscillation is amplified. On the other hand, if heat is added to the system at the moment of lowest pressure, or taken away from it at the moment of highest pressure then, the oscillation is damped, though the frequency is not effected by the heat transfer.

The gas vibrations in a combustion chamber of a spark ignition engine can be represented schematically by Fig. 5.1(a)., where the burned gas, flame front and the unburned gas are represented as lumped parameters. The displacement of the flame front due to the oscillations is given as  $S$ . The equivalent lumped system considering

a duct would be depicted as in Fig. 5.1(b), where the flame front separates the duct into a cold gas column of length of  $L_1$  and a hot gas column of length  $L_2$ . The organ pipe oscillation for this system can be represented by the following wave equation

$$c^2 \frac{d^2 S}{dx^2} = \frac{d^2 S}{dt^2} \quad 5.1$$

where  $S$  is the longitudinal displacement of the gas column, and  $C$  is the velocity of sound at temperature  $T$ .

The boundary conditions are:

when  $X = 0$  then  $S = 0$  and  $dS/dX \neq 0$

when  $X = L$  then  $S = 0$  and  $dS/dt = 0$

solution of the wave equation subject to the boundary conditions is

$$S = A \sin kx (C \sin w_k t + D \cos w_k t) \quad 5.2$$

in which the fundamental harmonic  $k = 1$ , is important.

Assuming that the oscillating flame front is momentarily fixed at a mean position the period of the fundamental harmonic in the cold and hot gas columns are

$$t_1 = 2 * L_1 / C_1 (1 + M_1^2) \quad 5.3$$

$$t_2 = 2 * L_2 / C_2 (1 + M_2^2) \quad 5.4$$

Since the cold and hot gas columns are interconnected at the flame front, the period of acoustic oscillation of the complete equivalent duct is

$$t_s = t_1 + t_2 = 2 * L_1 / C_1 (1 + M_1^2) + 2 * L_2 / C_2 (1 + M_2^2) \quad 5.5$$

where  $M_1$  and  $M_2$  are the Mach numbers in the cold and hot gas columns, and the acoustic frequency is

$$f_s = 1/t_s \quad 5.6$$

Any given mechanical system can be usually represented by an equivalent electrical circuit. Following Karplus [73] the wave equation for a one dimensional electrical system represented by the circuit in Fig. 5.3, where the inductance is  $L$  henrys per unit length and capacitance is  $C$  farads per unit length is given as:

$$\frac{\partial^2 V}{\partial x^2} = LC \frac{\partial^2 V}{\partial t^2} \quad 5.7$$

Introducing damping into the system the analog circuit could be represented by Fig. 5.4, which is known as the telegraph equation, since it is descriptive of the voltage distribution along telegraph transmission lines and is given as :

$$\frac{\partial^2 V}{\partial x^2} = LC \frac{\partial^2 V}{\partial t^2} + (LG+RC) \frac{\partial V}{\partial t} + RGV \quad 5.8$$

where  $R$  is the resistance (ohms) per unit length  
and  $G$  is the conductivity (mhos) per unit length.

Considering the system as a single lumped system rather than a number of discretized lumps the burning mass in the cavity could be represented as in Fig.5.4, the mechanical equivalent of which is given by Fig. 5.5.

Ning [74] considers the above system but with damping resistance  $R$  absent, the equivalent lumped system would then be represented by Fig. 5.6(a) the mechanical equivalent of which would be represented as shown in fig. 5.6(b).

Considering the circuit in Fig. 5.6(a) the current balance (Kirchoff's Law)

$$i_1 = i_2 + i_3 \quad 5.9$$

for an inductance coil  $V = L di_1/dt$

hence  $i_1 = 1/L \int V \cdot dt$

for a conductance  $i_2 = (e-V)G$

where  $e$  is the electro motive force ,  $V$  the voltage drop and  $G$  the conductance.

therefore  $i_2 = (e-V)/R$  as  $R = 1/G$

for a capacitor  $i_3 = C d(e-V)/dt$

as  $i_1 = i_2 + i_3$

$$1/L \int V \cdot dt = (e-V)/R + C d(e-V)/dt \quad 5.10$$

Differentiating the above equation with respect to  $dt$

$$V/L = 1/R de/dt - \frac{1}{R} \frac{dV}{dt} + C \frac{d^2 e}{dt^2} - C \frac{d^2 V}{dt^2} \quad 5.11$$

$$\text{hence } \frac{d^2 V}{dt^2} + \frac{1}{RC} \frac{dV}{dt} + \frac{V}{LC} = \frac{d^2 e}{dt^2} + \frac{1}{RC} \frac{de}{dt} \quad 5.12$$

### 5.3 Application of Relaxation Oscillation to Engine Geometry

The basis for calculating the change in displacement of the flame front is taken from Ning [74]. Ning compares ramjet combustion to an equivalent duct of uniform cross section, separated into a cold gas column of length  $L_1$  and a hot gas column of length  $L_2$  by a flame front (Fig. 5.1b). The flow prior to the duct is supersonic while inside the duct it is subsonic. At the inlet to the duct a normal shock wave is present separating the supersonic and subsonic flows. The pulsating pressure in the combustor causes the cold gas column to contract and expand being made to act as a buffer between the normal shock and the flame front.

The displacements of the normal shock wave and the flame front from their neutral positions are given as  $S_1$  and  $S_2$  (Fig. 5.1b) respectively. As the normal shock wave has to move against the flow in the system its displacement  $S_1$  is less than the displacement  $S_2$  of the flame front, thus bringing the cold gas column into compression while the flame front and the hot gas column are in full expansion. The mean pressure  $P$  is at its highest level here. As the flame front recedes downstream the flame front and hot gas column contract while the cold gas column expands. In this case the mean pressure level is at its lowest level. In between these two pressure levels each gas column oscillates about its own neutral position.

Given the pulsating pressure as

$$P_s = f \rho / 2 U^2 \quad 5.13$$

$$\text{then } dP_s = f \rho U dU \quad 5.14$$

the flow velocity in front of the oscillating flame front also fluctuates at audio frequency, which in turn results in a periodic damping force given by

$$dD_s = A f \rho U S_2 = A f \rho U \delta U \sin \omega_s t$$

Ning [74] suggests a non linear equation for the relaxation oscillation for the elastic flame front as :

$$m_2 \ddot{S}_1 + (A f \rho U) \dot{S}_2 + \frac{n \bar{P} A}{L_2} (1 + \frac{\delta P}{\bar{P}} \cos \omega_s t) S_2 = 0 \quad 5.15$$

where  $m_2$  = mass of the flame front  
 $S_2$  = Displacement of the flame front  
 $A$  = Area of cross section of the duct  
 $f$  = coefficient of friction  
 $\rho$  = Density of Burned gas  
 $U$  = Velocity of flow in the duct  
 $n$  = Ratio of specific heats for the burned gas  
 $\bar{P}$  = Mean pressure  
 $L_2$  = length of the burned gas column  
 $\omega_s = 2 \pi f_s$  where  $f_s$  = the natural frequency of the system

The phenomenon of Relaxation Oscillation is explained in Appendix C.

#### 5.4 Compression Waves in Bombs and Engines

As mentioned in section 1.5, Kogarko and Ryzkhov [31] found that the passage of compression waves through the flame front resulted in the amplification of the waves if their amplitude was over a given threshold. Leyer and Mason [29] found this threshold to be 50 mbar and have shown that the results obtained from open-closed tubes (i.e. tubes open at one end and closed at the other) could be applied to bombs. Thus considering the engine combustion as a lumped system, the fluctuations of the flame front due to combustion instability and pressure variations could be studied by solving the non linear equation of relaxation oscillation derived for the duct by equating the engine combustion chamber to an equivalent chamber (Fig. 5.1).

## 5.5 Application of Equation of Relaxation Oscillation

In the engine context the variables in equation 5.15 would have the following definition

- m2 = mass of flame front
- S2 = displacement of flame front (to be calculated)
- A = Area of flame front
- U = flame speed
- f = coefficient of friction assumed constant
- n = ratio of specific heats of burned gas
- P = cylinder pressure
- dP = pressure rise over interval considered
- L2 = Flame radius
- ws = Natural frequency of system given by equation 5.5

Of the variables present in equation 5.15 all except the mass m2 of the flame front can be obtained from the output of the computer program discussed in chapter III. Therefore it was considered necessary to rewrite equation 5.15 with reference to the engine variables which can be obtained from the output of the computer program "copred.fortran", which simulates the combustion in an engine .

It is assumed that at the time of consideration the thickness of the flame front is 't' and that the flame area 'A' is constant over the thickness 't', thus giving the volume of the flame front V as:

$$V = A*t \quad 5.16$$

Equation 5.15 can now be written as :

$$\ddot{S} + \frac{f u \dot{S}}{t} + \frac{n \bar{P} A}{L_2} \left(1 + \frac{\delta P}{\bar{P}} \cos \omega_s t\right) S_2 = 0 \quad 5.17$$

Experiments involving the measurement of turbulence in engines [49]

have shown that the thickness of the flame front is proportional to the integral length scale  $L$  which in turn is proportional to the instantaneous piston displacement from TDC. As the output trends are of interest the flame thickness is considered equal to the height of the chamber (Measurements in Bombs [63] have shown that this is quite an acceptable assumption). Equation 5.17 can now be written as:

$$\ddot{S}_2 + \left(\frac{u'}{h}\right)\dot{S}_2 + \frac{V_s^2}{hL_z} \left(1 + \frac{\delta P}{P} \cos \omega_s t\right) S_2 = 0 \quad 5.18$$

the square of the sonic velocity passing through a medium at a pressure  $P$  and density  $\rho$  with the ratio of specific heats given by  $n$  is given by the expression :

$$V_s^2 = \sqrt{\frac{nP}{\delta}} \quad 5.19$$

## 5.6 Solution of Equation for Relaxation Oscillation

The second order non linear differential equation given by equation 5.18 is solved using the Advanced Continuous Simulation Language (ACSL). This is a language designed for modelling and evaluating the performance of continuous systems described by time dependent, non linear differential equations.

Integration is a special ACSL operator that is accomplished by the operator INTEG.

The general second order differential equation is given as

$$A \frac{d^2x}{dt^2} + B \frac{dx}{dt} + C = 0 \quad 5.20$$

considering  $dx/dt = Z$  we have:

$$A \frac{dz}{dt} + BZ + C = 0 \quad 5.21$$

equation 5.20 is now reduced to two first order differential equations given as:

$$dZ/dt = -AZ - Bx + C \quad 5.22$$

$$\text{and } dx/dt = Z \quad 5.23$$

hence

$$Z = \int (C - AZ - Bx)dt$$

$$\text{and } x = \int Zdt$$

The program for integrating equation 5.10 is given in Appendix (D).

The algorithms available for integrating are:

1. Adams Moulton: variable step, variable order
2. Gears Stiff : variable step, variable order
3. Runge-Kutta First order or Euler
4. Runge-Kutta Second order
5. Runge-Kutta Fourth order

or any other algorithm supplied by the user.

The Adams Moulton, Gears Stiff and Runge Kutta fourth order were tried and no appreciable difference in the solution was found, also the time taken by the three methods were very similar to each other. The Gears stiff method was selected as it is known from experience (refer Chapter II and Appendix B) that the Gears algorithm has a wide applicability, i.e. it is equally good for both stiff equations and non-stiff equations.

## 5.7 Modelling Data from Lancaster's Thesis

why not own data?

Knocking cycles??

Lancaster [56] provides a set of experimental data for a CFR engine over a wide range of conditions. The combustion model was run with the data obtained from the thesis [56]. The frequency response was calculated from equation 5.13 at 10 degrees before top dead centre, top dead centre and 10 degrees after top dead centre. The variation of the chamber height being small over this range of crank angle, the combustion chamber volume can be considered to be constant over this range, thus making it possible to apply the equations derived for a duct (5.10). Fig. 5.7 to 5.10 show the response frequency against the crank position with various engine parameters being changed, for conditions with a shrouded and non shrouded intake valve. The common feature that stands out on these plots is that increasing the turbulence increases the frequency of the flame front at the initial stages of the combustion (irrespective of the piston position) though towards the later part of the combustion the difference is not appreciable.

One variable that is found to have an appreciable effect on the response frequency is the flame thickness. Increasing the flame thickness reduces the response frequency while reducing it increases the response frequency (Fig. 5.11). The natural frequency of the burned gas and unburned gas system increases as the combustion progresses (increasing the temperature increases the sonic velocity which in turn increases the natural frequency of the system)

The falling response frequency also indicates that the stiffness of the burned gas volume is decreasing. The spring stiffness of the hot gas column is given by Ning [74] as

$$K_2 = \frac{A dP}{S^2} = \frac{n P A}{L^2}$$

which for the engine combustion chamber is given as :

$$K_2 = \frac{n P R a}{R f}$$

$R_a$  = Flame area

$R_f$  = Flame radius

Low stiffness indicating a large burned gas volume (and large flame radius), low pressure and a low flame area. To keep the response frequency high (much above the natural frequency of the chamber) it would be necessary to have a stiff burned gas column, which would mean high pressures or low flame radii. Maxwell and Wheeler [3] as well as Egerton [13] have shown that with long tubes the tendency for vibrations to set in were higher than with shorter tubes, which would indicate that gas columns with low stiffness have a larger tendency to vibrate than gas columns with high stiffness.

#### 5.8 Effect of Fluctuating Flame Front on the Unburned Gas

The Flame front inside a combustion chamber can be considered to move like a diaphragm. The forward motion of the flame front would compress the unburned gas ahead of it and thus increase the temperature and pressure of the unburned gas. As the unburned gas is in a state of high reactivity any increase in the temperature would tend to increase the rate of the reactions occurring in the unburned gas.

A simple parametric study was conducted to investigate the effect of cyclic temperature rise of the unburned gas at the frequency of the flame front oscillations, on the occurrence of knock.

Fig. 5.12 shows the pressure crank angle history for the case with 90 RON fuel and spark timing advanced from MBT by 10 degrees and subjected to 8 and 17 pulses of 20 degrees C and 30 degrees C, the larger the number of pulses the earlier knock occurs in the engine cycle, and the more intense it is. Increasing the duration of the pulses also tends to cause knock to occur earlier in the cycle..

Increase in the amplitude of the flame front fluctuations would, increase the compression effects on the unburned gas thus, increasing the temperature and pressure momentarily. If the frequency of the flame front were to coincide with the natural frequency of the system resonance would occur, which would also amplify the waves.

Experiments conducted and results obtained are discussed in the next chapter.

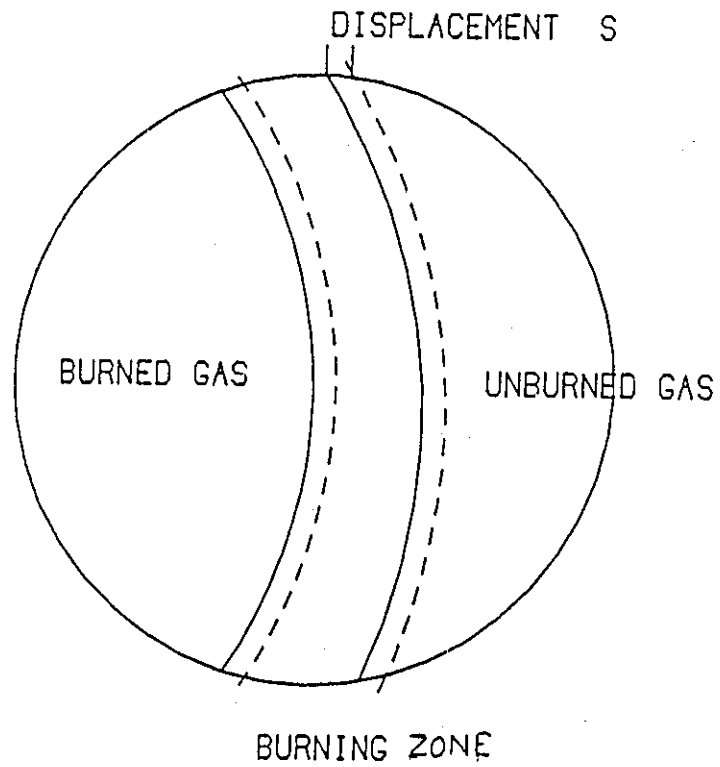


Fig. 5.1 (a) Schematic Diagram of Different zones  
in a combustion Chamber

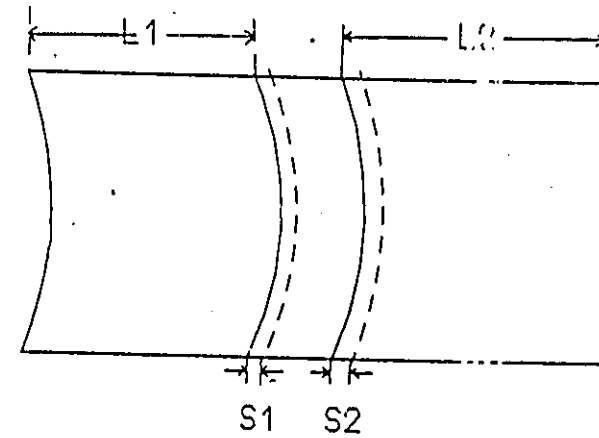


Fig. 5.1 (b) Equivalent Duct  
with uniform area of cross section

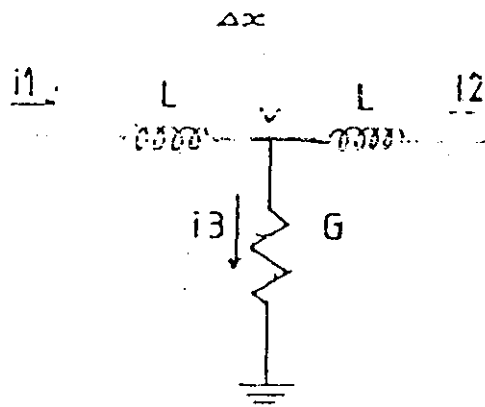


Fig. 5.2 Circuit Representing the Wave Equation

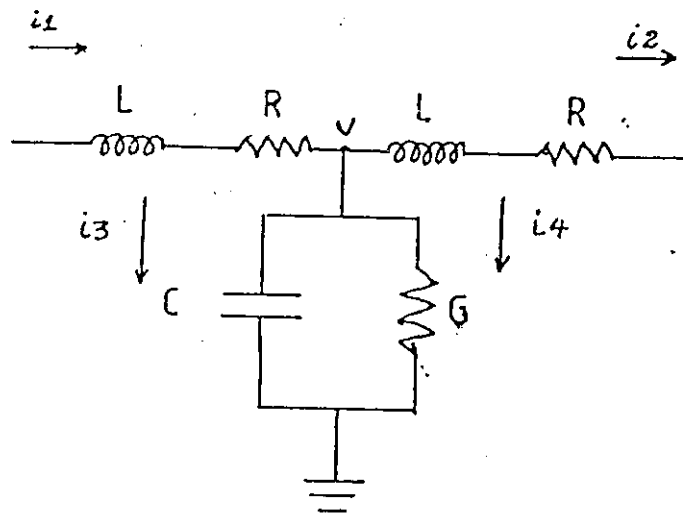


Fig. 5.3 Circuit Representing the Telegraph Equation

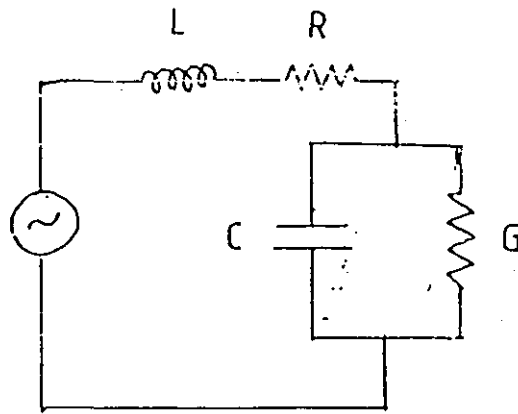


Fig. 5.4 Representaion of Telegraph Equation as Lumped Parameter

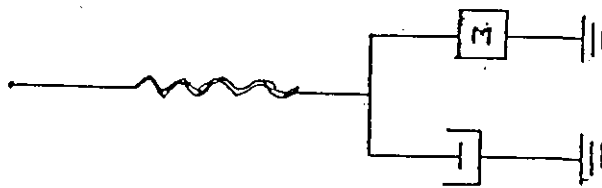


Fig. 5.5 Mechanical Equivalent of above Circuit

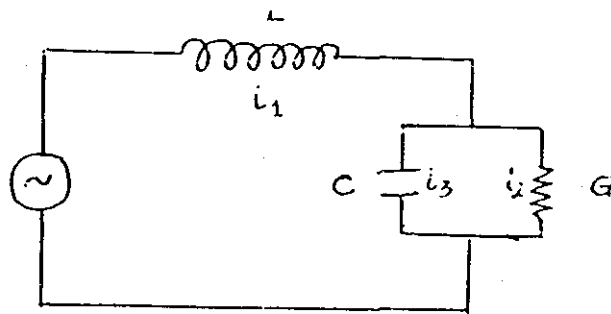


Fig. 5.6 (a) Representation of Telegraph Equation without the Resistive Element

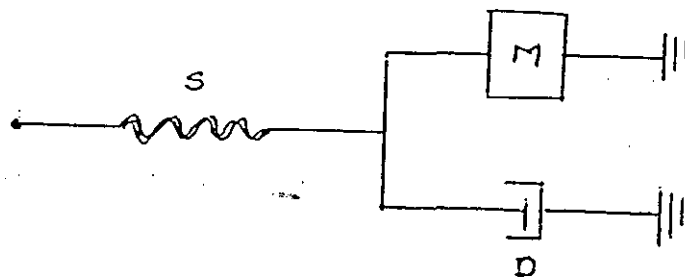


Fig. 5.6 (b) Mechanical Equivalent of above Circuit

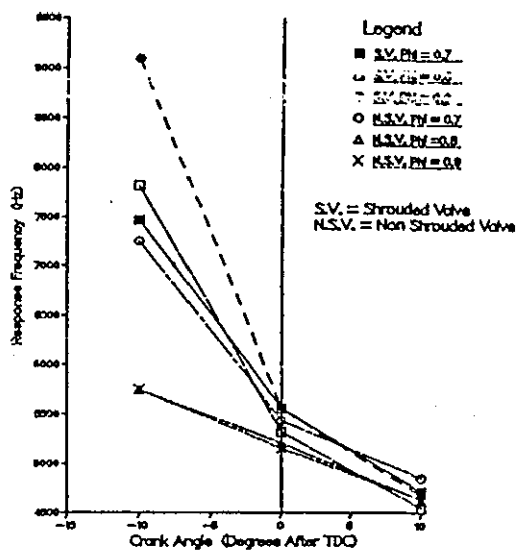


Fig. 5.7 Variation of response Frequency with Crank Angle with Change in Equivalence Ratio

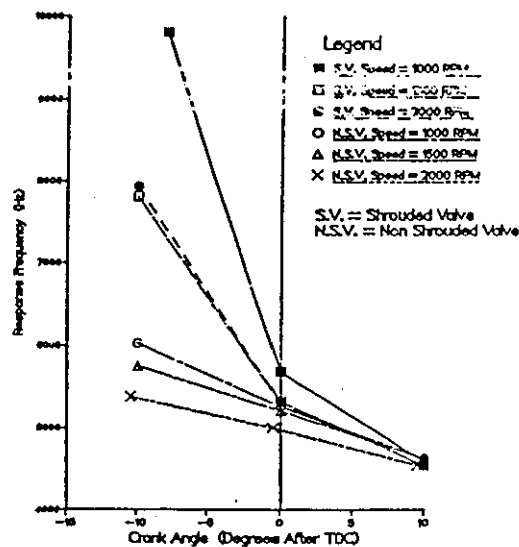


Fig. 5.8 Variation of response Frequency with Crank Angle with Change in Speed

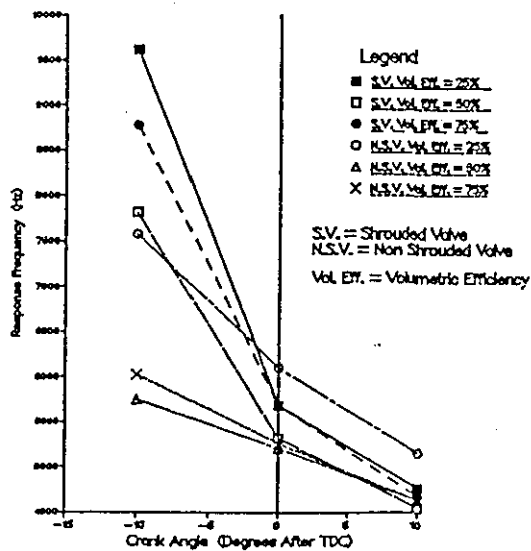


Fig. 5.9 Variation of response Frequency with Crank Angle with Change in Volumetric Efficiency

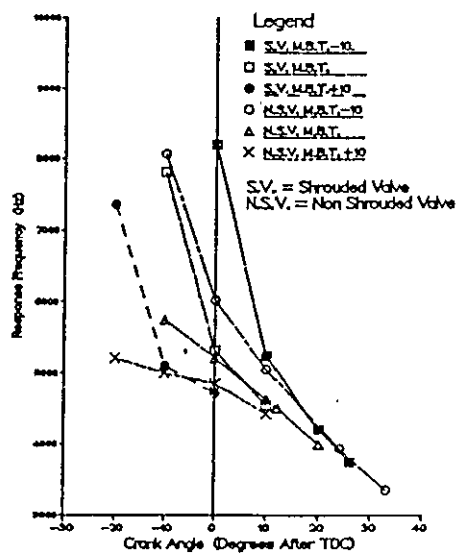


Fig. 5.10 Variation of response Frequency with Crank Angle with change in Spark Timing

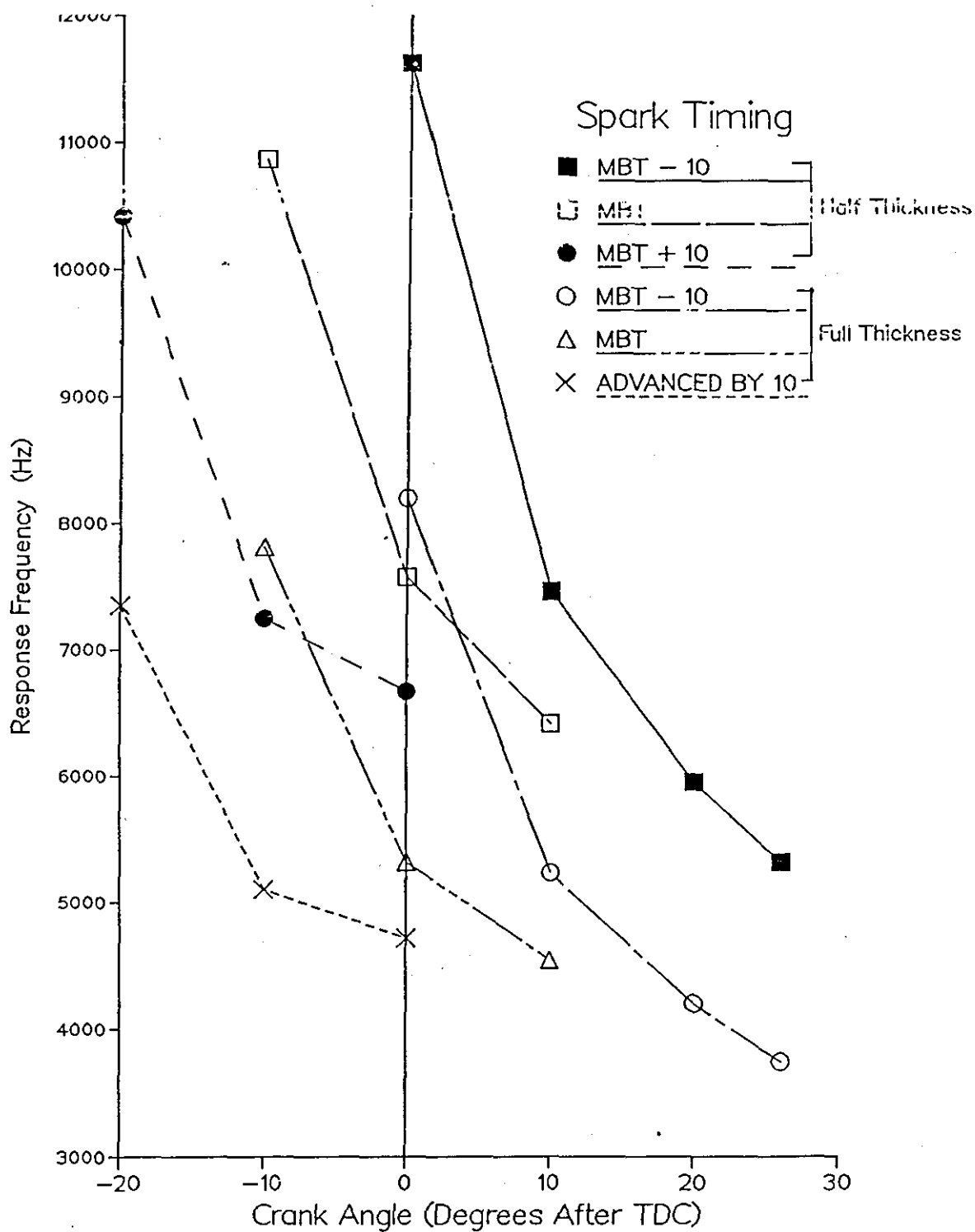


Fig. 5.11 Variation of Response Frequency with Crank Angle  
(Shrouded Valve)

## 90 RON Advanced

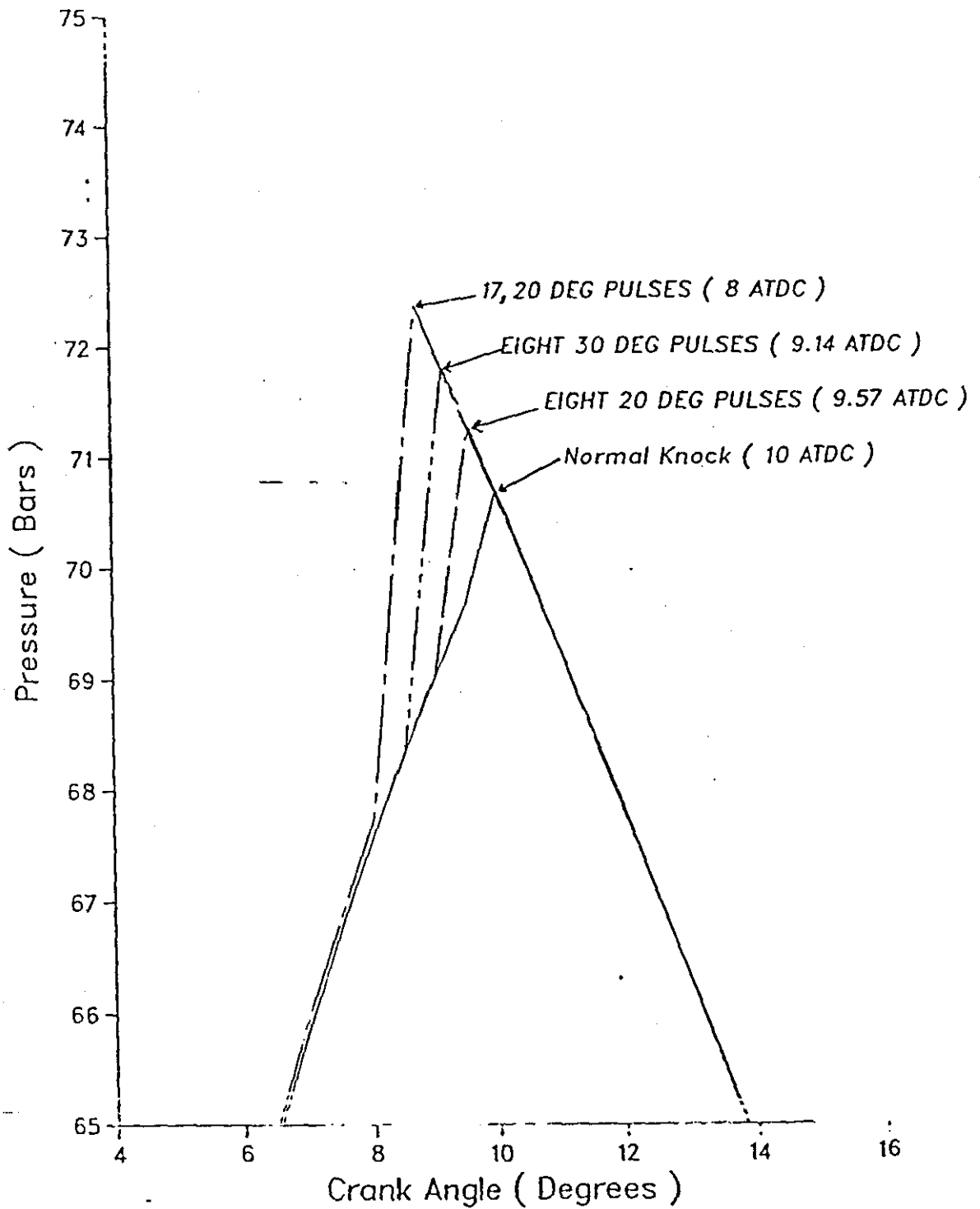


Fig. 5-12 Effect of Temperature Pulses  
on knock

## CHAPTER VI

### RESULTS AND DISCUSSION

#### 6.1 INTRODUCTION

The work reported in this chapter correlates the results obtained from engine experiments with the theoretical analysis presented in chapter V. Flame ionization probe responses at different positions from the cylinder periphery were recorded and analysed. The engine was run on propane, commercial Premium Grade Gasoline and 70 octane fuel made from mixing 70% by volume of iso-octane with 30% by volume of n-heptane, referred to as 70 RON PRF (Primary Reference Fuel)

The experimental results are compared to the results obtained from the model. The analysis from the model presented in Chapter V predict the response frequency of the flame front to be within the range 5000Hz and 9000Hz, depending on the time at which the flame position is considered. To measure the frequency of an oscillating flame by photographic means, it would be necessary to record the displacement of the flame front at a minimum of 2 positions (similar to sampling theory in digitizing analog signals - section 4.8). Therefore to record the flame movement photographically it would be necessary to have a camera that is capable of taking over 18000 frames a second. As such a camera was not available at the time of conducting the experiments. Hence, the flame ionization level was measured and the energy content in the power spectra of the ionization probe responses are compared at the frequencies closest to the natural frequency of the chamber and the knock frequency.

In the case of 70 RON PRF the ionization probe detects fluctuations in the ionization level at frequencies close to that of the pressure signal recorded during knock.

## 6.2 Comment on the Experimental Procedures

Selection of the test conditions were dictated by the endurance limit of the ionization probes in the combustion chamber under firing conditions. The tests were conducted with propane, Premium Grade Gasoline and 70 octane Primary Reference Fuel (PRF).

The test conditions selected with propane were: air-fuel ratios of 13:1; 15:1; and 17:1 to study the effect of mixture strength variations, with spark timing maintained at MBT, and to study the effect of change in the spark timing, with the air-fuel ratio maintained at 15:1 the spark timing was advanced and retarded by 10 degrees crank angle relative to MBT.

The engine compression ratio was kept at 9.3:1. This was the highest compression ratio possible with the introduction of the disc to locate the ionization probes. As explained in chapter IV the engine was fired once in three cycles. The engine had to be operated at no load to keep the engine speed at around 1500 rpm. Running the engine with one cycle in three firing did not produce knocking combustion under any of the above conditions, except with 70 Octane Primary Reference Fuel. (PRF). The reason for the engine not knocking even with very large advances (52 degrees before top dead centre which was 10 degrees advanced from MBT) in the spark timing for both Propane and Premium Grade Gasoline is because both fuels have very good anti-knock qualities, also the combustion chamber cools down between the fired cycles.

Running with Premium Grade Gasoline the compression ratio had to be reduced and the engine run with leaner mixtures (18.3:1) as there was carbon deposition on the ionization probe, which acted as hot spots when run with stoichiometric or rich mixtures. In an attempt to record the probe signal under these conditions quite a few probes were damaged. The compression ratio chosen for the runs with Premium Grade Gasoline and with 70 octane fuel was 8.7:1.

The probes were seated at a minimum depth of 4mm from the cylinder wall to a maximum depth of 35 mm when the engine was run on Propane, whereas when the engine was run with Premium Grade Gasoline and 70 RON PRF seating the probe any deeper than 21mm from the cylinder wall resulted in the probe being damaged due to overheating.

Though the probe location is fixed (i.e. the penetration into the chamber is constant) the flame arrival at the probe varied from cycle to cycle and from one condition to another. The legend 'probe location' on the graphs corresponds to the crank angle position when the probe picks up the flame arrival. To calculate the piston position at the time of flame arrival 10 random cycles were played back from the tape recorder on to the Nicolet FFT analyser. The time from spark to the arrival of the flame at the probe was measured in milliseconds, and knowing the engine speed from the time interval between two TDC marks, the crank angle at the time of flame arrival could be calculated.

The results are presented as frequency spectra of the ionization signal under different engine conditions, the response frequencies calculated from the model presented in chapter V for the positions corresponding to the probe location and the variation of the power content in the frequency components corresponding to 5500 Hz, 6500Hz and 7500 Hz. The natural frequency as calculated from eqn. 5.4 for the set of different engine conditions shown in table 3.1 is plotted in fig 6.17. At peak pressure point (just after top dead centre ) the natural frequencies for nearly all the conditions fall around 5500 Hz.

Draper [76] found in his experiments with a CFR engine running under knocking conditions that the most prominent frequency was 6500 Hz, while Hickling et. al. [77] found that the first mode of the resonant frequency in a spark ignition engine was around 7000 Hz. It would be appropriate to mention here that the resonant frequency of the combustion chamber is inversely proportional to the diameter of the chamber.

Performing a Fourier transformation on the pressure trace and the ionization trace with the Nicolet FFT analyser showed a sharp peak in the power spectrum at 7200 Hz for the pressure trace and at 7300 Hz for the ionization trace (Fig. 6.8). These values compare favourably with the value of 8KHz obtained by Schaefer and Lee [78] when testing the engine at 2000 rpm., Schaefer and Lee mention the fact that the engine speed did not have any significant effect on the knock frequency. Fig. 6.35 shows the variation in the natural frequency of the chamber as the speed is increased. This is due to the fact that for a given air fuel ratio and spark timing (MBT in this case) increasing the speed would result in increased temperatures and pressure in the cylinder. Increased temperatures would mean higher sound velocities which in turn would imply higher natural frequencies (eqn. 5.4).

### 6.3 Experimental Results from tests with Propane

Fig. 6.1 to 6.5 show the frequency spectra of the ionization signal at the different crank angle positions on the engine cycle and under the different engine conditions. The common feature that stands out in all cases is the fact that as the piston moves away from top dead centre the intensity of the overall signal dies down. Iinuma [71] and Kumagai and Kudo [58] found that the concentration of ions falls with fall in pressure. As the piston moves away from TDC the pressure in the chamber would drop resulting in lower concentrations of ions, the lower concentration of ions would therefore lead to a low intensity signal. The most intense signal is either at TDC or very close to TDC. Most frequency spectra show a smooth curve as they represent an ensemble average of 10 random cycles. As the combustion chamber comes closest to a thin disc at top dead centre the frequency spectra of the different probe signals are compared at TDC in Fig. 6.6 and Fig. 6.7

The probe response with lean mixtures (MBT spark Timing) and with stoichiometric mixtures and retarded spark timing are much weaker

than the signals with rich mixtures (MBT spark Timing), stoichiometric mixtures with MBT spark timing and 10 degrees advanced from MBT spark timing.(Figs.6.6 and 6.7) The frequency response of the flame front at the position corresponding to that when the flame hits the probe is plotted against the crank angle position in Fig.6.9. and against the mass fraction burned at that point (calculated from Appendix A) is plotted in Fig. 6.10.

Fig.6.11 to Fig.6.16 show the power in the frequency component corresponding to 5500 Hz, 6500 Hz and 7500 Hz. The lean mixture cases show a much weaker response signal than the others, this could be due to the fact that under lean mixture conditions the ionization level formed around the flame front is much less, as compared to that found with rich mixtures or stoichiometric mixtures [71].In the case of the rich mixtures at TDC, there is a sharp rise in the power followed by drastic fluctuations.The power at 5500 Hz is the highest of the three frequencies selected, this frequency is quite close to the natural frequency of the chamber. The response frequency of the flame front at the beginning of combustion is around 9500 Hz but falls steadily to 6500 Hz at around 66% burn (fig. 6.10). The fall in the case with a stoichiometric mixture is the least, while in the case of the lean mixture it is slightly higher.

Variation of spark timing shows an interesting feature in the response of the ionization probe. The case with MBT spark timing and retarded spark timing shows a steady rise in the power content as the combustion progresses, whereas with the advanced spark timing the response shows a marked rise and then a fall. The peak level is around 10 degrees before TDC, which corresponds to about 97% burn.

The fall in the energy level in the advanced case represents a situation where the major portion of the combustion is over, but the ionization level is still high enough to be recorded by the probe.

## 6.4 Results with Premium Grade Gasoline

Combustion in an engine with propane as a fuel represents a case when the fuel and air in the charge have undergone very good mixing. Propane having a RON (Research Octane Number) greater than 100 represents a case when the engine has to be run under severe conditions to obtain knock. Even when the engine was run with a spark timing of 54 degrees before top dead centre, and firing once in three cycles the engine did not knock. Of the commercially available liquid fuels Premium Grade Gasoline has the highest octane rating (98). A set of tests was therefore conducted with Premium Grade Gasoline.

Due to poor mixing (as compared to propane/air) combustion with Premium Grade Gasoline was much rougher. Rich and stoichiometric mixtures caused the probes to act as hot spots and cause back fire. The ceramic tube inside the probe sheath as well as the probe sheath could not withstand the heat in the engine and disintegrated at the ends. Therefore the engine was run at lean air-fuel ratios (18.3:1) and with varied spark timing.

The effect of varying the spark timing 10 degrees on either side of MBT at an air-fuel ratio of 18.3:1 on the ionization probe response is shown in Figs. 6.18 to 6.20.

The power spectra of the signals corresponding to the flame arrival at TDC are shown in Fig 6.21. In the case of advanced spark timing the combustion has reached a stage where the ionization probe could detect no signal. At 8 degrees before top dead centre all the probe signals show a similar response, though with advanced spark timing the low ionization levels show a low flame intensity, which is normally seen close to the end of combustion (Fig. 6.22). The combustion with advanced spark timing (54 degrees before top dead centre) has progressed to a level where more than 65% of the charge mass has burned.

In contrast to the case of retarded spark timing and stoichiometric air-fuel ratio with propane, the power spectra for retarded spark timing and lean mixtures with commercial Premium Grade Gasoline show a decrease in intensity as the combustion progresses. At the same time the response frequency shows a drastic fall (Fig.6.23). One of the reasons for the probe response being weak is due to dispersion of the ions which would also indicate the presence of a thick flame front. Fig. 6.36 shows the variation in flame thickness at different probe locations for engine runs with commercial Premium Grade Gasoline and 70 RON PRF. The flame thickness is calculated by first measuring the time difference between the recording of the first peak and the second peak in the flame ionization signal and then multiplying it by the average flame speed of Iso-octane. The flame speed used in these calculations are those published by Mattavi. et. al. [42]. Mattavi et. al. computed the flame speeds from cylinder pressure data for an engine with a disk shaped combustion chamber.

The Flame speed increases to a maximum at around 50% burn [42] and then drops down. An assumption of constant flame speed would therefore not show the true characteristics of the variation in flame thickness when calculated as described above. If the flame speed were assumed to be increasing as the combustion progresses then the curves depicting flame thickness for advanced spark timing and MBT spark timing would show an increase in thickness rather than stay approximately constant. This would compare with the finding of Mattavi et. al. that the flame thickness increases as the flame propagates.

The Figures 6.23 and 6.24 show the variation of the response frequency with crank angle for the case with Premium Grade Gasoline and lean air-fuel ratios. The tendency for the response frequency to fall as combustion progresses is seen in these figures, indicating a thickening of the flame front as well as a decrease in the stiffness of the system. The Flame thickness calculated as described above shows a decreasing tendency for retarded spark timing while a

steady and slightly rising tendency with MBT and advanced spark timing (Fig. 6.36). As explained above taking into account corrections to the flame speed this would show an increase in the flame thickness with MBT and Advanced timing. This compares favourably with the results of Fig. 6.23 and Fig. 6.24.

According to Iinuma, [71] the ion level is proportional to the pressure, a decreasing level of ion intensity would also indicate lower pressure and density levels. As compared to stoichiometric and slightly lean (around 16:1) mixtures, very lean mixtures develop lower pressures in the combustion chamber, which would indicate the reason for the low intensity levels with lean mixtures.

As with propane the power content in the frequency component corresponding to 5500Hz, 6500Hz and 7500 Hz are plotted in Fig. 6.25 to 6.27.

## 6.5 Results with 70 octane PRF

Running tests with propane and Premium Grade Gasoline showed the frequency response and the flame instability under conditions removed from knock. 70 RON PRF knocks in an engine even when fired once in three cycles, thus making it possible to record the ionization probe signals without damaging the ionization probes.

A mixture of 70 octane PRF at 16.4 air-fuel ratio and spark timing of 16 degrees before top dead centre produced a knocking cycle. The probe locations are closer to the wall as longer probes were damaged within 20 seconds of firing the engine.

Fig. 6.31 shows the probe response wherein the first pulse corresponds to the flame arrival, while the second set of pulses correspond to that of engine knock. Fig. 6.28 shows the frequency spectra of the ionization probe signal corresponding to the first pulse, (i.e. corresponding to the flame arrival.) and Fig. 6.30 shows

the frequency spectra for the second pulse. The sharp peak at around 7000 Hz shows the major frequency component at the time of knock.

Fig. 6.29 shows the variation in the power at the three selected frequencies against the position of the piston. The interesting feature of this figure is that there is very little change in the power content of the frequency component corresponding to 5500 Hz. The crank angle at which all the frequencies have the highest power corresponds to that when knock occurs, this is seen from Figs. 6.31 to 6.34 which shows the pressure pulse as well as the ionization probe response at knock.

The power content in the frequency component corresponding to 7500 Hz drops immediately after knock occurs.

The probes recording the flame arrival at crank angle positions corresponding to 2.0 degrees before top dead centre, 2.15 and 2.5 degrees after top dead centre recorded the knock fluctuations after recording the flame arrival whereas the probe which was closer to the wall only picked up the flame arrival pulse but not the knock.

The time interval between the flame arrival and the occurrence of knock is on an average between 2 degrees crank angle and 5 degrees crank angle. Fig. 6.31 which is a representative case for the probe located at 21 mm from the cylinder wall inwards, with both the probe signal and the pressure signal shows the start of pressure fluctuations to be around one degree after the flame arrival, though the ionization probe picks up the fluctuations in the ionization level about a degree later.

## 6.6 Discussion of Results

Interaction between pressure waves and the flame front has been noticed in combustion bombs by Kogarko and Rhyzkov [31] and Leyer and Mason[29]. Due to the lack of instrumentation to record the actual flame movement in the engine (i.e. Photographic equipment that could record the flame oscillations), the nearest feature correlating the frequency composition of the flame front was the power spectrum of the ionization probe signal. The variation in the power spectra of the ionization probe signal at different locations in the combustion chamber has been presented. The power content of the signals at around the natural frequency of the chamber at top dead centre (i.e. 5500 Hz) has been presented. The selection of 6500 Hz and 7500 Hz was based on the fact that various authors (76,77,78) have found the predominant knock frequencies to be in this range. The author has found from his experimental results (Fig. 6.8) that the most predominant frequency as recorded by an ionization probe is 7300 Hz under knocking conditions.

The digital Fourier transformation of any signal results in the power spectra at discrete frequencies, the step size of which is obtained by dividing the frequency range selected by the number of points in the sample. (in the present case it is 499 Hz). Propane and Premium Grade Gasoline having very high anti-knock qualities, no knocking could be produced under the conditions where the data was taken.

The results with 70 octane show an interesting feature in that the probe picks up a fluctuating ionization level when knock occurs after the flame front passes the probe but not before, i.e. if the probe were stationed in the unburned gas zone at the time of knock the probe does not pick up any fluctuating ionization levels( Fig. 6.37 shows a sketch of the flame front, autoignition zone and the probe location corresponding to the case when the ionization probe does not detect any fluctuating ionization levels) . This indicates that knock probably occurs between the flame front and the tip of

the ionization probe and when the end gas starts to autoignite the pressure waves push the ions out towards the burned gas. Fig. 6.31 to 6.34 show representative plots of the ionization probe signals during knocking combustion at four positions corresponding to 21mm, 18mm, 14mm and 4mm from the cylinder wall.

The occurrence of knock is about 2 degrees crank angle after the flame arrival at the probe positioned 14mm from the wall, and on average is about 5.5 degrees after top dead centre.

In section 1.1 the different theories as to the cause of knock were discussed. In section 5.8 it was proposed that the possible interaction between the compression waves and the chemically unstable end gas was a contributory factor to knock.

Following the theory for autoignition the complete unburned zone would ignite when the temperature and pressure reached the critical limit. Modelling knock in a spark ignition engine with the aid of a two-dimensional combustion model with a thick flame front Natarajan and Bracco [32] introduced the knock model proposed by Halstead et. al.[21] to calculate the low temperature ignition on the unburned side. The interaction of the high temperature regime with the low temperature reactions resulted in some of the species produced by the intermediate or high temperature reactions diffusing into the low temperature region at the foot of the flame, react with the low temperature radicals, and reduce their concentration. To overcome this drawback, Natarajan and Bracco [32] considered two cases, one wherein the flame inhibits the low temperature reactions and is not greatly affected by them and the second where the flame accelerates the low temperature reactions and is in turn accelerated by them. Natarajan and Bracco [32] report a better correlation between the computed and experimental data when the former theory (i.e. flame inhibition theory) was used, whereas applying the second criterion of flame initiation gave results which implied that knock originated just in front of the flame front. The results from the second case are shown to support Curry's [57] theory that knock was due to a

sudden flame acceleration.

Variation in the flame movement was recorded by Iwashita and Saito [82], the flame area normalized against the maximum flame area showed a sharp rise just before knock occurred (with 85 RON PRF). The standard deviation of the normalized flame area also showed a sudden increase indicating a sudden rise in the fluctuations in the flame area. As the frame speed (i.e. number of frames per second) used was between 4000 and 10000 and would not be high enough to resolve any fluctuations in the flame front at frequencies predominant at the time of knock (as the knock frequencies are around 7500 Hz and for frequency analysis at least 2.5 samples per cycle are required). Also the resolution of the television screen is not high enough to show the fine irregularities in the flame front. The ionization probe has an advantage here in that it can record the fluctuations in the ion density (which represents the flame front) both in forward and reverse directions.

Modelling the effect of temperature pulses on the unburned gas has shown that it advances the time knock occurs (Fig. 5.12.). Fig. 6.31 to 6.34 show that knock occurs at a point between the flame front and the wall, much closer to the probe that is situated 14mm from the wall. This shows that the unburned gas zone just ahead of the flame front autoignites, creating a high ionization level. The probe close to the wall picks up the flame arrival after knock occurs, but no fluctuating pulses. This could indicate that as autoignition takes place just ahead of the flame front, the pressure fluctuations set up by the autoignition push the ions back towards the burned gas zone. The moving flame in turn would push the ions forward towards the unburned zone, thus creating a fluctuating band of ions. The ionization levels do not reach very far ahead of the flame front due to autoignition as is evident from the fact that the probe close to the wall has not picked up any fluctuating pulses when knock occurs. The fluctuating ion levels picked up by the probes after the flame arrival could also indicate that, due to the interaction of the flame front instability with the unburned gas in front of the flame,

the unburned gas just preceding the flame front would autoignite causing the pressure waves to push the ion clouds back and forth between the autoignition zone and the burned gas zone.

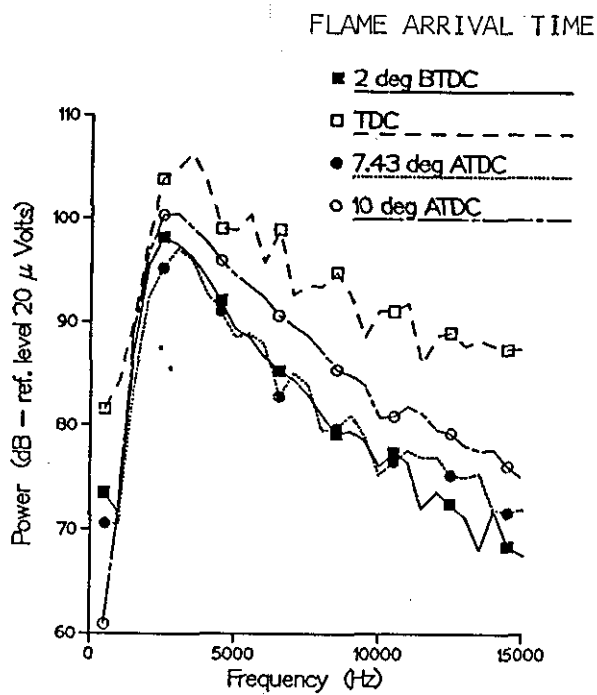


Fig. 6.1 Air-Fuel Ratio = 13.0  
Spark Timing 24° BTDC (MBT)

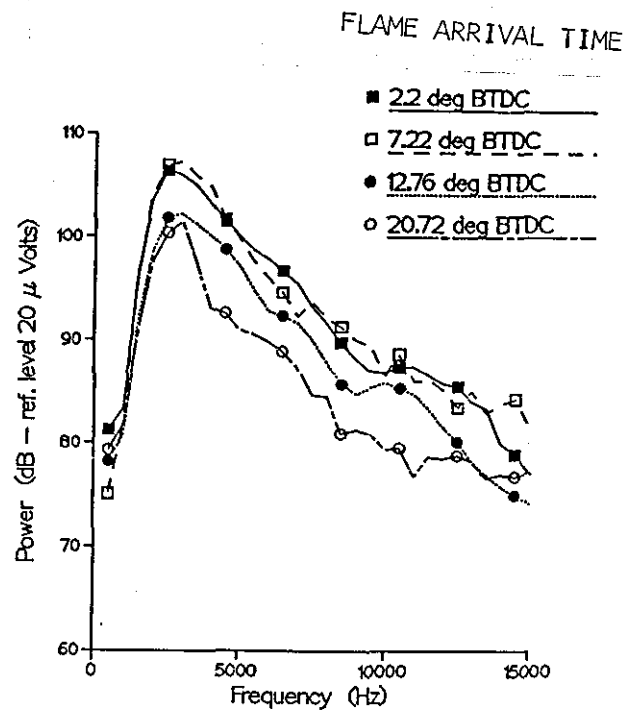


Fig. 6.2 Air-Fuel Ratio = 15.0  
Spark Timing 32° BTDC (MBT)

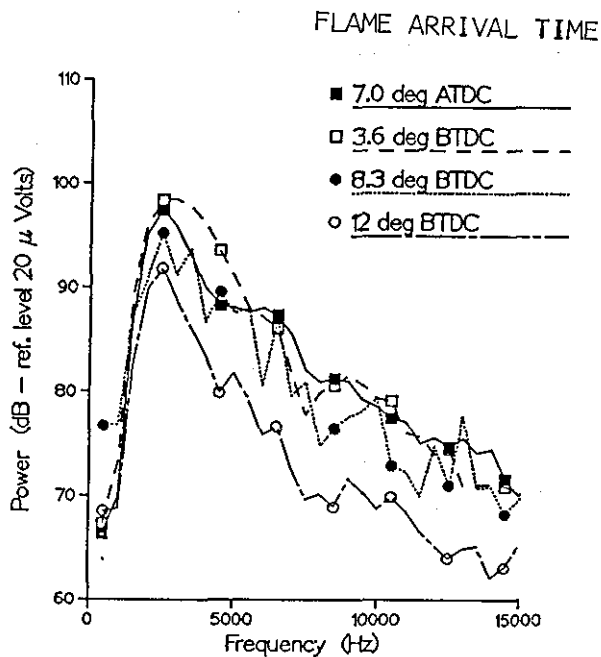


Fig. 6.3 Air-Fuel Ratio = 17.0  
Spark Timing 40° BTDC (MBT)

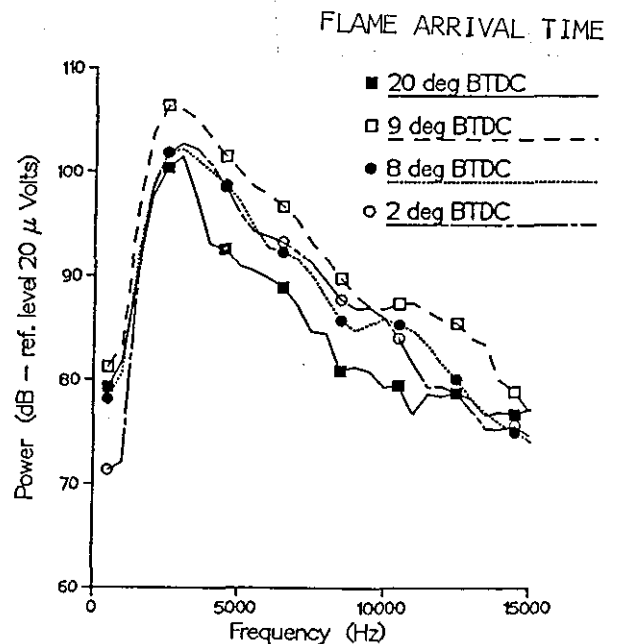


Fig. 6.4 Air-Fuel Ratio = 15.0  
Spark Timing 40° BTDC (ADV)

Power Spectra of Signals from Different Ionization Probes  
Ricardo E6 Engine, Fuel — Propane Gas  
Speed = 1500 RPM, Wide Open Throttle

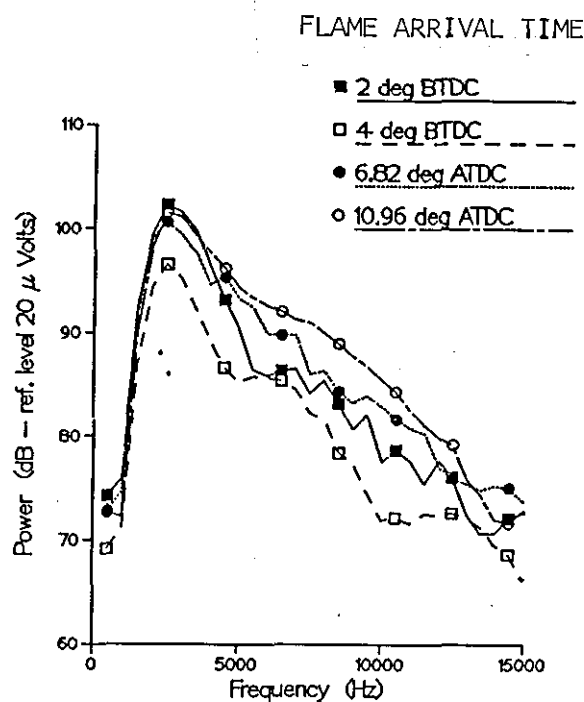


Fig. 6.5 Air-Fuel Ratio = 15.0  
Spark Timing 24° BTDC (RET)

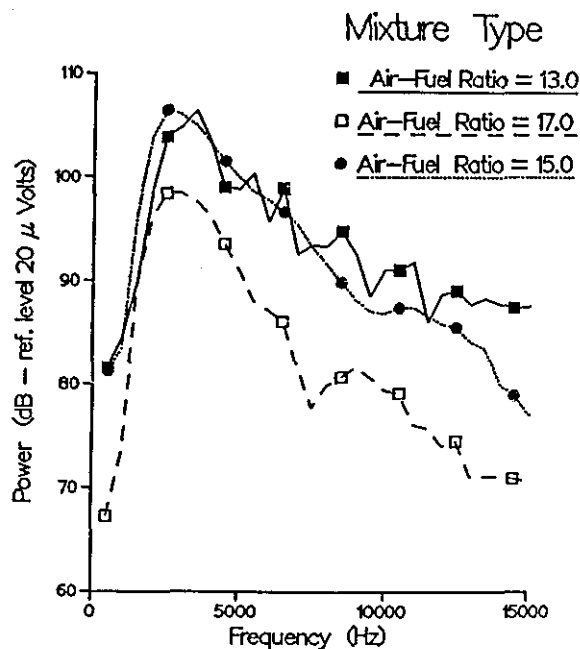


Fig. 6.6 Power Spectra of Signals at TDC  
Spark Timing MBT

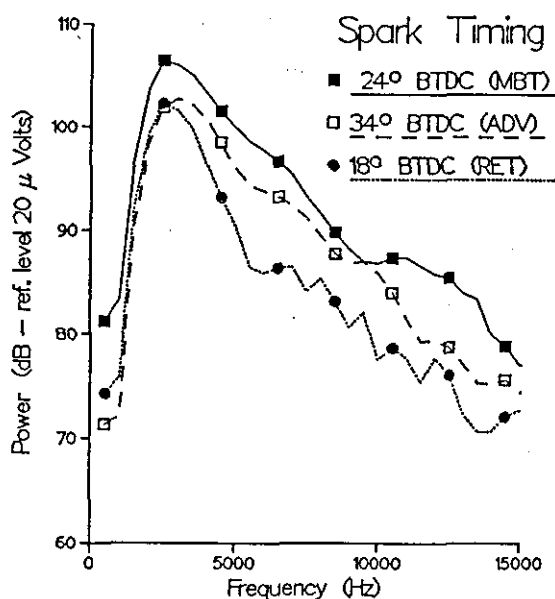


Fig. 6.7 Power Spectra of Signals at TDC  
Air-Fuel Ratio = 15.0

Power Spectra of Signals from Different Ionization Probes  
Ricardo E6 Engine, Fuel — Propane Gas  
Speed = 1500 RPM, Wide Open Throttle

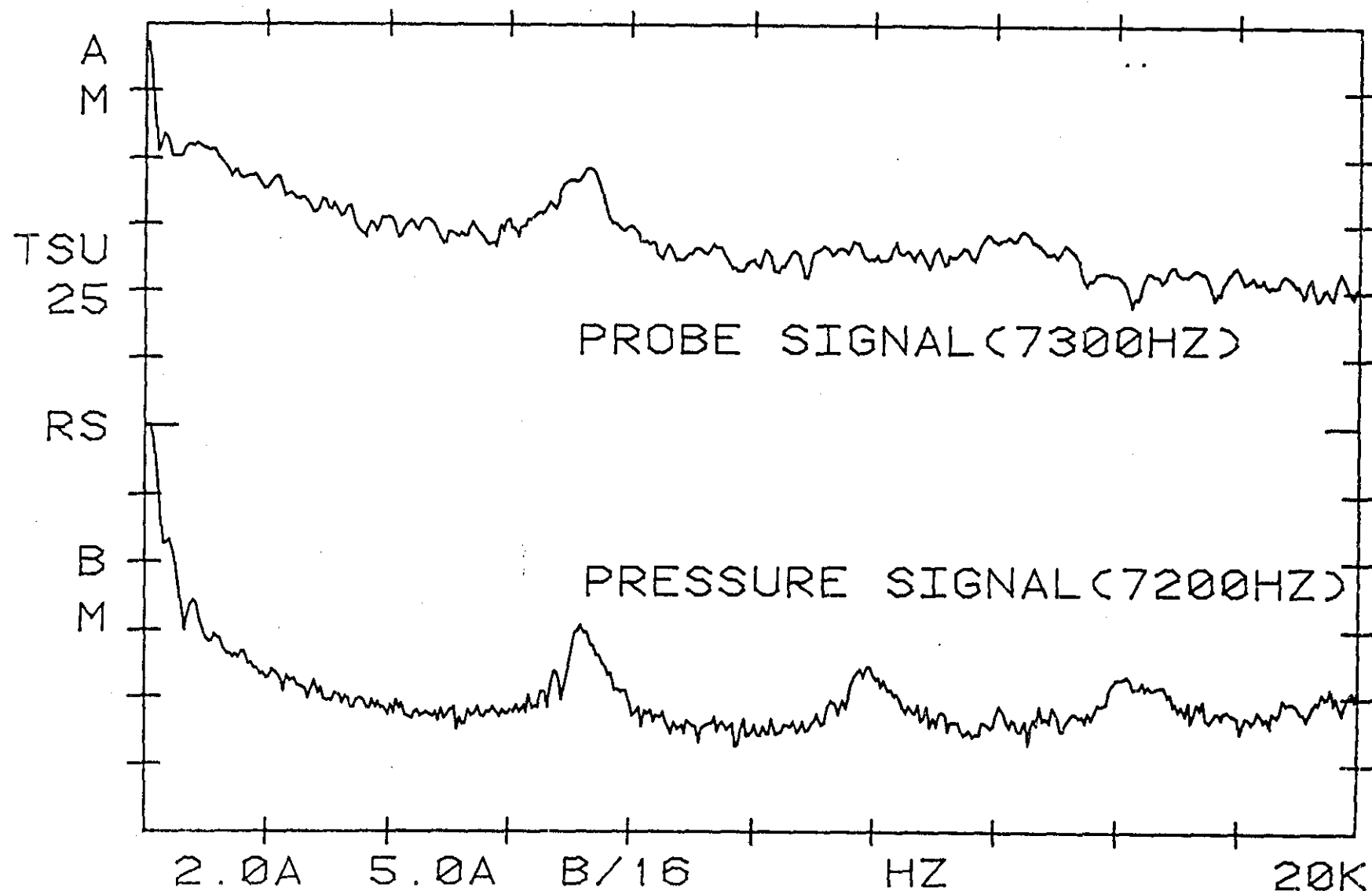
70 RON FUEL

100.-03 V

VLG

100.-03 V

T



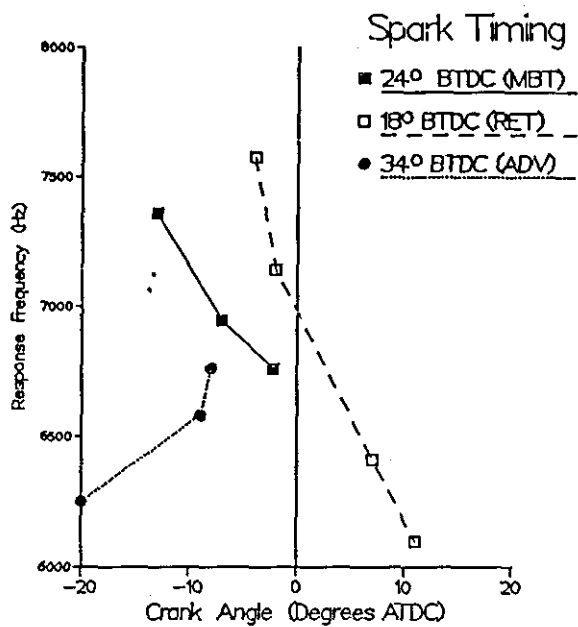


Fig. 6.9(a) Variation of Response Frequency with Crank Angle at  $\phi = 1.0$

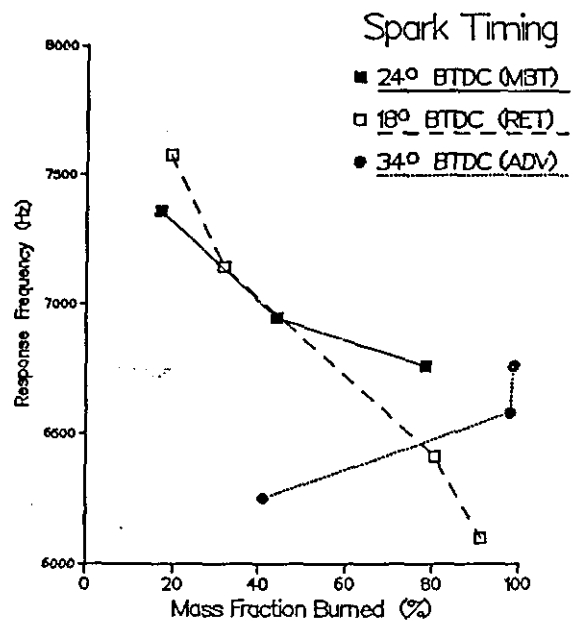


Fig. 6.10(a) Variation of Response Frequency with Mass Fraction Burned at  $\phi = 1.0$

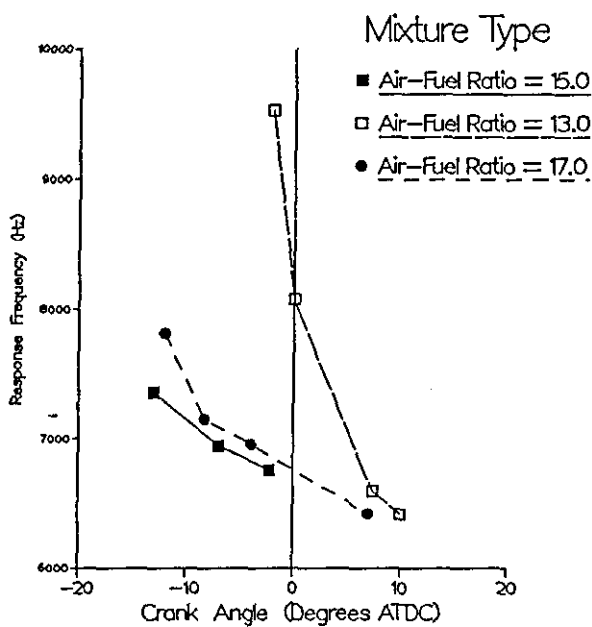


Fig. 6.9(b) Variation of Response Frequency with Crank Angle at MBT Spark Timing

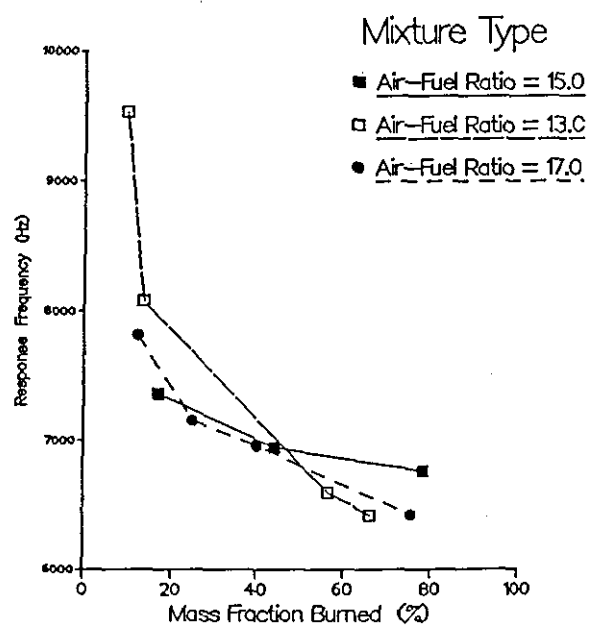


Fig. 6.10(b) Variation of Response Frequency with Mass Fraction Burned at MBT Spark Timing

Calculated Response Frequency at Probe Positions  
Ricardo E6 Engine, Fuel — Propane Gas  
Speed = 1500 RPM, Wide Open Throttle  
Compression Ratio = 9.3

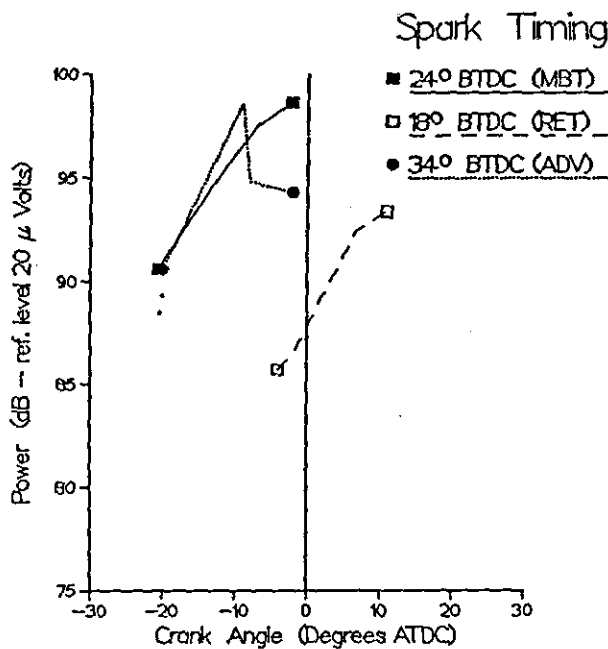


Fig. 6.11 Power Content of Signal at 5500Hz

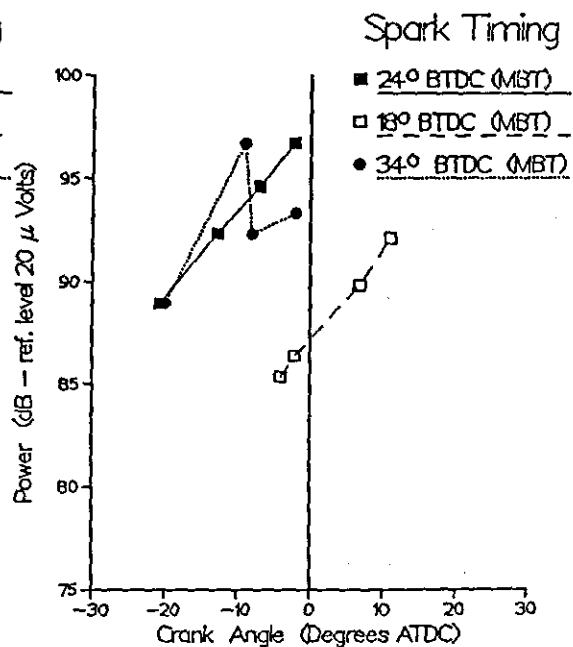


Fig. 6.12 Power Content of Signal at 6500Hz

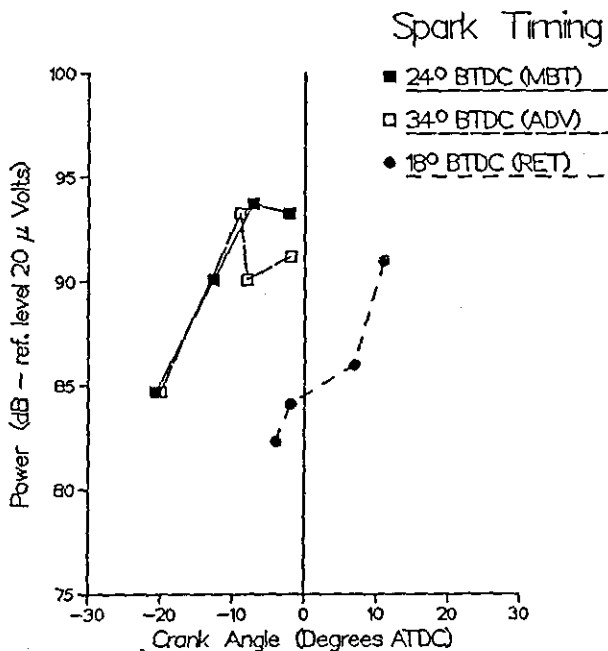


Fig. 6.13 Power Content of Signal at 7500 Hz

Power Content of Signals at Various Frequencies  
 Ricardo E6 Engine, Fuel — Propane Gas  
 Speed = 1500 RPM, Wide Open Throttle  
 Air-Fuel Ratio = 15.0, Compression Ratio = 9.3

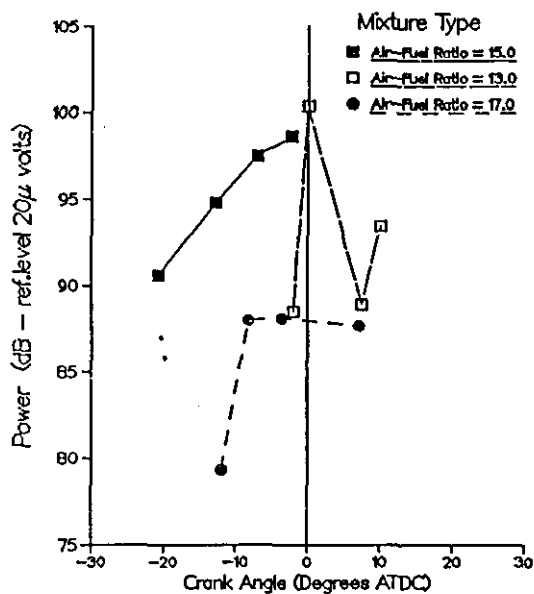


Fig. 6.14 Power Content of Signal at 5500 Hz

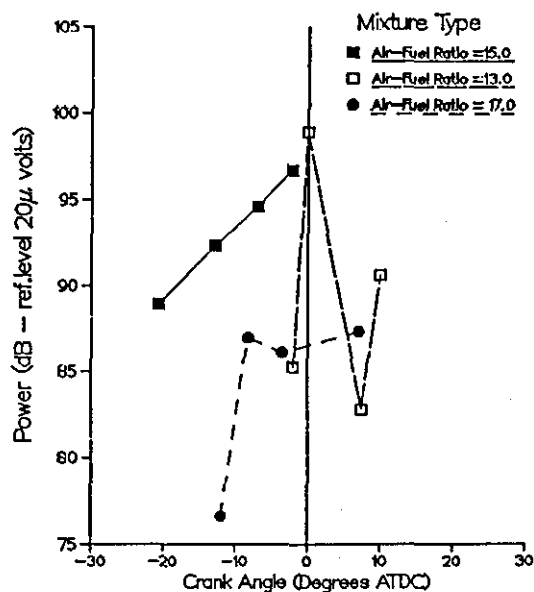


Fig. 6.15 Power Content of signal at 6500 Hz

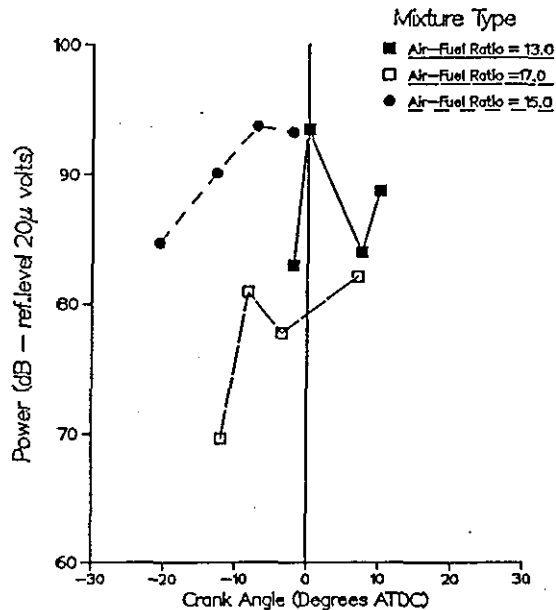


Fig. 6.16 Power Content of Signal at 7500 Hz

Power Content of Signals at Various Frequencies  
 Ricardo E6 Engine, Fuel — Propane Gas  
 Speed = 1500 rpm, Wide Open Throttle  
 Spark Timing = MBT, Compression Ratio = 9.3

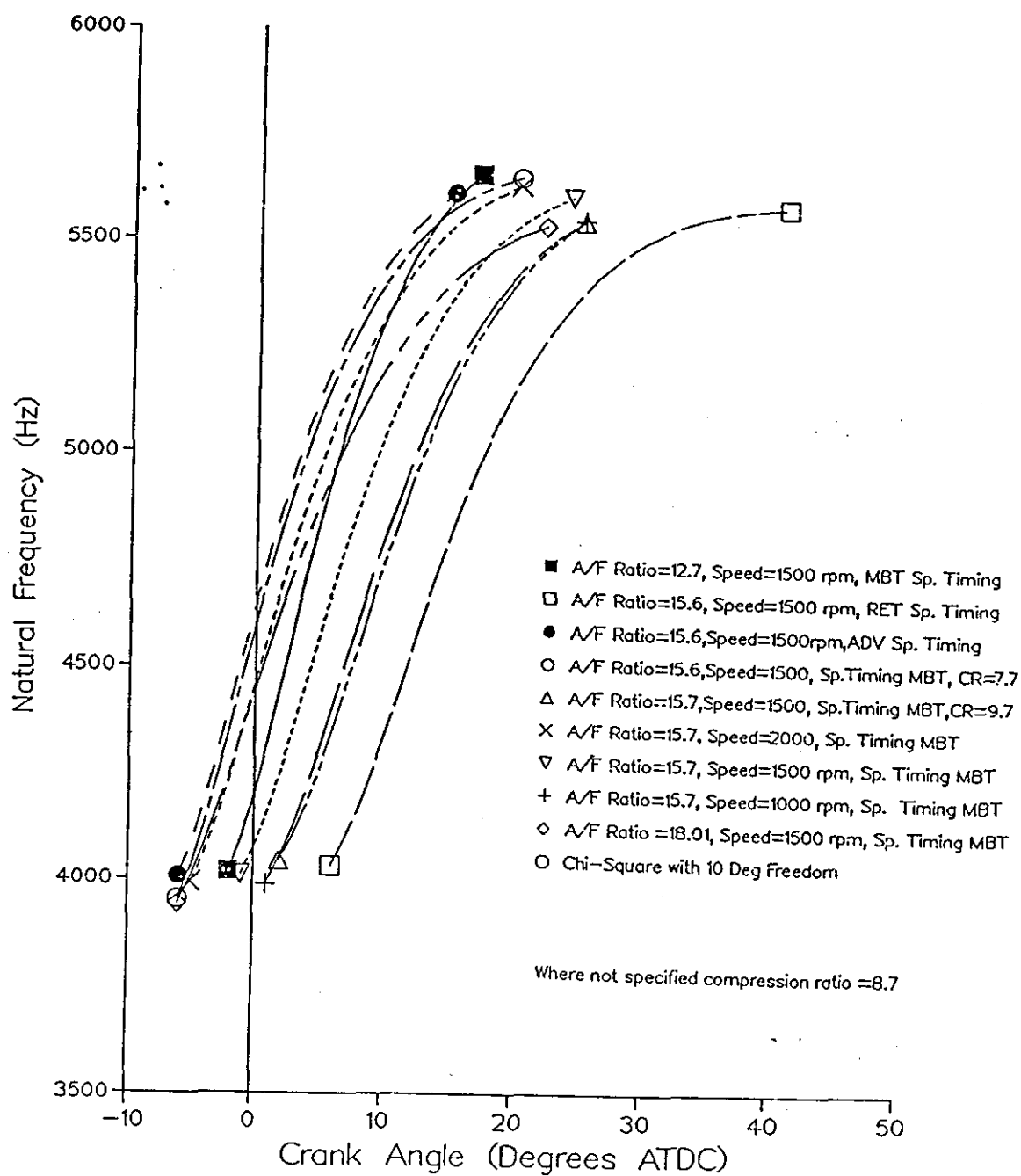


Fig. 6.17 Natural Frequency of Chamber at Different Conditions

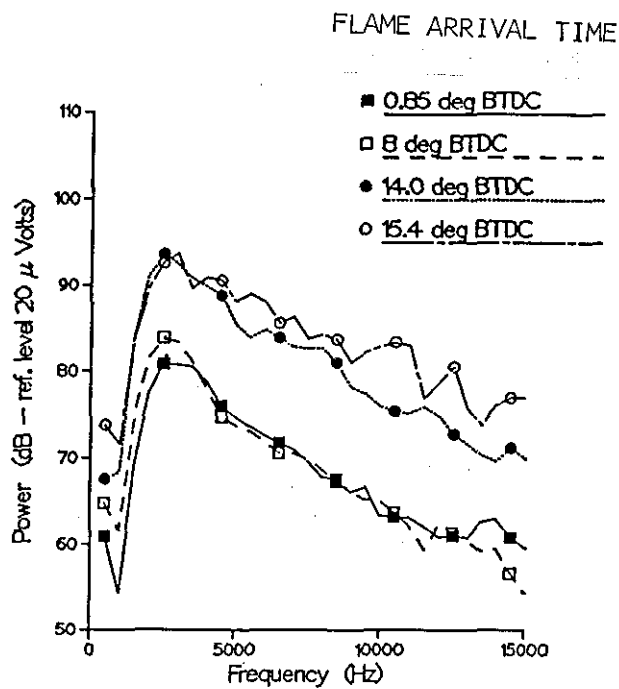


Fig. 6.18 Spark Timing 32° BTDC (RET)

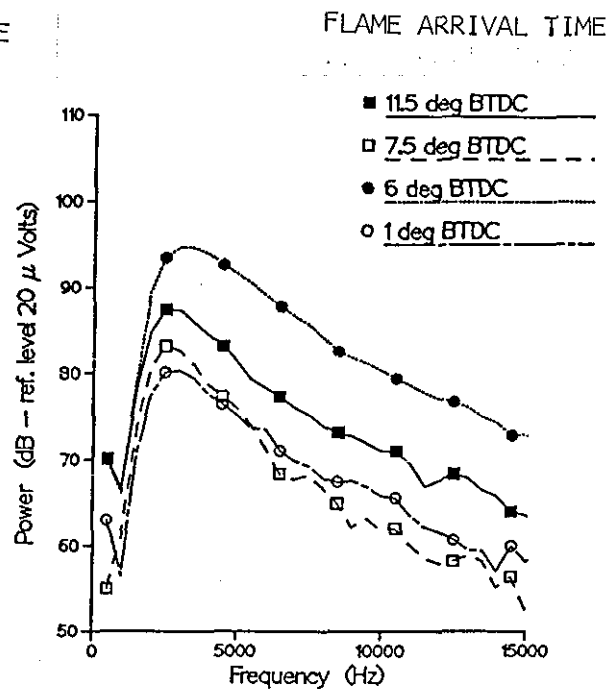


Fig. 6.19 Spark Timing 42° BTDC (MBT)

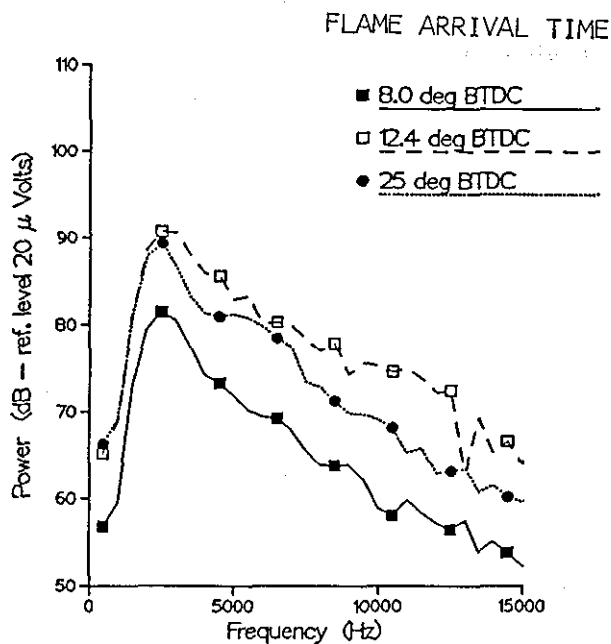


Fig. 6.20 Spark Timing 52° BTDC (ADV)

Power Spectra of Signals from Different Ionization probes  
 Ricardo E6 Engine, Fuel — Premium Grade Gasoline  
 Speed = 1500 RPM, Wide Open Throttle  
 Air-Fuel Ratio = 18.3, Compression Ratio = 8.7

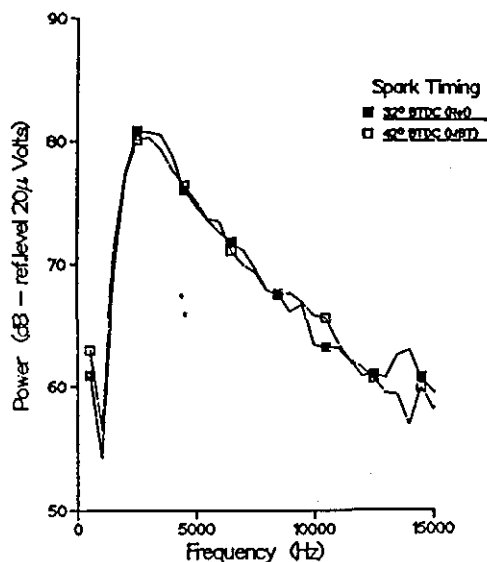


Fig. 6.21 Power Spectra of Signals at Top Dead Centre

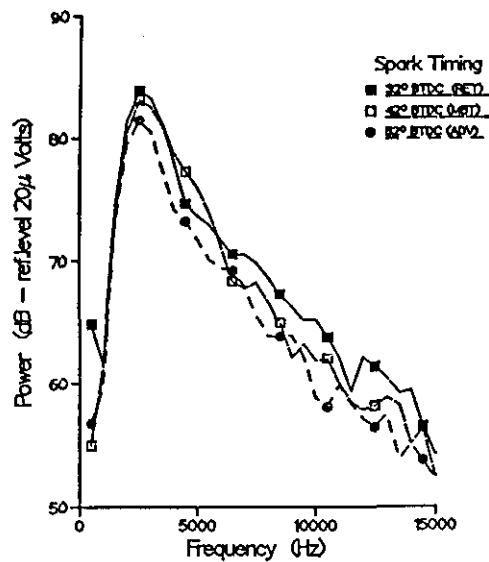


Fig. 6.22 Power Spectra of Signals 8° Before TDC

## Power Spectra of Ionization Probe Signals

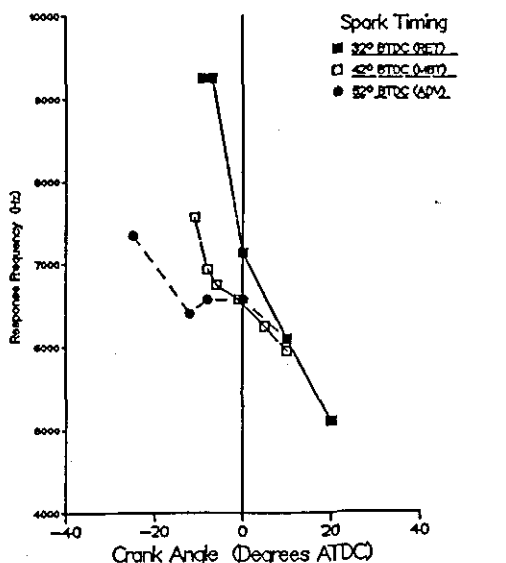


Fig. 6.23 Response Frequency (From Model) v/s Crank Angle

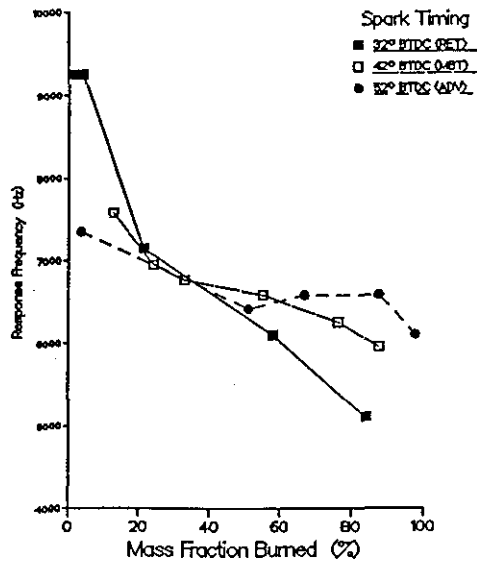


Fig. 6.24 Response Frequency (From Model) v/s % Mass Burned

Calculated (from Model) Response Frequency  
 Ricardo E6 Engine, Fuel — Premium Grade Gasoline  
 Speed = 1500 RPM, Wide Open Throttle  
 Air-Fuel Ratio = 18.3, Compression Ratio = 8.7

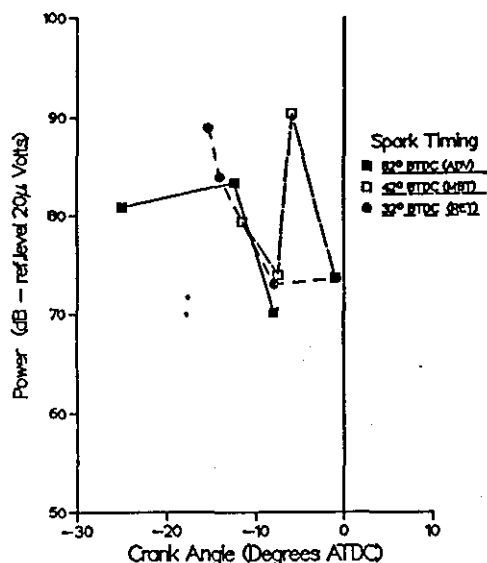


Fig. 6.25 Power Content of Signal at 5500 Hz

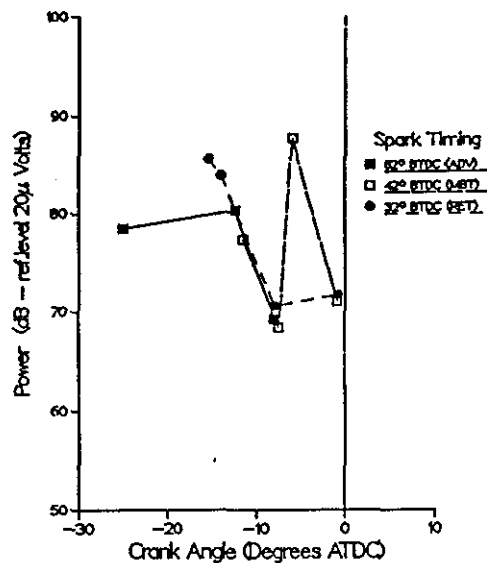


Fig. 6.26 Power Content of Signal at 6500 Hz

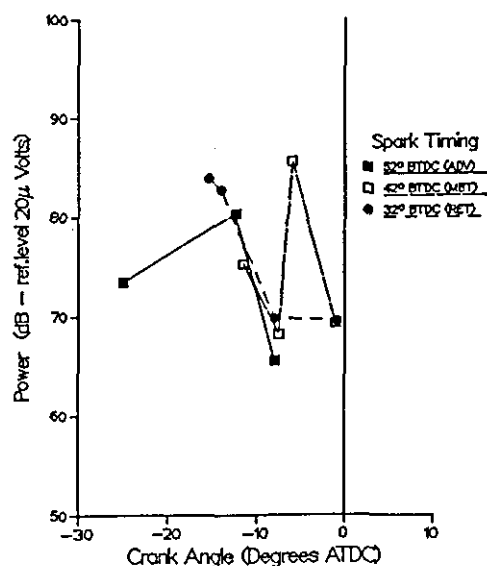


Fig. 6.27 Power Content of Signal at 7500 Hz

Power Content of Signals at Selected Frequencies  
 Ricardo E6 Engine, Fuel — Premium Grade Gasoline  
 Speed = 1500 RPM, Wide Open Throttle  
 Air-Fuel Ratio = 18.3, Compression Ratio = 8.7

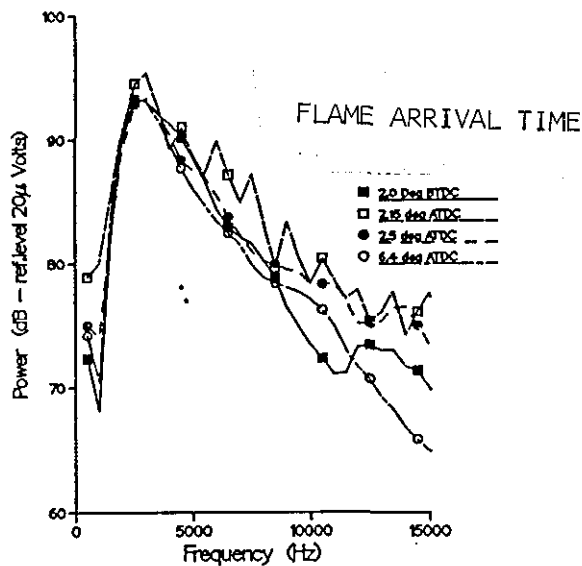


Fig. 6.28 Power Spectra from Different Probes

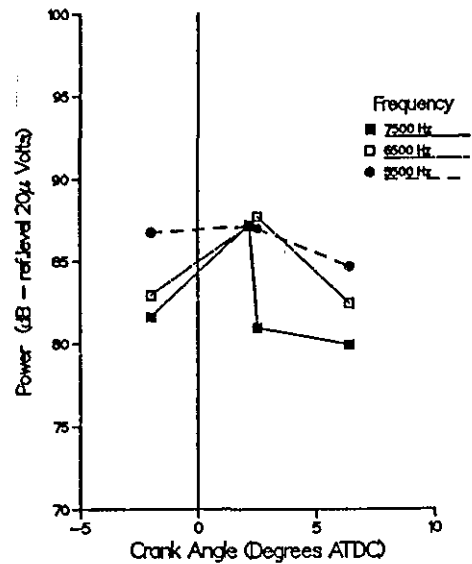


Fig. 6.29 Power Content of Signals at Selected Frequencies

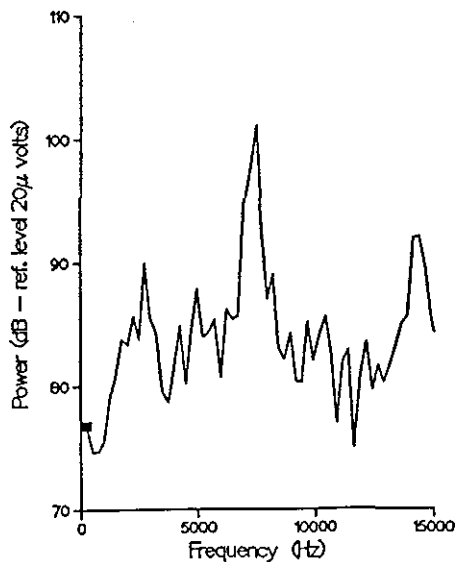


Fig. 6.30 Power Spectrum of Probe Signal at the time of Knock

Ricardo E6 Engine, Fuel — 70 RON PRF  
 Speed = 1500 RPM, Wide Open Throttle  
 Air-Fuel Ratio = 16.4, Compression Ratio = 8.7

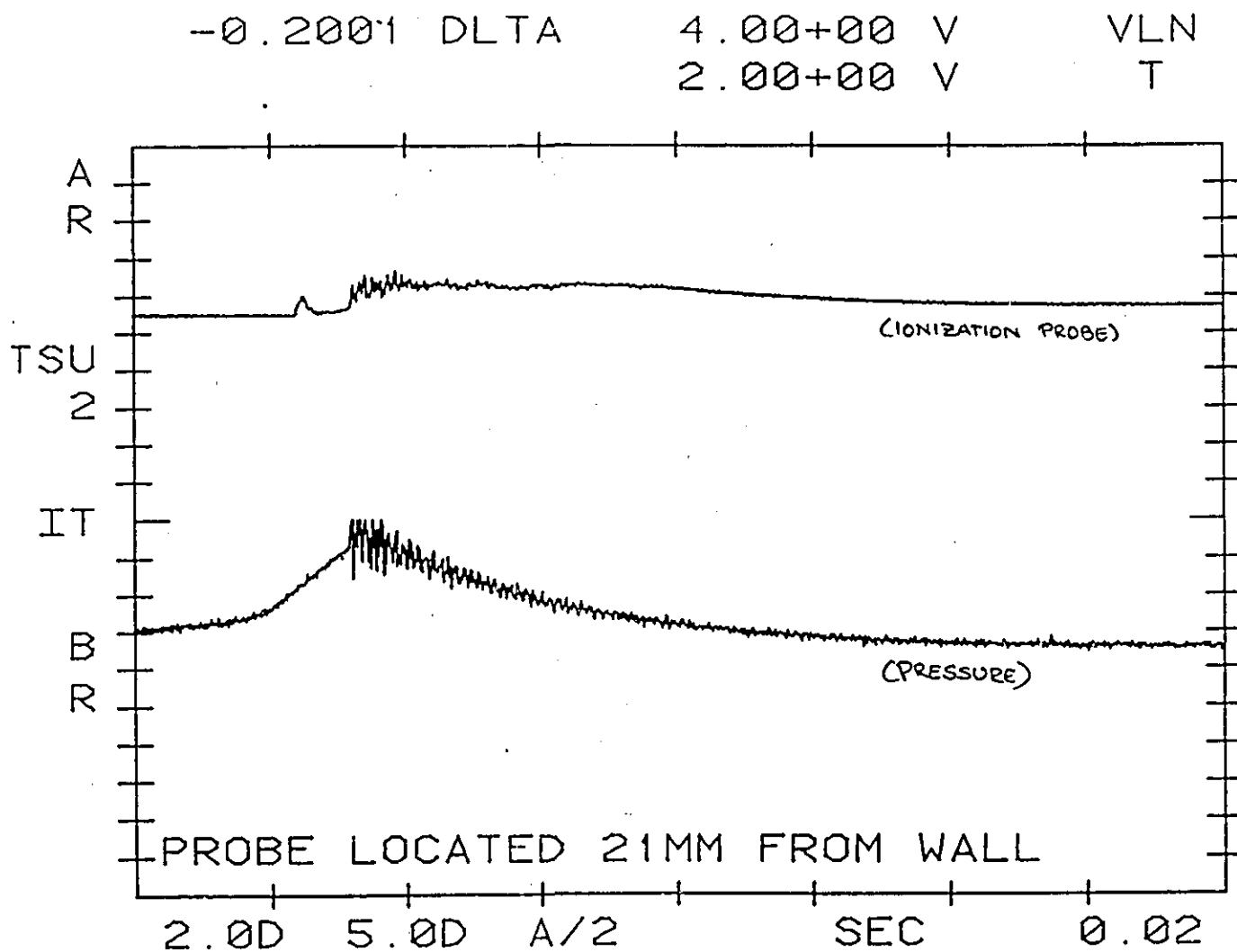


Fig. 6.31 Ionization Probe and Pressure Response with Knock  
 Ricardo E6 Engine , Fuel - 70 RON PRF  
 Speed = 1500 rpm, Air-Fuel Ratio = 16.4  
 Compression Ratio = 8.7

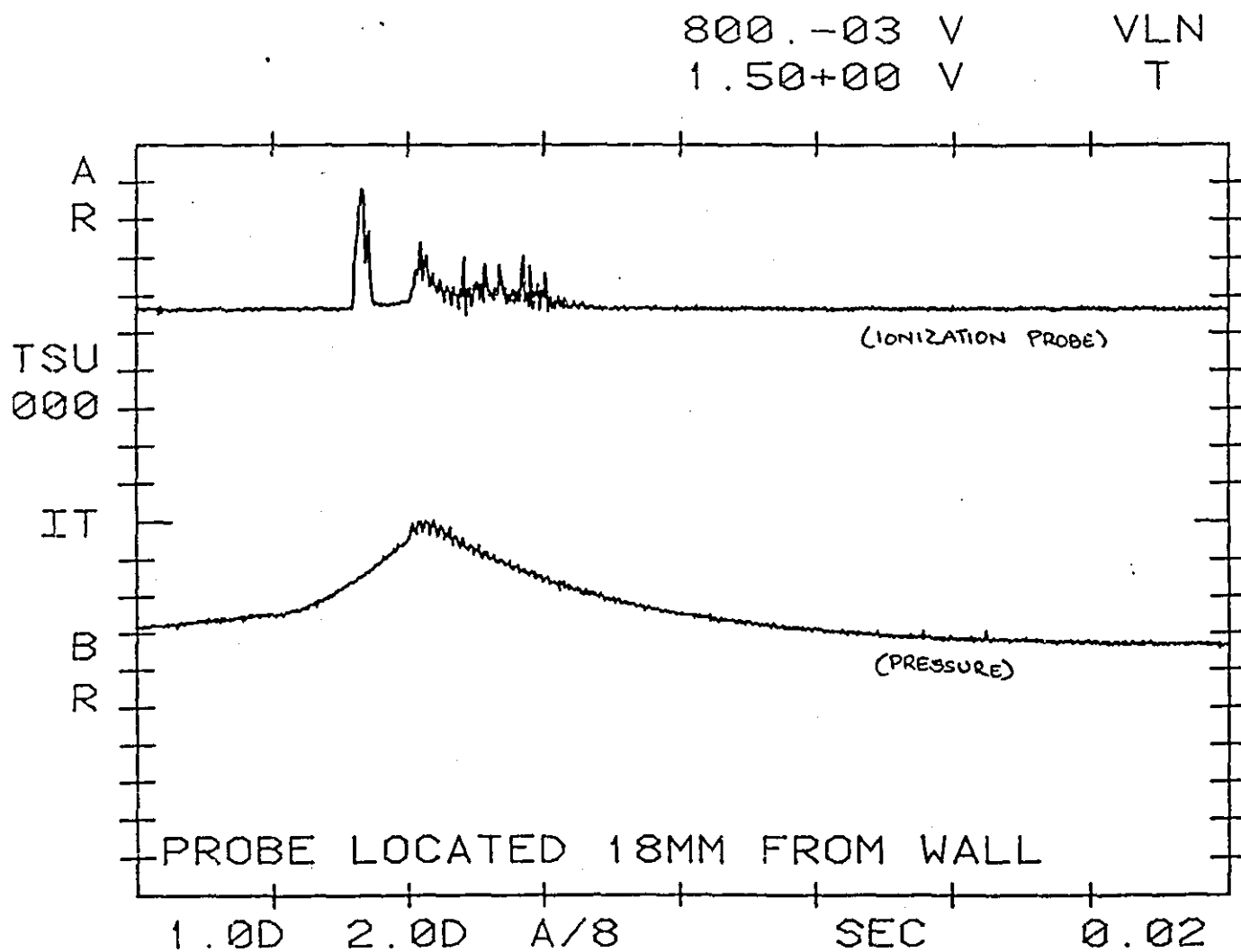


Fig. 6.32 Ionization Probe and Pressure Response with Knock  
Ricardo E6 Engine , Fuel – 70 RON PRF  
Speed = 1500 rpm, Air–Fuel Ratio = 16.4  
Compression Ratio = 8.7

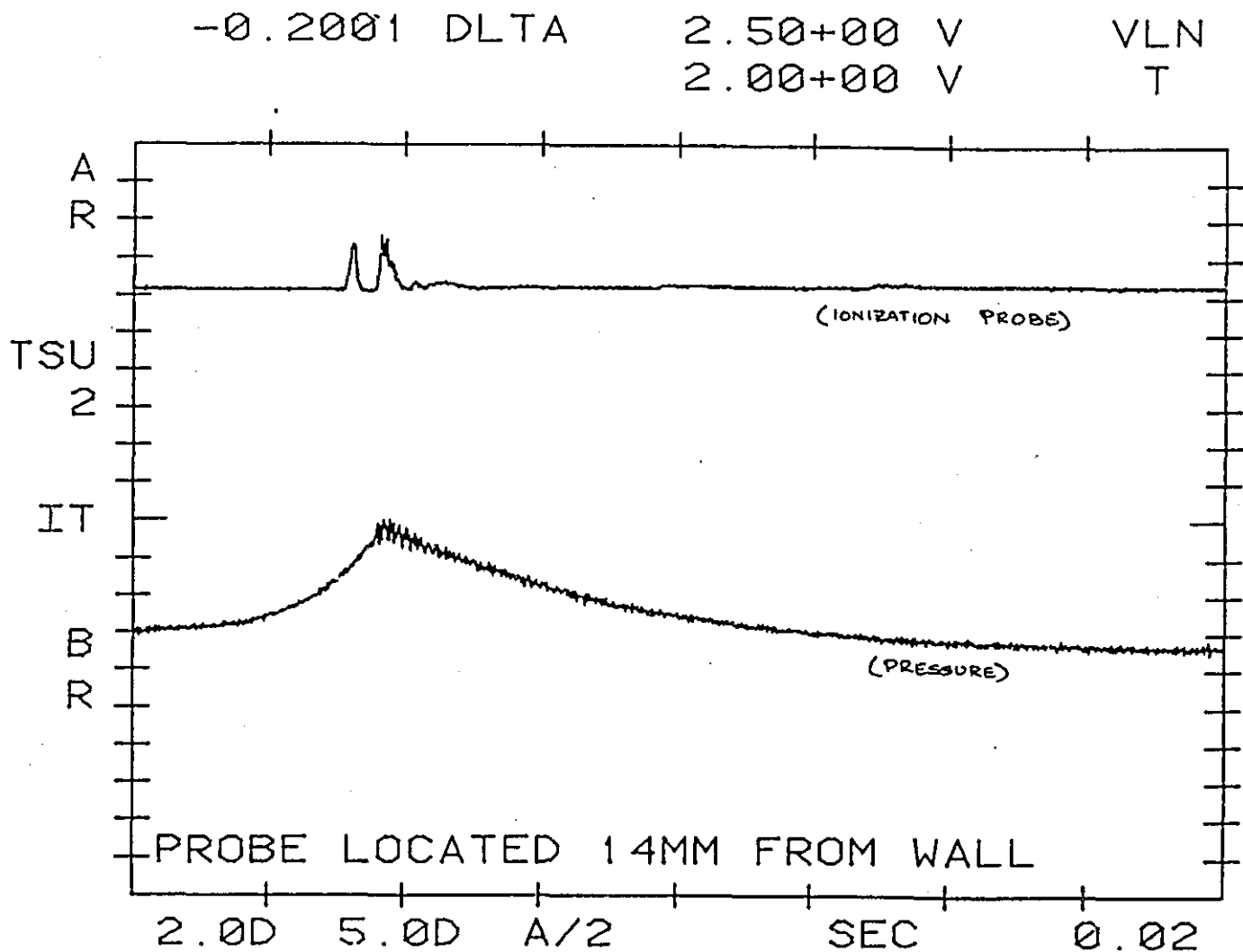


Fig. 6.33. Ionization Probe and Pressure Response with Knock  
 Ricardo E6 Engine , Fuel – 70 RON PRF  
 Speed = 1500 rpm, Air–Fuel Ratio = 16.4  
 Compression Ratio = 8.7

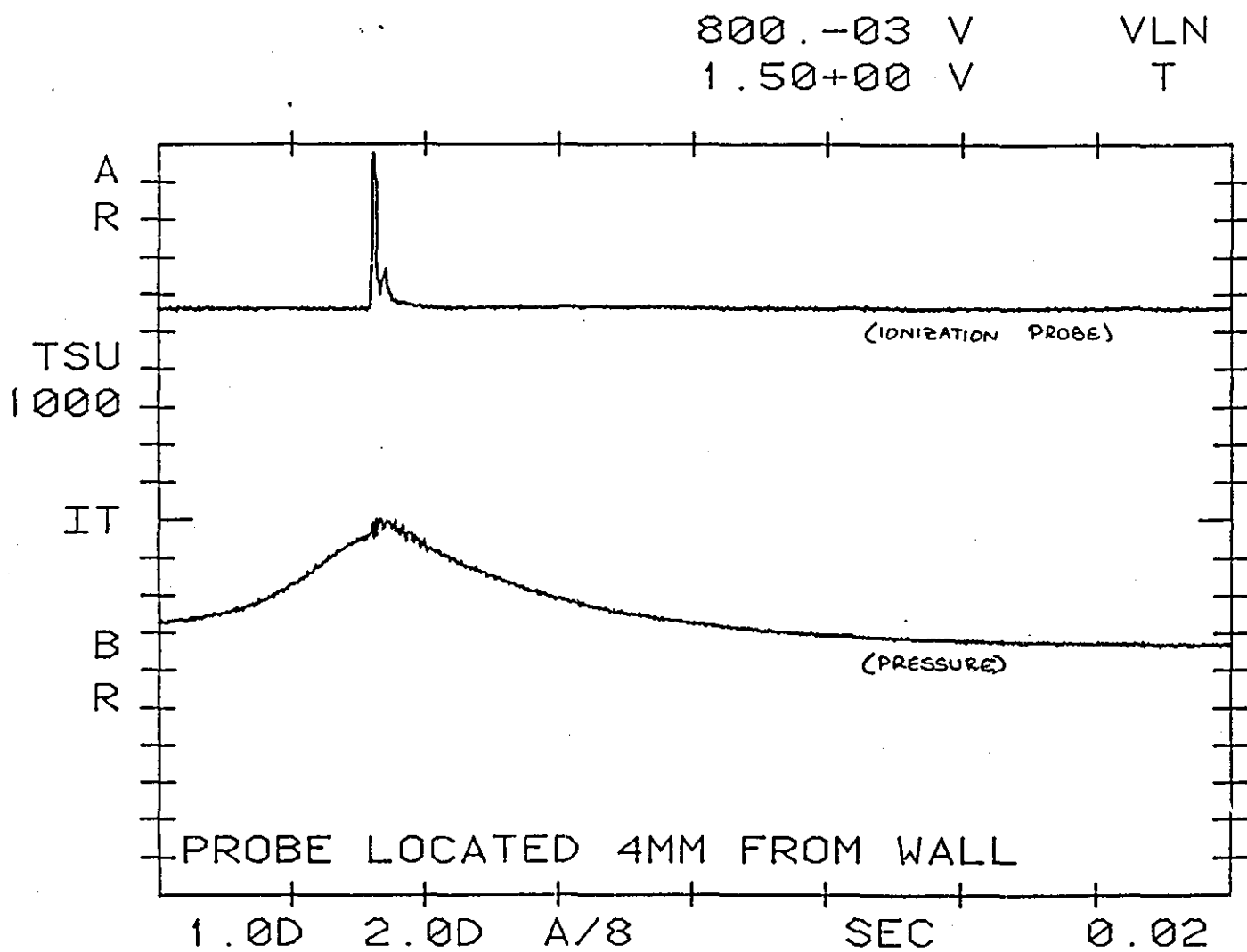


Fig. 6.34 Ionization Probe and Pressure Response with Knock  
 Ricardo E6 Engine , Fuel - 70 RON PRF  
 Speed = 1500 rpm, Air-Fuel Ratio = 16.4  
 Compression Ratio = 8.7

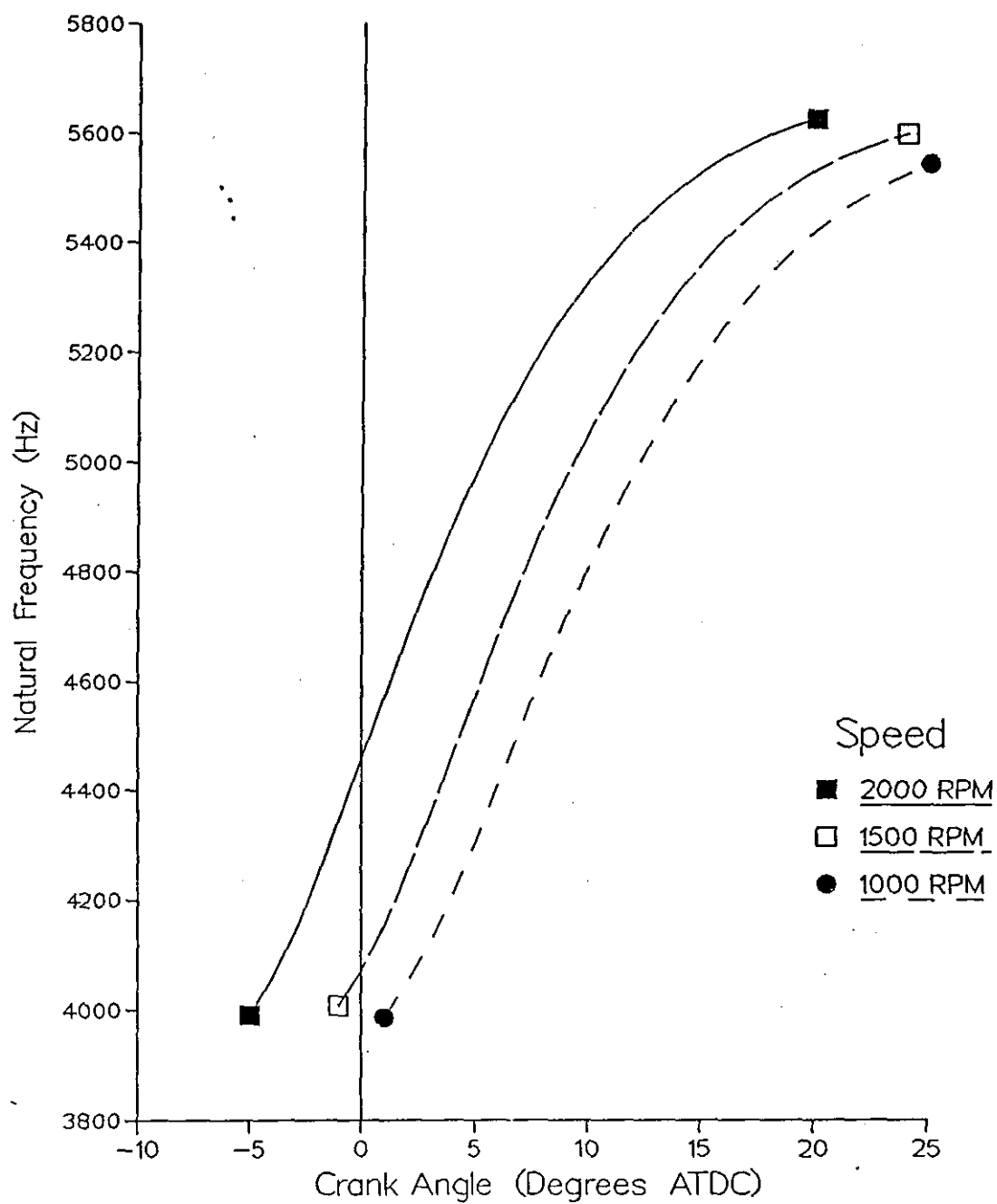


Fig. 6.35 Natural Frequency of Chamber v/s Crank Angle

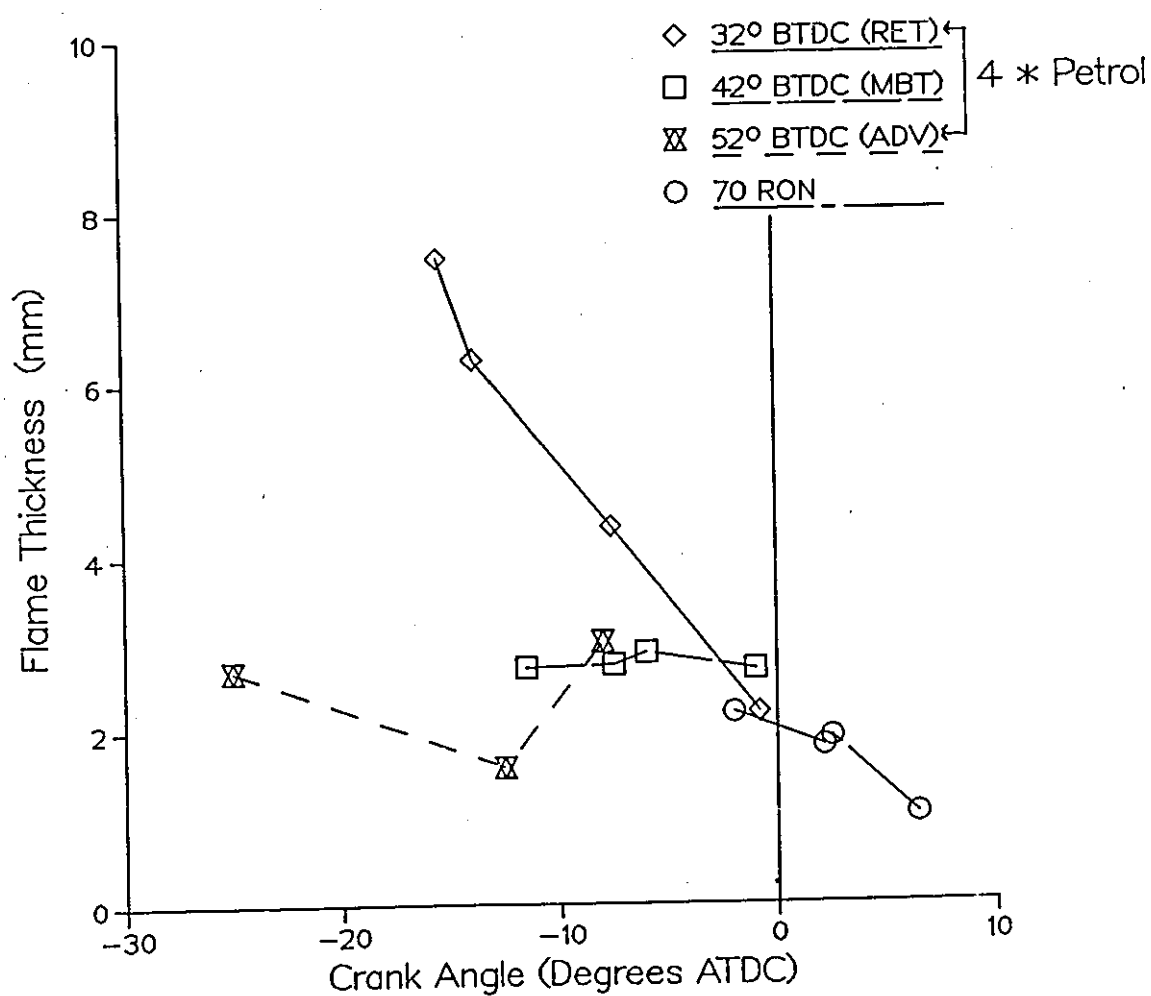


Fig. 6.36 Flame Thickness at Different Probe Locations

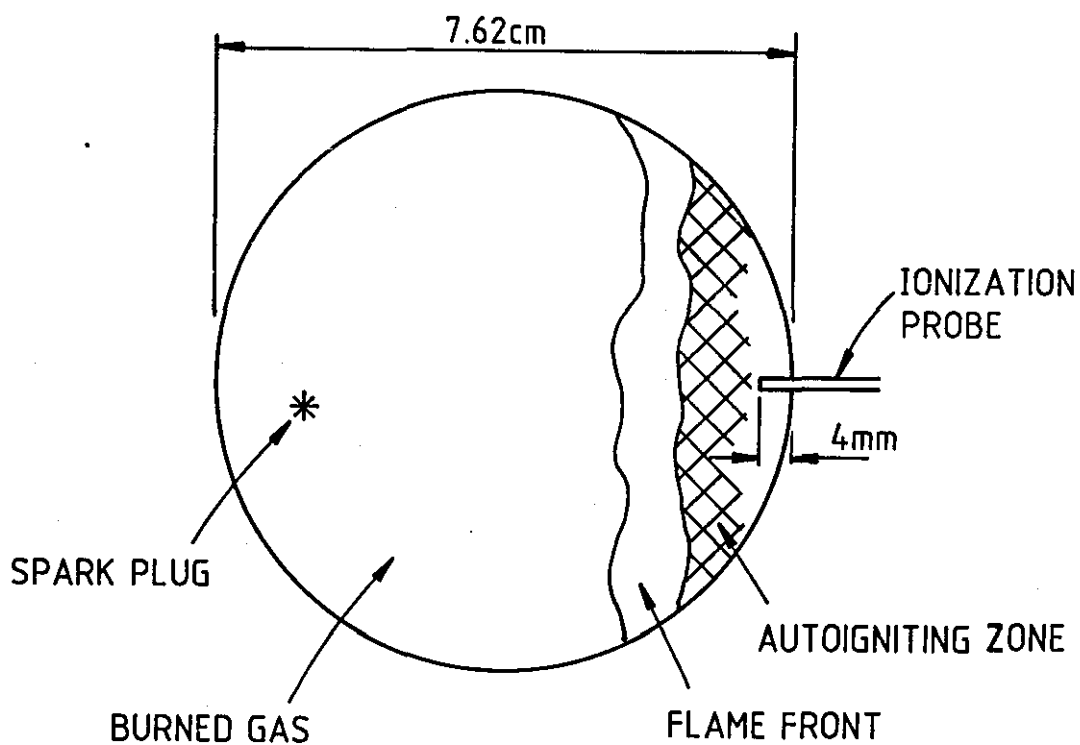


FIG. 6.37 SCHEMATIC REPRESENTATION OF FLAME, AUTOIGNITION ZONE AND IONIZATION PROBE CORRESPONDING TO THE CASE IN FIG. 6.34

## CHAPTER VII

### SUMMARY, CONCLUSIONS AND RECOMMENDATIONS FOR FUTURE WORK

#### 7.1 Introduction

The results from the chemical-kinetic model for autoignition of end-gases were presented in Chapter II. The results after incorporating this model into an existing combustion model were presented in Chapter.III, while, the model for the acoustic response of the flame front, due to pressure fluctuation was presented in Chapter V. In Chapter VI the results of the experiments conducted to correlate the acoustic frequency of the chamber, knock frequency and frequency composition of the flame front movement were presented and discussed.

#### 7.2 Summary

Three Kinetic models for the autoignition of hydrocarbons have been discussed. It has been shown that the model developed by Halstead et. al. [21] is the most suited for the purpose of the present investigation. A computer program to simulate the autoignition of hydrocarbons in a rapid compression machine was developed. The kinetic reaction constants published by Halstead et. al. in a later paper [41] were used for the simulation. The results are shown to compare favourably with those published by the authors.

This model for the autoignition of hydrocarbons was incorporated into the existing combustion model. The combustion in the main flame propagation sequence and the autoignition occur in parallel in the engine. In the computer program a time step of one degree crank angle is considered. It is assumed that over this small time step the error due to the two routines running in series would be negligible. The mass of fuel and air consumed due to autoignition in the unburned gas over the time step is added to the total mass

burned, thus effecting the pressure and temperature of the complete system.

After incorporating the knock model into the combustion model, it was tested against experimental data obtained on a single cylinder engine with Premium Grade Gasoline and 90 RON PRF. The combustion model starts at spark and ends at exhaust valve opening, using input data , such as, charge mass , air-fuel ratio, inlet pressure and temperature, and speed corresponding to experimental tests. The predicted and experimental pressure curves show a favourable comparison till the time knock occurs. After knock the predicted pressure is higher than that measured experimentally by about 3 to 4 Bars. The reason the predicted pressure curves are much higher than the experimental pressure curves (Fig. 3.25) during the expansion stroke is, because, at the time knock occurs, it is assumed that all the remaining unburned charge is burned instantaneously, thus creating a very large pressure and temperature rise. The combustion model follows a simple polytropic expansion after the end of combustion thus maintaining a higher pressure and temperature level till the exhaust valve opens.

In an engine running at MBT spark timing, advancing the spark timing suddenly, does not produce knock in the immediate next cycle. This is because, advancing the spark timing increases the peak pressures and inturn the peak cylinder temperatures which increase the charge temperatures. To consider this effect it was necessary to raise the temperature of the charge mass by 20 degrees C.

The occurrence of knock is defined as the crank angle period over which the temperature rise of the unburned gas due to autoignition is greater than 200 C, which is equal to  $1.8 \times 10^6$  degrees C per second. This is about one fifth the value considered by Halstead et. al. [41], but it does not make much difference to the time knock occurs, as, the temperature rise is sharp and very large at the time of autoignition. The value 200 C was used as the maximum rise in temperature, to avoid mathematical instability caused due to the

limitations and restrictions of the computer. (The maximum value that the computer handles is  $3.2 \times 10^{38}$ , if the restriction of 200 C is not used then in the next computational time step the concentrations of the various species would increase to a value greater than  $3.2 \times 10^{38}$  and cause the program to crash). The assumption that all the unburned gas remaining in the cylinder at the time of knock burns instantaneously is applicable in the case of heavy knock, but with light knock or trace knock all the end gas does not burn up as a unit but small pockets of unburned gas are still present in the combustion chamber as is seen from the photographs presented by [83].

As the combustion model considers the burned gas region and the unburned gas region as two zones separated by a flame front of negligible thickness, it is not possible to study the effect of the flame front on just a part of the unburned gas neighbouring the flame front. Any effect the flame front has to have on the unburned gas region would involve the complete unburned gas as a unit rather than a small portion of it, unless a multidimensional model is used

The system of burned gas and unburned gas divided by a burning zone of finite thickness is compared to a duct of equivalent length. Due to pressure disturbances the burning plug is set into an oscillatory motion, which has been described by a non linear differential equation of relaxation oscillation.

Solving the equation of relaxation oscillation for conditions corresponding to different positions of the flame front as the combustion progresses gives the frequency response of the flame front due to the pressure fluctuations. As the flame progresses the stiffness of the system decreases and so does the response frequency. At the same time the acoustic (or natural) frequency of the chamber increases (as the temperature of the system increases which increases the velocity of sound). The amplitude of these fluctuations are found to increase as the frequency falls.

The pressure waves developed during the combustion interact with the flame front and compress the unburned gas. Simulating such an effect in the end gas at a rate of one compression wave in one degree crank angle, and the effect of the pressure wave to raise the unburned gas temperature by 20 C, the occurrence of knock was found to advance by 2 degree crank angle.

The experimental results of Chapter VI show the autoignition to occur closer to the flame front rather than all over the unburned gas zone. This is seen from the fact that the probes close to the wall do not pick up the ion pulses at the time knock occurs, whereas the probes seated deep within the chamber pick up the fluctuations. The fluctuations occur within one to two degrees crank angle of the flame passing the probe and about 0.5 degrees crank after the pressure transducer pick up the pressure fluctuations.

### 7.3 Conclusions

The measurement of the ionization probe response in an engine fired once in three cycles and with three fuels namely: Propane, commercial Premium Grade Gasoline and 70 RON PRF are presented. The spectral distribution of energy in these signals show that at the time knock occurs the energy content in these signals is the highest. The frequency of knocking pulses recorded by the pressure transducer and the ionization probe match each other very closely and also match those published by other investigators [39,76,77].

The results with different lengths of ionization probes, show that autoignition occurs just ahead of the flame front. All the probes located in the burned gas zone at the time of knock recorded the fluctuations but not the one near the wall, it can be surmised that the unburned gas just ahead of the flame front, autoignites to push the ion clouds back and forth between the flame front and the autoigniting zone in the unburned gas. Natarajan and Bracco [32], suggested that if the flame front was to have the effect of accelerating the low temperature reactions in the unburned gases, then, the autoignition would take place at the foot of the flame. This would compliment the theory proposed by Curry [79] that knock is due to flame acceleration, though, Natarajan and Bracco do not consider such form of knocking combustion to be the usual case.

The probe near the wall, not picking up any fluctuations at the time knock occurs, could also indicate that the fluctuations are quenched by the time it reaches the cylinder wall. This would corroborate the trends shown by the plots for the response frequency in that, as the flame reaches the end of the chamber the response frequency falls.

#### 7.4 Recommendations for Future Work

As shown in the results of Chapter III and Chapter VI, the limitations of the phenomenological model are its inability to respond to change in geometry of the engine or the location of the spark plug. The effect of hot valves or any other hot spots cannot be simulated by this type of model.

It has been assumed in this work that the two electrode ionization probe can record the fluctuations of the flame front. Additional data regarding the behaviour of the flame front as combustion progresses, would be valuable. The use of multiple microstatic probes and high speed photography (over 18000 frames per second), could probably provide such information.

It would be desirable to have probes that could withstand the engine conditions even when placed deep inside the combustion chamber, and also be able to withstand conditions of knock. Running the engine with every cycle fired rather than the skip fired (i.e. firing once in three cycle) would be closer to realistic conditions, making it possible to study the effect of load and speed, as skip firing requires the engine to be motored or run on no load.

One of the major drawbacks of the combustion model output with respect to the relaxation oscillation model, was the lack of information regarding the flame thickness. Since the model assumes a thin flame front of negligible thickness, it was necessary to assume a flame thickness proportional to the height of the chamber. A multidimensional model using a finite flame thickness (like that of Natarajan and Bracco [32] or the KIVA code [80]) would give more information regarding the variation of the flame thickness as combustion progresses, thus giving a more realistic value to the input to the acoustic model as well as the output from the acoustic model.

#### REFERENCES

1. Oppenheim, A. K.; "The Knock Syndrome - Its Cures and its Victims ", SAE paper No.841339.
2. Ricardo, H.R.; "Recent Research Work on the Internal-Combustion Engine", The Journal of The Society of Automotive Engineers, vol 10, May 1922.
3. Maxwell, G. B. and Wheeler, R. V.; "Flame Characteristics of "Pinking" and "Non-Pinking" fuels", Journal of the Institute of Petroleum Technology, vol. 14., part 67.,1928.
4. Morgan, J. D.; "Some Experiments on Gas Explosions in Closed Tubes, with Particular Reference to 'Pinking'", The Automobile Engineer, Jan.1925.
5. Maxwell, G. B.; "Pinking in Internal Combustion Engines".Journal of the Institute of Petroleum Technology, Vol 14, 1928.
6. Withrow, L. and Boyd, T. A.; "Photographic Flame Studies in Gasoline Engines", Industrial and Engineering Chemistry, May 1931., Vol 23.
7. Taylor, C. F. and Taylor, E. S.; "The Internal Combustion Engine", Second Edition , International Textbook Company, Scranton, Pennsylvania.
8. Jost, W.; "Explosion and Combustion Processes in Gases", Translated by Huber O. Croft. McGraw-Hill Book Company Inc. 1946.

9. Gussak, L. A., Karpov, V. P. and Tikhonov, Yu. V.; "The Application of Lag-Process in Prechamber Engines"; SAE Paper 790692.
10. Lewis, B. and Von-Elbe, G.; "Combustion Flames and Explosion of Gases", Second Edition, Academic Press Inc. 1961.
11. Ball, G. A.; "Photographic Studies of Cool Flames and Knock in an Engine", Fifth Symposium (International) on Combustion, Pittsburgh (1954).
12. Sturgis, B. M.; "Some Concepts of Knock and Antiknock Action", SAE Transactions, Vol. 63. 1955.
13. Egerton, A. C.; "General Statement as to Existing Knowledge on Knocking and its Prevention", The Science of Petroleum vol IV, eds. Dunston, A. E., Nash, A. W., Brooks, B. T. and Tizard, H. T. Section 42 (1938).
14. Withrow, L. and Rassweiler, G. M.; "Formaldehyde Formation by Preflame Reactions in an Engine.", Industrial and Engineering Chemistry, Vol 26, no.12., Dec. 1934.
15. Schapertons, H., Gupta, H. C. and Lee, W.; "Preliminary Attempts to Simulate Knocking in Spark Ignition Engines with a Two-Dimensional Model", presented at the International Symposium on "Knocking of Combustion Engines", Wolfsburg Nov. 1981.
16. Livengood, J. C. and Wu, P. C.; "Correlation of Autoignition Phenomenon in Internal Combustion Engines and Rapid Compression Machines", Fifth Symposium (International) on Combustion, 1955.
17. Rifkin, E and Walcutt, C.; "A basis for Understanding Antiknock Action", SAE Transactions, Vol 65 (1957).

18. Burwell, W. G. and Olsen, D. R.; "The Spontaneous Ignition of Isooctane Air Mixtures under steady flow conditions", SAE Paper 650520.
19. Vermeer, D. J., Meyer, J. W. and Oppenheim, A. K.; "Auto-ignition of Hydrocarbons Behind Reflected Shock Waves", Combustion and Flame, Vol 18, pp.327-336, 1972.
20. Douad, A. M. and Eyzat, P.; "Four-Octane-Number Method for Predicting the Anti-knock Behaviour of Fuels and Engines", SAE paper 780080. Feb 1978.
21. Halstead, M. P., Kirsch, L. J., Prothero, A., Quinn, C. P.; "A Mathematical Model for Hydrocarbon Autoignition at High Pressures", Proc. Roy. Soc., London, A 346, pp. 515-538 (1975).
22. Warnatz, J; "The Mechanism of High Temperature Combustion of Propane and Butane", Combustion Science and Technology, vol.34, 1983.
23. Warnatz, J; "Chemistry of High Temperature Combustion of Alkanes up to Octane", 20th Symposium (International) on Combustion 1984.
24. Cox, R. A., and Cole, J. A.; "Chemical Aspects of the Autoignition of Hydrocarbon- Air Mixtures", Combustion and Flame, Vol 60, pp. 109-123 (1985).
25. Rothrock, A. M. and Spencer, R. C.; "A Photographic Study of Combustion and Knock in a Spark Ignition Engine", NACA Report NO. 622.
26. Payman, W.; "The Detonation Wave in Gaseous Mixtures and the Pre-Detonation Period", Proc. Roy. Soc. 1928, 120A, 90.

27. Miller, C. D. and Logan, W. O.Jr.; "Preknock Vibrations in a Spark Ignition Engine Cylinder as Revealed by high Speed Photography", NACA Report No. 785.
28. Fraser, R. P.; "Flame Propagation, Particularly with Reference to Vibratory and True Detonation Flames", The Science of Petroleum, Vol IV, Section 42, 1938.
29. Leyer, J. and Mason, N.; "Development of Vibratory Flame Propagation in Short Closed Tubes and Vessels".. Symposium (international) on Combustion.
30. Bone, W. A., Fraser, R. P. and Wheeler, W. H.; "The Phenomenon of Spin in Detonation ", Phil. Trans.235 A, 29 (1935).
31. Kogarko, S. M. and Ryzhkov, D. L.; "A study of the amplification of Compression waves during Compression", Soviet Physics - Technical Physics, vol. 6, no. 2, 1961.
32. Natrajan, B., Bracco, F. V.; "On Multidimensional Modelling of Auto-Ignition in Spark Ignition Engines", Combustion and Flame, vol. 57, pp. 179-197, 1984.
33. Schapertons, H., and Lee, W.; "Multidimensional Modelling of Knocking Combustion in SI Engines", SAE paper 850502 (1985).
34. Comprehensive Chemical Kinetics, "Gas Phase Combustion"; Eds. Bamford, C. H. and Tipper, C. F. H.
35. Douad, A. M.; "Modelling the Knocking Phenomenon in Engines : Application to identifying the autoignition delay of fuels and to optimizing the engine-fuel system", presented at the International Symposium on "Knocking of Combustion Engines", Wolfsburg Nov. 1981.

36. Pitz, W. J., Westbrook, C. K., Proscia, W. M., Dryer, F. L.; "A Comprehensive Chemical Kinetic Reaction Mechanism for the oxidation of N-Butane", Twentieth Symposium (International) on Combustion 1984.
37. Westbrook, C. K. and Pitz, W. J. "A Comprehensive Chemical Kinetic Reaction Mechanism for Oxidation and Pyrolysis of Propane and Propene", Comb. Sci. and Tech., Vol. 37, 1984.
38. Esser, C., Maas, U., Warnatz, J.; "Chemistry of the Auto-Ignition in Hydrocarbon-Air Mixtures up to Octane and its Relation to Engine Knock", Diagnostics and Modeling of Combustion in Reciprocating Engines, COMODIA 85, Symposium, Tokyo 1985.
39. By, A., Kempinski, B., Rife, J. M., "Knock in Spark Ignition Engines", SAE paper 810147, Feb. 1981.
40. Benson, S. W., "The Kinetics and Thermochemistry of Chemical Oxidation with Application to Combustion and Flames", Prog. Energy Combustion Sci. Vol. 7, pp. 125-134.
41. Halstead, M. P., Kirsch, L. J., Quinn, C. P., "The Autoignition of Hydrocarbon Fuels at High Temperatures and Pressures - Fitting of a Mathematical Model", Combustion and Flame vol. 30, pp. 45-60 (1977).
42. Mattavi, J. N., Groff, E. G., Lienesch, J. H., Matekunas, F. A., Noyes, R. N.; "Engine Improvements Through Combustion Modelling", Combustion Modelling in Reciprocating Engines. Eds. James N Mattavi and Charles A Ammann, General Motors research Labs. Plenum Press 1980.
43. Blizard, N. C. and Keck, J. C.; "Experimental and Theoretical Investigation of Turbulent Burning Model for Internal Combustion Engines", SAE 740191.

44. Tabaczynski, R. J., Ferguson, C. R. and Radhakrishnan, K.; "A Turbulent Entrainment Model for Spark Ignition Combustion", SAE
45. Lakshminarayanan, P. A., and Dent, J. C.; "Personal communications".
46. Lavoie, G. A. and Blumberg, P. N.; "A Fundamental Model for Predicting Fuel Consumption, NO<sub>x</sub> and HC Emissions of the Conventional Spark Ignited Engine", Combustion Science and Technology, 1980, Vol 21, pp225-258.
47. Ferguson, C. R. and Keck, J. C. and Oforah, O. ; "The Development of Performance Evaluation Criteria for Lean Operating Conventional Spark Ignition Engines", U.S. Department of Transportation Interim Report.
48. Martin, M. K. and Heywood, J. B.; " Approximate Relationships for the Thermodynamic Properties of Hydrocarbon-Air Combustion products", Combustion Science and Technology, 1977, vol15., pp1-10.
49. Hires, S. D., Tabaczynski, R. J. and Novak, J. M.; "The Prediction of Ignition Delay and Combustion Intervals for a Homogeneous charge, Spark Ignition Engine", SAE Paper 780232 (1978).
50. Woshni, G; "A Universally Applicable Equation for the Instantaneous heat Transfer Coefficient in the Internal Combustion Engine", SAE 670931.
51. Lakshminarayanan, P. A. and Dent, J. C.;"Generalised Procedure for Flame and Combustion Chamber Surface Determination in Spark Ignition Engines", SAE paper No. 821223.

52. Lavoie, G. A., Heywood, J. B. and Keck, J. C.; "Experimental and Theoretical Study of Nitric Oxide Formation in Internal Combustion Engines", Combustion Science and Technology; Vol 1, (1970).
53. Pollack, T. S.; Department of Mechanical Engineering, University of Technology, Loughborough.
54. Young, M. B.; "Cyclic Dispersion - Some Quantitative Cause-and-Effect Relationships ", SAE Paper no. 800459.
55. Krogh, F. T.; "A Variable Step Variable Order Multi-step Method for the Numerical Solution of Ordinary Differential Equations", Information Processing 68 - North Holland Publishing Company - 1969.
56. Lancaster, D.; "Effects of Turbulence on Spark Ignition Engine Combustion", PhD. Thesis - University of Illinois at Urbana Champaign. 1975.
57. Curry, S.; "Three Dimensional Study of Flame propagation in a Spark Ignition Engine"., SAE Transactions, Vol. 71 (1963), paper 452-B.
58. Kumagai, S. and Kudo, Y.; "Flame Studies by Means of Ionisation Gaps in a High Speed Spark Ignition Engine", 9th Symposium (International) of Combustion, (1962).
59. Warren, J. A. and Hinkamp, J. B.; "New Instrumentation for Engine Combustion Studies", SAE Transactions Vol. 64, pp 665-679, 1956.
60. Arrigoni, V., Calvi, F., Cornetti, G. M. and Pozzi, U.; "Turbulent Flame Structure as determined by Pressure Development and Ionization Intensity", SAE paper no. 730088.

61. Calcote, H. F. "Ion Production and recombination in Flames", 8th Symposium (International) in Combustion. (1960 ) .
62. Denniston ,D. W. Jr.; Oxendine, J. R.; Knapschaefer, D. R.; Burgess, D. S. and Karlovitz, B.: "Applications of the Electronic Probe to the study of Turbulent Flames", Journal of Applied Physics, vol28, No1. APL
63. Ohigashi, S., Hamamoto, Y. and Kizima A "Effects of Turbulence on Flame Propagation in Closed Vessels ", Bulletin of the Japanese Society of Mechanical Engineers, vol 14, no74, 1971.
64. Harrow, G. A. : "Some Applications pf Basic Combustion Research to Gasoline Engine Development Problems", SAE Paper No.680765.
65. Dryden, H. L.: "A Review of the Statistical Theory of Turbulence", Quarterly of Applied Mathematics, Vol 1., pp7-42, 1943.
66. Bendat, J. S. and Piersol, A. G.; "Random Data : Analysis and Measurement Proceedures", Wiley-Interscience Inc.
67. Newland, D. E.; "An Introduction to Random Vibrations and Spectral Analysis", Second Edition, Longman Group Ltd.
68. Ewins, D. J. "Modal Testing : Theory and Practice", Research Studies Press Ltd, John Wiley and Sons Inc.
69. Charch, W. H., Mack, E. Jr., and Boord, C. E.; "AntiKnock Materials - An Experimental and Theoretical Study", Industrial Engineering and Chemistry, Vol. 18, No. 4 (1926).
70. Winch, R. F. and Mayes, F. M.; "A Method for Identifying Preignition", SAE Trans. vol.61. (1953).

71. Iinuma, K; "Studies of Engine Combustion Processes by Ionization Current", Bulletin of Japanese Society of Mechanical Engineers, vol. 4, 1961.
72. Rayleigh "The Theory of Sound", Macmillan, 1929.
73. Karplus, W. J.; "Analog Simulation Solution of Field Problems", McGraw-Hill Series in Information Processing and Computers . 1958.
74. Ning, H.; "The Relaxation Oscillation in Ramjet Combustion"; Eighteenth Symposium (International) on Combustion ,1981.
75. Wood, A. B.; "A Textbook of Sound ", G. Bell and Sons Ltd. 1957.
76. Draper, C. S.; "Pressure Waves Accompanying Detonation in the Internal Combustion Engine", Journal of the Aeronautical Sciences, vol 5, no.6, 1938.
77. Hickling, R, Chen, F. H. K. and Feldmaier, D. A. ; "Pressure Pulsations in Engine Cylinders", Engine Noise - Excitation, Vibration, and Radiation, Edited by Robert Hickling and Mounir M. Kamal, G M Research Laboratories. 1982.
78. Schaefer, H. J. and Lee, W. "Analysis of Local Pressures, Surface Temperatures and Engine Damages under Knock Conditions", SAE paper 830508.
79. Curry, S.; "Effect of Antiknocks on Flame Propagation in a Spark Ignition Engine", 9th Symposium (International) on Combustion , 1962.
80. Amsden, A. A., Butler, T. D., O'Rourke, P. J., Ramsmah, D. J.; "Kiva : A Comprehensive Model for 2D and 3D Engine Simulations", SAE 850554.

81. Obert, E. F.; "Internal Combustion Engines", 3rd Edition, International textbook Company, Scranton, Pennsylvania. 1968.
82. Iwashita, Y. and Saito, A.; "Observation of Knock Using a High Speed Shetter TV Camera System", SAE Paper no. 831696.
83. Shiga, S., Kono, M., Iinuma, K., Karasawa, T. and Kurabayashi, T.; "Further Investigation of Knock Intensity by a Thermodynamic Model and Experiments using a Rapid Compression Machine", Diagnostics and Modeling of Combustion in Reciprocating Engines, COMODIA 85, Symposium , Tokyo 1985.
84. Morgan, C. R. and Hetrick, S. S., "Trade-Offs between Engine Emission Control Variables, Fuel Economy, and Octane ", SAE Paper no.750415

## Appendix "A"

### Calculation of Mass Fraction Burned from Experimental Data

The pressure signal obtained from the Kistler type 601A piezo-electric transducer is amplified by a Kistler type 5001 charge amplifier and fed to the Analog/Digital Convertor. The signal from the cam shaft triggers the computer to digitise the data at every second crank angle. A disc with 180 slots sends a pulse out to the Schmidt trigger on the computer.

The method for calculating the mass fraction burned and net heat release is as follows.

For an ideal gas the relation between the specific heat at constant pressure ( $C_p$ ) and the specific heat at constant volume ( $C_v$ ) and the universal gas constant is given as :

$$C_p - C_v = R \quad \text{A.1}$$

$$C_p/C_v = K \quad \text{A.2}$$

Substituting 2 in 1 and rearranging the terms we get:

$$C_v = R/(K-1) \quad \text{A.3}$$

For the ideal gas the state equation is

$$PV = mRT$$

P = Pressure

V = Volume

R = Universal gas constant

T = Temperature

m = mass

The equation of state for conditions (A.1) and (A.2) can therefore be written as:

$$P_1 V_1 = mRT_1 \quad \text{A.4}$$

$$P_2 V_2 = mRT_2 \quad \text{A.5}$$

Assuming the change in volume to be small enough to apply the specific heat at constant volume to calculate the internal energy, the change in internal energy for any process starting at (1) and ending at (2) would be given as :

$$\begin{aligned} d(u) &= mC_v(t_2 - T_1) \\ &= (mRT_2 - mRT_1)(1/(K-1)) \end{aligned}$$

which can be written as:

$$d(u) = (P_2 V_2 - P_1 V_1)(1/(K-1)) \quad \text{A.6}$$

The work done over the interval is:

$$dW = P dV \quad \text{A.7}$$

As mentioned earlier the interval assumed is so small that the pressure curve can be approximated to a straight line over the interval considered, thus obtaining

$$dW = (P_1 + P_2)/2 dV \quad \text{A.8}$$

The change in volume is  $dV = V_2 - V_1$

$$\text{Thus we get } dW = (P_1 + P_2)(V_2 - V_1)/2 \quad \text{A.9}$$

For any closed system the first law of thermodynamics states

$$dQ - dW = dU$$

$$dQ = (1/(K-1))(P_2 V_2 - P_1 V_1) + (P_2 + P_1)(V_2 - V_1)/2 \quad \text{A.10}$$

$dQ$  is the net heat released, which is the difference between the heat released due to combustion and the heat lost to the surroundings.

The ratio of specific heats is <sup>s</sup>assumed to be 1.35.

The mass fraction burned is given as:

$$m_{fb} = \frac{\int dQ}{Q_{tot}} \quad A.11$$

where  $Q_{tot}$  is the net heat released.

## APPENDIX - B

The Parameters used in the Integrating subroutine D02QBF are defined below: (for further details refer Nag Library document on D02QBF)

### 1. PARAMETERS

**X** - real.

Before entry, X must be set to the initial value of the independent variable T.

On exit, it contains XEND, unless an error or an interrupt has occurred, when it contains the current value of the independent variable. If the integration is to be continued after interruption or with a new value for XEND, X must not be changed.

**XEND** - real.

On entry, XEND must specify the end point of the range of integration. If  $XEND < X$  on entry, integration will proceed in the negative direction.

Unchanged on exit.

**N** - INTEGER.

On entry, N must specify the number of differential equations.

Unchanged on exit.

**Y** - real array of DIMENSION at least (N).

Before entry, Y(1), Y(2), ..., Y(N) must contain the initial value of the dependent variables,  $Y_1, Y_2, \dots, Y_N$ .

On exit, Y(1), Y(2), ..., Y(N) contain computed values of the dependent variables at XEND, unless an interrupt or an error has occurred when they contain computed values of the solution (dependent variables) at the exit value of  $T = X$ .

**CIN** - real array of DIMENSION at least (7).

CIN is used to control the calculation as follows:

CIN(1) indicates whether the user intends to set certain parameters, or to use default values. If CIN(1) = 0.0 on entry, the following are initially set to 0.0: CIN(I), I = 2,3,4,5, COMM(I), I = 1,2,3,4, CONST(I), I = 1,2, ..., 5 and the routine subsequently resets them as specified below. If CIN(1) = 1.0 on entry, the user must set all these parameters (see the detailed descriptions).

On a successful exit with X = XEND, CIN(1) is set to 2, with IFAIL = 0. For an exit due to a normal interrupt with X  $\neq$  XEND, corresponding to the use of COMM(2), COMM(3) or COMM(4), CIN(1) has the value 3.0, 4.0, 5.0 or 6.0 with IFAIL = 0. For an exit due to an abnormal interrupt (corresponding to the use of COMM(1), the error indicator IFAIL is set to 5 or 7. For all exits indicated by IFAIL = 2, CIN(1) has the value 7.0. For error exits indicated by IFAIL = 1, CIN(1) has a negative value.(as described in section 2.)

The user may continue integration after reaching XEND merely by resetting XEND and IFAIL, and calling D02QBF again with no changes to any other parameters. Integration may also be continued after a normal interrupt by resetting the corresponding interrupt variable (COMM(2), COMM(3) or COMM(4)) if required and also IFAIL, and calling D02QBF with no changes to any other parameters (except COMM(5) if COMM(4) < 0.0). After a normal interrupt corresponding to COMM(4) > 0.0 it is necessary to reset COMM(4) only if this interrupt is not required again. It is also possible to continue integration after an abnormal interrupt with IFAIL = 5, by resetting COMM(1) and IFAIL, and setting CIN(1) = 2.0.

Particular care should be taken when calling D02QBF again with CIN(1) = 5.0 or 6.0 (corresponding to a interrupt controlled by COMM(4)). In these cases, most of the checks on the parameter values are omitted to reduce computation time. If any other changes are made to parameters before re-entry, the user should set CIN(1) = 1.0, and CIN(5) should be set to CIN(6) if it is expected that

integration will proceed with a similar stepsize (alternatively CIN(5) should be set to 0.0).

CIN(2) controls the form of the local error test. On each step of the integration, an estimate  $E(I)$  of the local error in  $Y(I)$ ,  $I = 1, 2, \dots, N$ , is made and the current stepsize and order are modified, if necessary, so that the appropriate inequality below is satisfied.

Error Tests controlled by CIN(2):

CIN(2) = 0.0 (Mixed Error Test)

$$\frac{1}{N} \sum_{I=1}^N E(I)^2 \leq \text{TOL} \times \max\{1.0, \frac{1}{N} \sum_{I=1}^N Y(I)^2\}$$

where TOL is the local error tolerance (see below).

CIN(2) = 1.0 (Absolute Error Test)

$$\frac{1}{N} \sum_{I=1}^N E(I)^2 \leq \text{TOL}$$

CIN(2) = 2.0 (Relative Error Test)

$$\frac{1}{N} \sum_{I=1}^N E(I)^2 \leq \text{TOL} \times \max\left\{\frac{1}{N} \sum_{I=1}^N Y(I)^2, \text{dwarf/macheps}\right\}$$

(see the specification of COUT(11) AND COUT(12) below).

CIN(2) = 3.0 (Mixed Error Test applied componentwise)

$$\frac{1}{N} \sum_{I=1}^N \left[ \frac{E(I)}{W(I,19) \times \max(W(I,20), Y(I))} \right]^2 \leq \text{TOL}$$

(see the specification of W below).

CIN(2) = 4.0 (Absolute Error Test applied componentwise).

$$\frac{1}{N} \sum_{I=1}^N \{E(I)/W(I,19)\}^2 \leq \text{TOL}$$

(see the specification of W below). CIN(2) is unchanged on exit.

CIN(3) specifies a minimum stepsize permitted in the Gear method.

If CIN(3) = 0.0 on entry, the minimum stepsize, COUT(13) is set to  $\max\{COUT(11) \times |x|, 10.0 \times COUT(12)\}$  internally. This value is also used for the minimum stepsize if it is larger than the input value of  $|CIN(3)|$ . The sign of CIN(3) is immaterial. Setting CIN(3) = 0.0 is recommended.

CIN(3) is unchanged on exit.

CIN(4) specifies a maximum stepsize permitted in the Gear method.

If CIN(4) = 0.0 on entry, the maximum stepsize, COUT(14), is set to  $XEND - X$ . This value for the maximum stepsize is also used if it is less than the input value of CIN(4) in modulus. The sign of CIN(4) is immaterial. It is recommended that CIN(4) be set to 0.0 unless it is expected that the solution will have features which could be 'missed' if a long stepsize were taken. In this case, CIN(4) should be set to a value whose size permits resolution of the expected feature (e.g. half the distance over which the feature should be observed).

CIN(4) is unchanged on exit.

CIN(5) is used in the calculation of the initial stepsize when CIN(1) = 1.0. If CIN(5) = 0.0, a starting value for a stepsize iteration is calculated internally by D02QBF. If CIN(5)  $\neq$  0.0, and if it lies between the minimum and maximum stepsizes (see CIN(3) and CIN(4) above) and has the correct sign, then CIN(5) is used as the starting value; otherwise the starting value is computed internally. The initial stepsize iteration is used to calculate a suitable initial stepsize for integration from X using the starting value as first iterate. If the input value of CIN(5) is suitable then it is adopted as the initial stepsize. It is strongly

recommended that CIN(5) be set to 0.0 except when a suitable starting value is available (such as provided by a previous run of D02QBF on a similar problem). CIN(5) is not used on a call to D02QBF with CIN(1)  $\geq$  2.0.

On exit, CIN(5) contains the value of the initial stepsize used (not the starting value in the stepsize iteration).

CIN(6) specifies an initial stepsize used when CIN(1)  $\geq$  2.0. Normally on a call of D02QBF to continue integration, CIN(6) should not be changed from its value on exit from the previous call of D02QBF. CIN(6) is not used on a call to D02QBF with CIN(1)  $\leq$  1.0.

On exit, CIN(6) contains an estimate for the next stepsize unless an error has occurred when it contains the last step tried.

On exit when X = XEND, CIN(6) may have a small value due to the requirement to integrate to XEND exactly. If integration is to be continued with a new value for XEND, then the user should check whether CIN(6) is of acceptable size (possibly by comparing it with CIN(5) and COUT(4) - COUT(5)). If it is not acceptable, then a restart is recommended with CIN(1) = 1.0 and CIN(5) suitably chosen.

CIN(7) is used in conjunction with CIN(6) on calls to D02XGF and D02XHF for interpolation. On output it contains the current order of the Gear method. This parameter is not used for input.

TOL - real

On entry, TOL must specify a positive tolerance for bounding the local error. Its use is described under CIN(2) above.

Unchanged on exit.

FCN - SUBROUTINE, supplied by the user

FCN must evaluate the functions  $F_1$  (i.e. the derivatives  $Y_1'$ ) for given values of its arguments,  $T, Y_1, \dots, Y_N$ . Its specification is:

```
SUBROUTINE FCN(T,Y,F)
  real T,Y(n), F(n)
```

where  $n$  is the actual value of  $N$  in the call of D02QBF.

$T$  - real .

On entry,  $T$  specifies the value of the argument  $T$ . Its value must not be changed.

$Y$  - real array of DIMENSION (n)

On entry,  $Y(I)$  contains the value of the argument  $Y_1$ , for  $I = 1, N$

$F$  - real array of DIMENSION (n)

On exit,  $F(I)$  must contain the value of  $F_1$ , for  $I = 1, \dots, n$ .

FCN must be declared as EXTERNAL in the sub(program) from which D02QBF is called.

COMM - real array of DIMENSION at least (5).

COMM is used in specifying interrupts for D02QBF. Note that if  $CIN(1) = 0.0$  on entry, the components  $COMM(I)$ ,  $I = 1, 2, 3, 4$  are given default values 0.0. If  $CIN(1) = 1.0$ ,  $COMM(I)$ ,  $I = 1, 2, 3, 4$  must be set on entry. If  $2.0 \leq CIN(1) \leq 6.0$ ,  $COMM(I)$ ,  $I = 1, 2, 3, 4$  will already be set on return from a previous call of D02QBF but they may be reset before continuing the integration (see below). Note that even if an interrupt should occur on the last step of the integration (finishing at XEND), D02QBF will always exit with  $CIN(1) = 2.0$  on this step, overriding any possible return value of  $CIN(1)$  resulting from an interrupt.

Several interrupt checks may be made on each integration step. When one interrupt check is satisfied no further checks are made. The

checks are made in the following order: COMM(3), COMM(2), COMM(4), COMM(1).

COMM(1) specifies the maximum permitted number of function calls to the derivative evaluation routine FCN, or if MPED = 1, COMM(1) is a bound on the number of calls defined by: (number of calls to FCN) + N\* = (number of calls to PEDERV). If COMM(1) = 0.0, no check is made on the number of calls. If COMM(1) > 0.0, then on exit for any reason, COMM(1) contains its original value minus the number of calls to FCN (or -1.0 if this result is 0.0). If more than the specified maximum number of calls were made, the routine exits with IFAIL = 5 or 7.

If IFAIL = 5 on exit, the parameters of D02QBF contain sufficient information to continue the integration, or to permit interpolation using the routines D02XGF or D02XHF. To continue, CIN(1) should be reset to 2.0, COMM(1) reset to a non-negative value and IFAIL reset to its original input value, then D02QBF called again.

COMM(2). If COMM(2) = 0.0, this parameter has no effect. COMM(2) > 0.0 specifies an upper bound on the permitted size of  $\max|Y(I)|$ . If the bound is attained during the integration, the calculation is interrupted and the routine exits with IFAIL = 0. CIN(1) = 4.0 and COMM(2) = 0.0. To continue the integration, IFAIL should be reset to its original input value (and COMM(2) may be given a new value) then D02QBF should be called again. COMM(2) is always set to zero on exit when its input value is the cause of interruption to the integration, otherwise COMM(2) is unchanged on exit. Note that COMM(2) must be small enough to prevent overflow.

COMM(3). If COMM(3) = 0.0, this parameter has no effect. If COMM(3) = 0.0, a check is made on whether  $Y(I) - W(I,21)$  has changed sign on the current integration step for any value I, I = 1, 2, ..., N. Here, W(I,21), I = 1, 2, ..., N are values which must be specified by the user when COMM(3) = 0.0. If there has been a sign change in any component on the current step, the calculation is

interrupted with  $IFAIL = 0$ ,  $CIN(1) = 3.0$  and  $COMM(3) = 0.0$ . To continue the integration,  $IFAIL$  should be reset to its original input value and  $COMM(3)$  may be reset (in which case  $W(I,21)$ ,  $I = 1, 2, \dots, N$ , may also be reset), then  $DO2QBF$  should be called again.  $COMM(3)$  is always set to 0.0 on exit when its input value is the cause of an interruption to the integration, otherwise it is unchanged on exit.

$COMM(4)$ . If  $COMM(4) = 0.0$ , this parameter has no effect. If  $COMM(4) > 0.0$  the calculation is interrupted after every integration step.

On exit  $IFAIL = 0$ ,  $CIN(1) = 5.0$ ,  $COMM(4)$  is unchanged. To continue the integration,  $IFAIL$  should be reset to its original input value and  $DO2QBF$  called again.

If  $COMM(4) < 0.0$  a check is made for a change in sign of  $X - COMM(5)$  on the current integration step (where  $COMM(5)$  must be set by the user). If there has been a sign change, the integration is interrupted with  $IFAIL = 0$ ,  $CIN(1) = 6.0$  and  $COMM(4) = 0.0$ . To continue the integration,  $IFAIL$  should be reset to its original input value. If it is desired to reset  $COMM(4)$  to a negative value, then  $COMM(5)$  should also be given a new value, and  $DO2QBF$  called again.  $COMM(4)$  is always set to 0.0 on exit when a change in sign of  $X - COMM(5)$  is the cause of an interruption, otherwise it is unchanged on exit.

$COMM(5)$  is only active when  $COMM(4) < 0.0$ , in which case it specifies the point where the next interruption of the integration should take place (see above). When  $CIN(1) = 1.0$  on entry,  $COMM(5)$  must lie between  $X$  and  $XEND$ , otherwise  $COMM(5)$  must lie between  $COUT(4)$  and  $XEND$ .

$COMM(5)$  is unchanged on exit.

**CONST** - real array of **DIMENSION** at least (5).

**CONST** is used to control stepsize choice during integration. Normal entry is with **CONST(I)** = 0.0,  $I = 1, 2, \dots, 5$  and default values are then set in **D02QBF** as described below. On an error exit with **IFAIL** = 1, the default values of the components of **CONST** may not have been set. If not 0.0, each **CONST(I)** must be  $> 1.0$ , and, in addition, **CONST(2)**  $>$  **CONST(1)**.

**CONST(1)** and **CONST(2)** are factors used to bound stepsize changes. If the initial stepsize is  $H$ , then the modulus of the stepsize on the second step is bounded by **CONST(2)**  $\times |H|$ . At any other stage in the integration if the current stepsize is  $H$  then the modulus of the next stepsize is bounded by **CONST(1)**  $\times |H|$ . If **CONST(1)** = 0.0 on entry, it is given the default value 10.0 in **D02QBF**; if **CONST(2)** = 0.0 on entry, it is given the default value 100.0 in **D02QBF**.

**CONST(3)**, **CONST(4)** and **CONST(5)** are 'tuning' constants used in determining the next order and stepsize. They are used to scale the error estimates used in determining whether to keep the same order of the Gear method, decrease the order or increase the order respectively. The larger the value of **CONST(I)**,  $I = 3, 4, 5$  the less likely the choice of the corresponding order. The choice of these constants might be assisted by studying the appropriate sections of [2] and [3]. If any **CONST(I)** = 0.0,  $I = 3$  or  $I = 4$  or  $I = 5$ , on entry, then the corresponding default value is set as follows in **D02QBF**: **CONST(3)** = 1.2, **CONST(4)** = 1.3, **CONST(5)** = 1.4.

**COUT** - real array of **DIMENSION** at least (16).

**COUT** is used for output only. The components **COUT(I)**,  $I = 1, 2, \dots, 16$ , are set by routine **D02QBF** when **CIN(1)** = 0.0 or 1.0. On calls to **D02QBF** with **CIN(1)**  $\geq 2.0$ , **COUT(I)**,  $I = 1, 2, \dots, 16$  are updated or remain unchanged, and they should not normally be changed on interruptions of **D02QBF**. On an error exit with **IFAIL** = 1, values of the components of **COUT** may not have been defined. The output values of the components of **COUT** are:

#### COOT(1)

The minimum stepsize used in the integration to the current point. For smooth solution this will often be the initial step (output in CIN(5)).

#### COOT(2)

The maximum stepsize used in the integration to the current point.

#### COOT(3)

The number of successful integration steps (see COOT(8)) taken at the maximum permitted stepsize (given in COOT(14) on exit) or at a stepsize chosen so that the endpoint XEND is reached in the current step.

#### COOT(4)

The last integration point used before the current value of X.

#### COOT(5)

The last integration point used before COOT(4).

The value COOT(4) - COOT(5) may be a better choice of stepsize for continuing integration when XEND is changed than the value CIN(6).

#### COOT(6)

The maximum value of  $\max Y(I)$  occurring in the integration to the current point.

#### COOT(7)

The minimum value of  $\max Y(I)$  occurring in the integration to the current point.

#### COOT(8)

The number of successful integration steps used in the integration to the current point. An integration step is successful if it is used to advance the integration (that is if the local error test is satisfied).

#### COUT(9)

The number of unsuccessful integration steps used in the integration to the current point.

#### COUT(10)

is not used by D02QBF.

#### COUT(11)

When CIN(1) = 0.0 or 1.0 on entry, COUT(11) is set to macheps by D02QBF; macheps is the smallest positive number representable on the machine for which  $1.0 + \text{macheps} > 1.0$  (as given by the NAG Library routine X02AAF). On re-entry to D02QBF with CIN(1) = 2.0, COUT(11) is not recalculated and must not be changed between successive calls.

#### COUT(12)

When CIN(1) = 0.0 or 1.0 on entry, COUT(12) is set to dwarf by D02QBF; dwarf is the smallest positive machine-representable number (as given by the NAG Library routine X02ABF). On re-entry to D02QBF with CIN(1)  $\geq 2.0$ , COUT(12) is not recalculated and must not be changed between successive calls.

#### COUT(13)

The value used as a lower bound on the modulus of possible stepsizes in the integration up to the current point (see (CIN(3) above), COUT(13) is re-evaluated on each entry.

#### COUT(14)

The value used as an upper bound on the modulus of possible stepsizes in the integration up to the current point (see CIN(4) above). COUT(14) is re-evaluated on each entry except on entries with CIN(1) = 5.0 or 6.0 and COMM(4) > 0.0 respectively.

#### COUT(15)

The order of the method on the last successful step.

## COUT(16)

The number of evaluations of the Jacobian,  $(\partial F_i / \partial Y_j)$  (if MPED = 1, this is the number of calls to PEDERV).

## MPED-INTEGER

If MPED = 0 on entry, the Jacobian  $(\partial F_i / \partial Y_j)$  is calculated internally to D02QBF; whereas if MPED = 1 the Jacobian must be calculated in PEDERV.

Unchanged on exit.

PEDERV - SUBROUTINE, supplied by the user.

PEDERV must evaluate the Jacobian of the system (i.e. the partial derivatives  $\frac{\partial F_i}{\partial Y_j}$ ) for given values of the variables T,  $Y_1, \dots, Y_N$ . Its specification is:

```
SUBROUTINE PEDERV(T,Y,PW)
  real T,Y(n),PW(p,n)
```

where n and p are the actual values of N and IW in the call of D02QBF.

T - real

On entry, T specifies the value of the independent variable T.  
Its value must not be changed.

Y - real array of DIMENSION (n).

On entry, Y(I) contains the value of the variable  $Y_I$  for  $I = 1, 2, \dots, n$ .

These values must not be changed.

PW - real array of DIMENSION (p,n).

On exit, PW(I,J) must contain the value of  $\frac{\partial F_i}{\partial Y_j}$  for  $I, J = 1, 2, \dots, n$ .

PEDERV must be declared as EXTERNAL in the (sub)program from which D02QBF is called.

If MPED = 0, PEDERV can be a dummy routine.

PW - real array of DIMENSION (IW,q) where  $q \geq N$

Used as work space.

W - real array of DIMENSION (IW,IW1).

W is used partly as workspace and partly for input/output. The input values of W have been described above under CIN(2) and COMM(3). Note that if CIN(2) = 3.0, W(,19) and W(I,20), I = 1,2,...,N, must always be set; and if CIN(2) = 4.0, W(I,19), I = 1,2,...,N, must always be set. If COMM(3) = 0.0, W(I,21), I = 1,2,...,N, must always be set. The values are unchanged on exit.

On exit, W(I,J), I = 1,2,...,N, J = 1,2,...,6 contain values used by interpolation routines D02XGF and D02XHF, and should not be changed between successive calls to D02QBF. If COMM(3) = 0.0, W(I,22), I = 1,2,...,N, contains those values of the computed solution closest to the given values W(I,21) computed throughout the integration; that is

$|W(I,22) - W(I,21)|$  is equal to the minimum over all integration points of  $|Y(I) - W(I,21)|$

for I = 1,2,...,N

IW - INTEGER

On entry, IW must specify the first dimension of W as declared in the calling (sub)program.  $IW \geq N$ .

Unchanged on exit.

IW1 - INTEGER

On entry, IW1 must specify the second dimension of W as declared in the called (sub)program.  $IW1 \geq 18$ , except that in some circumstances IW1 must be larger ( $IW1 \geq 22$  is always sufficient).

if COMM(3) = 0.0 and CIN(2) = 3.0,  $IW1 \geq 20$ ;

if COMM(3) = 0.0 and CIN(2) = 4.0,  $IW1 \geq 19$ ;

if COMM(3) = 0.0,  $IW1 \geq 22$ .

IW1 is unchanged on exit.

## IFAIL - INTEGER

On entry, IFAIL must be set to 0 or 1. For users not familiar with this parameter the recommended value is 0.

Unless the routine detects an error (see next section), IFAIL contains 0 on exit.

For this routine, users are strongly recommended to set IFAIL = 1 before entry, because values of certain output parameters may be useful even if IFAIL = 0 on exit. It is then essential to test the value of IFAIL on exit (and if relevant, the value of CIN(1) also).

## 2. ERROR INDICATORS AND WARNINGS

Errors or warnings specified by the routine:

IFAIL = 1

On entry a parameter has an illegal value. The output value of CIN(1) determines which error has occurred, as follows:

CIN(1) = -1

$N \leq 0$

or  $IW < N$

or  $IW1$  too small

CIN(1) = -2.

$TOL \leq 0.0$ .

CIN(1) = -3.

$CIN(1) < 0.0$

or  $CIN(1) > 6.0$ .

CIN(1) = -4.

$CIN(2) < 0.0$

or  $CIN(2) > 4.0$ .

CIN(1) = -5

$W(i,19) \leq 0.0$

for some  $I$ ,  $1 \leq I \leq N$ .

CIN(1) = -6.

indicates  $CIN(2) = 3.0$ ,

$Y(I) = 0.0$  and  $W(I,20) \leq 0.0$

for some  $I$ ,  $1 \leq I \leq N$ .

CIN(1) = -7.

For some  $I$ ,

$CONST(I) < 0.0$ .

CIN(1) = -8.

For some  $I$ ,

$0.0 \leq CONST(I) \leq 1.0$ ,

or  $CONST(2) \leq CONST(1)$ .

CIN(1) = -9.

indicates  $COMM(1) < 0.0$  on entry.

CIN(1) = -10.

indicates  $COMM(2) < 0.0$  on entry.

CIN(1) = -11.

indicates  $\max |Y(I)| \geq COMM(2) > 0.0$  on entry.

CIN(1) = -12.

indicates  $COMM(3) = 0.0$  and

$Y(I) = w(i,21)$ ,

for some  $I$ ,  $1 \leq I \leq N$ , on entry.

CIN(1) = -13.

With CIN(1) = 1.0 and

COMM(4) < 0.0 on entry,

COMM(5) does not lie between X and XEND inclusive.

CIN(1) = -14.

With CIN(1) = 1.0 and

COMM(4) < 0.0 on entry, the points

COOT(5), COOT(4), X and XEND are

not ordered correctly.

CIN(1) = -15.

With CIN(1)  $\geq$  2.0 and

COMM(4) < 0.0 on entry,

COMM(5) does not lie between

COOT(4) and XEND inclusive.

CIN(1) = -16.

CIN(3) > CIN(4) > 0.0.

CIN(1) = -17.

Two successive calls have been made to D02QBF with X  
set to XEND on entry.

CIN(1) = -18.

MPED  $\neq$  0 and MPED  $\neq$  1.

IFAIL = 2

To satisfy the local error bound the integration step H needed is so  
small that  $H < COOT(13)$ .

IFAIL = 3

The problem cannot be solved to the required accuracy. This error  
exit is unlikely to occur. A further explanation is given in [3].

IFAIL = 4

TOL is too small for an initial step to be taken or corrector convergence could not be achieved on the first step.

IFAIL = 5

More than COMM(1) function calls have been made (when COMM(1) > 0.0 on entry). The output from D02QBF is in the correct form for interpolation using D02XGF or D02XHF and for continuing the integration.

IFAIL = 6

A relative error test failure with CIN(2) = 3.0; that is, for some value  $I$ ,  $1 \leq I \leq N$ , with  $W(I,20) \leq 0.0$ , either  $Y(I) = 0.0$  or a component of the solution has different signs at the points  $T = X$  and  $T = COUT(4)$ .

IFAIL = 7

More than COMM(1) function calls have been made (when COMM(1) > 0.0 on entry) before sufficient progress has been made in the integration for any useful information to be produced (neither D02XGF or D02XHF can be used with the output from D02QBF).

IFAIL = 8

Indicates that corrector convergence could not be achieved for a stepsize greater than COUT(13) in modulus.

## Appendix C

### The Idea of Relaxation Oscillation

The amplitude of any oscillating mass would decay due to the influence of dissipative or frictional forces. Assuming that the damping force on a vibrating particle of mass  $m$  is proportional to the velocity, the equation of motion for a system with a stiffness factor (or restoring force)  $S$ , and retarding force per unit velocity (i.e. resistance constant)  $r$ , is given as:

$$m \frac{d^2x}{dt^2} + r \frac{dx}{dt} + sx = 0 \quad C.1$$

$x$  being the displacement and  $t$  the time.

If the resistance constant ' $r$ ' were to be negative, i.e. instead of a retarding force acting on the mass a periodic accelerating force were to be acting then the equation C.1 would be rewritten as:

$$\ddot{x} - \frac{r}{m} \dot{x} + \frac{s}{m} x = 0 \quad C.2$$

thus implying that the amplitude in this case would increase infinitely. Though this condition is physically impossible, eqn. 5.8 could be applicable for small values of  $x$  [75].

If  $r/m$  could be given by the value  $2k$  and  $s/m$  equated to  $n^2$ , and introducing the term  $(1-x^2)$  to make the resistance to the oscillating system a function of the displacement the equation of motion could be written as :

$$\ddot{x} - 2k (1-x^2) \dot{x} + n^2 x = 0 \quad C.3$$

representing an oscillatory system in which the resistance is a function of the displacement. When ' $k$ ' is a positive quantity the system has a resistance which, for a small amplitude, is negative. Therefore the position  $x=0$  is unstable. When, further,

$$k^2 \gg n^2$$

C.4

it can be shown that as long as  $x^2 \ll 1$  the variable  $x$  will initially leave the value aperiodically, but when  $x^2 > 1$  the resistance changes signs and becomes positive.

The fundamental period of such a vibration is, apart from a numerical constant, defined by a quantity involving the elastic forces and resistance only. Such oscillations are described as 'relaxation oscillations'. They differ very markedly from the sinusoidal oscillations of a mass controlled by a spring, for the resistance may now be negative (as in analogous electrical cases), increasing to a positive value as the displacement increases. The displacements take place in sudden jumps which recur periodically.

The properties of relaxation oscillations are :

1. Their time period is determined by a time constant, or relaxation time, dependent on resistance and elastic forces only.
2. Their wave form is far from simple harmonic. Very steep parts occur on 'relaxation' of the resistance, and as a consequence many harmonics of large amplitude are present.
3. A small impressed periodic force can easily bring the relaxation system into step with it (automatic synchronization), whilst under these circumstances the amplitude is hardly influenced at all.

# APPENDIX D

## PROGRAM ON ACSL

PROGRAM ACOUSTIC WAVE

INITIAL

```

    CONSTANT WS = 5924. , TSTOP = 0.2000E-03
    CONSTANT PR = .33797E+07 , XL = .68737E-01
    CONSTANT GN = 1.1505
    CONSTANT RHO = 4.3073
    CONSTANT XC = 0.97E-02
    CONSTANT DP = 0.325E+05
    CONSTANT UP = 2.870E+00
    CONSTANT IC2 = 0.0
    CONSTANT IC3=2.870E+00
    CINTERVAL CINT = 1.00E-06
    ALGORITHM IALG=2
    Z = UP/XC
    VS = SQRT(GN*PR/RHO)
    CZ = COS(WS*2.*3.14159*T)
    XZ = VS*VS/XC/XL
    DZ=XZ*(1+DP/PR*CZ)

```

END \$ 'OF INITIAL'

DYNAMIC

DERIVATIVE

```

    SD= INTEG(-Z*SD-DZ*S,IC3)
    S = INTEG(SD,IC2)

```

END \$ 'OF DERIVATIVE'

TERMT (T.GT.TSTOP)

END \$ 'OF DYNAMIC'

END \$ 'OF PROGRAM'

